Rationally designed DNA origami hosts for protein guests

Inaugural-Dissertation zur Erlangung des Doktorgrades

-Dr. rer. nat.-

der Fakultät für Biologie an der Universität Duisburg-Essen

vorgelegt von

Andreas Jaekel (M. Sc.)

aus Greifswald

August 2021

Der vorliegenden Arbeit zugrundeliegenden Experimente wurden im Zeitraum von Februar 2017 bis Juli 2021 im Arbeitskreis von Prof. Dr. Barbara Saccà am Zentrum für medizinische Biotechnologie an der Universität Duisburg-Essen durchgeführt.

Tag der Disputation: 12.11.2021

1. Gutachter: Prof. Dr. Barbara Saccà

2. Gutachter: Prof. Dr. Hemmo Meyer

Vorsitzende des Prüfungsausschusses: Prof. Dr. Elsa Sanchez-Garcia

DOI: 10.17185/duepublico/74992
URN: urn:nbn:de:hbz:465-20240723-113347-8

Table of contents

List of abbreviations

Abbreviation	Description
2D	two dimensional
3D	three dimensional
[x]	molar concentration of x [mol/l]
°C	degree celsius, T(°C)= T(K)-273.15 K
Å	ångström
A	adenine
AAA	ATPase associated with diverse cellular Activities
Ab	antibody/immunoglobulin G
ADP	adenosine diphosphate
AFM	atomic force microscopy
AGE	agarose gel electrophoresis
APS	ammonium persulfate
Arg	arginine
ATP	adenosine triphosphate
AuNP	gold nanoparticles
BG	benzylguanine
bp	base pair
c	molar concentration [mol/l]
C	cytosine
cs	core staples
Cdc48	cell division control protein 48
CTF	contrast transfer function
CuAAC	copper(I)-catalyzed azide-alkyne cycloaddition
Cys	cysteine
d	diameter [m]
Da	dalton [$1.66 \cdot 10^{-27}$ kg]
DLS	dynamic light scattering
DNA	deoxyribonucleic acid
ds	double stranded
DX	double cross-over
E	Echo (lower half-prism origami)
EDC	1-ethyl-3(3-dimethylaminopropyl)carbodiimide hydrochloride
Etbr	ethidium bromide
ex	extruding edge handles
f	factor
FAM	6-carboxyfluorescein
FnS	Freeze and Squeeze
G	guanine
H	Halotag
His	histidine
p97H	p97-Halotag
Sp97H	Snaptag-p97-Halotag
hybr	hybridization staples

in	intruding edge handles
k_x	reaction rate of x
K	kelvin
K_D	dissociation constant
l	left ring protruding arms
L	left origami edge staples
Lys	lysine
M	Molar concentration unit (=mol/l)
MALDI	matrix-assisted laser desorption/ionization
ml	middle left ring protrusions
mr	middle right ring protrusions
MWCO	molecular weight cut-off
N	Narcissus upper half-prism origami
N-in	N/D1 domain oriented towards origami center
N-out	N/D1 domain oriented towards origami edge
NE	Nemesis (full origami prism)
NHS	N-hydroxysuccinimide-ester
N_L, N_R, N_T,	modified Narcissus staple sets
Npl4	nuclear protein localization 4
NTA	nitrilotriacetic acid
NZA	NZ-Amine
OD	optical density
OGT	O^6-alkylguanine-DNA alkyltransferase
PA	protruding arms
PAGE	polyacrylamide gel electrophoresis
PBS	phosphate buffered saline
PCR	polymerase chain reaction
PEGx	polyethylenglycol of weight x in Da
pH	negative common logarithm of hydronium ion concentration
pix	pixel
POI	protein of interest
PP1	protein phosphatase 1
PUB	peptide: N-glycanase and UBA or UBX-containing proteins
r	right ring protrusions
R	right origami edge staples
rcf	relative centrifugal force [$kg \cdot m \cdot s^{-1}$]
rel	release strand
RNA	ribonucleic acid
rpm	rounds per minute [60^{-1} s^{-1}]
RT	room temperature (21°C)
S	Snaptag
SBP	streptavidin binding peptide
SDS	sodium dodecyl sulfate
Sds22	suppressor of Dis2 mutant 2
SEC	size exclusion chromatography
SMCC	succinimidyl 4-(N-maleimidomethyl)cyclohexane-1-carboxylate
SPDP	succinimidyl 3-(2-pyridyldithio)propionate

SPIE	Sds22/PP1/I3-Eos complex
ss	single stranded
STV	streptavidin
T	thymine
TAMRA	tetramethylrhodamine
TBTA	tris(benzyltriazolylmethyl)amine
TCEP	tris(2-carboxyethyl)phosphine
TEM	transmission electron microscope/microscopy
TEMED	tetramethylethylenediamine
T_m	melting temperature [°C]
Tw	CLR01 molecular tweezer
Ufd1	ubiquitin fusion degradation protein 1
UV	ultraviolet
V	volt ($kg \cdot m^2 \cdot A^{-1} \cdot s^3$)

1. Introduction

1.1. Bionanotechnology

Nanotechnology is the science that deals with matter at the nanometer scale[1–3] and is considered a key technology to reach todays requirements to materials and chemicals with increasing numbers of patents, firms and public financing around the globe.[4–6]Typically, nanomaterials are composed of particles that are larger than the size of an atom or small molecule but smaller than roughly one micrometer in one dimension. This rather arbitrary range of sizes originates from the definition of colloidal particles in solutions at the beginning of the 20th century with the upper limit compelled by the optical resolution of light microscopy.[1] The fact that the size of nanomaterials is comparable to the wavelength of visible light allows the manipulation of quantum effects, such as localized surface plasmons[7] or surface based catalytic activity[8–11] for designer physical properties.[12] On the other hand, the high surface to volume ratio of a nanoobject facilitates the fine tuning of such properties for their use in bulk studies.

Nanoparticles have been used by humans through millennia. Examples of applications range from coating of materials with carbon nanotubes[13], increasing metal stability by cementite nanowires[14], introduction of glittering effects by copper and silver nanoparticles' layers[15] or production of dichroic glass by inclusion of gold nanoparticles.[16] Those manufacturing techniques were however carried out without much understanding of the physical properties of nanoscale objects until first pioneering studies at the second half of the 19th century by Graham and Faraday[17,18].

The finding and development of various technologies such as the Rayleigh light scattering[19] and electron microscope[20] allowed first insights into the nanoparticles at play. However, the potential of harnessing molecules at the nanoscale remained largely unrecognized until the 1980s[21,22], two decades after the pioneering talk by Richard Feynman ´There´s plenty of room at the bottom´[2] where the seminal ideas of the Nanotechnology Era were firstly laid down. The consciousness of a still largely unexplored world in the nanosized dimension boosted scientific efforts that finally culminated in the development of the scanning tunneling microscope[23], the atomic force microscope[24], the discovery of fullerenes[25] and the proof of concept of precise atomic placement[26]. This led to largely increased research in this field and the usage of the term `nanotechnology´ for it. Nowadays many products like batteries or sunscreens contain some nanotechnological engineered particles[27,28].

Two approaches can be used to build nanosized objects: a top-down approach, where a nanosized object is generated or manipulated by a larger object and a bottom-up approach, where a nano-object is built from smaller molecules. Modern top-down or miniaturization approaches, such as extreme UV-lithography[29] and inject-printing[30,31] share the same principle: the exploitation of the laws of physics to pack a huge amount of information on an exceedingly small space. However, these techniques are challenged by the small size of things that can be manipulated, resulting in drawbacks such as limited precision, reduced sample

throughput and high costs.[32] In bottom-up approaches instead, nanomaterials are grown by self-assembly or polymerization procedure. Having access to the growth process not only allows to control the dimensions of the target object but also enables the pre-designed placement of other molecules and chemical functionalities. However, the self-assembly of nanomaterials through nucleation and growth mechanisms can be difficult to control.[33–35]

As a solution to the growth control of nanoparticles finite-sized, information-bearing molecules like proteins and nucleic acids can be used as building blocks for bottom-up materials, that are programmable on the molecular to atomic level, as theorized already in 1981 by Drexler.[22] Since these biomolecular polymers display structural features in the low nanometer range[36–38], they can be advantageously used as construction materials for nanotechnological purposes. Within this broad field, the utilization of those biomolecules for artificial or semi-artificial nanomaterials is sometimes referred to as bionanotechnology.[39,40] Here, the boundaries to other technologies like protein engineering and biotechnology are not always very clear and often are solely a matter of definition. In the most widely accepted sense, bionanotechnology is a discipline at the interface of nanotechnology and biology and essentially makes use of biomolecules (both engineered or of natural origin[33,41]) and biological mechanisms for nanotechnological purposes.[39,40]

Some examples of this kind are nanopores spanning lipid bilayers, either derived from natural membrane-spanning proteins or made of artificial DNA constructs (See example in Figure 1-1 A and B). These structures can be used to detect and even sequence DNA strands or polypeptide stretches.[42–45] They were also reported to be capable of size-dependent transport across a membrane.[44] Another relevant example is the usage of DNA as a data storage molecule for archiving. The technique was already theorized in 1964 by soviet scientist Neiman[46] and consequently further developed allowing storage of hundreds of megabytes[47,48] and possibly even several gigabytes[49] of information in DNA today (see Figure 1-1 C for basic layout). Applying increasingly sophisticated designs of bionanomaterials, several nanomachines have been developed where the mechanical movement of the single component is triggered from an external source[50–53]. Potential usage in targeted drug delivery[54–56], tunable optical properties of materials[57–60] and programming of chemical synthesis routes[61–66] have been also reported.

Bionanomaterials, as their natural counterparts in biological self-assembled systems, are often held together by supramolecular non-covalent bonds. Exploiting the occurrence of known interactions between biomolecules, as for example specific protein-protein interactions[67,68] or nucleobase pairing in DNA and RNA[69,70], desired macromolecular structures can be designed. Polyvalent ion and hydrogen bonds as well as dipole-dipole interactions and covalent bonds are often simultaneously at play, complicating the

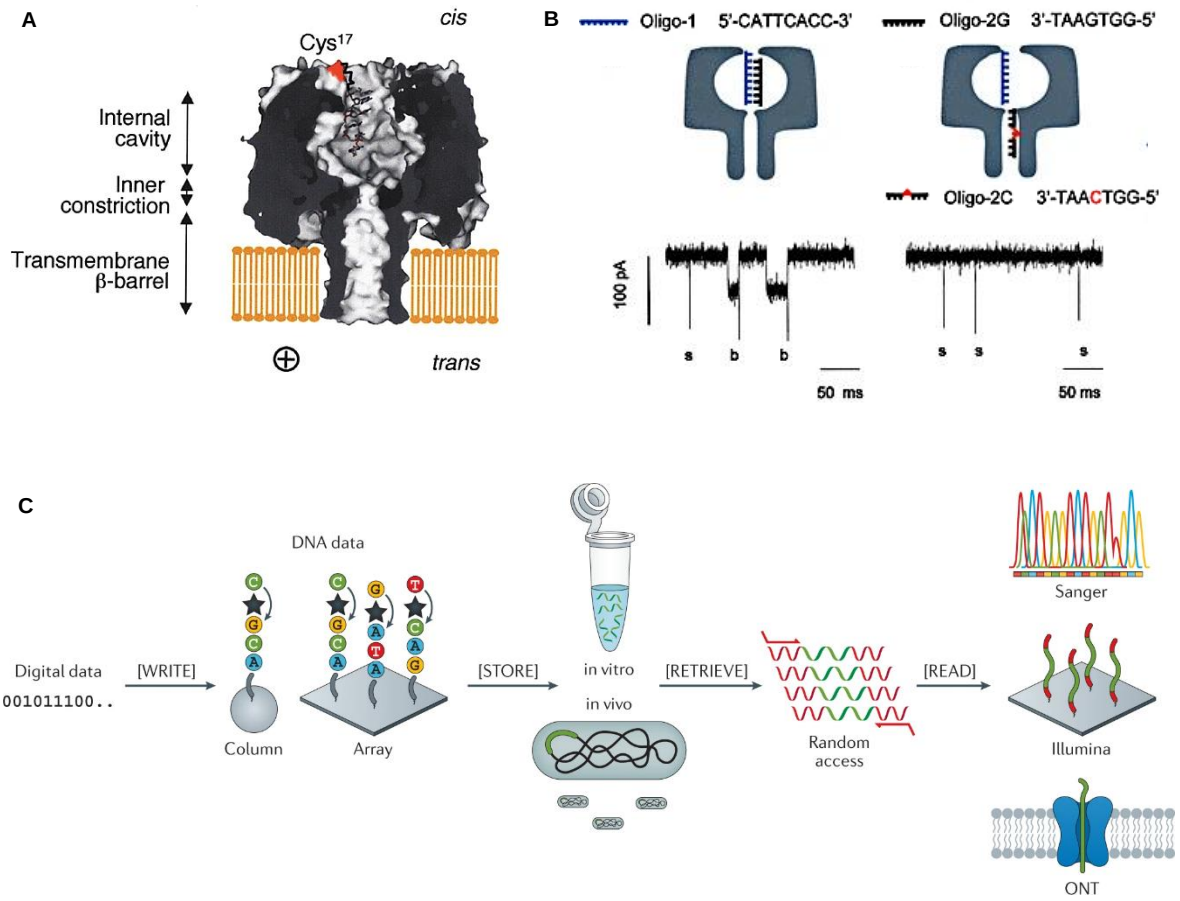

Figure 1-1: Examples of bionanomaterials. **A** The outline of a membrane spanning nanopore based on α-hemolysin. One cysteine at the pore entry was modified with a DNA oligonucleotide. **B** When electric field was introduced across the membrane, binding of complementary oligonucleotides could be detected by decrease of ion flux and hence total current. **C** Common workflow of molecular data storage with DNA. Binary data is parted in strings and mapped into DNA sequences. The sequences are synthesized by solid phase phosphoramidite synthesis on solid support. After cleavage, the DNA strands are stored *in vivo* or *in vitro* where they can later be retrieved and sequenced by Sanger sequencing, sequencing-by-synthesis, or nanopore sequencing. **A** and **B** were reprinted with permission from reference 42, copyright 2021 Springer Nature **C** was reprinted with permission from reference 48, copyright 2021 Springer Nature.

programmability of the object of interest. The design process is also often assisted by computer simulations and various *in silico* studies, both at the level of polypeptide chains and nucleic acids.[71–74] These tools, together with the advancement of bioconjugations methods, led to the foundation of new fields of science, such as protein origami[75], as well as DNA and RNA nanotechnology[76,77] all of which allow the programmable construction of molecular structures with almost any desired shape and a size of few tens to several hundred nanometers (see Figure 1-2 for examples[78,79]).

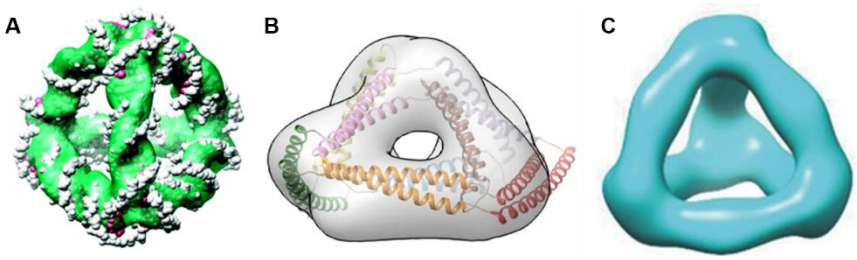

Figure 1-2: Structural reconstruction of tetrahedrons (not to scale) designed by **A** DNA nanotechnology **B** protein origami and **C** RNA nanotechnology. **A** and **C** were reconstructed from cryo-EM maps. **B** was reconstructed from negative stain TEM maps. **A-C** reprints with permission from references 78, 75 and 79, copyright 2021 Springer Nature and 2021 John Wiley and sons.

1.2. DNA as a construction material

While RNA- and protein-based objects are more feasible for applications with living matter[72,75,80–83], DNA nanomaterials profit of their easier design rules and high stability *in vitro*[84–86]. DNA nanotechnology has been an active field of scientific research for already a few decades, during which theoretical frameworks and experimental procedures have been constantly evolved. This increasing development makes possible nowadays to design and realize – in a reproducible manner – molecular objects with predictable nanosized features and with sizes that range from only three to several hundred or even thousands of oligonucleotides, shaped into kDa to GDa-large arbitrary architectures[87–89] as well as 2D and 3D patterns and crystals[90–95].

1.2.1. DNA nanotechnology

The fundamental building block for every DNA nanostructure is DNA. Hence, the understanding of the chemical-physical properties of this polymer is necessary when the purpose is to design ordered assemblies thereof. Single-stranded DNA (ssDNA) consists of nucleotide monomers which are composed of three subunits: a phosphate, a deoxyribose and one of the four nucleobases. adenine, guanine, thymine or cytosine.[96–98] The usage of DNA as a building material however is nearly exclusively based on the structure of double stranded (ds) B-DNA. In B-DNA two antiparallel strands of DNA form a right handed double helix with the nucleobases pointing inward (Figure 1-3 A).[36,99] The major driving force in forming a duplex is the stacking interaction of consecutive DNA bases.[100–104] However, the double-stranded structure requires hydrogen bonds between the bases of each strand to be stable. This process is called base pairing because each nucleobase pairs only with a specific other nucleobase of the opposing strand. In the canonical Watson-Crick base pairing adenine pairs with thymine and guanine pairs with cytosine.[36] This rule is the basic law of any DNA design: once a DNA sequence is given, its complementary sequence is also defined.

The increasing interest for artificial DNA sequences to be used in genetic experiments led to initial breakthroughs in *de novo* chemical synthesis of DNA strands in the 1960s and 1970s[105–107]. In this way, single-stranded DNA of any sequence and their corresponding duplexes could be easily accessed. However, to build two and three-dimensional DNA structures, stable junction points between the constituent dsDNA stretches are necessary. Depending on the sequence at the junction bases can be exchanged between dsDNA stretches, leaving the junction mobile[108]. Here, for stability it is intended that the junction between the duplexes is not migrating, i.e. it is immobile. The theoretical description as well as the experimental realization of the first immobile four way junction was reported by Seeman and Kallenbach in 1983 and hence marked the beginning of structural DNA nanotechnology (Figure 1-3 B).[89,109] Regrettably, those single junction motifs, despite being immobile, are structurally very flexible and do not allow for a high degree of shape control for higher ordered structures.[110–112] Few years later, meso- and antijunctions were also developed, whose even higher structural flexibility limited their further implementation for nanotechnological applications.[113]

The circular stepping of bases around the B-DNA central axis allows in principle to introduce chemical modifications at every phosphate positions with one step being approximately 34° and 3 Å apart from the next one.[36,114] Hence, it is also possible to locate a second crossover every integer multiple of a half-helical turn, thus joining two immobile junctions into a so-called double cross-over tile[115] (or DX). The DX motifs overcame the high flexibility issue of the single junction and allowed the successful production of 2D DNA lattices[116] (Figure 1-3 C and D).

Other tile structures, including additional helices and/or DNA crossovers, were lately introduced and used for the production of a variety of arrays[94,117–120]. Several of those were further employed to precisely place proteins[118,121–123] or metal nanoparticles[61,124,125] on a DNA array within nm precision. Despite the development of DNA tiles allows the controllable placement of molecular moieties with almost molecular resolution, thus overcoming other technologies, the method suffers from important drawbacks, such as the lack of full control over the self-assembly mechanism[126] and the requirement of known concentration and purity of each strand involved[115].

Tiles could also be programmed to build small finite objects or small lattices by hierarchical and algorithmic self-assembly[126–133], but the focus of the research community shifted after the publication of a scientific breakthrough in 2006. Aiming to build finite-sized objects of arbitrary shapes and inspired by the work of Shih[134] and Yan[135], Rothemund developed the scaffolded DNA origami method. In this technique a long ssDNA strand (termed scaffold) is folded into arbitrary two-dimensional shapes by designed, artificial, shorter oligonucleotides (termed staple strands) binding to distinct parts of the scaffold strand (Figure **1-3** E)[136]. This technique was quickly further developed making it possible to build three-dimensional[91], curved[137] and less space-filled structures (Figure 1-4 A)[137–140]. One big advantage of this method is the high yield of formation of the goal structures[141]. Progress in design software[73,142–144], optimization of design rules[143,145,146] as well as development of assembly[86,147,148] and purification[149–152] methods made the DNA origami method a reliable workhorse of structural DNA nanotechnology.

Since, the 5´ and 3´ ends of the staple strands can be placed at desired positions of a DNA origami, elongations and chemical modifications pointing out of the DNA origami surface can be easily introduced and are separately addressable[136]. Similar to DNA tiles, DNA origamis can be programmed to build larger, up to several GDa finite-sized objects[87] and even meta-DNA structures which can be further assembled into junctions, tiles and arrays (Figure 1-4 B and C)[153]. Several hierarchical constructs, such as filaments[154–159], 2D lattices[92,160,161] and 3D crystals[162] could be developed, enabling this technology to exceed the nm regime.

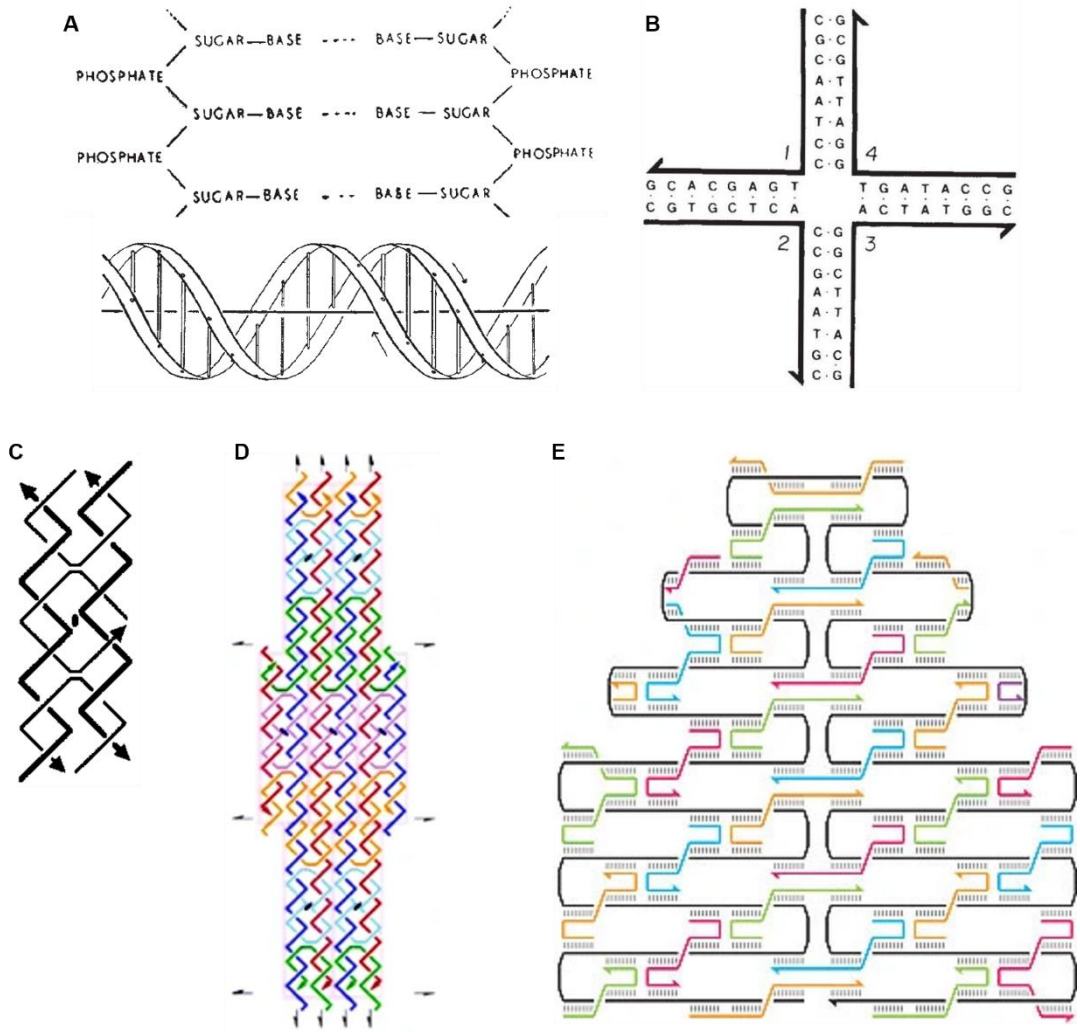

Figure 1-3: **A** The structure of dsDNA as supposed by Watson and Crick, later verified for B-DNA. **B** An immobile Holliday junction developed by Seeman and Kallenbach. **C** A DNA double crossover tile with even integer number of half helical turns and antiparallel dsDNA stretches. One of five possible double cross-over designs developed by Seeman and Fu. **D** A 2D array based on the double crossover tile developed by Winfree *et al.* . **E** Conceptual design of a DNA origami developed by Rothemund. **A-E** were reprinted and adapted with permission from references 36, 89, 115, 116 and 136. **A**, **B**, **D** and **E** Copyright 2021 by Springer Nature. **C** Copyright 2021 by American Chemical Society.

A major advancement in the tile-based approach occurred few years ago, with the development of the single-stranded tile or DNA brick technology. This method enables the building of large arbitrary shapes (Figure 1-4 D and E)[120,163] starting from a mixture of several hundreds of short oligonucleotides. The absence of a scaffold makes the self-assembly mechanistically different from that of a DNA origami and has been source of intense theoretical studies for its similarities to a nucleation-and-growth crystallization-like process[88,164–166]. Even though the DNA bricks strategy overcame the high purity requirements of former tile approaches, the bottleneck of this method remains the low yield in the target structure and the long assembly procedures[167–170].

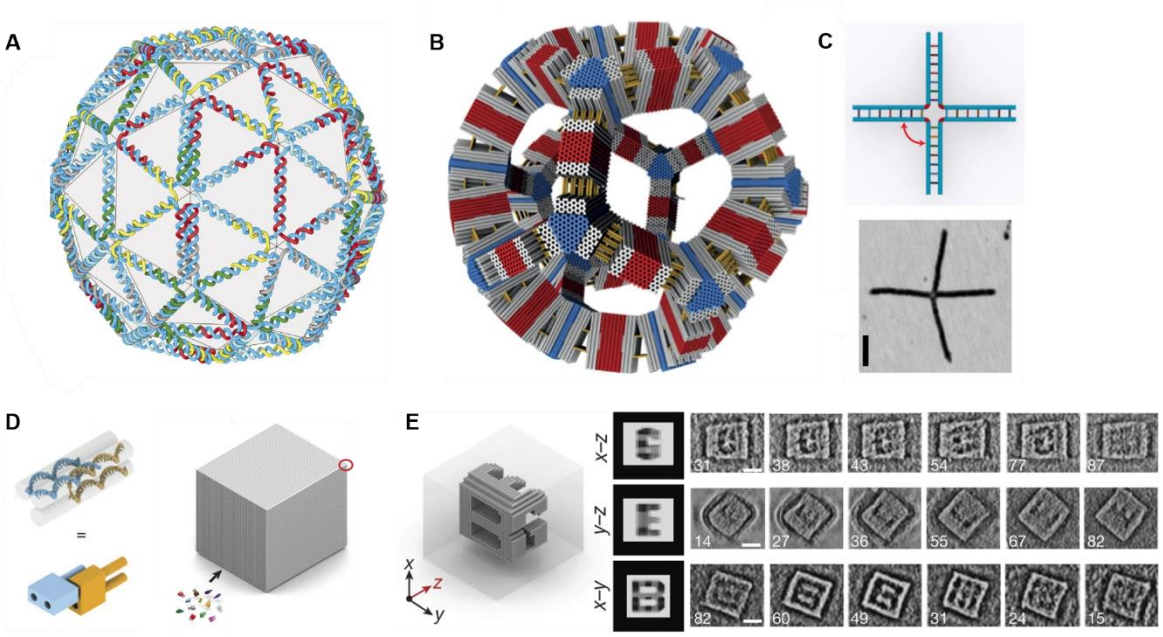

Figure 1-4: Structural DNA nanotechnology developments of the last ten years. **A** DNA meshes or wireframe origami allow less space filling structures. **B** Larger particles could be built from origami subunits, the one of the largest to date is shown here consisting of 220 origamis. **C** DNA origami can be used as meta material where an origami (blue) with oligonucleotide protrusions (other colors) mimic single stranded DNA. Structure shown here is a Holliday junction inspired DNA origami multimer (top) with respective AFM image (bottom). **D** DNA brick technology parts its used oligonucleotide in four domains allowing programmable binding sites for each brick. Domains are parted in voxels which can be singularly addressed. **E** DNA brick-based cavity can be achieved by leaving out respective staples. Here an example design is shown (left) with its respective electron tomographies (right). **A-E** adapted from references 140, 87, 153 and 88. Copyright 2021 by Springer Nature.

1.2.2. Strategies for binding proteins to DNA nanostructures

One way to functionalize DNA nanostructures is to attach molecular entities like metal nanoparticles or enzymes[57,60,155,171–177]. Solid-phase synthesis of DNA oligonucleotides enables production of desired sequences with high yields and makes the exchange and addition of various building blocks very feasible. Those can be further processed allowing the placement of either small molecules or large protein complexes onto DNA nanostructures. The various nature of those modifications were well reviewed by Madsen and Gothelf in 2019[178].

Especially proteins are very interesting to combine with DNA nanotechnology, since their native function and structure can not only be taken out of context but also put in spatially defined positions in relation to other substances of interest as cofactors, ligands, or other proteins. This led to the engineering of several nanomachines and enzyme cascades[179–187], some of them displayed unforeseen properties such as increased activity for increasingly shielded and spatially dense protein cascades[180].

Proteins can be bound onto DNA origamis using either covalent or non-covalent chemistry, with the linkage being either regioselective or non-regioselective (Figure 1-5)[188]. Which approach is more convenient is mostly dependent on the particular application sought for, the knowledge at hand about the protein as well as the nature and binding affinity of the ligand.

DNA constructs are usually used in low μM to low nM concentrations. While covalent bonds circumvent the problem of finding ligands that interact strongly enough with the protein of interest, they ultimately change the surface of the protein. Additionally, non-regioselective bifunctional crosslinking molecules like

succinimidyl 4-(N-maleimidomethyl)cyclohexane-1-carboxylate (SMCC) or succinimidyl 3-(2-pyridyldithio)propionate (SPDP), which establish a bond between amino and thiol residues, may indeed address several reactive sites on a protein surface, resulting in a heterogeneous mixture of products which are often extremely difficult to distinguish and isolate.[189–192] Nevertheless, for most applications, this approach is still suitable and is therefore well-established in the field, due to the rapidity and versatility of the bioconjugation strategy.[178]

The regioselectivity of binding can be achieved by introduction of tags into the protein of interest. Self-labelling enzymes, such as halo-, snap- or clip-tag, and peptide tags, are only few examples of protein tags that allow bioconjugation, either by means of so-called suicide ligands or additional enzymes like transglutaminase, sortase A or terminal deoxynucleotidyl transferase. In other cases, azide moieties can be employed for successive cycloaddition or Staudinger ligation. These techniques and other were reviewed already several times and their orthogonal usage in DNA nanotechnology proven[178,188,192–194]. However, they require a genetic modification of the protein of interest either via fusion with a distinct protein domain or elongation with a specific peptide sequence.

The usage of non-covalent bonds in DNA nanotechnology is mainly restricted to the avidin biotin interaction and applied to topologically mark certain sites in a designed object, to link proteins of interest (POI) to the DNA strands or to immobilize the DNA nanostructure on a surface[125,129,194–199]. Other non-covalent strategies rely on strong antigen-antibody interactions[118], cofactor-apoenzyme binding[200,201] or DNA binding domains[186,202,203]. A special case, reported by our group, describes the encapsulation of a multimeric DegP protein by a peptidic ligand which was radially distributed within the inner of a DNA origami prism[204].

Finally, the usage of non-covalent non-regioselective interactions is somewhat unusual as they aim to either reconstruct the native environment of the protein in a defined space or to shape an artificial environment which the protein ´prefers´ over its current surroundings. So far membrane proteins could be stabilized in solution and simultaneously marked for further investigation without changing the protein by lipid decorated DNA origamis[205,206].

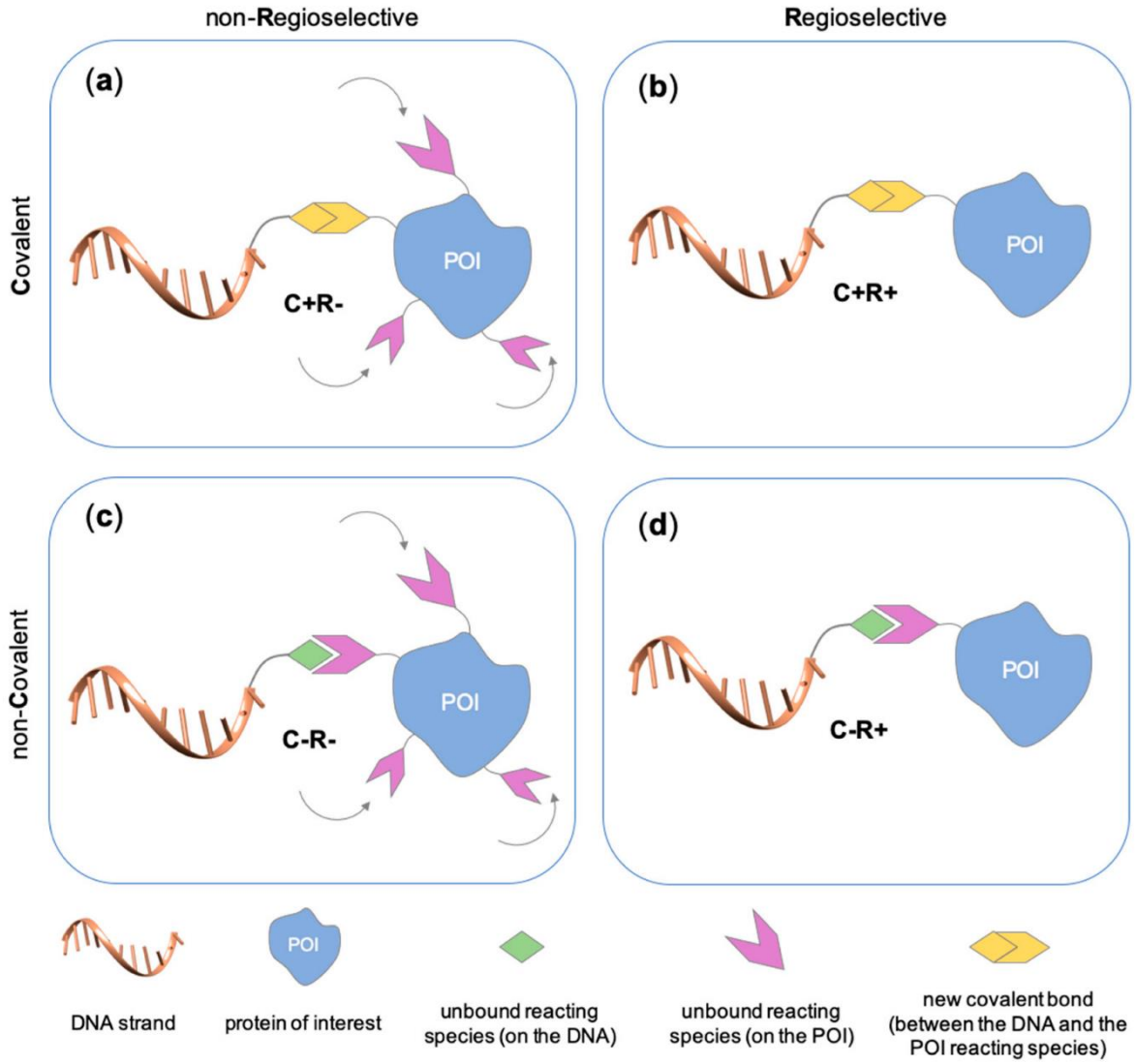

Figure 1-5: Binding proteins to DNA nanostructures can be done either covalently or non-covalently addressing the protein either regioselectively or non-regioselectively. Reprinted from reference 188.

2. Objective of this work

The aim of this work is to develop nanosized DNA cavities for proteins. Most of the DNA-scaffolded protein systems that make use of the DNA origami technology consist of enzyme cascades positioned on a DNA platform at a defined intermolecular distance.[181,183,207,208] The majority of the studies reported so far in this field deal with the horse radish peroxidase and glucose oxidase pair, and only recently, more complex enzymatic reactions, like the transcription and processing of RNA within a DNA capsule, have been described[186]. Here, the semi-synthetic system essentially works as an RNA-extruding nanofactory, with DNA-scaffolded protein components that engage, process and finally transport the substrate along a defined direction. Along this line, the present work aims at developing a DNA-scaffolded translocation and protein unfolding device that can be employed as an up-stream module in multifunctional nano-fabrication devices.

In parallel, different strategies have been explored to extend the toolbox of available methods for protein attachment to DNA. Non-covalent and non-regioselective encapsulation of proteins into a DNA-scaffolded environments is currently of increasing interest as a potential aid in the structural elucidation of membrane bound proteins.[205,206,209,210] In a similar fashion, we here investigate the encapsulation of proteins within DNA cavities using low affinity ligands for distinct amino acid groups distributed on the protein surface. In this way, the protein will be immobilized in various orientations within the DNA chamber, facilitating its structural elucidation and 3D model reconstruction, as theorized before[188].

We applied some of the abovementioned strategies to three different proteins: (i) p97 ATPase (in cooperation with the group of Prof. Dr. H. Meyer, UDE), (ii) the DegP serine protease (in cooperation with the group of Prof. Dr. M. Ehrmann, UDE) and (iii) an engineered thermophilic O^6-alkylguanine-DNA alkyltransferase (OGT) from *Sulfolobus solfataricus* (in cooperation with the group of Dr. G. Perugino, University Naples, Italy).

2.1. Forced orientation of p97 inside DNA nanostructures

2.1.1. p97

The ATPase p97 is involved in several essential cellular functions, mainly in the protein quality control up-stream to the endoplasmatic reticulum associated degradation, as well as mitochondria and chromatin associated degradation (Figure 2-1 A).[211–216] p97 is a translocational motor implicated in the extraction of misfolded or ubiquitinylated proteins from protein complexes, membranes, ribozymes, or DNA, with function and substrate specificity achieved through various cofactors.

Structurally, p97 is classified as an ATPase belonging to the superfamily of the ATPase associated with diverse cellular Activities (AAA+ ATPase). More precisely p97 and its yeast homolog Cdc48 are considered proteins of the Cdc48 family of the classical AAA ATPase clade.[217,218] p97 and other proteins of this family contain two conserved AAA+ motifs in each monomer (D1 and D2 motif) as well as an regulatory N-

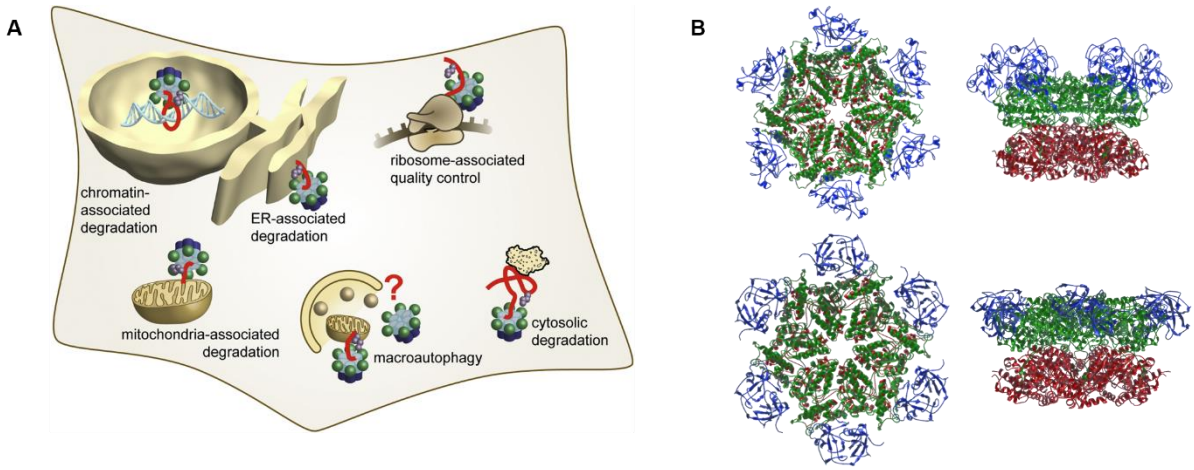

Figure 2-1: **A** Graphical presentation of p97(blue/green) involvement in several cellular processes. **B** Flipping of N-terminal domains (blue) depending on nucleotide state in D rings (top row with ATPγS, bottom row with ADP). D1 domain are depicted in green and D2 domains are shown in red (pdb files 5ftn and 5ftk). **A** was reprinted with permission from reference 216. Copyright 2021 by Elsevier.

terminal domain.[219] As native structure of p97 is a homohexameric complex, each p97 contains twelve nucleotide binding sites arranged around a central pore. Both D domains are functional as conformational changes in the complex were reported dependent for nucleotide binding state in the D1 and D2 domains. While nucleotide exchange in the D1 reflects in very drastical mechanical movements of the N-terminal domains (Figure **2-1** B),[220,221] the C-terminal D2 ATPase ring is described essential for substrate threading through the p97 inner pore and its structure-function relationship is in good agreement with other AAA ATPases.[218,222] Substrate channeling is generally described starting from the N-terminal pore entry with successive complete threading through the central protein pore. However, incomplete threading events have been also theorized in the literature. [215,223–225] Increasing structural evidence supports the view of a staircase mechanism of substrate threading within the protein pore, similar to other AAA ATPases. According to this hypothesis, each D domain would engage differently with the substrate dependent on the state of the nucleotide bound and mechanical coupling to neighboring domains.[218,226,227]

One of the functions of p97 is the regulation of protein phosphatase 1 (PP1) by the unfolding of inhibitor-3 from a complex. Generally, PP1 function is suppressed shortly after translation by the formation of a complex with Sds22 and inhibitor-3. Together with its cofactor p37, p97 unfolds inhibitor-3, releasing PP1 and consequently permitting its downstream association with other cofactors (Figure 2-2). For in vitro analysis of p97 function the unfolding of the substrate can be investigated by the usage of fluorescent proteins fused to it.[228,229]

For this purpose, a fluorescent monomeric Eos protein (mEos) is linked to the inhibitor-3 (I3) substrate molecule, resulting in a fused complex that emits in the 516 nm region (therefore commonly described as the green species). Upon irradiation with near UV light, a backbone break is introduced between the C_α and amide nitrogen of His^{62} of mEos, shifting the fluorescence emission signal to the 581 nm.[230,231] This leads to the so-called red species.. Most importantly, this "light activated" mEos species is uncapable to refold, providing a means to monitor substrate unfolding by p97 using mEos fluorescence decrease. [232]

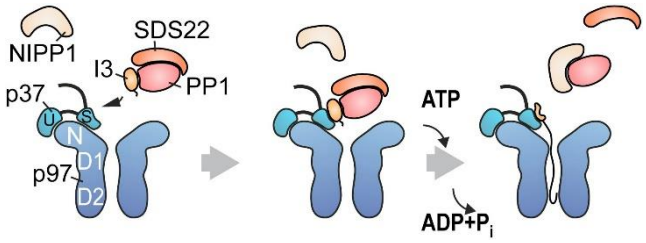

Figure 2-2: Proposed mechanism of inhibitor-3(I3) unfolding from complex with PP1 and Sds22 and successive formation of PP1 complex with substrate specifier NIPP1. Reprinted from reference 228, copyright 2021 by Elsevier

Despite recent progress in structural elucidation and biochemical investigation of substrate-bound p97 and its yeast homolog, some questions about the structure-function relation of p97 subunits remain open. Mainly the unfolding the role of the D1 domains for substrate unfolding is partially unclear to date[226,227,233]. Although full understanding of p97 working mechanism and cellular function requires further studies, we chose this protein as an interesting candidate for our purposes, as the construction of our DNA-origami/p97 complex could help in the elucidation of some aspects of the p97-mediated translocation process and may serve as a module unit for future DNA-based nanomachines.

2.1.2. Design of a semi-artificial translocation device

For making such a construct, several bottlenecks had to be tackled. Firstly, the DNA origami chamber has to have proper dimensions to hold p97 with its central pore aligned to the long axis of the chamber itself. Indeed, only a coaxial orientation of the two objects will enable the engagement of the substrate on one side of the DNA chamber and its extrusion on the other side. Assuming one attachment site per monomer, the design of the DNA chamber must allow for a radial distribution of attachment points around the internalized protein. Furthermore, the design should also allow for outer modifications of the DNA shell in order to potentially transfer it into other media or immobilize the construct on a surface. Hence, a rather bulky DNA origami structure around the p97 is required.

An important point to consider is the functionality of the encapsulated protein, which of course should be preserved. Until now, only a handful of enzymes were described to maintain their full functionality once entrapped inside DNA origami constructs; therefore, the first issue to face was to verify whether encapsulation would be disadvantageous or even fatal for the p97 protein. Finally, the orientation of p97 inside the DNA origami has to be described and controlled. This would allow development of more advanced nanostructures, where the directionality of the overall process is caused by the unfolding through p97.

2.2. Usage of thermophilic proteins

Thermophilic proteins have a multitude of desirable properties that make them especially interesting for biotechnological uses such as high chemical and physical stability, fast and simple purification methods and high performance at elevated temperatures[234,235]. To my knowledge, they have not yet been investigated as single enzymes or enzyme cascades arranged onto DNA-origami scaffolds.

To combine DNA with thermophilic proteins is theoretical very similar to mesophilic proteins. As a model system, we used protein tags for binding to the DNA origami surface. A few years ago, the group of Perugino developed a thermophilic protein tag derived from the archaeal thermostable alkylguanine-DNA-alkyl-transferase (OGT) expressed in the *Sulfolobus solfataricus* (H^5*Ss*OGT)[236–238]. In a cooperation with this group, we investigated the feasibility of the usage of these tags on DNA origamis as a proof of concept for future encapsulation of thermophilic proteins.

2.3. Random orientation of proteins within DNA nanocavities

Non-covalent and non-regioselective encapsulation of proteins into DNA origami cavities might be very interesting for structural purposes. Indeed, in those systems, proteins will be encapsulated in various orientations within the DNA cavities, leading to an ensemble of all possible two-dimensional projections of the protein on a plane. Linking multiple DNA-origami cavities into extended lattices would enable sampling of several protein orientations simultaneously. Such lattices could be then automatically screened by transmission electron microscopy (TEM) for structural elucidation of the protein. While lattice formation was already described for various DNA origami designs, the general feasibility of this encapsulation technique was not shown until now.

Basically, protein encapsulation could be driven by any type of small molecule that shows a binding affinity to the protein of interest. Limitations arise as soon as ligands must be chemically linked to DNA. Additionally, they should not have considerable DNA binding capacities to avoid self-binding of ligand modified oligonucleotides. For initial proof of concept of this encapsulation method, a molecular tweezer (CLR01) motif was used. This molecule binds preferably to lysin and arginine residues.[239,240] DNA-origami cavities modified with molecular tweezers were used to encapsulate various types of proteins, namely the serine protease DegP in its hexameric form and p97.[204]

Molecular tweezers show a K_D in the μM range for various proteins[241–243], while DNA origami structures are usually obtained in the low nM range. Therefore, it was concluded that the inner surface of the origami chamber needed to be modified with a high number of ligands to ensure sufficient binding affinity as a consequence of a high local concentration of interacting species and, possibly, multivalent cooperative binding. Of course, DNA origami cavities should minimize binding issues derived from steric hindrance.

2.4. Design of adequate DNA origamis

The design requirements highlighted above led to the conclusion to build hollow DNA-origami prisms. This would allow proteins to enter the DNA chamber, while providing substantial shielding. Inner decoration of the origami structure can be easily achieved by extension of selected staple strands at the nucleobases that point within the inner space of the cavity.

Generally, oligonucleotides with attached molecules of interest can be introduced to an DNA origami structure binding either to the scaffold ssDNA stretch or to a staple strand protrusion. When ligand-modified oligonucleotides are designed such to be partially complementary to the staple strand protrusions, toehold strand displacement reactions can be performed. That enables later release of the DNA-tagged ligands and removal of the specific binding interactions between the protein of interest and the inner surface of the origami prisms. This could be useful to understand the effect of DNA encapsulation on a particular protein property when compared to the same situation in bulk conditions. Hence, in our constructs, the design of the protruding arms was always performed to allow a strand displacement reaction.

3. Methods

Details of the chemicals, oligonucleotides, buffers and equipment used in this work can be found in section Appendix I p.98 and following.

3.1. DNA conjugations

Conjugation of primary NH_2-residues via N-Hydroxysuccinimide-esters(NHS): NH_2-modified oligonucleotides were precipitated by addition of the same volume 3 M $NaCH_3COO$ and eight volumes isopropanol. The suspension was mixed and then centrifuged for 30 min at 21,000 rcf at 4°C. The precipitate was washed in 100% ethanol three times, dried and re-dissolved in phosphate buffered saline (PBS) pH 7.6. The NHS modified substance was added in five- to tenfold excess and the reaction was incubated at 21°C for at least two hours. The obtained sample was further purified either by precipitation with 5 M NH_4CH_3COO, as described above, exchanging phosphate buffer with water through at least five ultrafiltration steps in 3 kDa molecular weight cut-off (MWCO) filters or by extraction from denaturating polyacrylamide gel electrophoresis (PAGE) as described in section 3.2.

Copper(I)-catalyzed azide-alkyne cycloaddition (CuAAC) based conjugation: Azide modified oligonucleotides at 100 µM concentration were incubated with two to five-fold (tweezer) or tenfold (dodecyne) excess of alkyne modified ligand, 50 µM tris(benzyltriazolylmethyl)amine (TBTA), 1 mM $CuSO_4$ and 16 mM sodium ascorbate at 60°C for 2 h.

Conjugation of thiol-moieties with maleimide: Disulfide-protected oligonucleotides were reduced with 100-fold excess of tris(2-carboxyethyl)phosphine (TCEP) for one hour at room temperature. Excess TCEP was removed by elution over NAP™5 and successively over NAP™10 columns in PBS pH 6.5. Oligonucleotide solutions were concentrated over 3 kDa MWCO filters and then incubated with 25-fold excess of maleimide modified ligand.

Thioether formation for DNA oligonucleotide decoration of gold nanoparticles (AuNP): AuNP (diameter 10 nm) stabilized in polysorbate 20 or cetrimonium bromide were provided by Michael Erkelenz from the group of Prof. Dr. Sebastian Schlücker (UDE). The AuNP solution was treated with 0.1% sodium dodecyl sulfate (SDS) to exchange the positively charged stabilization agents. Disulfide modified oligonucleotides were reduced by incubation with 50 equivalents TCEP for one hour at room temperature. Thiol-oligonucleotides were then washed three times over 3 kDa MWCO filters with MilliQ water. Oligonucleotides were added in 1,000-fold excess over gold nanoparticles and the sodium concentration was increased in 50 mM steps each 15 min of incubation up to a total concentration of 250 mM. Final incubation was performed overnight at room temperature. Obtained particles were washed over 100 kDa MWCO filter devices and their concentration measured by optical density at 400 nm.

Phosphate hydrazide conjugation: This conjugation was performed through activation by 1-ethyl-3(3-dimethylaminopropyl)carbodiimide hydrochloride (EDC) and imidazole. For this 2 mg EDC were weighed; subsequently, 15 µl of a 100 µM solution of 5´phospho modified oligonucleotide, 2.5 µl imidazole pH 6 at 1 M concentration and 7.5 µl of a 20 mM hydrazide-modified ligand were added. The solution was mixed and let sit for two hours at room temperature. The oligonucleotide was then precipitated in isopropanol and NH_4CH_3COO and successively washed in 100% ethanol as described above.

3.2. Gel electrophoresis

Agarose gel electrophoresis (AGE): Agarose gels were prepared using either 0.75% agarose in TBEMg buffer for the 6p120 prism or 1% agarose in TBEMg11 buffer for all other purposes. Agarose was weighed and suspended in the respective buffer, cooked, cooled to 50°C and then casted in a gel sledge and let harden. Running buffer was added and the DNA samples were applied to the gel pockets upon mixing the sample solution with an agarose loading dye. Gels were run at 80 V for at least 1.5 h, keeping them cool through immersion of the gel chamber into a water ice bath. After running, fluorescently-labelled samples were visualized by scanning the gel with a Typhoon FLA9000 prior staining the gel with ethidium bromide (Etbr) or Sybr green I. Stained gels were scanned with Typhoon FLA9000 as well.

Native AGE: Agarose concentration was 2% and the ice-bath cooled gel was run at 100 V for at least 1 h. Native AGE buffer and loading dye were used.

Extraction from AGE: Tetramethylrhodamine (TAMRA) labelled or Etbr stained DNA origami bands were illuminated by ultraviolet (UV) light using an Intas gel documentation system, excised with a clean razor and applied to commercially available Freeze´n´Squeeze DNA gel extraction spin columns. Gel pieces were squashed on the column and then spun at 16,000 rcf for 5 min, as reported elsewhere.[152]

Denaturing DNA PAGE: DNA oligonucleotides were isolated and extracted by this method either for analysis or further processing. Depending on the oligonucleotide length, 15%-25% (m/v) acrylamide in denaturating DNA PAGE buffer was polymerized by addition of 0.07% (w/v) ammonia persulfate (APS) in the presence of 0.07% (v/v) tetramethylethylenediamine (TEMED). Gels were pre-equilibrated for 30 minutes at 180-220 V, depending on the percentage of acrylamide. Gel pockets were carefully washed to eliminate traces of urea and samples mixed with den. PAGE loading buffer were finally applied. For analysis purposes, 2 µl of 10 µM oligonucleotides solutions or 2 µl of 1 µM fluorescently-labelled oligonucleotides were applied per pocket. For preparative gels, at least 100 µl of a 50 µM oligonucleotide solution was applied per gel. Gels were run at 180-220 V for 45 min in TBE buffer. Analytical gels were either scanned to monitor fluorescence and/or stained with SYBR Gold and then scanned by Typhoon FLA9000. Preparative gels were illuminated by UV light (230 nm) on a thin layer chromatography plate to identify and finally excise the desired band.

Extraction from den. PAGE: Preparative gel bands were cut out and squashed in a falcon tube. Gel pieces were suspended in 5 ml MilliQ water or TEMg buffer and the DNA sample was eluted at room temperature overnight or longer using a rotary device. The solution was then carefully transferred to a second tube. Water volume was decreased by repeated addition of n-butanol, upon shaking, spinning and discarding the upper phase. Volume reduction was alternatively performed by concentrating the solution over 3 kDa MWCO cutoff-filters. When only approximately 100 µl solution was left, the oligonucleotide was precipitated in 0.15 M $NaCH_3COO$ and 80% isopropanol and successively washed with 100% ethanol. Samples were finally dried and resuspended in MilliQ water.

SDS-PAGE: Depending on the protein size investigated 8-12% acrylamide was polymerized in the buffer used for the lower (separating) gel using APS and TEMED as described for the denaturating DNA PAGE. Casted lower gel was covered with a few drops isopropanol to avoid air bubbles and let harden. The isopropanol was discarded and the upper (stacking) gel was casted on top of the lower gel. The stacking gel typically contained 4% acrylamide polymerized as usual. Samples were heated at 95°C in an SDS-containing loading dye for 10 min and shortly cooled to room temperature before applying them to the gel. For protein size estimation, a protein broad range or low range ladder was applied in one gel pocket. Gels were in SDS running buffer at 140-180 V for at least 1 h. If necessary, fluorescently-labelled samples were initially monitored by scanning the gel with a Typhoon FLA9000 under illumination at a desired wavelength. Gels were stained with Coomassie R by firstly gently washing off SDS-PAGE running buffer and successive cooking the gel in a Coomassie staining solution for one minute in a microwave oven. The gel was then let cool for at least 30 min in the staining solution. Destaining was performed by rinsing the gel with water, performing two successive soaking in 10% acetic acid in a microwave oven and discarding the solution. Finally, the gel was photographed.

Native PAGE: Native PAGE was performed as described for the SDS-PAGE with upper and lower gels in their respective buffers. The lower gel contained 4% (w/v) acrylamide, the upper gel contained 2% (w/v) acrylamide. Samples were mixed with a native PAGE loading dye and the gel was run in native PAGE buffer at 90 V for 3 h while cooled in an ice bath. Gels were stained and investigated as described above for the SDS-PAGE.

3.3. High resolution microscopy

Atomic force microscopy (AFM): For imaging in air, 5 µl of sample was applied to freshly cleaved mica and let sit for 3 min. Then the mica was rinsed with a few drops of water and dried with a gentle air flow. For measurement in liquid, 5 µl of the sample was applied and incubated on the mica for 3 min as well. It was then mounted in the AFM sample holder. The liquid handling cell was added and brought close to the sample. Then the cell was flooded with 40 µl buffer and laser alignment was performed. For both kinds of measurements, the ScanAsyst mode was used.

Negative stain transmission electron microscopy (TEM): DNA origami samples used for TEM imaging had a maximum concentration of 10 nM while protein solutions were up to 200 nM in concentration. Formvar/coal coated copper grids were glow discharged at 10 mA for 30 s. 3-5 µl sample were applied and incubated for 2 minutes. For origami samples the liquid was dried off with a filter paper and 5 µl of a 1% uranyl formate staining solution was added and quickly dried in the same way. Then 5 µl staining solution was added, let soak for 2 min and finally dried with a filter paper.

For protein investigation, the sample was incubated for 2 min on the grid and dried off with a filter paper. Then the grid was washed two times with 5 µl water and two times with staining solution before applying 5 µl staining solution for 2 min.

Grids were further dried in air for a few minutes prior to investigation with TEM. TEM imaging was performed at the imaging center Essen using a JEOL JEM 1400Plus equipped with a 120 kV beam from a LaB_6 or tungsten filament. Images were manually obtained near the Scherzer defocus (highest contrast near the focus).

The structures of interest were counted in TEM images using the cell counter plugin for the software FiJi. Data were interpreted by resampling the images to obtain around 200 structures per subset. Standard deviation and average were derived from these subsets. Alternatively, if the total sample size was <300 structures, image to image variance was calculated. Both resampling techniques were done to estimate to what extent the TEM sample was representative of the bulk sample.

TEM class averages: Class-averages were obtained by using Eman2. Images were imported and their Contrast transfer function (CTF) checked for absence of drift or stigmatism. Contrast was set at 60-80 and Å/pix resolution was adjusted, depending on the image used. A spherical aberration of 3.4 was set as provided by the instrument vendor. CTF were fitted as recommended for negative stain TEM. Particles were picked manually. Particle sets low-pass filtered for 20 Å were used to obtain 2D class-averages.

3.4. DNA origami production

Scaffold production: 25 µl of chemical competent *Escherichia coli* were thawed and transfected with 5 µl of a 100 µM desired scaffold sequence via heat shock at 42°C for 30s and recovered in 1 ml NZ-amine (NZA) medium. 200 µl of this solution were plated on NZA medium agar plates containing 28 µM tetracycline and were incubated overnight at 37°C. Simultaneously, 200 ml overnight culture of *E. coli* XL-1 Blue were grown in NZA medium while shake incubated at 180 rpm at 37°C. The next day, 3 l of prewarmed 2xYT medium were inoculated with 75 ml of the overnight culture and its optical density at 400 nm (OD_{400}) was monitored. When an OD_{400} of 0.3 was reached, plaques containing transfected cells were scratched from the agar plate and injected into the growing *E. coli* culture. *E. coli* cells were allowed to grow further well vented at 37°C and 180 rpm for 4 h. The cell suspension was centrifuged at 4,000 rcf at 4°C for 15 min. The supernatant was mixed to 40 g/l PEG8000 and 30 g/l NaCl. The mixture was mixed for 45 min while cooled by ice. Precipitated phages were pelleted by centrifugation at 4,000 rcf at 4°C for 15 min. The supernatant was discarded. Pellets were suspended in 10 ml of a 10 mM Tris pH 8.5 buffer solution. Residual *E. coli* cells

were pelleted by centrifugation at 20,000 rcf at 4°C for 15 min. The clear supernatant was frozen at -20°C and further processed the next day. Thawed phages were lysed by addition of two volumes of lysis buffer and gentle inversion. 1.5 volumes of neutralization buffer were added, and the sample was incubated in ice for 15 min. The suspension was centrifuged at 16,000 rcf at 4°C for 10 min and the precipitate discarded. The scaffold was precipitated in 50% ethanol with successive centrifugation at 16,000 rcf at 4°C for 15 min, further washing in 1.5 ml 75% ethanol and repeated centrifugation. The pellet was dried and then resuspended in 10 mM Tris pH 8.5. AGE was used to check for absence of bacterial genomic DNA. The sample was fully sequenced for possible mutations with primers P1-18 (see Table 0-48 page 130).

DNA origami self-assembly: Assembly was performed using 5 or 10 nM scaffold strand with five- or ten-equimolar amount of each staple strand according to a thermal annealing and cooling ramp as described in the results (section 4.1 and 4.3). The strands complementary to the protrusion arms of the origami were used in 1.5-fold excess to ensure binding. The thermal ramp was performed in a thermocycler with lid temperature slightly above (10 K) the highest assembly temperature. The assembly volume per reaction tube was never higher than 100 µl.

Polyethylenglycol (PEG) assisted purification: To purify DNA origami structures from excess staple strands, the assembled samples were mixed 1:1 with PEG precipitation buffer and inverted a few times. Samples were centrifuged at 16,000 rcf for 25 min and the supernatant was discarded. The DNA origami pellets were redissolved in the buffer of choice over several hours at room temperature.[244]

Purification with cut-off filter: Beside agarose gel excision and PEG precipitation, DNA origamis were purified from excess staple strands by ultrafiltration, using 100 kDa or 50 kDa MWCO centrifugal devices. Samples were washed for six or seven times, depending on the initial staple excess over the scaffold. Centrifugation was performed at around 8,000 rcf as higher forces are reported to reduce sample recovery.[152] This technique was also used to simultaneously exchange the buffer of the sample.

3.5. Protein conjugation

Proteins: $DegP_6$ was provided as inactive variant (serine/alanine exchange) by Pierre Stegemann (our group) and produced/purified with equipment from the group of Prof. Dr. Ehrmann (UDE). DegP was expressed in *Escherichia coli* and purified by affinity chromatography via His_6 tags and further purified by size exclusion chromatography (SEC). p97 constructs, p37 constructs and the complex of suppressor of Dis2 mutant 2 (Sds22), protein phosphatase 1 (PP1) and mEos-I3 (IE) and Ubiquitin fusion degradation protein 1 (Ufd1) and nuclear protein localization 4 (Npl4) were produced and purified by Dr. Johannes van den Boom and Dr. Matthias Kracht (Group of Prof. Dr. Meyer, UDE). Human p97 constructs were expressed with a His_6 tag and purified by affinity chromatography and size exclusion chromatography. Human p37 were expressed in *E. coli* with a N-terminal GST-tag. The protein was purified by GST-tag affinity chromatography with subsequent GST-tag removal and further purified by SEC. The complex of Sds22, PP1 and His_6-IE (SPIE) was expressed in insect cells and purified via affinity chromatography, ion exchange chromatography and SEC. Ufd1 and Npl4 were expressed in *E. coli* with GST and His_6 tag and purified by GST-tag affinity chromatography and SEC. The peptide N-glycanase and UBA or UBX-containing proteins (PUB domain) was produced during a lab exchange period, together with Mike Blüggel (group of Prof. Dr. Bayer, UDE). PUB was expressed in *E. coli* with a His_6 tag and further purified by His_6-tag affinity chromatography and SEC.

Conjugation via maleimides: Cysteine/maleimide conjugation was used either for labelling purposes (e.g. attaching a fluorescent dye to the p97) or to modify proteins with DNA (e.g. linking a maleimide-modified DNA strand to a single cysteine residue of the PUB domain). For the former type of application, 20-fold excess of maleimide fluorophore was added to the protein solution and let react for 30 min at 0°C. The excess of unbound fluorophore was removed using the provided dye removal columns and the success of the conjugation was checked by SDS-PAGE. For DNA attachment to the PUB domain, two equimolar amounts of protein were used and incubated overnight at 4°C. Samples were further purified by size-exclusion chromatography and conjugation was verified by SDS-PAGE.

Conjugation via self-labelling tag proteins: Expressed and purified Snap or Halotagged fused proteins were incubated with fivefold excess of oligonucleotides bearing the respective ligand (benyzlguanine or chloroalkane) at 8°C overnight. Conjugation of DNA to Snaptag-p37, p97-Halotag and Snaptag-p97-Halotag was carried out in p97 storage buffer, while DNA conjugation to H^5SsOGT was performed at 50°C for one hour in FluoReaction buffer. The reaction mixtures were then purified by size exclusion chromatography (SEC) and ultrafiltrated over size respective MWCO filter devices in the case of the p97 and p37 constructs. Successful conjugation was verified by SDS-PAGE. Further treatment of H^5SsOGT is described in section 4.3.

3.6. Other methods

SEC of protein-DNA conjugates and DNA origami: SEC was performed using the equipment available in the laboratory of our cooperation partners. A Superose 6 10/300 column was used to purify p97 constructs and DNA origami. For purification of the Snaptag-p37 DNA-conjugate, a Superdex 200 10/300

column was employed, whereas for purification of the DNA-PUB conjugate a Superdex 75 pg 16/60 was chosen. All SEC columns were initially equilibrated in the target buffer and then the sample was eluted at isocratic flow slightly below the critical pressure. Generally, samples were eluted in 500 µl fractions. Aliquots were tested either for fluorescence or presence of protein/origami by SDS-PAGE, AGE or by applying droplets on Typhoon FLA9000 stage. Fractions of interest were pooled and concentrated over ultrafiltration centrifugal devices with appropriate cut-off. DNA origami purification with SEC was performed with at least 100 µl 20 nM of DNA origami.

Pulldown by magnetic beads: 35 µl of a streptavidin-coated magnetic bead solution were shortly spun and the particles were washed with 400 µl TEN100 buffer four times before incubation with 0.5 nmol bt-T10-cF9(22) at 8°C overnight. Excess DNA was removed by washing three times with 400 µl p97 storage buffer. The beads were incubated with 20 µl of the DNA origami sample containing F9-modified p97H for at least 2 h at 8°C to pull-down the excess of modified protein.

Pulldown by BG-modified agarose beads: 200 µl BG-modified agarose beads were spun down and subsequently washed with 200 µl FluoReaction buffer. 100 µl of 80 µM H^{5}*SS*OGT partially conjugated with F9(16) were added to the 40 µl resin and incubated at 4°C overnight in a roll shaker. In this way, the unmodified protein remained bound to the beads and the DNA-modified species could be recovered.

Dynamic light scattering (DLS): This technique was used to monitor the time-dependent change of the hydrodynamic diameter of DNA origami structures. For this purpose, 10 nM of an origami solution was measured and the parameters were optimized. Refractive index for the buffer was obtained with Zeta Analyzer Software built-in calculator. Attenuator 11 was chosen to keep the particle count approximately constants. For kinetic measurements, one data point consisted of four measurements, with each measurement about one minute long. Derived volume peak was monitored.

Matrix-assisted laser desorption/ionization (MALDI): Mass/charge values for oligonucleotides were obtained to verify the extent of conjugation with ligands and oligonucleotide purity. Oligonucleotides at 10-100 µM were mixed 1:1 with matrix. 1 µl thereof was placed on the MALDI stage and let dry. Three to four different oligonucleotides spanning the mass range of interest were used as mass standard and placed on the stage in a similar fashion. Laser power, spot size and frequency were adjusted to allow detection of the heaviest oligonucleotide of the standard with good signal to noise ratio. The mass spectra were gauged and samples measured. Obtained sum spectra were baseline subtracted and exported.

DNA concentration estimation: The concentration of the oligonucleotides was measured by recording the absorption at 260 nm using a DS11 spectrophotometer. The signal from the buffer was subtracted and the concentration was calculated via the extinction factor provided by the vendor. DNA origami concentration was estimated by calculating the mass concentration. Averaged extinction coefficient for DNA of 0.02 ml/µg was used.[245,246] The DNA origami mass was estimated to be approximately twice the mass of the scaffold strand, which is 2.24 MDa for p7249 and 2.33 MDa for p7560 according to the vendor tilibit nanosystems. Estimated molar extinction coefficients would hence be around $8.96 \cdot 10^{6} cm^{-1} \cdot M^{-1}$ and

$9.32 \cdot 10^6 cm^{-1} \cdot M^{-1}$ for p7249 and p7560 based origami, respectively. For a DNA origami loaded with 54 cF9/F9(16) duplexes, the theoretical mass of 4.48 MDa was estimated to be increased by $2 \cdot 54 \cdot 0.0049$ MDa or 0.53 MDa.

Protein concentration estimation: Depending on the protein (PUB or p97), the Bradford assay or the tryptophane absorption were used to estimate protein concentration (performed by our collaboration partners). In this work, the concentration of p97-conjugates was estimated by Coomassie stained SDS-PAGE, using different concentrations of an unconjugated p97 applied to the same gel as a reference standard curve.

Unfolding assay for p97: Unfolding of 35 nM Sds22/PP1/Inhibitor3-mEos (SPIE) substrate complex was carried out in p97 unfolding buffer at 37°C in presence of 500 nM p37 and using a 384 well plate with a final volume of 35 µl per sample. The fluorescence decrease was monitored by a Tecan Spark 10 M at 540/580 nm through the transparent flat bottom of the plate. SPIE substrate complex, p37 and buffer were prepared in a master mix prior to each experiment and aliquoted for technical replica. p97 or DNA constructs were added at a concentration of 1 nM, if not stated differently. Samples were equilibrated for 20 min at 37°C and their fluorescence monitored. Prewarmed E-Mix (ATP and creatine phosphate based enzymatic recycling system) was quickly added and the sample was mixed by pipetting. The unfolding process was monitored collecting one data point per minute for approximately five hours. and the fluorescence values relative to the equilibration phase were considered for analysis.

4. Results

4.1. Development of DNA origami structures for encapsulation

Hollow DNA origami structures with a hexagonal cross section (herein referred to as hexaprisms) were chosen as suitable structures for our purposes. Not only the design of such structures is quite feasible, but their nearly tubular shape well adapts to the C6 or spheroidal geometry of the target protein cargos. The DNA helices of the origami sheets were chosen to run parallel to the central axis of the prism that passes through its interior. In this way, the angles between adjacent sheets can be adjusted via staple crossover sites, rather than imposing helical bending.[137]

4.1.1. Simplification and extension of monolayered hexaprism

For the encapsulation of DegP multimers via peptidic linkers, a monolayered hexaprism DNA origami (called 6p120) was used in a former study.[204] The structure consists of six monolayer sheets of DNA helices, four of them approximately 23 nm x 49 nm and two opposing sheets 23 nm x 56 nm in size (Figure 4-1 A). Staple cross-overs were designed at the edges of adjacent sheets to impose a 120° relative orientation between them (Figure 4-1 B). Up to 18 positions, radially distributed around the central cavity of the origami, were chosen for elongation and encapsulation purposes (shown in Figure 4-1 A). DNA origami edges (located in the front and back of the prism) were passivated using thymine loops consisting of five bases. The design was not twist corrected. This origami could quickly be assembled by heating to 95°C for 10 min and cooling down with a rate of -1°C/min.

This DNA origami was designed with the help of the SARSE software (no more available in the web) and only partially converted into Cadnano2 for graphical representation of the structure. To allow for protein encapsulation via low affinity binders, more modification sites were introduced reaching a total number of 54 possible anchoring sites (Figure 4-1 C) (6p120_54cF9). Two different lengths of protruding handles were

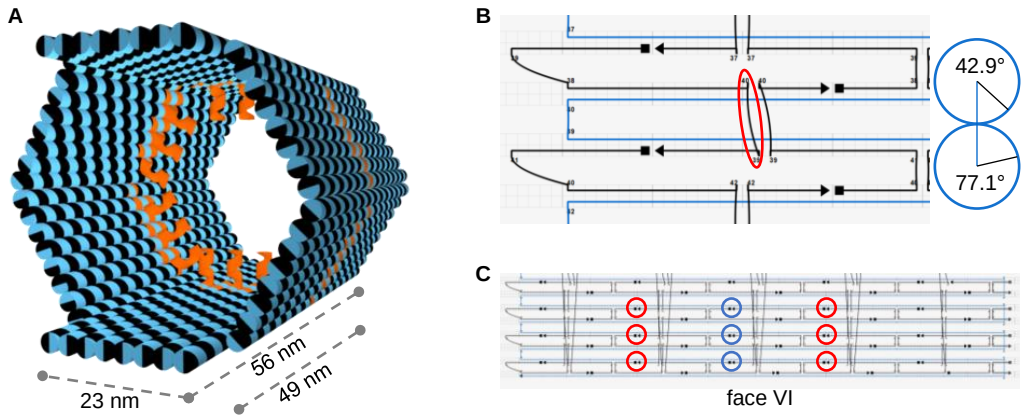

Figure 4-1: **A** The monolayered hexaprism origami 6p120 and its dimensions as published before. 18 protruding arms in the inner ring are shown in orange. **B** The hinge region of 6p120 in the cadnano depiction is shown. Scaffold depicted in blue and staples in black. The angles at the red marked crossover position will result in a total angle of 120° in the hinge region as shown right. **C** Additional sites for protruding arms for the 6p120_54cF9 construct were introduced. One of the six faces of the prism with original PA positions (blue) and newly introduced PA positions (red) are shown here in the cadnano representation.

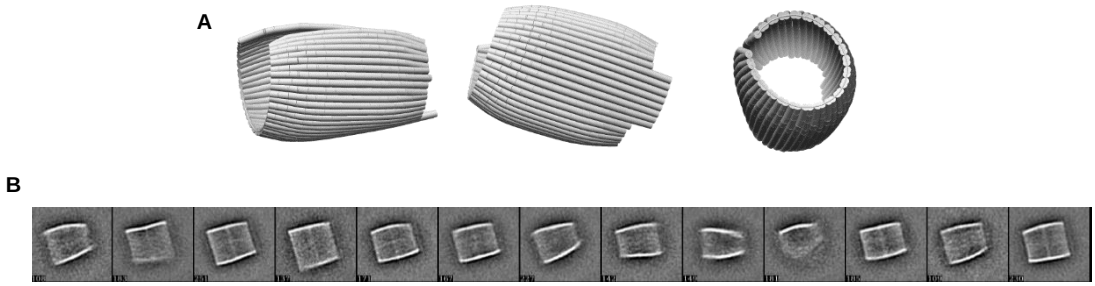

Figure 4-2: **A** Cando output for the 6p120 construct when one scaffold crossover in the hinge between face I and VI is deleted. **B** Class averages from 6p120_18cF9 published in the thesis of Andreas Sprengel (reprinted from reference 247) were in good agreement with the Cando output and indicate a rather flexible construct.

designed, consisting of either 22 or 32 nucleotides, thus enabling the placement ligands at various distances from the origami walls. Such handles will be here named as cF9(22) and cF9(32), respectively (consistently to already published results from our group). The strand F9(16) is partially complementary to the cF9(22) and cF9(32) and hybridizes to the last 16 bases of the handles near to their 3' terminus. The F9(16) sequences are used to place molecules inside the origami. This leaves a 5´ toehold on the protruding handles, which is at least 6 bases-long and can be advantageously employed for later release of the inner decorations. The resulting staples strands were newly sorted, allowing for an easy and quick pipetting. The full design can be found in appendix section II.a, p.134. Type and number of protrusions were included in the nomenclature of the origami structure. Thus, for example, the 6p120_18cF9 describes a hexagonal prism DNA origami structure with 18 protrusions of cF9(22) sequence.

It was found that when deleting the scaffold crossover between sheet VI and sheet I *in silico*, made it possible to successfully model the shape with the online software tool CanDo. The found very flexible and tube-like structure is fitting negative stain TEM images of the structure obtained during the thesis of Andreas Sprengel (Figure 4-2.)[247]. While also fitting well to the flexibility of two-dimensional DNA origami sheets and the internal twist between the helices[248], the obtained model was not able explain the two classes of orientation found in AFM that were published.

4.1.2. Shape self-complementary half-prism in honeycomb lattice

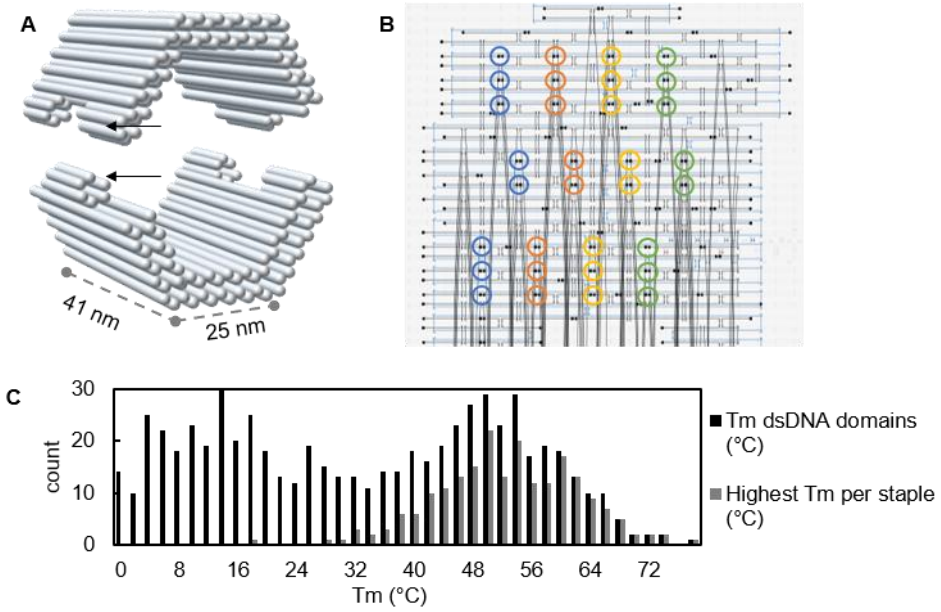

Figure 4-3: **A** A three-dimensional model of two identical half-prisms with fitting six helix protrusions and recessions(arrows) and its dimensions. **B** 32 protrusion positions per half-prism were distributed in four rings: left (blue), middle left (orange), middle right (yellow) and right (green). **C** Scaffold start positions were checked for monodisperse distribution of melting temperature using DNAanalyzer_app. Results of the used design shown here.

To overcome the flexibility of the 6p120 prism a second prism was designed to be structurally more rigid, maintaining approximatively the same dimensions (Figure 4-3 A). Higher rigidity was achieved using two instead of one single layer of DNA helices. As a consequence, two DNA origami structures had to be designed such to be assembled together in a final prism, which is 41 nm deep, has a total height of 53 nm and an inner radius of 15 nm. Each half prism displays a short six-helix bundle extrusion on one edge and a shape complementary intruding site on the other edge. This results in the homodimerization of the half-prism by blunt end stacking between its shape complementary features, giving rise to a full hexaprism. Hence, the design was termed Narcissus after the mythological man damned to love himself[249] and abbreviated with the letter 'N'. Staples were designed to have at least 14 bp continuous dsDNA regions and deviations from this rule are found only in the edge regions of the origami. All staples ending or starting at an outer helix were designed with their 5´ or 3´ends pointing outside the origami, to allow outer modifications of the structure.

To modify the inner side of the prism, 32 positions were chosen per half-prism, however they were not equally distributed per prism side. While two sides contained each twelve sites, one side of the prism displayed only eight handles. A full prism displayed then a total of 64 possible attachment points for staple strand elongations, organized into four layers, or rings, each one containing 16 attachment points. The location of these rings along the full prism finally dictates the position of the encapsulated cargo within the prism. The four rings were termed as left, middle left, middle right and right (and indicated as l, ml, mr and r, respectively) (Figure 4-3 B), where the left and right side of the origami structure refers to the design map provided as default by the caDNAno software tool. For all rings, the staple strand elongation (or protruding handle) was the 22 nucleotide long sequence, called cF9(22). Ligand attachment was performed by binding

the single-stranded protrusions via the partially complementary 16 nt-long oligonucleotide F9(16), leaving again six bases between the origami surface and the so-formed duplex. Also in this case, addition of the fully complementary F9(22) was then used for ligand release from the DNA prism.

Passivation of the DNA origami edges was achieved by a combination of four base scaffold and T4 overhangs. Edge staples binding to <10 bases-long scaffold domains were left out for passivation.

3D printing of the model revealed steric hinderance of dimer formation and the helices in the protrusion/recession regions of the N half prism were adjusted accordingly. Note that the designed stacking interaction would result in a homo-dimer with 5´ to 5´ and 3´ to 3´ orientation of the blunt ends. Finally, the DNAanalyzer_app tool was used to analyze the staples pools of various virtual scaffold starts. The search was terminated when a monodisperse melting temperature was found for the most-stable dsDNA domains. A good result was found for scaffold break position [8]126 in the Cadnano file (Figure 4-3 C).

Staple sequences were finally generated and sorted in sets as shown in Table 4-1. Suffixes were used to indicate the number, ring position and type of protrusions (P). For example, P_{3mlcF9} stays for three cF9 protrusions in the ml ring whereas P_0 indicate the absence of any protrusions. Later also other suffixes were introduced for the edge staple sets. throughout this work, the term 'left' and 'right' always refers to the left and right of the DNA origami structure as indicated by default in the Cadnano design file.

Table 4-1: Narcissus staple set nomenclature

Staple set	Acronym	Description
Protruding arms	P	Staples that can be 3´ modified with e.g. cF9 leading to an inner decoration of the prism
Left edge	L	All staples that end or start at the left origami edge
Right edge	R	All staples that end or start at the right origami edge
stack	stack	Staples responsible for the stacking interaction between the six-helix protrusion/recession
Core	cs	All other staples

A thermal ramp was developed in which the solution was cooled down slowly with intermediate longer steps around the melting temperature of the most-stable dsDNA domains in staples, especially 64°C, 54°C and 50°C. This was done to avoid the formation of kinetic traps (Figure 4-4 A).

N with cs and P_0 staple sets were assembled at various magnesium concentrations and analyzed by 1% AGE. Mainly monomeric bands were found for the origami over the range of 4-24 mM. Clustering appeared at higher Mg^{2+} concentrations. EtBr fluorescence was highest for the bands at 16 and 20 mM magnesium concentrations, indicating high yield formation of dsDNA (Figure 4-4 B). As higher Mg^{2+} concentrations might increase the self-dimerization yield, TEMg20 was used as folding buffer. Structures were purified by FnS and investigated by AFM. The six helix-bundle protrusions of the N half-prism were visible in most structures. The electrostatic interaction between the mica surface and the DNA origami structure was strong enough to flatten-out the hinge regions, hence observable half-prisms had a total length of approx. 65 nm, corresponding to the three sides of the prism with 22 nm length each. Their width was 40 nm and their

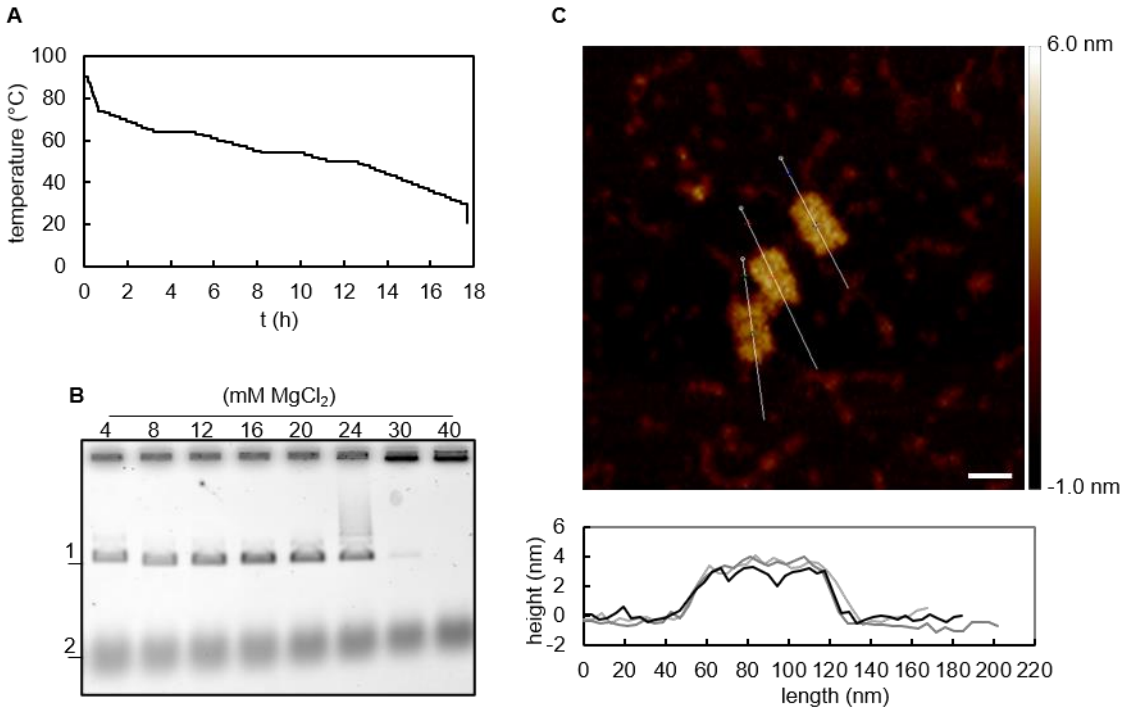

Figure 4-4: **A** Thermal ramp program that was developed with long incubation times around estimated melting temperatures of most stable dsDNA segments, especially at 64°C, 54°C and 50°C. **B** Assembly screened by AGE for optimal Mg^{2+} concentration. Bands for origami (1) and staples (2) can clearly been seen. **C** Successful formation of half-prisms were confirmed by ScanAsyst AFM scans in air. Scale bar is 50 nm. Half-prisms were only found collapsed on the mica. Height profiles (bottom) along the depicted lines in the image show a plateau around 4 nm height corresponding to two dsDNA helices.

height was evenly about 4 nm corresponding to two layers of dsDNA (Figure 4-4 C). Side views of Narcissus were not obtained by AFM as only structures with a high contact area to the mica are sufficiently stable for AFM imaging.

The Narcissus half-prism was then assembled with added L and R edge staple sets and analyzed by 1% AGE, revealing that this initial design of the edge staples (set 1) was insufficient to suppress unspecific dimer and multimer formations. Two new sets of edge staples were designed by either leaving four bases of the scaffold as overhangs (set 2) or extending the edge staples by six thymine residues (set 3) (Figure 4-5 A). The first alternative, edge staple set 2, resulted in even stronger dimerization and multimerization, while the latter (set 3) led to clear monomeric bands with only weak signal for unspecific dimers and was further used for edge passivation and termed L_{6T} and R_{6T} respectively (Figure 4-5 B).

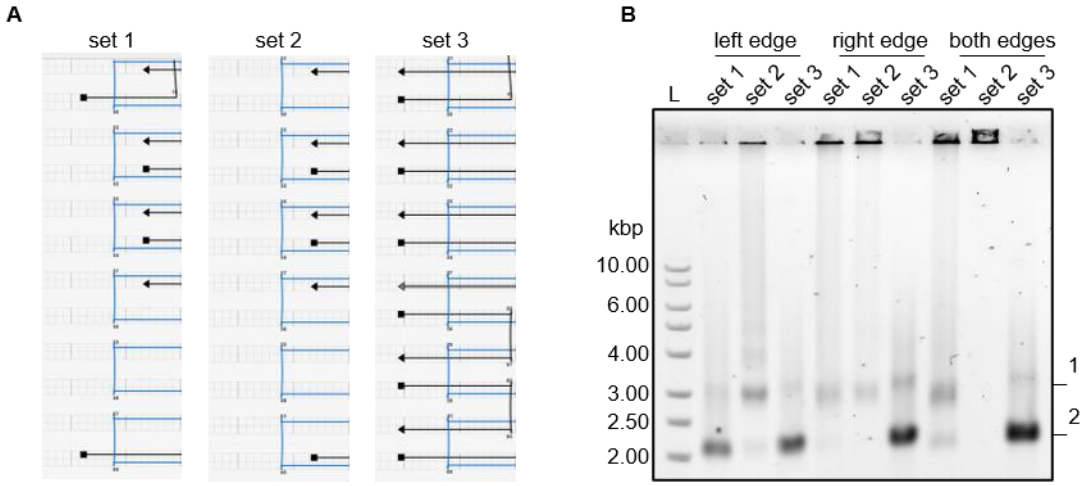

Figure 4-5: **A** Three edge staple sets were tested. Set 1 with a combination of passivation with four thymines and at least four bases long scaffold overhang, set 2 with only scaffold overhangs and set 3 with passivation by six thymine overhangs. Here shown is the same site in the cadnano file for all three sets of the left edge as example. **B** AGE of the three edge staple sets with unspecific dimers (1) and the desired monomeric half-prism (2).

Dimerization via blunt end stacking of male and female Narcissus parts was not obtained immediately after thermal ramp assembly. However, self-dimerization was observed by investigating samples that were incubated for a few days at room temperature (Figure 4-7 A lane 6). and confirmed by AFM analysis. However, a considerable amount of the observed dimers was either not closed or was formed incorrectly (Figure 4-7 B).

The Narcissus structure was purified by FnS and analyzed by negative stain TEM imaging. Three main structures were found. Each structure could be explained as the result of one of the half prism sides laying on the surface while the rest of the origami collapsed on it, with some species similar to those regularly observed by AFM (Figure 4-6). Upright structures were only found near to clusters, most likely due to a thicker staining layer, allowing a typically unfavorable orientation of the bilayer, with the DNA helix axes of the structure pointing outward during drying. These structures however confirmed the correct orientation of the individual sheets of the half-prism to each other. TEM images were used to generate class averages of the three main orientations.

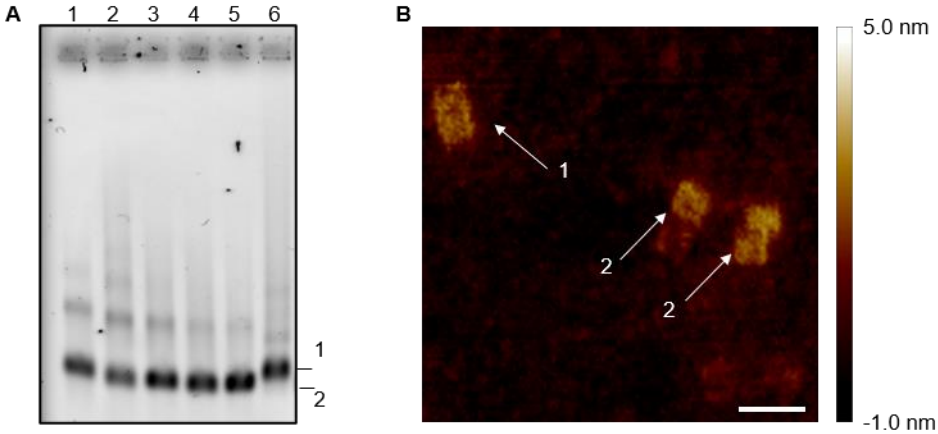

Figure 4-7: A DNA origami assembled with successive addition of staple sets and analyzed by AGE. Lane 1 contained only the core staple set, lane 2 as in lane 1 with additionally protrusion staple set (P_0), lane 3 -5 as lane 2 but with the right edge (R_{6T}) or left edge staple sets (L_{6T}) or both added, respectively. Lane 6 as lane 5 but with stacking staples allowing self-dimerization to form the dimer (1) running slower than the monomer (2) in lane 5. **B** The same sample as in lane 6 investigated by AFM. Dimers could be found (1), however often not formed properly (2). Scale bar is 100 nm.

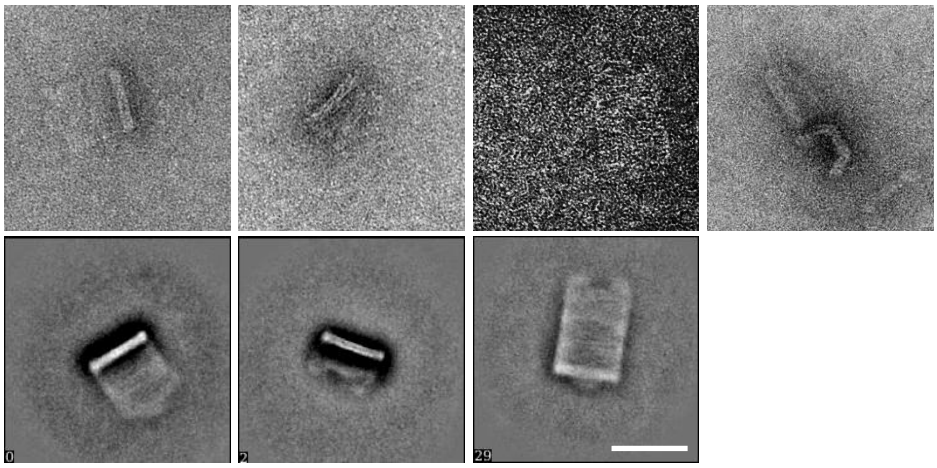

Figure 4-6: Successful formation of the half-prism could also be confirmed by negative stain TEM images (top row) and respective class averages thereof (bottom row). 4,641 particles were picked at 3.83 Å/pix. 384 px was used as box size, particles were sorted and averaged in 30 classes. Scale bar is 50 nm.

4.1.3. Second half-prism and full hexaprism prism in honeycomb lattice

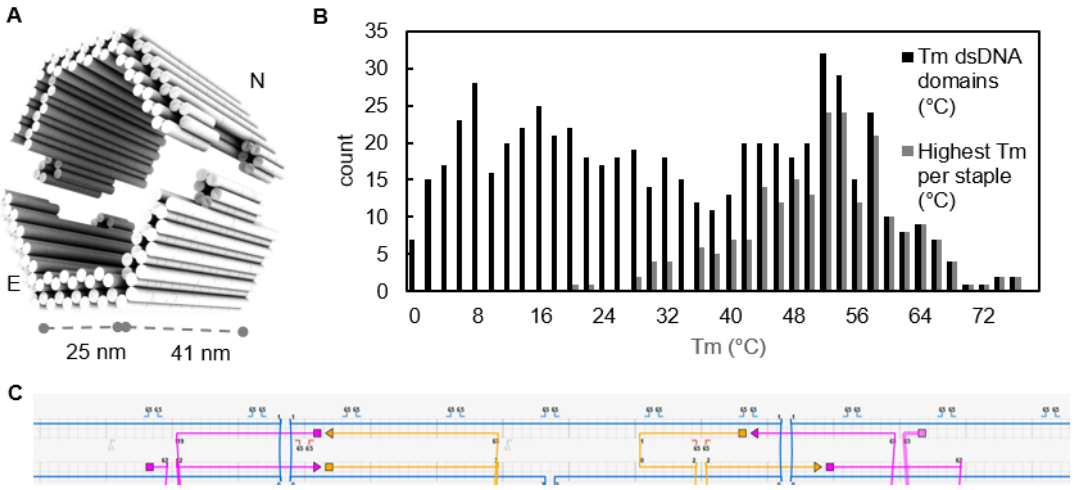

Figure 4-8: **A** Three dimensional model of upper half-prism (N) and lower half-prism (E). The dimensions are similar as before for 6p120. **B** Melting temperature of dsDNA region were optimized for monodisperse distribution for the lower half-prism. Results for the used staple sequences shown here. **C** Hybridization staples were developed with four base overhangs complementary to the respective other half-prism. Exemplary region shown here with hybridizing staples from N (yellow) and E (pink).

In order to achieve a reliable dimerized hexaprism, a second half prism was designed to be complementary in shape to Narcissus (Figure 4-8 A). The structure was termed Echo after the mythical woman who fell in love with Narcissus.[249] This design was abbreviated with the letter 'E'. The scaffold path was designed to be like Narcissus but turned by 180° around the central axis of the hexaprism, thus avoiding the face-to-face orientation of the blunt ends as in the Narcissus homo-dimer. Also in this case, staple strands were designed such to contain 14 bp long continuous dsDNA and 32-point modification were introduced in four rows, as described above for the Narcissus structure. Core staples and edge staples were also designed similarly to the Narcissus analog, and finally the six-helix bundles extruding and intruding from both structures were designed such to enable their hybridization (staple set hybr). Hybridization was achieved by four base-long overhangs spanning the matching helices (Figure 4-8 C). Naming of staple sets was based on the staple sets in Narcissus (Table 4-1).

Also for the Echo structure, the design_analyzer.app was used and a reasonable narrow distribution of melting temperatures for the longest continuous dsDNA segments was found for scaffold break position 69[57] (Figure 4-8 B).

The full origami structure, formed by hierarchical assembly of Narcissus and Echo was termed Nemesis after another character of the Greek mythology in the mythos about Echo and Narcissus[249] and conveniently allowed combining the acronyms N and E for the half-prisms into NE for the full prism.

Assembly conditions were taken from former experiments with the Narcissus design and were used to check the correct assembly of Echo. Assembled structures were characterized using 1% agarose gel electrophoresis. Magnesium screening and check of staple sets was similar to Narcissus, hence assembly conditions were kept the same for both half-prisms (Figure 4-9 A and C). AFM analysis confirmed correct formation of Echo. As expected, Echo structures flattened-out onto the mica surface with well visible six-

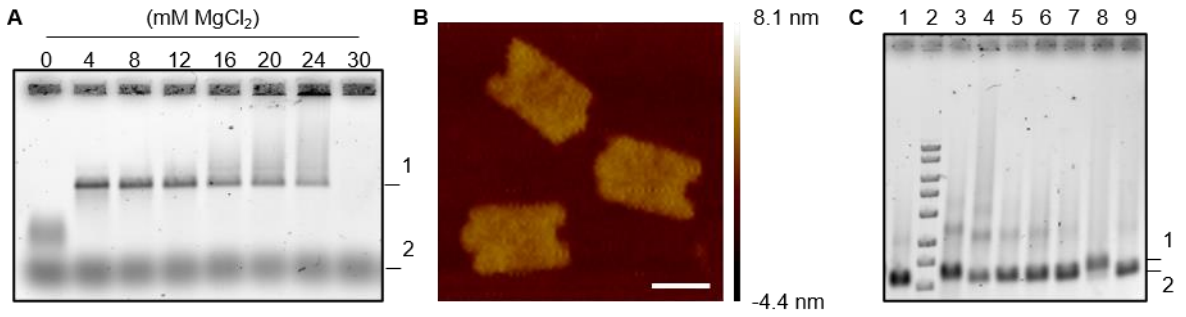

Figure 4-9: **A** The assembly procedure as described before was screened for optimal Mg^{2+} concentration. The final assembly Mg^{2+} concentration was 20 mM as for N. **B** AFM image of the lower half-prism confirm successful formation during the assembly. Scale bar is 50 nm. **C** Staple sets were tested as before for N: Lane 3 contained only the core staple set, lane 4 as in lane 3 with additionally protrusion staple set (P_0), lane 5 -7 as lane 4 but with the right edge (R_{6T}) or left edge staple sets (L_{6T}) or both added, respectively. Lane 8 as lane 7, but with stacking staples allowing homodimerization of Echo. Dimer formation can be found with a band of slower mobility (1) compared to the monomers (2). Lanes 1 and 9 contained N and E with the staple sets as in lane 7 but with the hybridization staple set.

helix protrusions (Figure 4-9 B). From there on, the half-prisms were usually assembled with the following staple sets: cs$PR_{6T}L_{6T}$hybr (see Table 4-1 for details on the nomenclature).

Using negative-stain TEM images, three possible orientations of Echo were found, with class averages being more detailed than for Narcissus due to better stained samples (Figure 4-11 A). This allowed to visualize the occurrence of some structural defects associated to neighboring helices connected only by few staple crossovers (Figure 4-11 B). The protruding six helix bundle was not placed exactly in the middle of the half prism due to the intrinsic structural features of connected DNA duplexes in the origami design. This results in a 10.0 nm and a 13.6 nm offset on opposite sides of the six helix bundle protrusion, as clearly visible by TEM imaging. The orientation of these two offsets in respect to the structure indicates that half-prisms most likely bound to the grid surface via their concave site before collapsing onto the surface due to electrostatic interactions.

Dimerization was investigated using labelled half-prisms. Each half-prism was assembled with three cF9 protrusions hybridized to fluorescently-labelled complementary strands. In particular, the Echo half was FAM-labelled and the Narcissus half was TAMRA-labelled. After assembling 10 nM of each half-prism, 10 µl of each monomer were kept as control samples. Three reaction conditions were investigated: PEG purification prior dimerization, increased temperature and increased magnesium ion concentration during dimerization. Higher magnesium concentrations were anticipated to overcome repulsion of the negatively charged nanoparticles. Mild heating was supposed to suppress unspecific multimer formation and mismatching of hybridization oligonucleotides with excessive staple strands. For the same reason, origamis were PEG purified before combining them. Incubation took place overnight and structures were checked afterwards with agarose gel electrophoresis. Dimerization was shown to take place with good yield in all conditions. However, pre-purified samples suffered from an increased clustering. Dimerization was hence always performed directly after half-prism assembly without any previous purification (Figure 4-10).

The same samples were investigated by AFM, confirming the correct formation of the expected dimer. Opened dimeric structures were rarely found, indicating good stability of the correctly folded full prism. However, the height profile of the structures observed at the AFM indicates that the hollow prisms collapse

either during AFM sample preparation or scanning with the AFM tip (Figure 4-12). Also, the sixfold pseudosymmetry of the structure could not be confirmed by this technique.

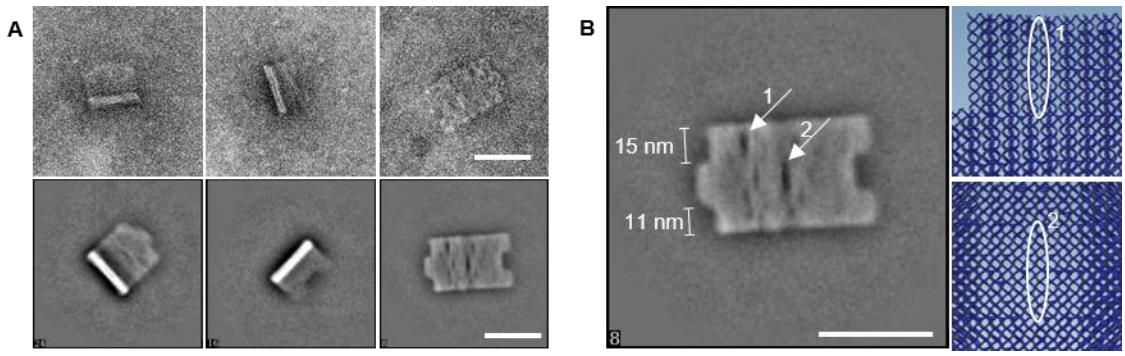

Figure 4-11: **A** Formation of E could also be confirmed by negative stain TEM (upper row) and the respective class-averages (lower row). 2,973 particles were picked at 3.83 Å/pix. 384 px was used as box size, particles were sorted and averaged in 32 classes. Scale bar is 50 nm. **B** Better stained samples allowed more precise measurement of the sample dimensions. Also, weak points with low crossover density can be seen (1 and 2). The corresponding regions are depicted right with a zoom in into a three-dimensional model of E.

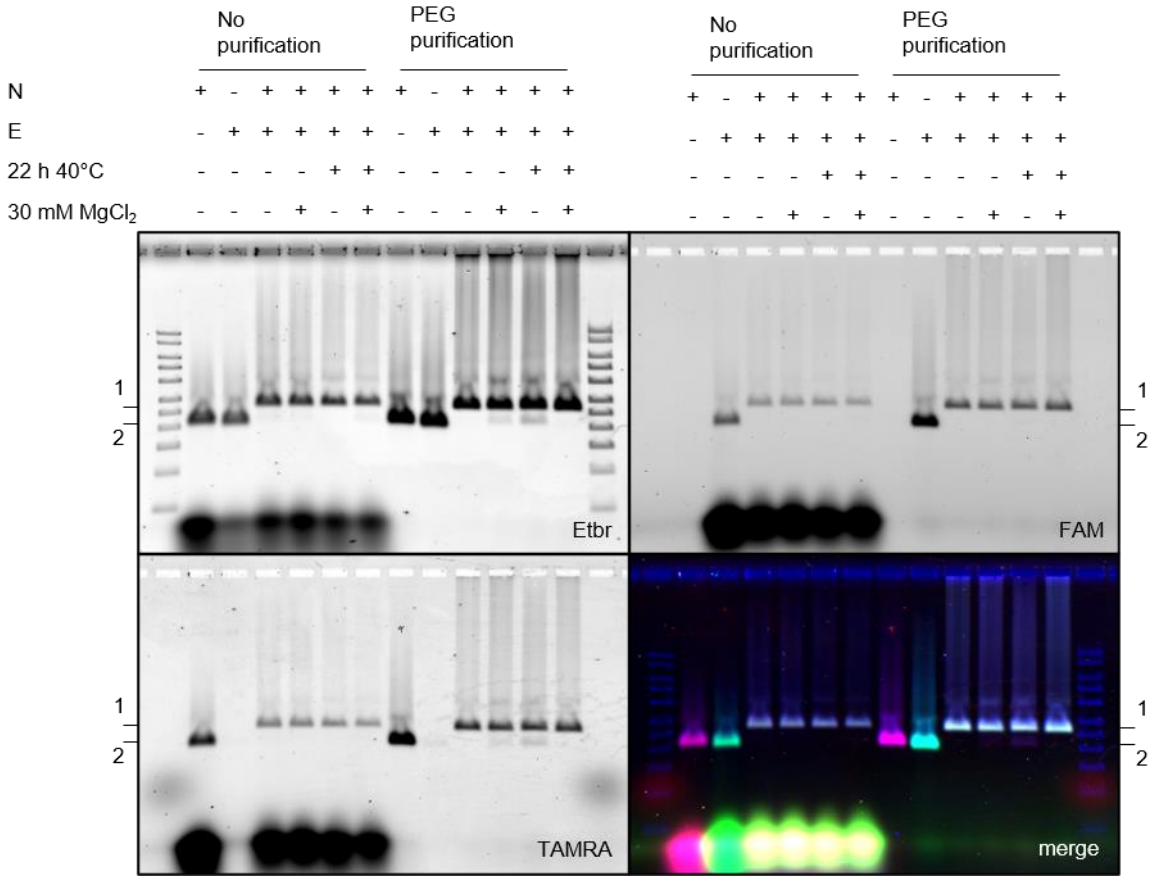

Figure 4-10: Dimerization NE(1) from TAMRA-labelled N and FAM-labelled E(2) was tested on a variety of conditions. AGE results shown here. Merge image from TAMRA (red) and FAM (green) fluorescence as well as Etbr signal after staining (blue)

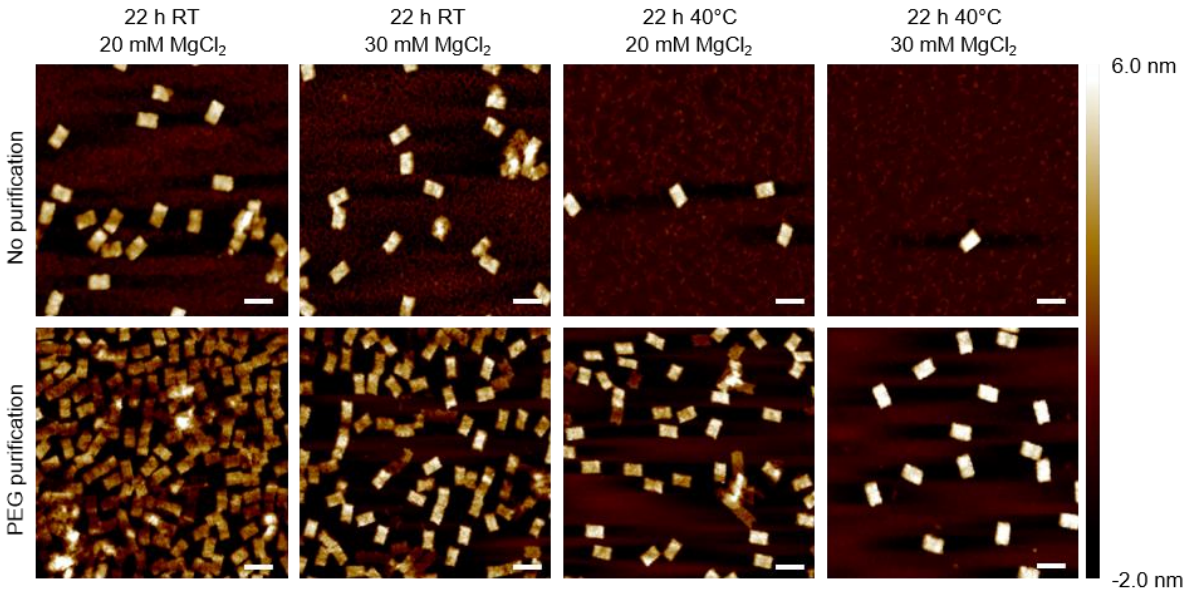

Figure 4-12: Dimerization of N and E to form NE. AFM results shown here. Scale bars are 100 nm.

Dimers in the expected size range where also found by TEM inspection. Notably, dimers were not found to open on the TEM grids, suggesting a high structural stability of the construct. Nemesis structures appeared in three distinct orientations. Two of them were interpreted to be prisms laying either on a side or a collapsed edge, resulting in either shorter or longer apparent diameter. In the third orientation the helical axes were parallel to the axis of vision, i.e. perpendicular to the grid; an orientation that was only rarely found for the half-prisms. Class averages were generated for all three orientations confirming the results for single images. The depth of the whole structure was confirmed to be around 41 nm, both for the full prism as for the half-prisms. However, the inner diameter as well as the height were about 15% smaller, probably as a consequence of sample shrinking during the staining process or miscalculation of the interhelical spacing, where half a nanometer was assumed for the helix-helix distance and two nanometers were considered for the diameter of each single helix (Figure 4-13).

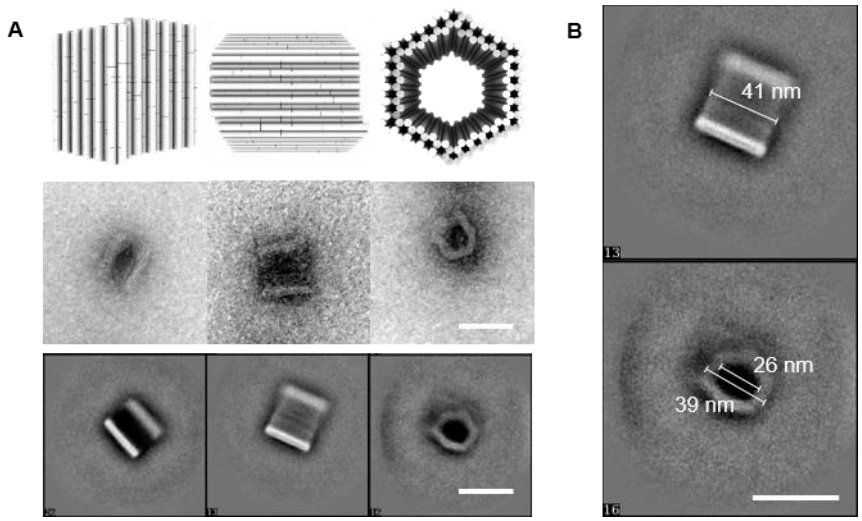

Figure 4-13: **A** Successful formation of the hexaprism can be confirmed by negative stain TEM. Orientation interpretitions of found particles are depicted in three dimensional models (top row). Single images (middle row) and class-averages thereof (bottom row) are shown. 3,065 particles were picked at 3.83 Å/pix. 384 px was used as box size, particles were sorted and averaged in 32 classes. Scale bar is 50 nm. **B** Dimensions differed from the designed inner cavity of approx. 30 nm diameter to be rather 26 nm.

Dimerization kinetic was further investigated using DLS by combining unpurified Narcissus and Echo and measuring the reaction course over night at room temperature. The resolution of the DLS was assumed not to be able to separate the hydrodynamic diameter of the monomer and dimer simultaneously, but rather average the hydrodynamic diameters of the particles. The observed diameter d_{obs} was assumed to result from the contribution of all species present in solution, each one contributing equally, leading to Equation 1:

$$d_{obs} = \frac{[N]}{c_{total}} d_{mono} + \frac{[E]}{c_{total}} d_{mono} + \frac{[NE]}{c_{total}} d_{dim} \qquad \text{Equation 1}$$

where d_{mono} and d_{dim} are respectively the hydrodynamic diameters of monomeric and dimeric structures, Narcissus [N], Echo [E] and Nemesis [NE] are the concentrations of the single species at a given time and c_{total} is the total concentration of all species at that given time: c_{total} = [N] + [E] + [NE]. Since N and E were used in equimolar amount ([N]=[E]) the formula can be written as

$$d_{obs=} \frac{2[N]}{2[N] + [NE]} d_{mono} + \frac{[NE]}{2[N] + [NE]} d_{dim} \qquad \text{Equation 2}$$

Also, as [N]+[NE] will always be the initial concentration of one monomer N_0 the formula can be rewritten as

$$d_{obs=} \frac{2[N]}{[N] + N_0} d_{mono} + \frac{N_0 - [N]}{[N] + N_0} d_{dim} \qquad \text{Equation 3}$$

And simplified to

$$d_{obs=}\frac{N_0 d_{dim} + [N](2d_{mono} - d_{dim})}{[N] + N_0} \qquad \text{Equation 4}$$

As the formation of NE from equal amounts of N and E should follow second order kinetics, the concentration of N can be described by:

$$[N] = (\frac{1}{N_0} + kt)^{-1} \qquad \text{Equation 5}$$

Where k is the second order rate constant over time t: The insertion of Equation 5 in Equation 4 gives Equation 6.

$$d_{obs=}\frac{N_0 d_{dim} + (\frac{1}{N_0} + kt)^{-1}(2d_{mono} - d_{dim})}{(\frac{1}{N_0} + kt)^{-1} + N_0} \qquad \text{Equation 6}$$

Which gives simplified Equation 7:

$$d_{obs} = \frac{N_0 d_{dim} kt + 2d_{mono}}{2 + N_0 kt} \qquad \text{Equation 7}$$

The measured hydrodynamic diameter d_{obs} by DLS for N_0 of 5 nM at room temperature was fitted to the described Equation 7, resulting in a rate constant of 0.139 $nM^{-1}h^{-1}$ or $3.85 \cdot 10^4$ $M^{-1}s^{-1}$ (Figure 4-14). Hence, dimerization at room temperature was performed overnight.

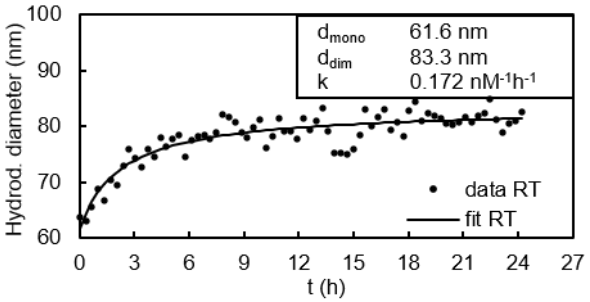

Figure 4-14: The dimerization process at room temperature was analyzed by DLS. Peak positions of measured hydrodynamic diameter were used as datapoints over time. Fit results are shown in box.

4.1.4. Assembly protocol optimization

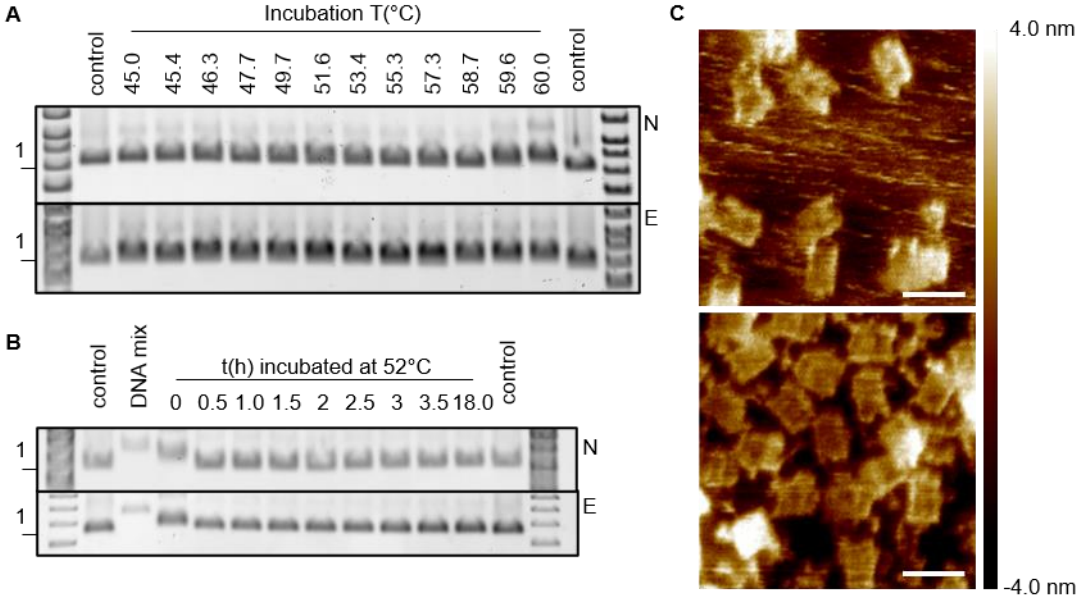

Figure 4-15: **A** Isothermal assembly was investigated by AGE for samples assembled at a temperature range from 45°C to 60°C after the initial denaturing step at 65°C. Control samples were folded origamis (1) assembled in a thermal ramp. **B** Isothermal assembly at 52°C with samples token over time analyzed by AGE with folded controls (1) as in **A**. **C** Narcissus (top) and Echo (bottom) assembled for two hours at 52°C investigated by AFM. Scale bars are 100 nm.

For assembly at higher scaffold concentrations (>10 nM) see appendix section II.b page 136.

The assembly procedure for a full prism as described above takes about two days, therefore the development of a faster protocol was desired. In 2012 Sobczak *et al.* described a fast isothermal assembly slightly below the global melting temperature of a given DNA origami.[147] The optimal assembly temperature was screened by using a gradient PCR cycler in a temperature range from 45°C to 60°C for 18 h after an initial melting step of ten minutes at 65°C. A sample volume of 50 µl for both Narcissus and Echo structures was used, with the staple set combination $csP_0R_{6T}L_{6T}$hybr. Well-defined bands formed for all screened temperatures, however a slower migration rate was observed for Echo assemblies above 57.3°C and Narcissus assemblies above 58.7°C indicating the formation of less compact structures above these temperatures (Figure 4-15 A).

A temperature value of 52°C was chosen for the investigation of the kinetics of the assembly. For this purpose, small aliquots were taken from the assembly mixture during a time course of several hours and stored on ice. The reaction volume was kept above 25 µl to avoid high concentration-dependent effects and all samples were then analyzed by agarose gel electrophoresis. The expected bands appeared already after 30 min isothermal reaction, with seemingly less smearing when compared to a control reaction performed applying a thermal ramp (Figure 4-15 B). AFM analysis of both half-prisms assembled at 52°C indicate well-formed origamis (Figure 4-15 C). Due to good results at this temperature, isothermal assembly was then performed at 52°C. The final assembly protocol was however prolonged to two hours instead of 30 minutes, since the published investigation of the sequence of events of a similar DNA origami structure formation was shown to take around 2 h to achieve completion.[250]

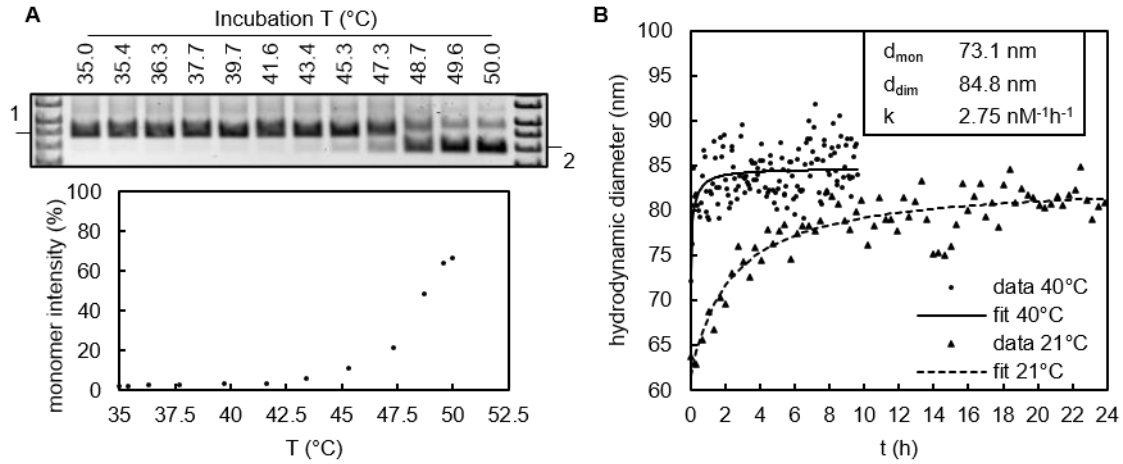

Figure 4-16: **A** Melting of NE was investigated by heating overnight to the shown temperatures. Samples were then kept on ice until quickly being investigated by AGE (top). Relative monomer band intensity plotted vs. temperature (bottom) indicate a melting temperature around 48°C. **B** Dimerization was carried out at 40°C and monitored as described before by DLS. Here depicted with data at room temperature for comparison. Fit parameter for the dimerization process at 40°C shown in box.

Additionally, the dimerization process was investigated. upon overnight incubation at several temperatures, the melting of the dimers was observed for a temperature around 48°C (Figure 4-16 A). Thus, a temperature of 40°C was chosen to perform dimerization. At this temperature, the dimer is formed in a relatively short time and no increased formation of monomers is observed. DLS was used to investigate the dimerization process using Equation 7(Figure 4-16 B). The estimated rate constant was 2.75 $nM^{-1}h^{-1}$ ($7.63 \cdot 10^5$ $M^{-1}s^{-1}$), which is too fast for a DLS investigation with datapoints generated only every four minutes. The dimerization process was assumed to be complete after three hours at 40°C which was confirmed by AGE, negative stain TEM and AFM (figures in section 4.1.5 and 4.2).

For the development of DNA brick inspired topologically markers see Appendix section II.d page 140. For the full cadnano design files of N and E see Appendix II.a, page 134 and following. For the sequences of all DNA strands see Appendix section I.b, page 99 and following.

4.1.5. Multimerization of the full prism

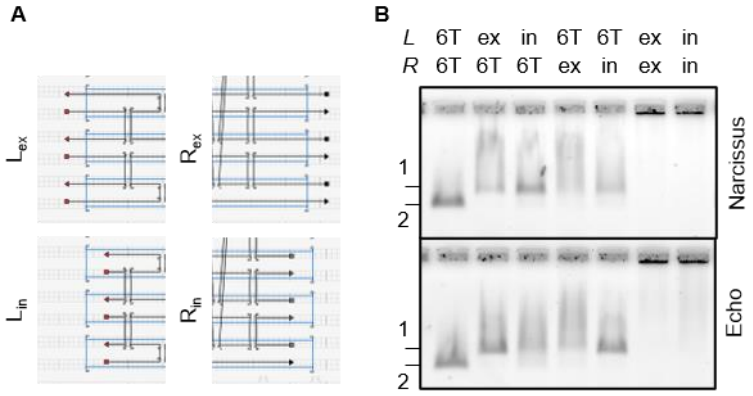

Figure 4-17: **A** New staple sets with protrusions (ex) complementary to the scaffold overhangs in the shortened staple strands (in) Here the same exemplary helices in N are shown. **B** AGE of assembled DNA origami structures with the new staple sets. Usage of the new edge staple sets ex or in in left (L) (lanes 2 and 3) and right (R) (lanes 4 and 5) edge led to unspecific dimers (1) in single prism assembly as found by AGE. When used simultaneously no monomers could be observed anymore (lanes 6 and 7) Lane 1 represents the monomeric 6T passivated half-prism(2).

The next step was to link multiple origami chambers in a row, i.e. three consecutive NE units. The initial Nemesis edges had to be modified to allow well defined interaction from one prism to another. Hence, hybridization staples were designed to extend of four bases from one edge of the prism and to hybridize to four complementary bases of the unpaired scaffold on the opposite edge of the same helix. There are two options to achieve this: either the staples protrude from the L edge staple set and hybridize to the intruding R edge or vice versa. This resulted in two sets of extruding L_{ex} and R_{ex} staples and two sets of intruding R_{in} and L_{in} staples (Figure 4-17 A). These new staples were tested using agarose gel electrophoresis and showed that origamis containing only one of the four possible sets, i.e. L_{ex}, R_{ex}, L_{in} or R_{in}, already undergo self-dimerization. When both extruding or intruding sets are present within the same structure, multimers are formed (Figure 4-17 B). A change in the design of the staples was therefore necessary.

As shown for other DNA origami structures with many potential stacking interactions the best way to achieve a desired hierarchical assembly, is the usage of a combination of both thymine passivating staples and hybridizing staples.[62] A low number of hybridizing strands might result in no or partial dimer formation, resulting in leaking structures. On the other hand, as shown above, a high number of hybridization strands results in unspecific dimer formation of the subunits.

In an initial trial, staples were designed to achieve NN and EE dimers, i.e. dimers of the half-prisms. To simplify the nomenclature, the left origamis were named A and the right origamis B, leading to four kinds of half-prisms, namely N_A, N_B, E_A and E_B (Figure 4-18 A). In order to find the optimal connectivity, sets of edge staples were designed where an increasing number of 6T passivating oligonucleotides were exchanged against the protruding version of that oligo in the left edge and shortened version on the right edge. The helices involved in the connection in the four investigated staple sets can be seen in Figure 4-18 B.

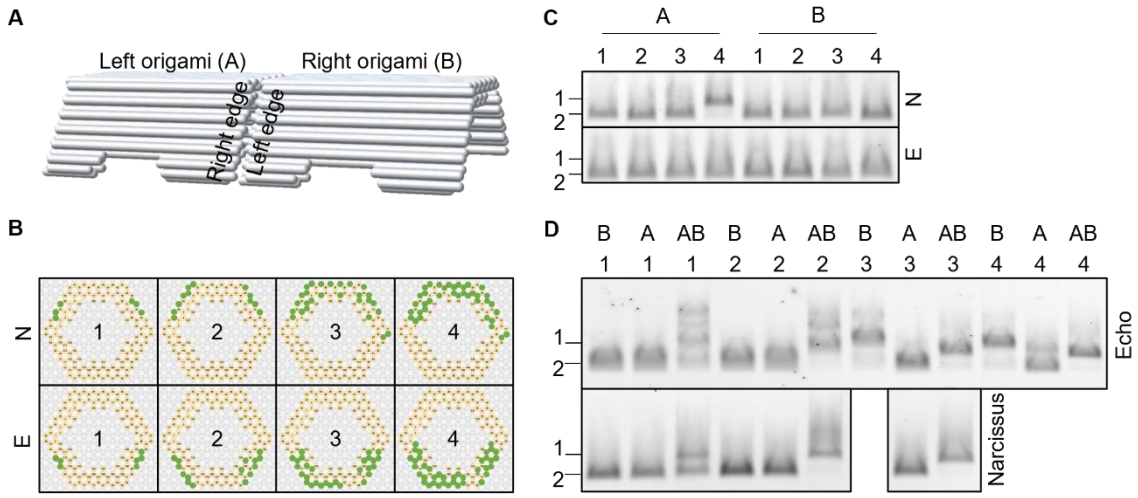

Figure 4-18: **A** Two N hybridizing along their axis resulting in NN. The origamis were The right edge of an origami A binds to the left edge of an origami B. **B** Sets of different connectivity were investigated. Connecting helices between N_A and N_B or E_A and E_B are shown in green, all others were passivated by six thymine overhangs. The left origamis A were used with R_{in} staples, the right origami B with the L_{ex} staples for interaction. **C** AGE of half-prisms (2) for the two full-prism setups shown in **A**:N_A, N_B, E_A and E_B. The numbers above lanes indicate the used connectivity as shown in **B**. Unspecific dimerization (1) for connectivity set 4 in N_A (in lane A 4) led to the exclusion of that set. **D** Assembled half-prisms (2) and their dimerization as shown in **A** investigated by AGE. A and B are the respective origami, the numbers correspond to the connectivity sets used. AB samples contain an equimolar amount of A and B origami incubated at room temperature overnight

These connectivities were investigated for their suitability to form stable monomeric half-prisms when assembled (Figure 4-18 C). Sets that resulted in considerable self-dimerization were not used in further experiments like set 4 for N_A. Note that the resolution of bands was not very good in this gel and led to the overlooked fact that also usage of connectivity sets 3 and 4 in E_B led to a considerable amount of self-dimers as shown in Figure 4-18 D, upper gel.

Assembled A half-prisms were combined with their corresponding B half-prisms resulting in NN and EE dimers by incubation overnight at room temperature. Those were also investigated by AGE revealing the expected dimer formation for connectivity set 3 both in N and E as well as connectivity 4 in E. This was somewhat surprising as the respective E_B staple set led to unspecific dimerization (Figure 4-18 D). Since the unspecific interaction could seemingly be overcome, the formation of a three-chambers system was investigated.

The three full origami prisms were named (from left to right) as NE_A, NE_B and NE_C or A, B, C. The fully 6T passivated origami (uncapable to link to any other origami or to itself) was used as control and named D. Multimerization of middle prism B can be avoided by using either extrusions or intrusions on both the left and right side of the structure (Figure 4-19 A). An initial attempt was performed using the connectivity sets 3 for both N and E at L and R edges of chamber B without further adaptation (Figure 4-18 B, third column). When extruding staples were used on both sides of B (B_{ex}), the structures N_B, E_B and NE_B underwent self-multimerization (Figure 4-19 B upper gel, lanes 2, 6 and 10). However, when only intruding staples were used (B_{in}) for the assembly, monomeric NE_B prism formed correctly, though the NE_C prism seemed to form higher molecular weight construct (Figure 4-19 B middle gel, lane 7 and 11). These interactions were further optimized (see Appendix section II.c page 137) resulting in set B_{in+} with the

respective three monomeric NE_A, NE_B and NE_C prisms (A, B and C prisms) ready for hierarchical assembly (Figure 4-19 B, lower gel).

Multimerization of the so-formed prisms into the corresponding dimers or trimers was confirmed by both AGE and negative stain TEM. It should be noted that the interaction site is most likely not completely closed for all structures, as gaps and bends in the interaction region are visible in negative stain TEM images (Figure 4-20).

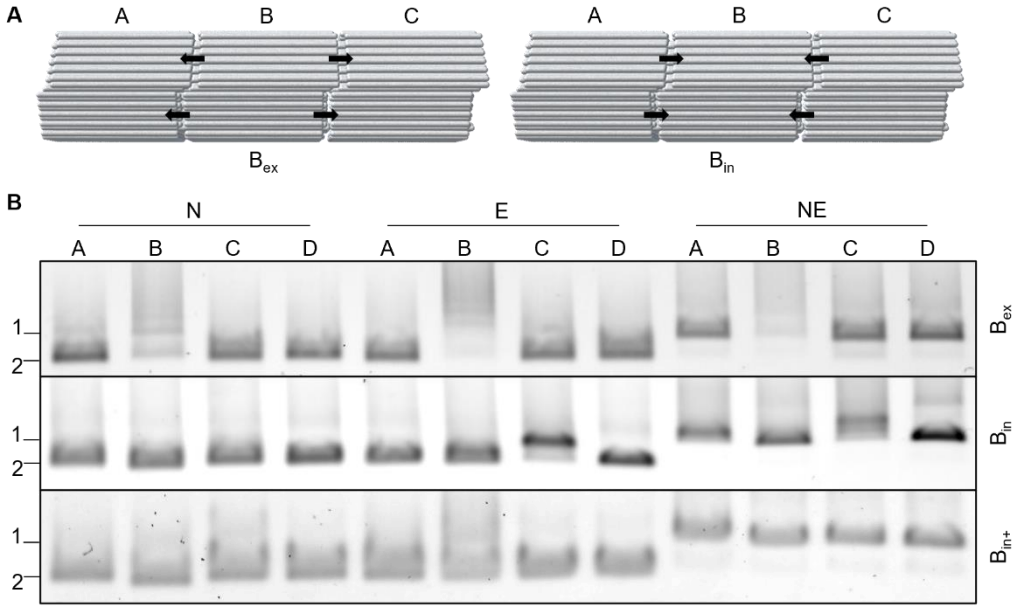

Figure 4-19: **A** Three prism setup can be theoretically done with the same multimerization staple set if the middle prism is using protrusions left and right(left) or has the corresponding staple recessions left and right(right). **B** AGE image of a B prism with only extruding connectivity set 3 led to the unsuccessful formation of the full prism (1) B and respective half-prisms (2) (B_{ex}, upper gel image). When using the respective intruding connectivity staple sets all B origamis were well formed, however E_C and NE_C were multimerizing (B_{in}, middle gel). This interaction was further optimized resulting into a combination B_{in+} allowing well-formed monomeric full prisms (bottom gel).

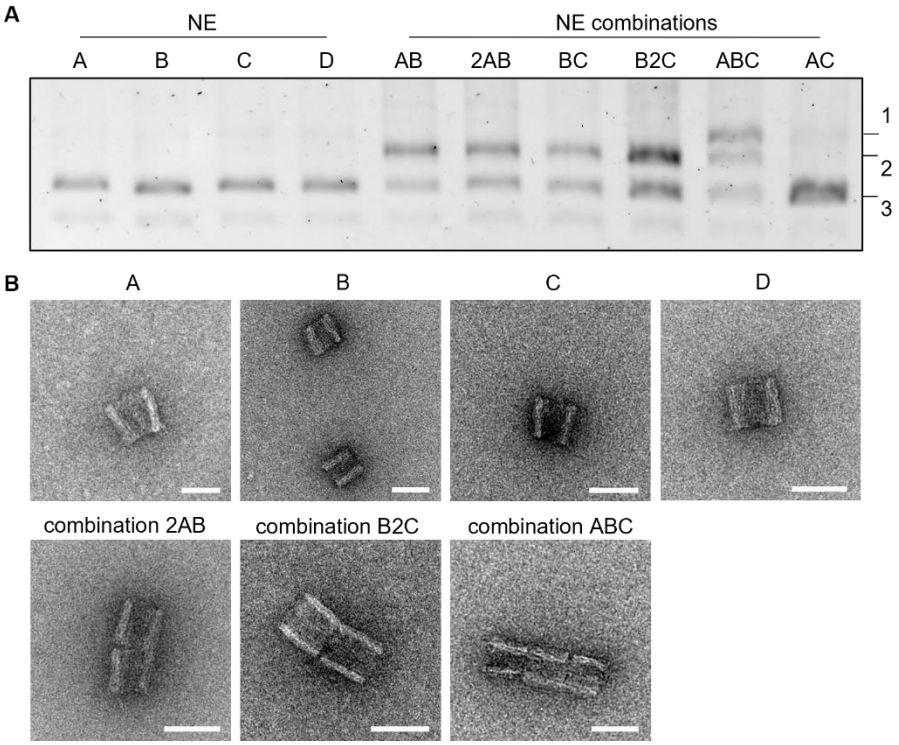

Figure 4-20: **A** AGE of multimerization of the prisms in p97 storage buffer. B prisms at 5 nM A and C either equimolarly added or in twofold excess (indicated by number two) shown by AGE. Formation of trimers (1), dimers (2) and monomeric (3) prisms was confirmed. **B** Interactions from **A** were investigated by negative stain TEM. Structures form as designed, however there were small gaps between the prisms. Scale bar is 50 nm.

4.2. Encapsulation of p97 in forced orientation

4.2.1. Encapsulation via Halotag

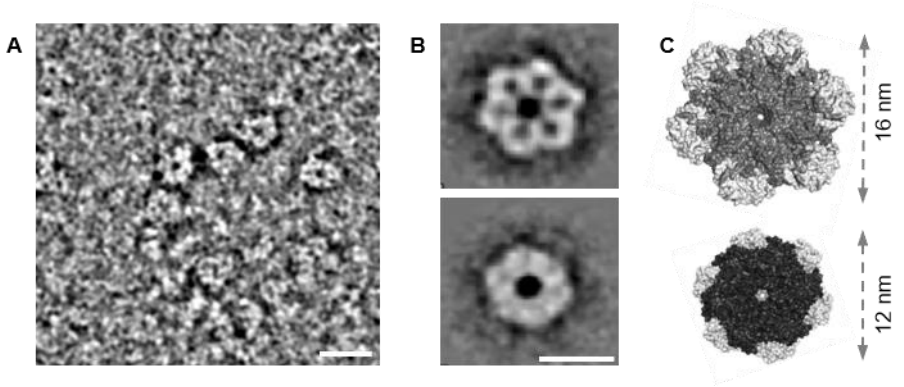

Figure 4-21: **A** Bandpass filtered negative stain TEM image of p97-His_6. Scale bar is 20 nm. **B** Exemplary class-averages were generated from particles picked from images as in **A**. 13,819 particles were picked at 2.39 Å/pix. 120 px was used as box size, particles were sorted and averaged in 100 classes. Scale bar is 10 nm. **C** Three-dimensional surface model of p97 in resting state (pdb: 5ftk) aligned to images in **B** for better visibility. Top row in **B** was interpreted as N/D1 domain visible while bottom row was interpreted as C-terminal D2 domains. Side-views were not found in class-averages.

The correct formation of p97 hexamer was investigated by negative stain TEM. The hexameric structure and the dimensions were clearly visible in single images and even more in class-averages. Most of the protein structures appeared with the central axis parallel to the axis of view, indicating a strong interaction between the grid and protein surface (Figure 4-21) and hence a strongly biased protein orientation.

When correct protein structure was confirmed, two first attempts were made to encapsulate it into NE. As initial approach PUB domains were chosen as they were reported to bind to the C-terminus of p97.[251,252] These small protein ligands were envisioned to localize p97 inside the origami prism. As an alternative streptavidin binding tag SBP introduced to the p97 C-terminus were investigated. As streptavidin binds strongly to SBP[253] and biotin[254], this tetrameric protein was anticipated to span biotin modified oligonucleotides in the origami interior and p97 C-termini. However, binding via PUB domain or streptavidin binding peptide (SBP)-tag were insufficient (see page 143 appendix section III.a). Then encapsulation via a Halotag-fused domain was envisioned. A rough model of the encapsulated complex was made in pymol, to better estimate the dimensions of the final protein cargo (Figure 4-22 A). The Halotag sequence was cloned at the C-terminus of p97 and the full complex was expressed and finally purified by His affinity chromatography. An amino-modified oligonucleotide (NH_2-F9) was conjugated to an NHS-modified chloroalkane, and successful conjugation was confirmed by denaturating PAGE and MALDI (Figure 4-22 B, C). The conjugated oligonucleotide was purified by precipitation in isopropanol/ethanol, re-dissolved in tris buffer and finally reacted with the p97-Halotag (p97H) overnight at 8°C. The final DNA-protein conjugate was isolated by size-exclusion chromatography (SEC). Unreacted protein, as well as excess DNA could be clearly separated (Figure 4-22 D), DNA-protein conjugate containing fractions were collected, pooled and concentrated over 100 kDa MWCO filter. The concentration of p97 and conjugation efficiency were estimated by Coomassie gel band intensities with the aid of a standard curve of unconjugated p97 in the same gel. For this the gel analyzer of the software FiJi was used. Yield of DNA conjugation was

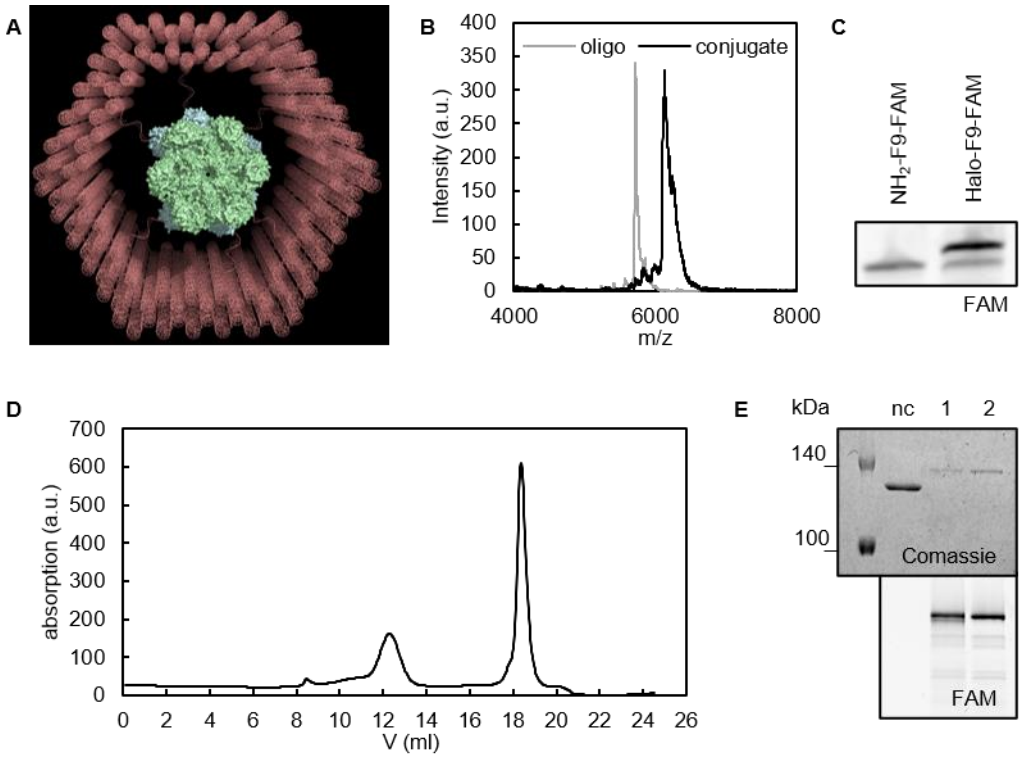

Figure 4-22: **A** Model of p97H encapsulated in NE hexaprism (red). p97(pdb 5ftk) is shown in green, Halotags in blue (pdb 5y2x). **B** MALDI spectra of F9 oligonucleotide bound to Halotag linker. Measured mass difference was 390 Da, theoretical mass difference was 393 Da. **C** The same samples as in **B** investigated by denaturing PAGE. **D** Elution profile of SEC of p97H conjugation mixture. Sample elutes between 11 and 13 ml. and oligonucleotides after 17 ml. **E** p97H conjugation with FAM labelled F9 oligonucleotide could be confirmed by SDS-PAGE (1). The conjugate was purified by SEC and concentrated over 100 kDa MWCO filter (2). Negative control (nc) is unconjugated p97H. Yields per p97 monomer were regularly between 70-100% (calculated from gel band intensity).

usually at least 70%. Assuming the formation of a nearly homogenous compound, this would correspond to 90% of p97 hexamers having at least three DNA strands attached to it (Figure 4-22 E).

N and E were assembled with and without one or two protruding arms (cF9) complementary to the F9-tagged Halo-p97 and further linked into NE full-prisms. The full prism and the half-prisms were then purified by PEG precipitation. The p97H-DNA conjugate displayed a FAM dye at the 3´ end of the F9 oligo and was used as a fluorescent marker. The p97H construct was added in 60X excess to the origami samples and let incubate at 4°C overnight. Samples were then investigated using AGE (Figure 4-23 A). FAM-labelled p97H hexamers were found to migrate faster than the origami structures, in absence of protruding arms. On the contrary, in presence of protruding arms, the FAM signal associated to the DNA-protein conjugate was colocalized with the DNA origami bands and resulted in one single band that migrates slightly slower than an empty DNA origami prism. Unpurified samples were imaged by AFM in air conditions and by negative stain TEM (Figure 0-13 in section III.b page 146 and Figure 4-23 B) and the encapsulation events were counted. For a full prism containing three protruding arms, the encapsulation yield estimated by TEM was about 45% (Table 4-2).

The question arose why so many DNA origami did not incorporate a p97 even though sufficient protein should be available in solution. From the AGE, AFM and TEM results it became clear that the Nemesis samples with three PAs had a higher encapsulation yield than the Echo sample containing two PAs, and

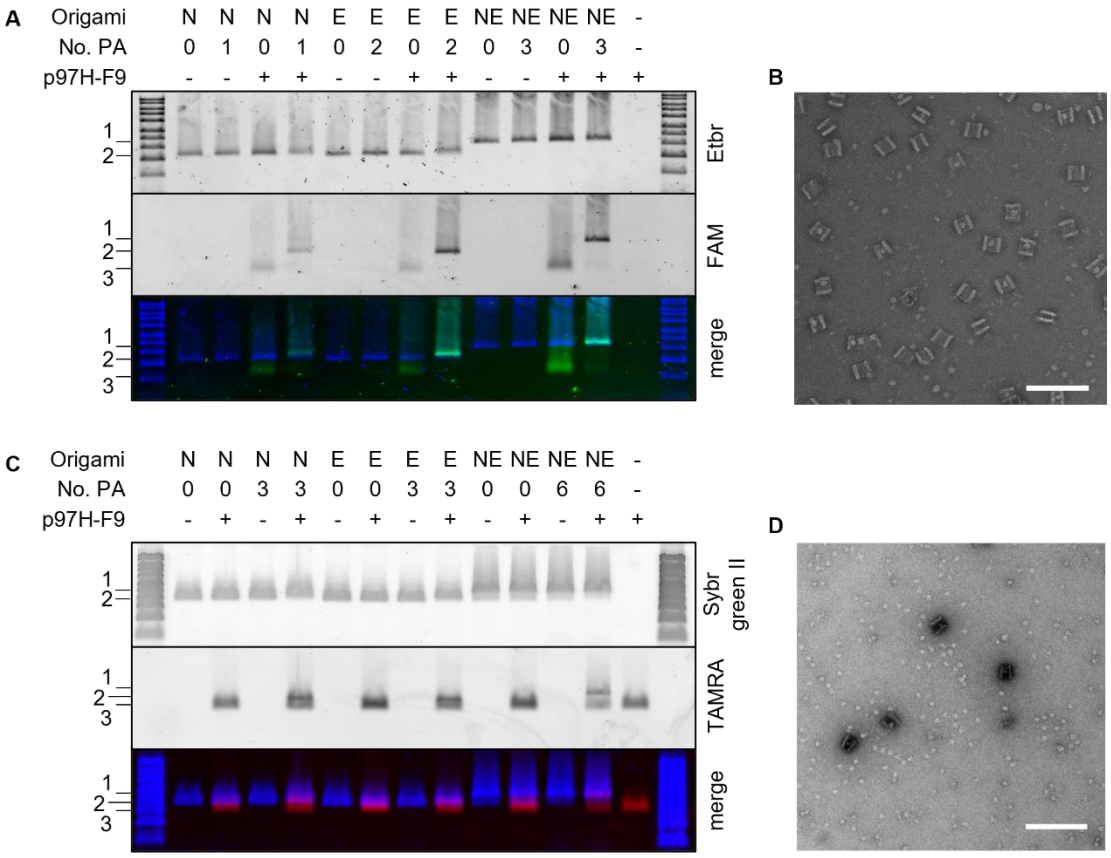

Figure 4-23: **A** AGE show a specific interaction between p97H conjugated to FAM labelled F9 to origamis with cF9 protrusions. Note that band intensity for FAM fluorescence increases with increasing number of protruding arms. Merge image of FAM channel (green) and Etbr signal (blue) proved colocalization of bands. **B** Exemplary negative stain TEM image of NE with three PA incubated with p97H gives an encapsulation yield of approximately 45% **C** The same as **A**, however with higher number of PA and TAMRA labelled F9. Merge image of TAMRA channel (red) and Etbr signal (blue). **D** Exemplary negative stain TEM image of unpurified sample of NE with six PA incubated with p97H show encapsulation yield between 80 and 95%. Scale bars are 200 nm.

this latter had a higher encapsulation yield than Narcisuss with only one PA. Hence, the issue was tackled by using a total of six PAs per prism, i.e. three PAs in N and three PAs in E. Again, these samples were investigated by AGE and negative stain TEM (Figure 4-23 C and D). In this case, there was no strong increase of colocalized fluorescence band intensity between half-prisms and full prism, indicating that p97H binds to a half-prism with a similar yield as to the full prism. Estimation of the yield by negative stain TEM

Table 4-2: Encapsulation yield of p97H into half-prisms and full prisms counted by AFM and negative stain TEM.

		AFM		TEM	
	No. PA	count	yield (%)	count	yield (%)
Echo	0	106	2.8		
	2	97	13.4	111	25.2
	3			104	75.0
Narcissus	0	44	2.3		
	1	105	13.0	161	17.4
	3			111	73.0
Nemesis	0	59	3.4		
	3	63	34.9	484	45.4
	6			115	86.1

was in this case about 86% and along this work and for similar constructs, typically varied between 80% and 95%.

It should also be noted, that when p97H was not encapsulated the pore structure and its sixfold symmetry could be seen in negative stain TEM (Figure 4-23 B and D). This is however not true when p97H was encapsulated in a DNA origami prism. In these cases an unsymmetric oval between the DNA origami walls could be found. These findings indicate, that p97H central axis was most likely never aligned perpendicular to the DNA origami central axis.

4.2.2. Purification of the encapsulated protein

Several purification methods for DNA origami protein complexes were published and investigated to date.[149] However, many of them are limited in recovery and may still contain a considerable amount of contamination. For this work, two techniques were tested: size exclusion chromatography and pull-down of protein excess with magnetic beads. Note, that only purified p97H constructs were used for encapsulation into NE prisms, so free oligonucleotide should only be present if later introduced.

For the first technique, a Superose 6 10/300 column was used for purification of p97 and the conjugations thereof as well as DNA origamis upon equilibration in p97 storage buffer. The elution profiles of an unpurified DNA origami solution, a conjugation mixture containing p97H and chloroalkane-modified oligonucleotide and an encapsulation mixture of DNA-tagged p97H and the NE prism were compared (Figure 4-24 A). Due to the size of the DNA origami, it eluted within the dead volume at about 8 ml. The elution peaks of p97 and its conjugation species appeared later (page 43 Figure 4-22). Unreacted oligonucleotides eluted mainly after 15 ml. Altogether, SEC demonstrated to be a good candidate technique for purification of DNA origami species (both unloaded or loaded with p97H). For purification, 200 µl of a 20 nM NE, previously purified from excess staples, was incubated with F9 conjugated p97H overnight at 8°C and successively applied to the column. Void fractions were collected, concentrated, and investigated by negative stain TEM (Figure 4-24 B). Free p97 hexamers were very rarely found in TEM images (also see Figure 4-31 B and Figure 4-34 B), demonstrating that the purification method successfully isolates unbound protein from DNA origami species. Later investigations by AGE confirmed the absence of free p97H (see section 4.2.4 page 48).

The biggest drawback of the SEC method is the low yield of recovered sample. Additionally, it could not be used to parallelly purify multiple samples. Hence, for quick investigations of several samples another technique was tested. In the reaction mixture of interest, there are mainly three species: empty prisms, prisms with encapsulated protein and excessive DNA modified protein. As in a Southern blot analysis[255] the latter can be specifically bound to a surface leaving only DNA origami species in solution. Similarly, commercially available streptavidin-modified magnetic beads were used to capture excess F9-conjugated p97H. For this, the beads were modified with a 5´ biotin-T_{10}-cF9 and therefore they present the same protruding arms as the DNA origami. This technique was highly efficient and allowed to optimize the encapsulation strategy by purifying several reaction mixtures with different protein to origami stoichiometric ratios, which were

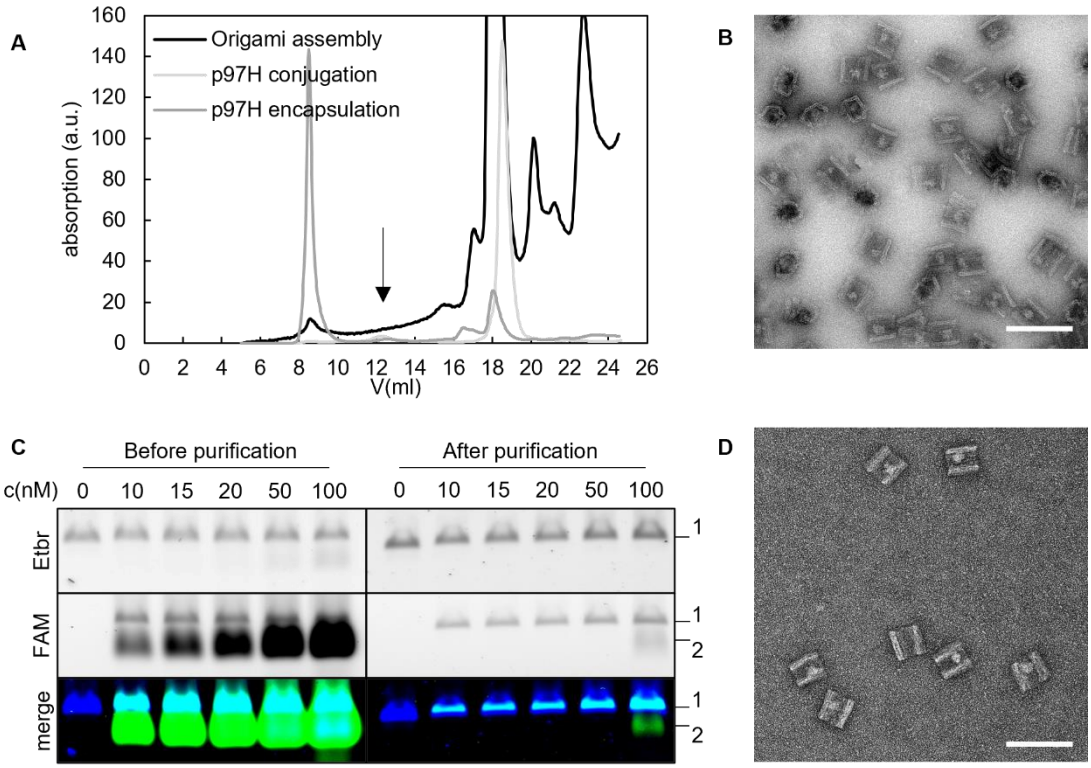

Figure 4-24: **A** SEC of 200 µl 20 nM assembled origami, p97H conjugation reaction mixture and p97H encapsulation mixture show that origamis elute in the column void around 9 ml. p97H elutes between 11 and 13 ml (arrow). DNA oligonucleotides after 13 ml. Absorption values of the three curves were manipulated to give similar strong signals for peaks of interest for presentation. **B** Negative stain TEM image of encapsulated p97H purified by SEC. Scale bar is 100 nm. **C** AGE of 10 nM NE with noted concentration of p97H conjugated to FAM-labelled F9 (left). The same samples after purification of 20 µl of it with 35 µl cF9 decorated magnetic beads (right). Merge image of FAM (green) and Etbr (blue) channel.**D** Negative stain TEM image of encapsulated p97H purified with magnetic beads. Encapsulation yield was not increased when more than 1.5fold excess p97H hexamer was used over NE prism. Scale bar is 100 nm.

further analyzed by AGE and TEM (Figure 4-24 C and D). According to these findings p97H was used only in slight excess (1.5X-3X) to NE in the following experiments, since encapsulation yield did not increase at higher concentrations, rather, a large excess in p97H was more difficult to remove.

Overall, the modified beads were able to pull-down approx. 25 amol p97H hexamers per µl bead solution, as demonstrated by AGE (Figure 4-24 C). Negative stain TEM images bead purified DNA origami samples show rare events of unbound p97, as expected, since statistically not all p97H would contain a DNA strand. While allowing easy parallel purification, this technique´s cost and handling are mainly suitable for purification of small amounts of sample.

The strong excess fluorescence band for p97H in Figure 4-24 C for low protein concentrations indicated also, that the concentration estimation of protein and origami was systematically flawed. This was most likely due to different techniques for concentration estimation.

4.2.3. Investigation p97 position

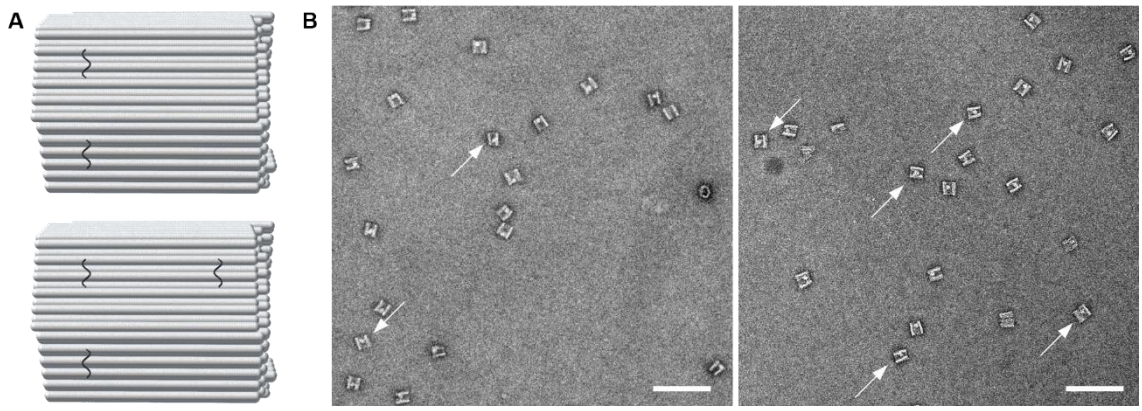

Figure 4-25:**A** Model of protrusion arm distribution. Either six protrusion arms were used in the left row (top) or five in the left and one in the right (bottom). **B** Negative stain TEM images of bead purified encapsulated p97H into NE with six PAs in the left ring (left) and NE with five PAs in the left ring and one PA from the right ring (right). p97H positioned at the center of NE are marked with arrows. Scale bar is 200 nm.

With a good encapsulation yield and purification method at hand, the placement of p97 at a certain site within the NE prism was confirmed by suitably modifying the design used. While up to here, all inner protruding arms were places on the left side of the prism, in the next experiment one of the inner-pointing arms was placed at a distal position, on the right side of the prism (Figure 4-25 A). Assuming that all arms can simultaneously bind to the same protein, this configuration was expected to lead to a larger amount of protein cargos positioned towards the center of the prism. DNA origami modified with cF9 handles were assembled as before, purified and incubated with F9-p97H and finally investigated by negative stain TEM (Figure 4-25 B). As expected, a larger fraction of species with a centered encapsulated protein was found (Table 4-3).

Table 4-3: Encapsulation yield and centered p97H counted from samples shown in Figure 4-25

protrusions	counted	yield (%)	centered (%)
6 left	758	88.5	8.2
5 left, 1 right	522	85.8	33.9

4.2.4. Activity of the encapsulated protein

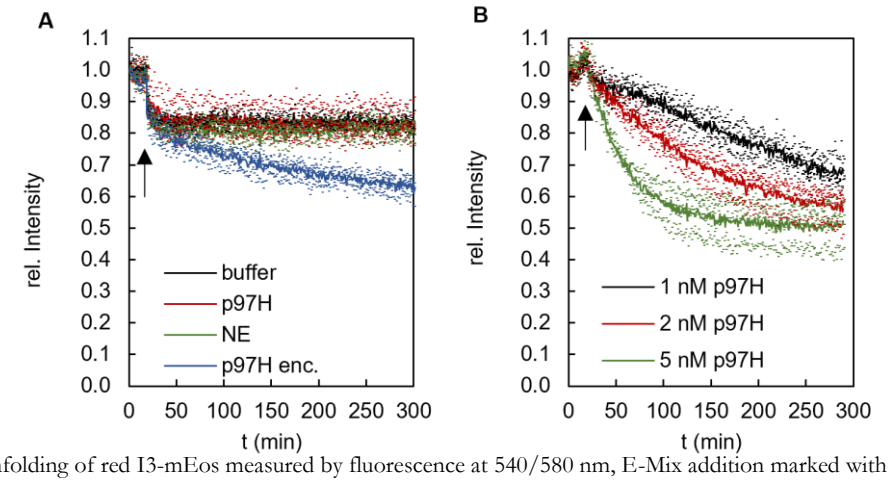

Figure 4-26: Unfolding of red I3-mEos measured by fluorescence at 540/580 nm, E-Mix addition marked with arrow. Small dots were data of each triplicate, solid lines depict the average thereof. **A** Fluorescence time-course for encapsulated p97H. DNA origami and free p97H were used at 1 nM. **B** Unfolding reaction of p97H-DNA conjugate at three different concentrations.

The activity of the p97H when encapsulated in a NE prism was investigated using the I3-mEos as substrate and measuring the extent of unfolding by the decrease in the fluorescence signal associated to this species. Upon illumination at 350-400nm, a backbone break was introduced in the Eos protein making it unable to refold and thus to recover its fluorescence after unfolding. Backbone break efficiency was estimated to be approximately 35% (measurement done in the group of our cooperation partner). DNA origami bound or free DNA-conjugated p97H were purified and diluted to 5 nM concentration and then used at 1 nM for technical triplicates. The reaction mixture containing encapsulated p97, SPIE substrate complex and p37 was first incubated at 37°C for approx. 20 min. Then prewarmed ATP containing E-mix was quickly added and the solution was mixed. Assays were monitored for at least 4.5 h. Note, that relative intensity used for analysis always was red mEos fluorescence (ex/em 540 nm/580 nm) intensity of a sample divided by the first measured value of red mEos fluorescence intensity in that sample. In these conditions, unfolding activity was observed only for p97H encapsulated into DNA origami, however not for free p97H (Figure **4-26** A).

It was then investigated if this behavior was based on protein handling. To minimize sample loss due to adhesion to reaction tube walls, purified p97H-DNA conjugate was diluted to 50 nM in a protein low-binding tube and then further diluted in a 384-well plate in which the SPIE unfolding assay took place. The protein was found active for concentrations as low as 1 nM (Figure 4-26 B) with a similar unfolding rate as the encapsulated protein, despite the effective concentration of origami and p97H might be slightly different from the nominal value.

In order to compare the unfolding activity of free and encapsulated p97H in a more reliable fashion (independent on the correct estimation of sample concentration), one single sample was used to investigate both types of constructs. For this purpose, the p97H-DNA conjugate was released from the DNA origami prism by using the toehold in the cF9 sequence as mentioned in section 4.1.1 from the inner of the prism. F9(22) was added in tenfold excess (60 nM) to the protruding arms cF9 and incubated for approx. 30 min at 37°C to enable the p97H release from the prism.

The feasibility of this method was checked with the release of a p97H-DNA conjugate labelled with TAMRA at the DNA sequence. Encapsulated and purified p97H was incubated with the release strand for 30 min at 37°C and successively investigated by AGE (Figure 4-27 A). Both a single construct (B) and a dimeric prism construct (AB) were tested. For samples incubated with the release strand, a band with higher migration rate corresponding to the p97H appears, while the fluorescence signal in the origami band decreases. The absence of p97 bands prior to the release process proved the absence of free p97 after purification.

Encapsulation yield after release was also estimated by negative stain TEM imaging of the same sample used for the unfolding assay (Figure 4-27 B). Note that, in this experiment, the DNA origami was strongly diluted and the quality of the TEM images strongly decreased due to the presence of the accessory proteins (adapter, substrate and energy mix enzymes) needed for the assay. On the other hand, the effective release of the majority of p97H from the prisms could also be microscopically confirmed.

The influence of free origami prism (NE) and release strand F9(22) on p97H unfolding activity was also tested (Figure 4-27 C, D). For a better comparison of the unfolding data obtained, the slope of the relative fluorescence signal at the beginning of the unfolding reaction was used. Since a rapid decrease in fluorescence after addition of E-mix was found in all samples and controls, the initial rate was calculated in the linear phase of the signal decay, included between 50 min and 200 min. The reason for the rapid drop in the fluorescence signal was attributed to sample temperature re-equilibration after E-Mix addition and was not further investigated. p97H unfolding rate was not significantly influenced by 1-5 nM free origami or 60 nM F9(22). However, when p97 was released from a DNA origami the unfolding rate significantly decreased (Z-test, $p<0.01$) (Figure 4-27 E, F).

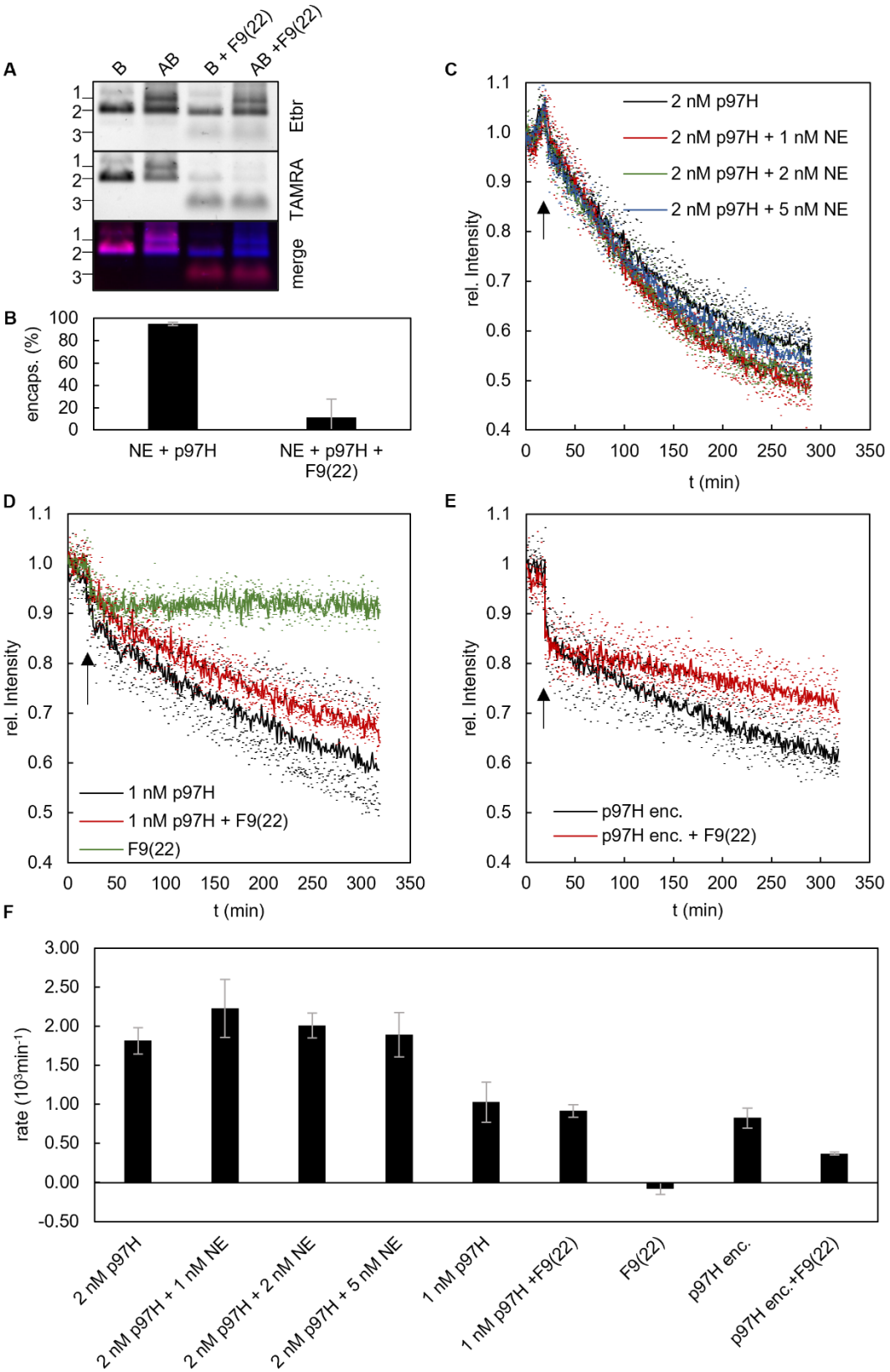

Figure 4-27: **A** AGE of SEC purified NE_B with encapsulated TAMRA labelled p97H (2) and AB dimeric prism construct based on this sample(1). Incubation with release strand resulted in emerging p97H band with higher mobility (3). **B** Encapsulation yield of p97 inside a NE prism before and after equilibration for unfolding assay with release strand. Analysis with negative stain TEM. Image to image variance used due to small population for NE+p97H+F9(22). **C** Red I3-mEos unfolding by 2 nM p97H-DNA conjuagte with various concentrations of NE (without protrusions) prism. **D** Red I3-mEos unfolding with 1 nM p97H incubated with 60 nM F9(22). **E** Unfolding rate of an encapsulated p97H and a released p97H. **C-E** Dots represent single curves of technical triplicates, solid lines the averages thereof. **F** Summary of the slopes between the 50th and 200th minute of samples in **C-E**.

4.2.5. Designing p97 entry into DNA origami prisms

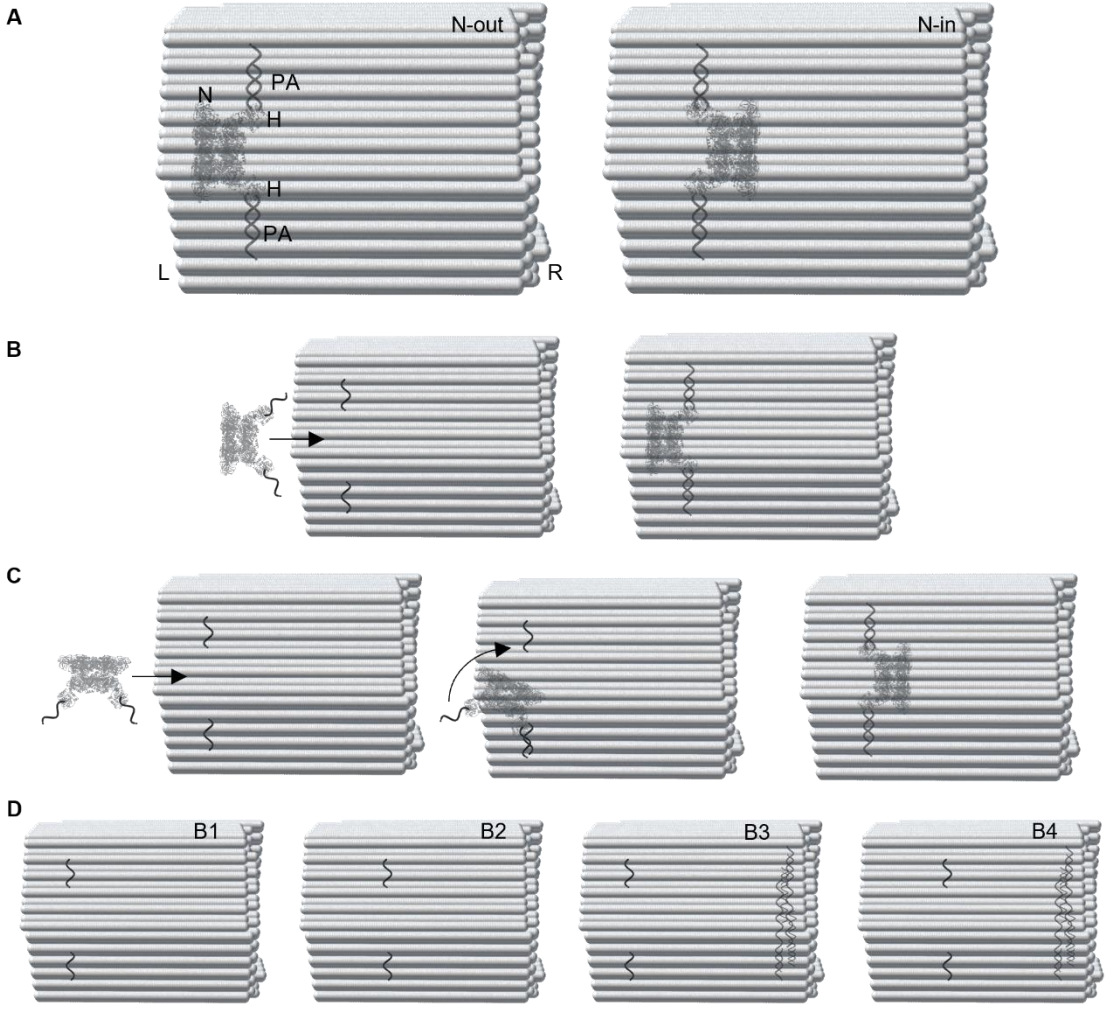

Figure 4-28: **A** When p97 would be encapsulated via its Halotags (H) and protruding arms (PA) with its central pore parallel to the prism axis, it could be oriented with D1 ring and N domains (N) either to the left (L) of the origami (N-out) or right (R) (N-in). **B** p97H entrance into the prism with its pore parallel to the DNA origami pore. **C**. p97H entrance into the prism with its pore perpendicular to the DNA origami pore. **B,C** As examples only entry from the left is shown. **D** Four constructs were investigated. B refers to the position of these in a three-prism setup. B1 and B3 have six protrusions in the left PA ring. B2 and B4 have six protrusions in the middle left ring. Additionally, diffusion barriers were designed for constructs B3 and B4, ideally leading to preferential p97H entry from the left.

The next goal was the control of p97H orientation inside the hexameric prism, with the N-terminal domains and D1 domains that either face towards the outer (N-out) or the inner (N-in) side of the DNA origami prism (Figure 4-28 A). Four routes were theorized to result in these two final orientations. The routes differ in the position of protein entrance into the prism (from the left or right side) and in the orientation of the p97 pore in respect to the cage during the entry process. For the p97 pore orientation basically two modes were assumed: a former, with the p97 pore oriented parallel to the origami prism and a latter, with the p97 pore oriented perpendicular to it (Figure 4-28 B and C left). In the pore-to-pore parallel case, p97 binding would result, respectively, in a N-in or N-out orientation if entering from the left side of the chamber with the N- or C-terminal part (Figure 4-28 B). The opposite orientations would be obtained when the protein enters from the other side of the DNA cage.

Contrarily to this, when the p97 and the DNA chamber cavities are aligned and are more perpendicular one to the other, initial binding between the DNA origami handle and the complementary sequence at the C-fused Halotag would result in the sequential binding of the next Halotag, pushing the p97 hexamer into an orientation where its pore would again lay parallel to the DNA origami pore (Figure 4-28 C). The resulting species would be N-in for entry from the left side of the cage and N-out for the entry from the right side of the cage. Of course, these are speculative considerations assuming only extreme geometric orientations of the two binding partners and serve only to illustrate the complexity of the problem.

In the attempt to control the resulting orientation, two design changes were applied on the basis of this simplified geometric model. A first modification relied on the blocking the right-side entrance of the DNA origami cage with a diffusion barrier, favoring protein entrance on the left side. A second change was the positioning of the PAs more towards the center of the DNA origami prism, thus prolonging the diffusion pathway to the first binding event. This was envisioned to make the pore-to-pore parallel orientation less prone to binding due to unfavorable steric hindrance inside the prism. The two changes resulted in four prism designs termed B1 to B4 with B corresponding to the central cage of a three-prism setup (Figure **4-28** D) (see also page 40 Figure 4-19).

For blocking one entry of the DNA origami prism, eight PAs were designed per half-prism, for a total of 16 PAs for each the left and right PA rings. Three blocking strands species were designed, each containing three segments: a 16 bases-long stretch that binds to the protruding arms, a 16 bases-long toehold for further displacement and a 0, 16 or 29 bases-long segment pointing towards the inner side of the prism to create a sort of steric blockage. The different blocking strands species were termed after their ssDNA blockage length: short (S), middle (M) and long (L) block. The block oligos were optionally 3´ Cy5 modified for tracking of binding and releasing events and 5´ NH_2 modified to allow further elongation with NHS-PEG5000 (Figure 4-29 A). The oligonucleotides were conjugated with NHS-PEG5000 as described above. Successful conjugation was shown by den. PAGE (Figure 4-29 B). MALDI spectra confirmed expected increase in mass despite low signal to noise values (Figure 4-29 C). The unusual behavior of these strands is described in appendix section III.c page 147.

Blocking strands were investigated for their capability to hinder p97 entrance into a DNA origami. For this purpose, a full prism was realized having both entries blocked by 16 blocking oligos. Encapsulation of the F9-p97H conjugate was ensured by the presence of six cF9 protrusions in the ml ring of the DNA prism. The origamis were assembled with either S-block, M-block, or L-block, using block oligos either with or without a PEG5000 elongation. As control, a full prism was used with the same PA layout but without the blocking strands. The origami units were assembled and purified from excess staples with MWCO filter. Then they were incubated with a doubly-labelled Snaptag-p97-Haloptag (Sp97H), further investigated later in this work (section 4.2.8, page 60). Besides displaying a FAM-labelled strand linked to the Halotag, this protein construct contained a N-terminal Snaptag conjugated to a TAMRA-labelled oligonucleotide. The performance of the barrier to block molecules that are smaller than the >800 kDa Sp97H was tested by incubation of the origamis with a FAM-labelled F9 oligonucleotide. The incubation took place overnight at

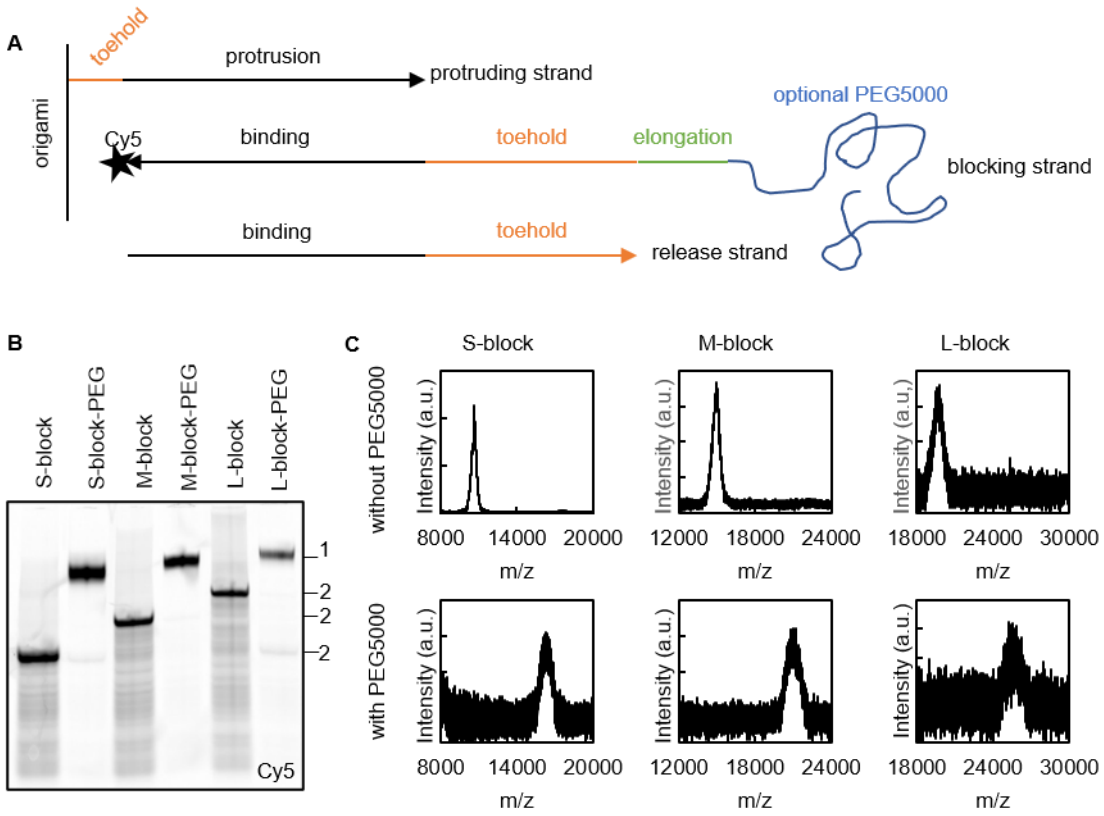

Figure 4-29: **A** The setup of the used diffusion blockage. A 22 bases long protrusion was designed pointing to the inner of the origami (upper strand). It contains a six base long toehold (orange) and a 16 base long binding region (black) to the block oligonucleotide. Three block oligonucleotides were designed (middle strand). They contained a 3´ binding region to the protruding arm (black), a 16 base toehold (orange) and an elongation (green) of 0, 16 or 29 nt for S-, M- and L-block, respectively. All block oligos were 5´ NH_2 modified allowing further attachment of an NHS-PEG5000 (blue) and could additionally be modified with a 3´ fluorophore. Finally, a release strand was designed with complementary sequence to the block strand binding domain and the 16 base toehold. **B** Denaturing PAGE of used blocking strands (2) and the purified block-PEG strands (1). **C** Conjugation of PEG5000 could be confirmed with MALDI mass spectra by mass increase of approx. 5,800-6,100 Da.

8°C and samples were investigated by AGE. The data show that increasing the length of the blocking oligonucleotides, less Sp97H was bound inside the prism (Figure 4-30 A). Additionally, when the blocking strands were PEG-modified even S-block strands could observably block Sp97H entry. For the F9 oligonucleotide only a small decrease of incorporation can be seen for PEG-modified blocking strands.

Furthermore, it was checked if these blocking strands could be reliably released so a free diffusion of molecules could be re-established in the B3 and B4 prisms after p97H encapsulation. For this, both NE entrances were blocked as described before with L-block strands, with or without PEG and an unblocked cage was used as control. The samples were purified and, prior to the overnight incubation at 8°C with p97H, the block release strand was added. The yield of p97 encapsulation upon block release was estimated by negative stain TEM (Figure 4-30 B).

Altogether, the data show that the presence of either L-block or PEG-L-block decreased the encapsulation yield drastically, however does not suppress binding completely. When the release strand was added, encapsulation efficiency was restored similar to samples without blockage, although to a minor extent in the case of the PEG-L-block sample. These findings suggest that the oligo barrier only partially hinder protein diffusion into the DNA prism and that the release of the PEG-containing oligos was not complete.

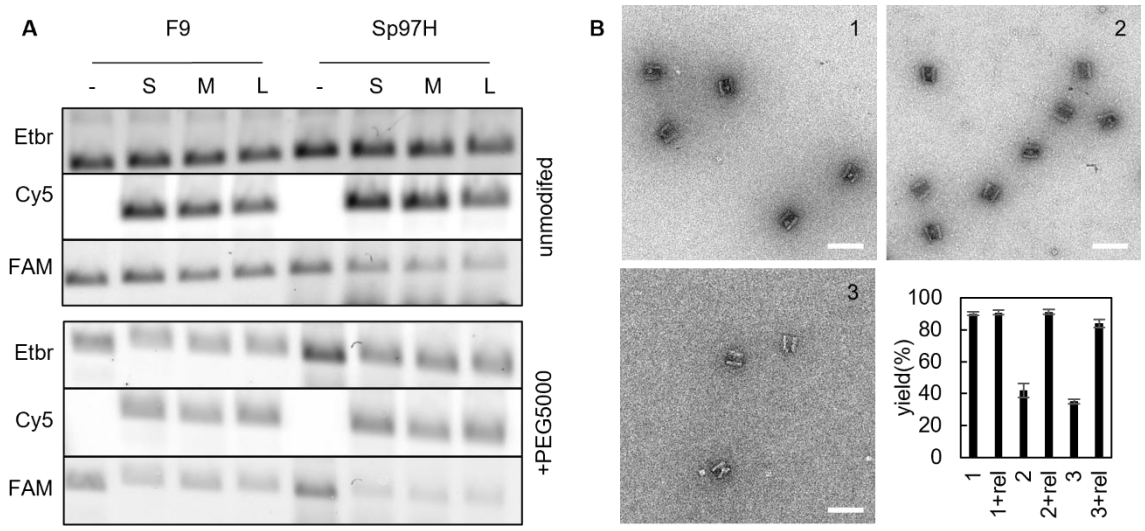

Figure 4-30: **A** NE with six cF9 protrusion in the middle left PA ring was blocked using all 16 protrusions in the left and 16 protrusions in the right PA ring with block oligos with or without PEG5000. Samples were purified from excessive staples and incubated overnight at 8°C with either FAM-labelled F9(left) or Sp97H conjugated with FAM-labelled F9 (right) and investigated by AGE. **B** Negative stain TEM images were used to calculate p97H encapsulation yield into NE with blocked entry. Encapsulation yield was as high as 90% for the unblocked sample (1) and dropped to 42% for the L-block containing sample (2) and 35% for the PEG-L-block sample (3). When release strand was added in tenfold to the block protrusions (+rel) prior to the incubation with p97H, encapsulation yield could be restored in sample 2 and also largely in sample 3 to 91% and 84% respectively. Scale bar is 100 nm.

The confirmation of successful release of L-block would allow further usage of B3 and B4 prism for activity assays later in this work without unwanted hindrance of diffusion of reactants.

4.2.6. Single molecule investigation of p97 orientation

After the development of the blocking strands, p97H orientation inside the prisms was investigated by negative staining TEM. The prisms B1 to B4 were assembled, purified, and incubated with p97H; then they were purified by SEC and submitted to the microscopic investigation. A biased orientation of p97H was expected to be visible from class averages of the structures. Hence, images were taken for all constructs and the DNA origami images were picked. The generated class-averages however did not have the spatial resolution necessary to distinguish the N-terminal domain inside the prism (Figure 4-31 A). The apparent oval shape for p97 in the prisms had similar dimensions as a p97 seen perpendicular to its pore: approx. 12 and 8 nm. In some classes, Halotags could be clearly seen, however their size and flexibility allowed no further structural insights. Proteins were found sometimes located around the center of the prism, however classification remained difficult, as also intermediate classes were obtained. Hence, no clear information about the orientation could be derived from TEM class-averages.

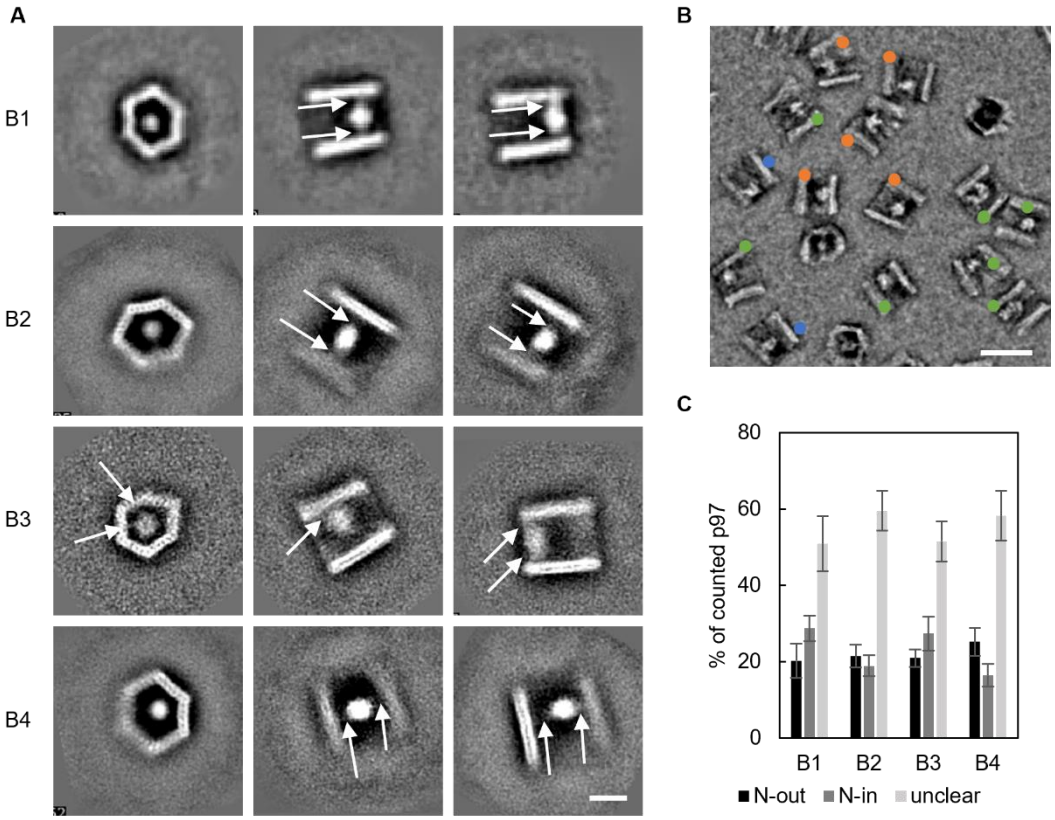

Figure 4-31: **A** Representative class averages of the four p97H containing NE constructs. Classes were sorted if p97 was more (middle column) or less (right column) in the center of the origami. Stain absence that could be interpreted as Halotags are indicated by arrows. 1,989 particles were picked for B1, 6,668 for B2, 1,619 for B3 and 7,780 for B4 at 3.71 Å/pix. 288 px was used as box size, particles were sorted and averaged in 60 classes. Scale bar is 20 nm. **B** Negative stain TEM images were bandpass filtered to cancel noise. Orientation was estimated by longest axis of protein and its relative position to the protein center of mass. Exemplary image of B1 shown here with structures interpreted as N-out (blue dots), N-in (orange dots) and unclear (green dots). Scale bar is 100 nm. **C** Approximately a thousand structures were counted for each construct as shown in B, resampled in groups of approx. 200 for estimation of sample average and variance.

In a second attempt, class-averages were analyzed such to sort p97H orientation by hand. The method applied assumes that the C-terminal Halotag domains were located along the long axis of the p97H (see also page 43 Figure 4-22) whereas the p97 occupies the majority of the protein complex mass. The distance between the long protein axis and the center of mass was used to estimate the orientation of the protein inside the prisms (Figure 4-31 B). For all B constructs, approximately 1,000 structures were categorized in this way (Figure 4-31 C), however the majority of orientations could not be categorized and the differences between N-in and N-out were not significant (Z-test>0.01).

4.2.7. Investigation of p97 orientation based on biased activity

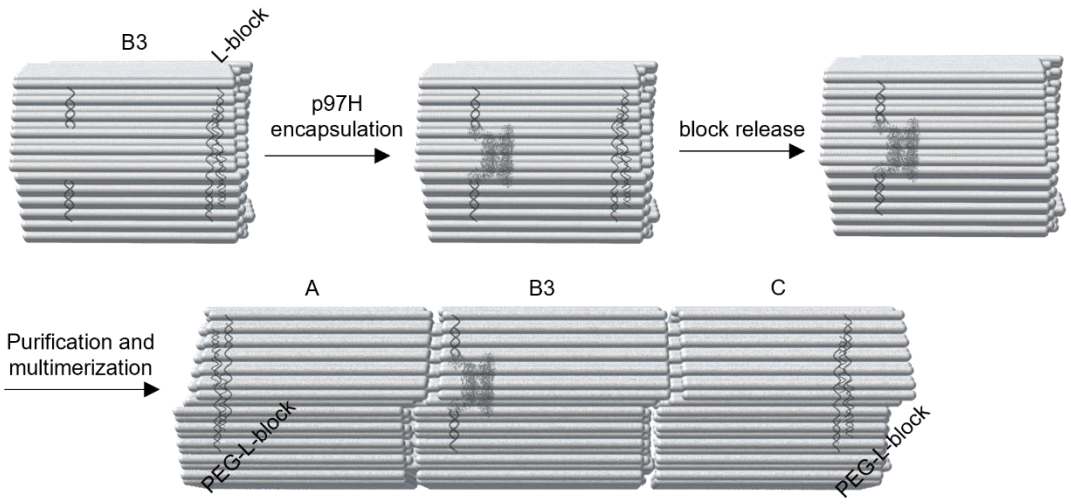

Figure 4-32: Workflow for sample preparation for biased unfolding assay. As an example, p97H encapsulation into a B3 prism is shown. Block strands had to be released after encapsulation for activity assay and the construct purified from excess protein and released blocking strands. Then the PEG-L-block containing A and C prisms were added in two-fold excess to form the respective prism multimers. Here a AB3C construct is shown.

Since the single molecule analysis did not solve the orientation issue to a reasonable extent, an unfolding assay was envisioned to verify whether a possibly biased p97H orientation could result in different unfolding profiles. Samples were prepared in a workflow as depicted in Figure 4-32. p97H was encapsulated into a B prisms and the block strand was released afterwards. Encapsulated p97H was purified from protein and DNA oligonucleotide excess by SEC. Then A, C or both AC prisms were added, which contained PEG-L-block respectively on the left and right side of the prism, thus resulting into a multi-chamber system partially blocked at both entries. This was expected to slow down SPIE and p37 diffusion, resulting in a slower unfolding rate. The decrease in reaction speed was thought to be dependent of the fraction of p97H oriented N-out or N-in, since either of them would be mostly affected by only one of the adjacent prisms, namely, N-out by the A cage and N-in mostly by the C cage. As a negative control an ABC construct was built, where the reaction was expected to be the slowest. To ensure multimeric formation, A and C prism were used in two-fold excess over the B prism.

The unfolding assays for the B1 constructs showed that the unfolding rate is surprisingly faster for AB, BC and ABC constructs when compared to the single B1 construct (Figure 4-33 A), despite the usage of the PEG-L-block barrier. This suggested that, contrarily to p97, the smaller p37 protein and SPIE complex were seemingly not hindered to enter the inner cavity of the prisms even in presence of a PEG-L barrier (compare Figure 4-30 A p. 54). The permeability of the barrier to small (or unstructured) proteins may also explain the lack of accumulation of unfolded substrate in the A or C prisms of the AB and BC constructs, when imaged by negative stain TEM (Figure 4-33 C and D).

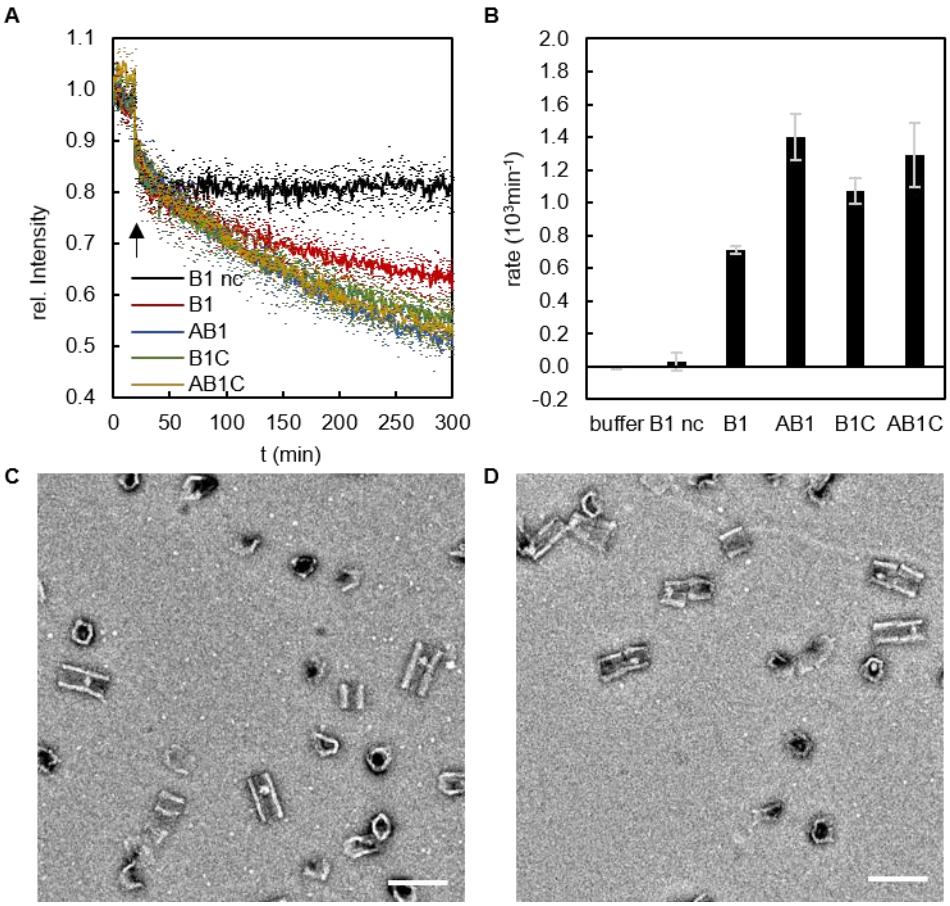

Figure 4-33: **A** Unfolding reaction of the multiprism constructs. B nc was a B prism control without p97H. Arrow indicates E-Mix addition. **B** Decrease of relative fluorescence between 50 and 200 minute. **C** Bandpass filtered negative stain image of the AB1 construct after 300 minutes of the assay. **D** Bandpass filtered negative stain image of B1C construct for the same conditions. No accumulation of unfolded species can be found in A or C prisms. Scale bars are 100 nm.

To compare the reaction rates of the different constructs, the linear decrease of the relative fluorescence in the 50-200 min time range was taken for each sample (Figure 4-33 B). As the reaction rate was influenced positively by addition of A and C prisms, the usage of PEG-L-block in them was dismissed. All B constructs were made, p97H was encapsulated, and the samples were purified by SEC. Multimerization was done by addition of the respective purified A and C prism in two-fold excess over the B prism. The multimeric prism setups devoid of p97 were checked by AGE (Figure 4-34 A), whereas the p97 loaded analogs were analyzed by negative stain TEM (Figure 4-34 B).

DNA origami structures were used at 1 nM concentration of B prism for all samples. The unfolding reaction was monitored in triplicates for all samples and interpreted as described before (Figure 4-35). The TEM data were used to calculate the encapsulation yield in the B constructs and the reaction rate was normalized to the same p97H concentration of approximately 1 nM (Figure 4-35 E). An increased activity was found for all multimeric prism setups when compared to the monoprism counterpart. Time courses of the triplicates were found to be quite similar (with very few exceptions, like one curve in B3, B3C and B4 nc), with comparable linear phases. AB, BC and ABC unfolding rates were quite similar for the same B species. The highest unfolding rate was observed in the B2 constructs, despite their similarity to the B4 prism after

L-block release. However, comparison between sample should be carried out with care due to possible unprecise concentration measurements.

Surprisingly, ABC construct show a similar activity increase as AB and BC constructs. The possible reasons for this remained elusive and are discussed in section 5.2.

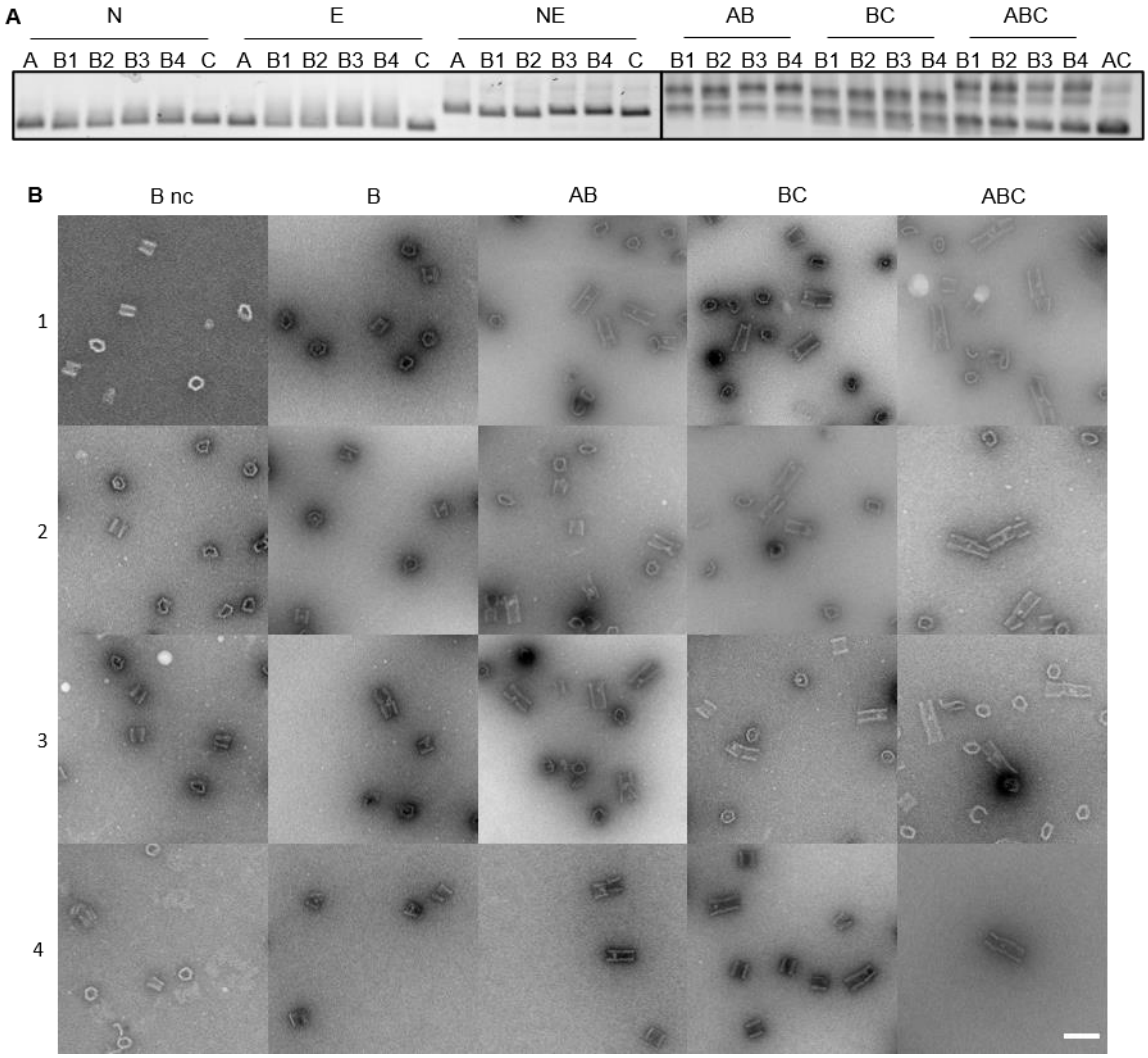

Figure 4-34: **A** AGE of all origami constructs used in the SPIE unfolding assay. **B** Exemplary negative stain TEM images of most of the constructs measured in the unfolding assay. Scale bar is 100 nm.

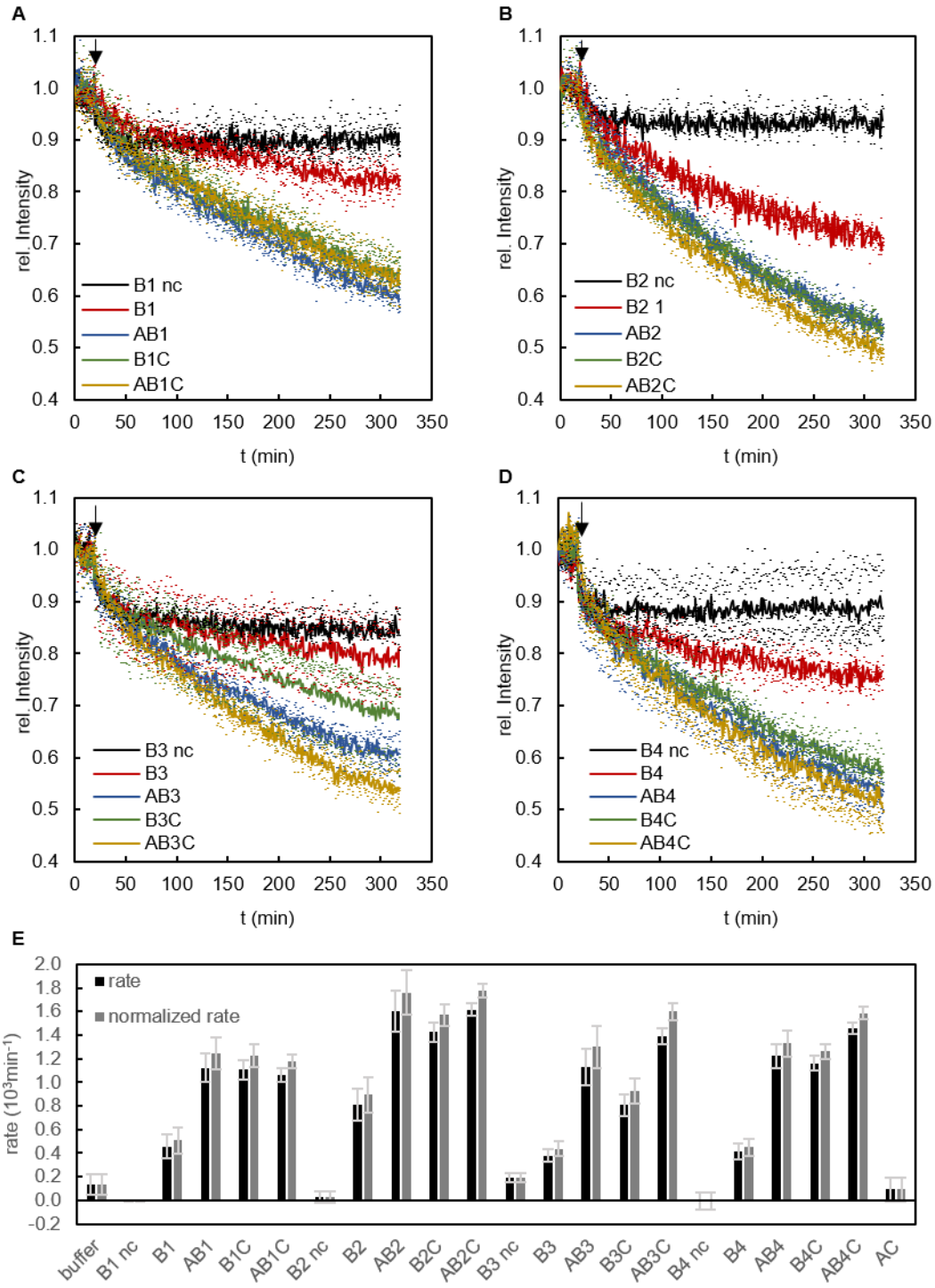

Figure 4-35: **A**-**D**: Activity assay of the B1-B4 and their multimeric constructs containing p97H compared to origami only samples (B nc). Dots show data points for each triplicate and solid line the average thereof. Arrows indicate E-mix addition. **E** Rates for all samples investigated. Buffer curves and AC curves were not shown in **D**.

4.2.8.Topological marking orientation of p97

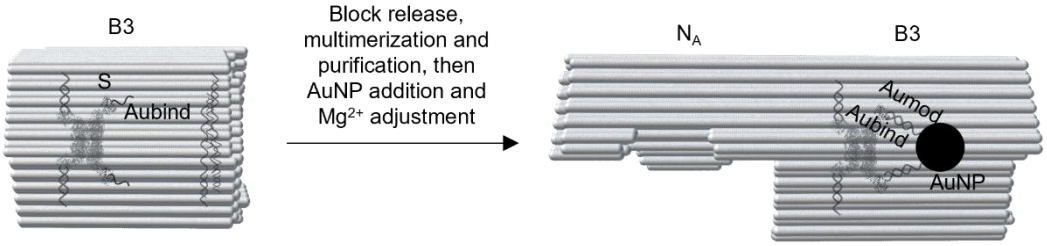

Figure 4-36: Schematic workflow for marking of p97 with AuNP inside a DNA origami prism. Sp97H was labelled with Aubind via its Snaptags (S) and encapsulated in a construct of choice (here B3). It was incubated with block release and an additional origami as a marker (N_A). Successive purification via FnS and incubation with AuNP in 50 mM Mg^{2+}.

Another strategy was considered to investigate the orientation of p97 inside the prisms: The idea behind this approach was that the N-terminal domain should be well accessible in the DNA origami cavity and could potentially been used for topological marking. Initial attempts with primary and secondary antibodies against the N-terminal p97, further linked to AuNPs, as well as with the Ufd1-Npl4 adapter or incubation with Snaptagged p37 bound to AuNPs failed; however gave some insights over AuNP handling in this setup (see appendix section III.d, page 148 and following). In a further attempt, Snaptags were cloned to the N-terminus of p97H resulting in Sp97H. This large construct was envisioned to be encapsulated into the DNA origami prism in a similar way as the p97H, with the advantage to provide an additional point of attachment at the N-terminus of the protein. The Snaptags were conjugated with a 16 bases long oligonucleotide called Aubind partially complementary to a strand Aumod used to decorate small AuNPs. The latter contained a 5´thiol group for attachment to the AuNP, a T_{10} sequence to ensure flexibility and spacing and a four bases toehold for further displacement.

The labelling of the N-terminus with AuNP was performed (Figure 4-36), upon release of the blocking strands, similar to the experiments described above. To better distinguish the left and right of the DNA prism, additional N_A half-prism was added as topological marker.

For conjugation to the Snaptag, 5´ NH_2 modified Aubind was conjugated to NHS-BG derivative (Snap) and purified from excess ligand (Figure 4-37 A). Sp97H was simultaneously reacted with Halo-F9-TAMRA and Snap-Aubind-FAM overnight at 8°C. The resulting conjugate was successfully purified by SEC (Figure **4-37** B). Analysis of the fluorescence gel band intensity in the Coomassie gel band intensity in SDS-PAGE showed double label efficiency of approximately 48% and an additional single label efficiency of 30% for the Halotag and 14% for the Snaptag (Figure 4-37 C).

The DNA sequences at the N-termini of the Sp97H construct allowed not only the theoretical labelling with nanoparticles but also an additional binding site to the DNA origami prism. Thus, the original B2 prism, bearing six (ml) protrusions for encapsulation of p97 at the C-terminal Halo tag, was modified with one (B5) or three (B6) Aumod protrusions in the mr ring of Narcissus to catch the protein at the N-terminal Snaptag. Similarly, B7 and B8 were derived from B4 (Figure 4-38 A).

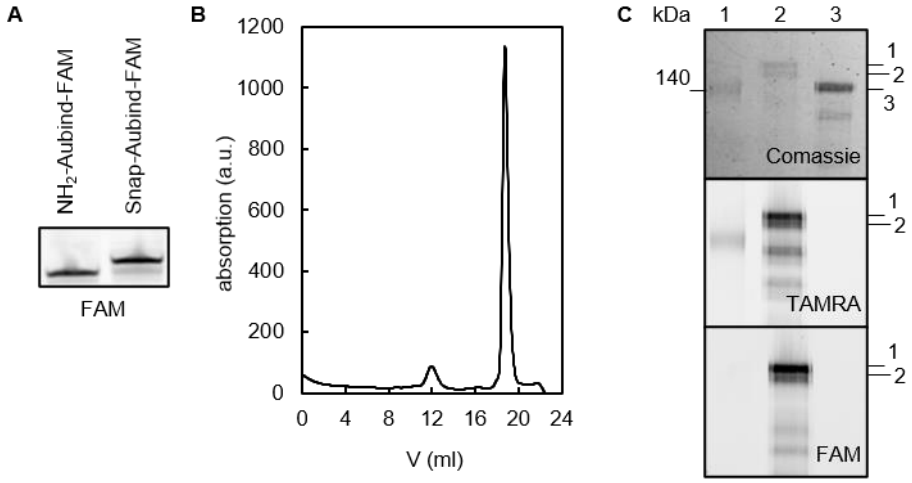

Figure 4-37: **A** Snaptag linker conjugation was confirmed by denaturating PAGE. **B** SEC elution profile of parallel conjugated Sp97H via Halotag and Snaptag. **C** SDS-PAGE confirmed successful double conjugation with FAM labelled Aubind and TAMRA labelled F9 with both single-(2) and double labelled (1) protein bands in the conjugate sample (lane 2). Negative control loaded in lane 3 (nc) was Sp97H only (3). Broad range ladder (lane 1) was used. Double label efficiency of p97 monomers was calculated from band intensities in the different channels to be 48%. Single label efficiency was 30% for the Halotag and 14% for the Snaptag. The residual 8% were potentially unconjugated p97 monomers, which could not be visualized.

The samples were assembled, purified and incubated overnight at 8°C with tenfold excess of Sp97H. Block release strands were added to the constructs B3, B4, B5 and B6 in tenfold excess over the block protrusion and the topological marker N_A was added to all samples. Incubation was performed at room temperature for 5 h. Successive purification was done by FnS from AGE to allow simultaneous removal of excess DNA strands and protein. AuNP were decorated with Aumod and purified from excess DNA strands with 100 kDa MWCO filter. Purified DNA origami samples were adjusted to 50 mM $MgCl_2$ and incubated with AuNPs overnight at RT. Then all samples were investigated by negative stain TEM (Figure 4-38 B).

Encapsulation yield, AuNP label efficiency of the protein and position of that label were counted from the respective images (Figure 4-39). Encapsulation yield was around 80% except for B4 and B8, most likely due to unprecise Sp97H concentration as a consequence of protein precipitation. Label efficiency was between 15% and 25%, hence most of the orientations of Sp97H remained unknown. Labelled structures showed no significantly preferred positioning of the AuNP in respect to the topological marker except an unforeseen N-out orientation for B5.

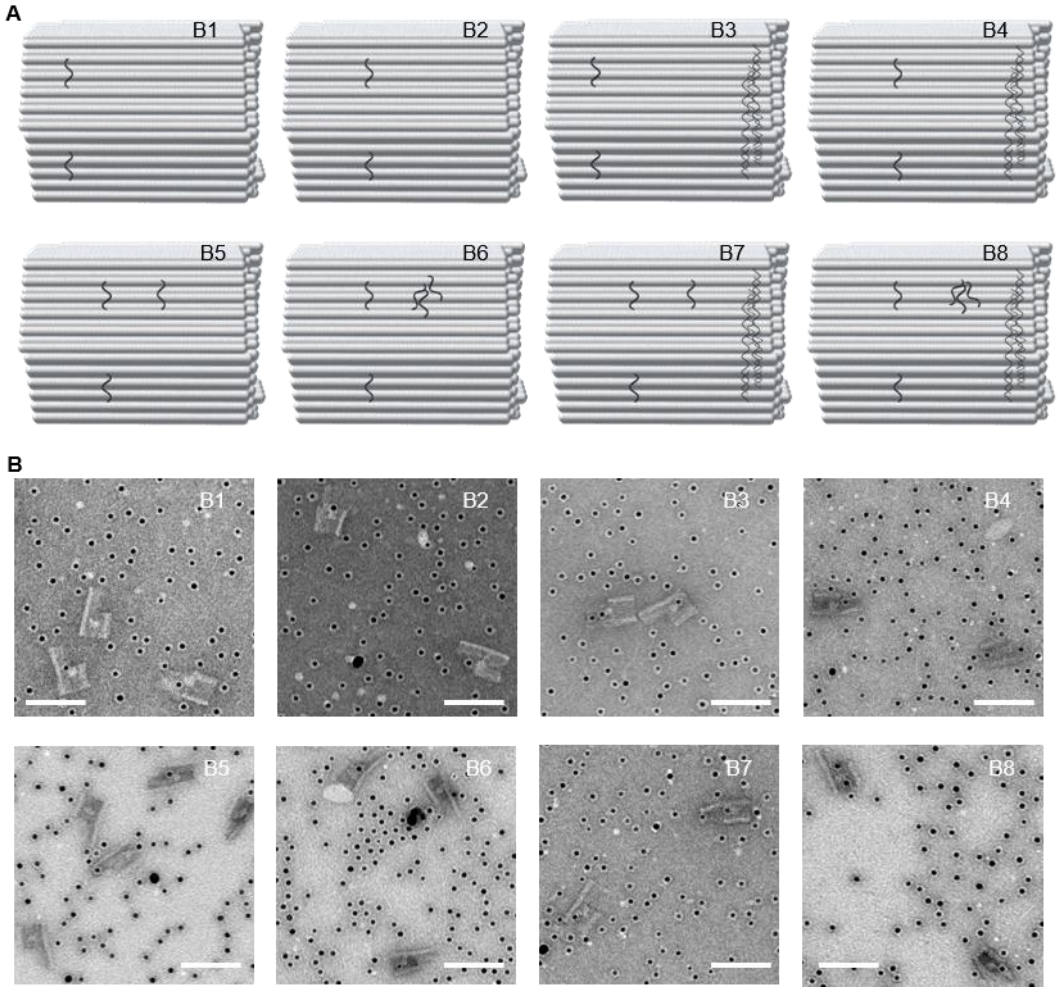

Figure 4-38: **A** Aubind oligonucleotides were allowing an introduction of a second anchoring point for Sp97H. Constructs B1-4 were the same as before, B5 and B6 were derived from B2 with six protrusions in middle left position but with one or three additional Aumod protrusions in the middle right position respectively. This allowed additional binding of the Snaptags of Sp97H to N_B. B7 and B8 were similarly derived from B4. With six cF9 protrusion in the middle left position and L-blockage on the right but again with one or three Aumod protrusions for the Snaptags of Sp97H. **B** AuNP binding to Sp97H in all eight constructs was investigated by negative stain TEM. Scale bars are 100 nm.

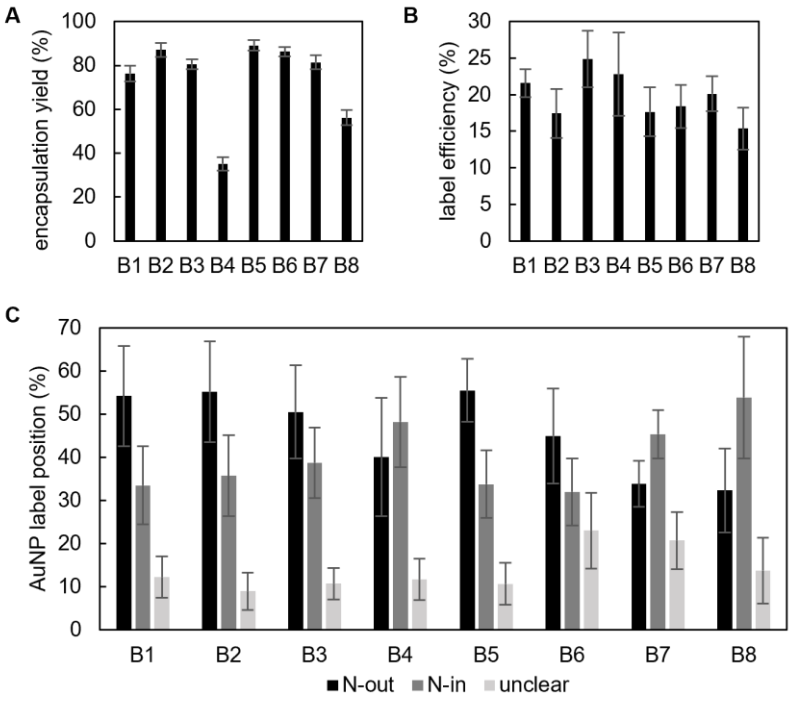

Figure 4-39: **A** Encapsulation efficiency was generally high at around 80%, however not for B4 and B8. **B** Label efficiency with AuNP of encapsulated Sp97H was between 15% and 25%. **C** Label positions indicate some preference for N-out or N-in some samples. Unclear label positions were p97 labelled between origami wall and protein or p97 labelled simultaneously for both N-out and N-in. Average and variance data obtained by resampling in groups of approx. 200 structures.

4.3. Binding of thermophilic proteins to a DNA origami

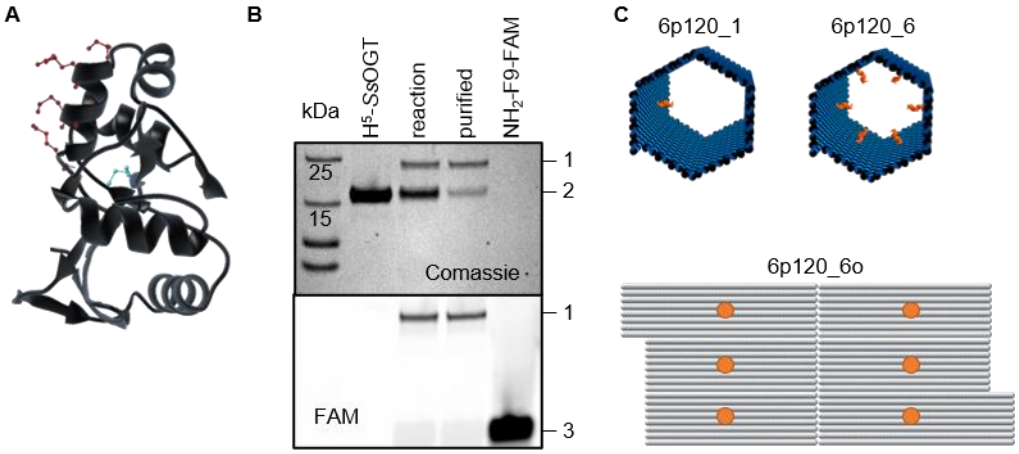

Figure 4-40: **A** Crystal structure of *Ss*OGT (pdb 4zye). Mutated amino acids in H^5 variant are shown in red. Catalytic active cysteine is shown in cyan. **B** SDS-PAGE was confirming reaction between BG-modified and FAM labelled F9 oligonucleotide (3) with H^5-*Ss*OGT (2). Purification by BG modified beads shows specific pull-down of excess active *Ss*OGT over the conjugate (1). **C** Origami used in this project were 6p120 hexaprisms with one (6p120_1) or six protrusion (6p120_6). Also, one open form of the latter was developed by leaving out staples in two hinge regions leading to a nearly rectangular origami with two rows of three protrusions (6p120_6o, orange dots indicate protrusion positions).

In order to enable work with thermophilic proteins in a DNA nanotechnology context, a thermophilic protein tag was investigated. H^5*Ss*OGT is a DNA alkyltransferase (enzyme class: 2.1.1.63) mutated to suppress DNA binding (Figure 4-40 A). This mutant form can react with O^6-alkyl guanine derivatives via its catalytic Cys_{119} thiol group, thus maintaining the catalytic activity similar to the commercially available Snaptag however surviving at higher temperatures (T_m at 75°C).[236] The H^5*Ss*OGT used here were produced in the laboratory of Dr. G. Perugino at the Institute of Biosciences and Bioresources (Neaples, Italy) as already published[238]. Protein samples were sent to our laboratory and conjugation to the benzylguanine (BG)modified oligonucleotide F9(16)-FAM was carried out with excess of protein over the oligonucleotide at 50°C for 1 h. Excess H^5*Ss*OGT was pulled down using benzylguanine modified agarose beads in a roll shaker overnight at 8°C. The conjugate appeared as the major product band in SDS-PAGE, however around 40% of protein was still unconjugated (Figure 4-40 B). This purification method was not further optimized due to the facts, that the unconjugated protein does not bind DNA and will be separated in later AGE based purification.

Three DNA origami were used for initial principal investigations: a closed monolayer DNA prism (6p120) with either one or six protrusion arms and one with six protrusion arms, however lacking two hinge staples leading to a planar open form of the construct called 6p120_6o (Figure 4-40 C). The latter was developed in order to make the proteins better visible under AFM imaging, with no DNA layer on top of them.

All three constructs were assembled using the following thermal gradient: an initial temperature of 65°C for 10 min, and a decrease to room temperature with a rate of -2°C/min. Two experiments were performed: in the first, protein conjugates were added after the assembly of the DNA origamis and in the second, they were added already prior to the assembly. In the first experiment, four samples for each origami were

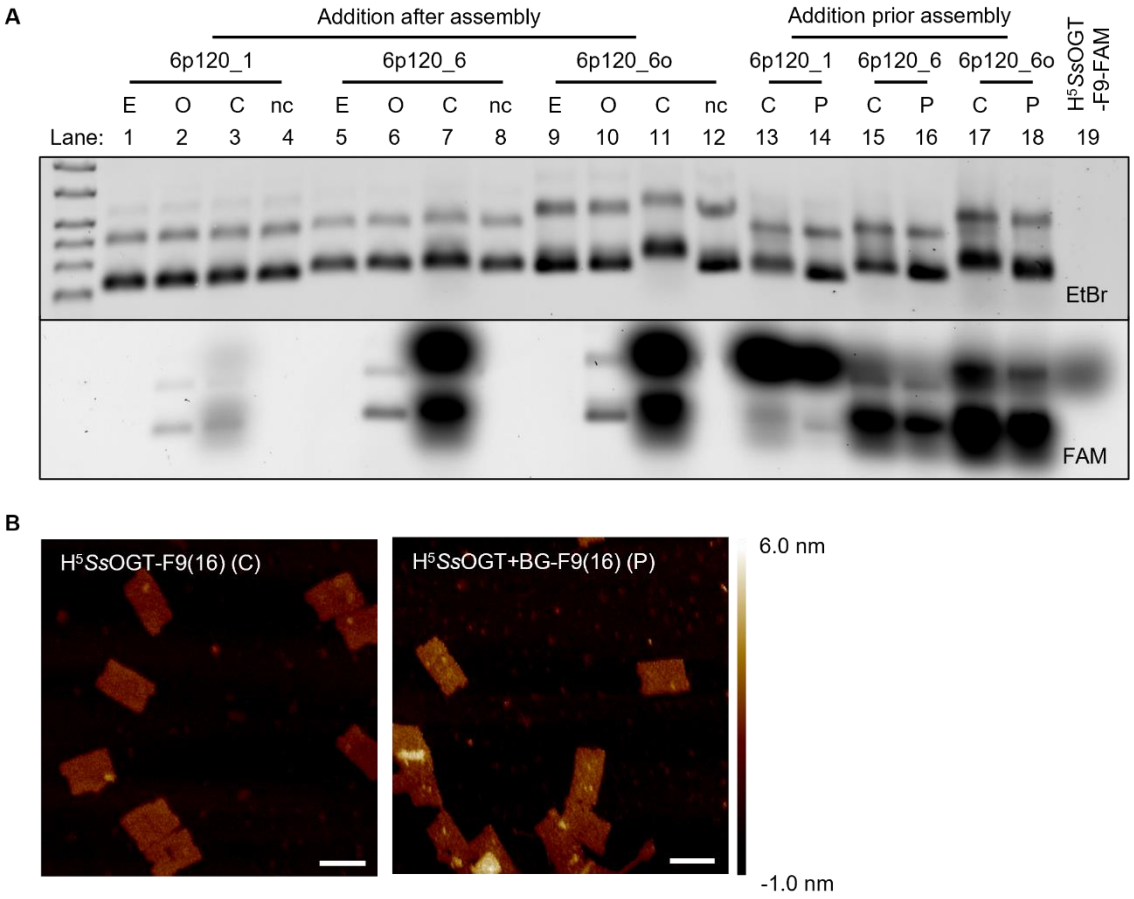

Figure 4-41: **A** AGE of empty origamis (E), with addition of either F9(16)-FAM (O), H5SsOGT-F9-FAM conjugate (C),H5SsOGT (nc) or BG-F9(16)-FAM and H5SsOGT separately (P). Addition was done either after or prior to an adjusted assembly procedure. **B** AFM images of 6p120_6o incubated with the conjugate (left) or the DNA and the protein separately (right) during the assembly. Scale bars are 100 nm.

prepared: the empty construct with only the protruding cF9 strand, the same construct with the complementary F9-FAM, the construct with the H5*Ss*OGT-F9-FAM conjugate and finally the construct with H5*Ss*OGT as negative control. Conjugate and F9 were added in ten-fold excess to the protrusions. For the second experiment, either 10-fold excess benzyl guanine-F9-FAM and 20-fold excess H5*Ss*OGT over the cF9 were used or 10-fold excess of the pre-formed conjugate were used. Samples were investigated by AGE (Figure 4-41 A). 6p120_6o samples were also investigated by AFM (Figure 4-41 B).

The gel results showed that the conjugated H5*Ss*OGT shows similar electrophoretic mobility as the origami dimer band (Figure 4-41, lower image, lane 19) and when bound to the complementary cF9 staples present in the assembly mixture, its migration was similar to the monomeric DNA origami (Figure 4-41 A, lower image, lanes 3, 7, 11, 12-19). This impeded the clear visualization of protein binding to the DNA origami in the FAM channel. The signal obtained in the FAM channel confirmed binding of the F9 DNA strand to the origami as expected (Figure 4-41 A, lower image, lanes 2, 6, 10). Successful conjugation between the protein and the oligonucleotide during DNA origami assembly could be also confirmed, resulting in similar bands as for the H5*Ss*OGT-F9-FAM conjugate used after assembly(Figure 4-41 A, lower image, compare lanes 7 and 11 with lanes 14, 16 and 18)

Addition of the conjugate always led to a decreased electrophoretic mobility of the origami band, especially for the 6p120_6o construct (Figure 4-41 A, upper image, lanes 3, 7, 11, 13, 15, 17). This was also true when the construct was added already prior to the assembly. Separate addition of modified oligonucleotide and H^5*Ss*OGT was not resulting in any considerable shift (Figure 4-41 A, upper image, lanes 14, 16, 18).

Unexpectedly, AFM images showed modified origami sheets both when reacted with a pre-formed conjugate and when H^5*Ss*OGT and benzylguanine modified oligonucleotide were added separately (Figure 4-41 B) prior to the assmembly. As the conjugate is reported to be less thermostable than the unconjugated protein (T_m below 65°C)[236], one explanation might be that proteins found in AFM imaging were in different states. A denatured conjugate would result in a less dense total DNA-origami structure and could account for the stronger shift in electrophoretic mobility. The H^5*Ss*OGT conjugated during the DNA origami assembly would lead to incorporation of the more compact native proteins. In both cases protein could be found in AFM attached to the DNA origamis. Alternatively, H^5*Ss*OGT was unspecifically binding to the DNA origami, however washed away during gel electrophoresis.

Nevertheless, the one-pot binding of the DNA-protein conjugate to the origami was confirmed and hence its potential usage for protein encapsulation during DNA origami assembly is feasible. However, the project was not continued due to problems in production of thermophilic proteins tagged with H^5*Ss*OGT.

4.4. Encapsulation of proteins in random orientation

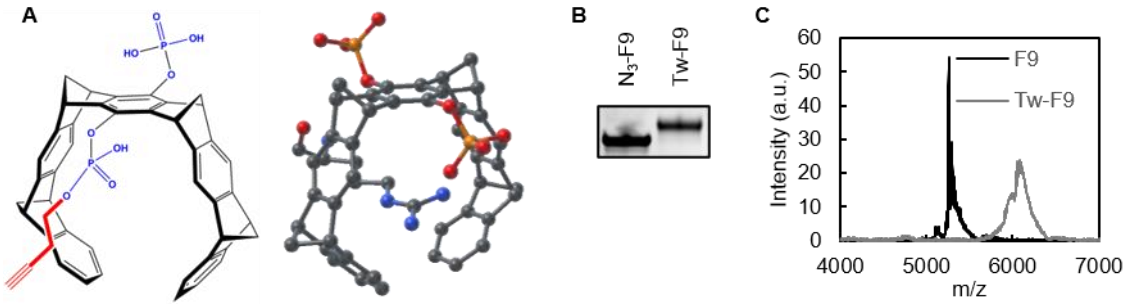

Figure 4-42: **A** Alkyne modified (red) molecular tweezer CLR01 (left) and three-dimensional structure of a similar unmodified tweezer coordinating an arginine (right). **B** Denaturing PAGE confirm successful conjugation of F9 to tweezer by click chemistry and purification thereof. **C** MALDI spectra of the same oligonucleotide and conjugate (theoretical 5,262 Da and 6,038 Da).

The usage of low affinity binders to encapsulate proteins in DNA origami structure is up to now an unusual approach. However, the possibility to use multiple weak binders simultaneously can be interesting to develop multivalent systems for encapsulation purposes. One strategy is to address charged amino acid residues, such as lysine, on protein outer surfaces, using lysine-selective molecular tweezers. To achieve this goal, a cooperation project started with the group of Prof. Dr. T. Schrader (UDE) and his former PhD student Dr. Christian Heid kindly provided the alkyne modified tweezer CLR01 (Tw).[256] This ligand was described to bind to lysins and arginines with a K_D in the medium μM range (Figure 4-42 A)[241–243].

The tweezers were conjugated to the azide modified oligonucleotide F9 using copper(I)-catalyzed azide-alkyne cycloaddition. The conjugate was successfully purified by denaturating PAGE and precipitation in isopropanol and the formation of the conjugate could be confirmed by a shift in PAGE and mass increase in MALDI (Figure 4-42 B and C). Note, that for the latter an additional increase of 17 Da was found, most likely due to incomplete dilution of NH_4^+ salt.

As a model protein for multivalent tweezer binding, the oligomeric $DegP_6$ was used since it contains a high amount of lysine and arginine residues (Figure 4-43 A). The protein was produced by Pierre Stegemann in our lab, who also works on DNA-driven protein encapsulation via a different approach. The protein was further mutated to be inactive (SA mutant) and to contain one cysteine per subunit which can be used for labelling, in this case with Alexa650-malemide.

In the first trial, the inner of 6p120_18cF9 was decorated with Tw-F9 during DNA origami assembly. The origamis were then purified by PEG precipitation and 5 nM was incubated with 50fold excess of Alexa650 modified $DegP_6$ and incubated at 8°C overnight. Investigation by AGE did not show any binding to the origami. This called for an increase of protruding arms in the 6p120 as described in section 4.1.1. All 54 protrusions were used to decorate the inner cavity with tw-F9. Purified origamis were again incubated with the labelled protein and binding events were found in AGE (Figure 4-43 B). Note, that there was also some considerable unspecific binding to the prism in the absence of tw-F9. The samples were purified from the gel by FnS and investigated by AFM, confirming protein encapsulation (Figure 4-43 C).

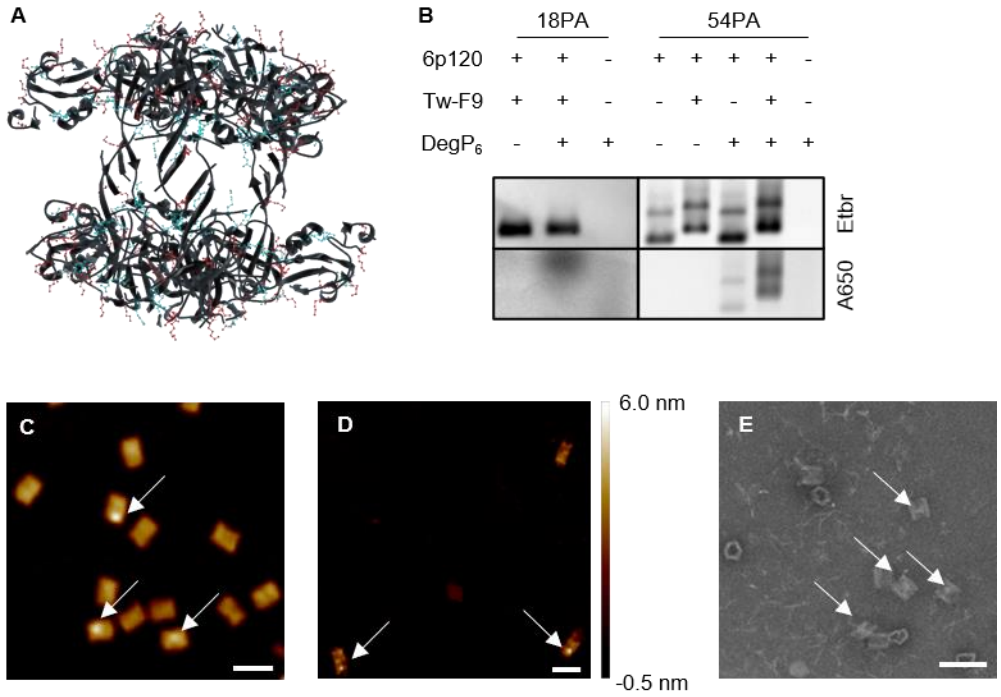

Figure 4-43: **A** Model of $DegP_6$ with marked lysins (red) and arginines (cyan). The total complex has 108 lysins and 66 arginines. **B** AGE shows that decoration of 6p120 with 18 protrusions with tweezers was not sufficient to bind A650-DegP6(SA). However, when number of protrusions was increased to 54, binding of the protein became evident. **C** AFM image of the FnS purified of encapsulate DegP6 in 6p120. Encapsulated DegP6 is marked with arrows. **D** AFM of N with 32 protrusions decorated with tweezers led also to the binding of $DegP_6$. This construct was also purified by FnS and shown here. Bound $DegP_6$ indicated by arrows. **E** Negative stain TEM imaging confirms the binding to NE with 64 tweezer moieties after purification. Scale bars are 100 nm.

In a similar attempt, Narcissus was decorated with 32 protrusions and bound to tweezers to encapsulate $DegP_6$. Binding was confirmed under AFM inspection of FnS purified samples (Figure 4-43 D). Using the full NE prism with 54 protrusions precluded analysis via AFM, probably due to the higher stability and thickness of the bilayer structure. Nevertheless, encapsulated protein was found when FnS purified samples were investigated by negative stain TEM (Figure 4-43 E).

To test if the lysine-specific tweezer ligand could be used for several proteins, p97 was used as a second model protein. With a few hundred lysine and arginine residues, this protein was supposed to be an ideal candidate (Figure 4-44 A). However, no binding could be detected by AGE (Figure 4-44 B). Various conditions as incubation time, temperature, protrusion arm length and pH were investigated by Michelle Hechler during her master thesis (our group), but no encapsulation events were found.

In a further experiment, different buffers were tested that do not contain amines. Additionally, magnesium iones were removed, since it was reported that the CLR01 tweezer might have a binding affinity to zinc[257] which has a similar ion radius as magnesium. Hence, cacodylate buffer at pH 6 was chosen and the assembly of 6p120 was screened for optimal calcium concentration (Figure 4-45 A). Formation however was not as well as for the TEMg buffer, so the structural stability of origami and p97 were investigated when the buffer was exchanged to caco7ca. Both species showed native dimensions for these conditions when investigated by AFM (Figure 4-45 B). Furthermore, samples were not purified by FnS to avoid electric and centrifugal forces. Samples were simply applied on mica, dried and the colocalization events of p97 and the origami counted.

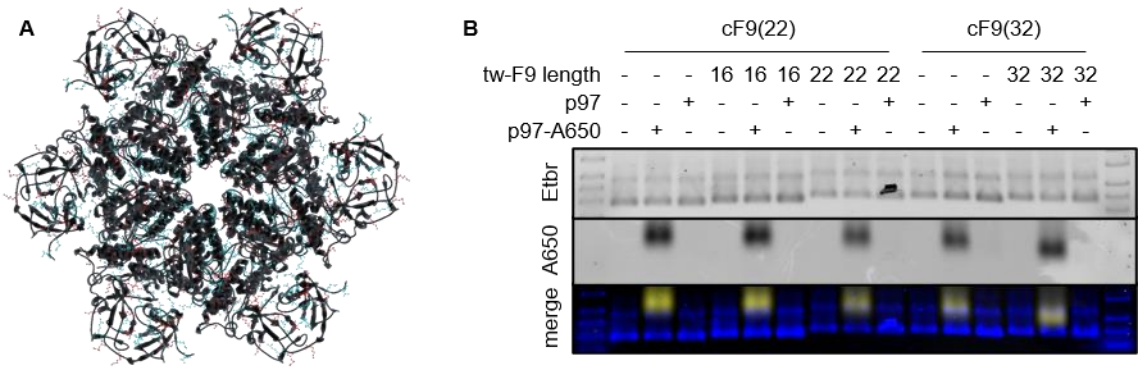

Figure 4-44: **A** Model of p97 in the resting state (pdb 5ftk) with marked lysines (red) and arginines (cyan). The protein complex contains 264 lysines and 312 arginines. **B** AGE results from master thesis of Michelle Hechler showed that independently of protrusion length and protrusion stiffness, p97 binding was not evident in this technique.

The results indicate a protein association to DNA origami modified with tweezer, however the sample-to-sample variance was immense (Table 4-4). The encapsulation strategy was stopped due to hardly reproducible results and low yields. Another promising attempt using Nitrilotriacetic acid (NTA) modified DNA strands as described by Ouyang et al.[258] failed similarly (see appendix section IV.a, p.151). Other ligands that were conjugated to the F9 oligonucleotides, however not further investigated, can be found in appendix section IV.b, p.153.

Table 4-4: Encapsulation yields and calculated K_D between p97 and decorated origami derived thereof for four different samples.

	sample		control		
condition	counted	yield (%)	counted	yield (%)	K_D (nM)
5 nM origami-tw, overnight 8°C	2439	2.6	5460	1.1	13128
5 nM origami-tw, 4 h RT	314	17.8	1570	4.8	1334
3.5 nM origami-tw, overnight 8°C	1193	10.2	1100	3.9	2971
5 nM origami-tw, overnight 8°C	2720	7.0	2085	1.4	3367

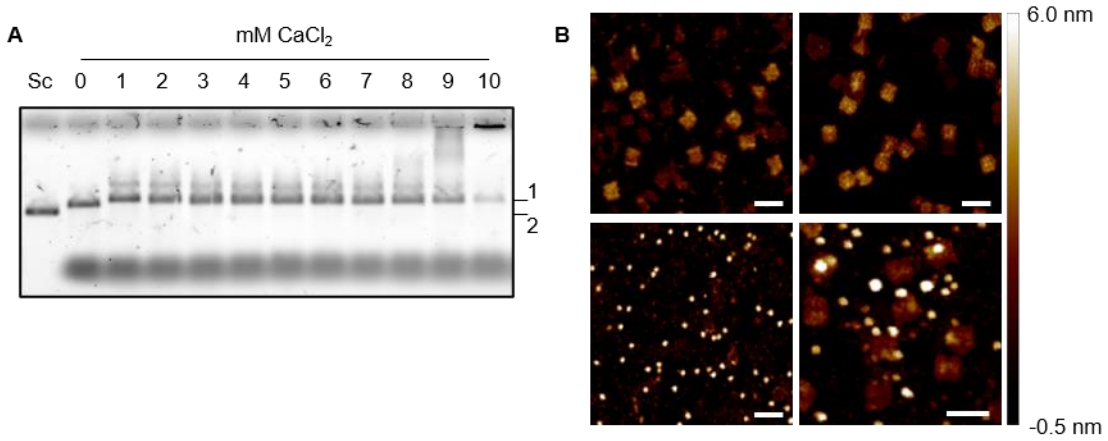

Figure 4-45: **A** AGE of an calcium screening for 6p120 assembly in cacodylate buffer. **B** AFM images of origami assembled in caco7Ca (top left), assembled in TEMg and washed with caco7ca over 100 kDa MWCO filter (top right), p97 (bottom left) and tweezer decorated 6p120_54 incubated with p97 in caco7Ca (bottom right). Scale bars are 100 nm.

5. Discussion and outlook

5.1. DNA constructs

A new DNA origami shape was designed to encapsulate large protein cargos (max ca. 30 nm in diameter) overcoming previous issues due to structural flexibility of the prism. This DNA chamber is formed by two shape-complementary origami units (N and E) bound together by base-hybridization. The design of the first half (N) had to be optimized to hinder unspecific interactions between the origamis. Four bases-long unstructured loops were reported in the literature[136,204] to be sufficient to ensure DNA origami passivation, however scaffold overhangs of four bases were not sufficient in our case to hinder self-association (Figure 4-5 p.28 and Figure 4-17 p.38). DNA origami structures fully lacking the edge staples resulted into unstructured single-stranded regions of the scaffold about 11 to 36 bases long and were instead stable in the monomeric form, similar to what has been described for other structures.[73,137,154] Unspecific base stacking interactions could be also successfully suppressed by a six thymine-elongation of the edge staples along the DNA helical axis.

Self-dimerization of the N structure by stacking of six helix bundles implied a 5´-5´ and 3´-3´orientation of the interacting helices. This configuration is rarely used and investigated in the field, however also reported to allow DNA origami stacking[159]. Structural investigation of the dimers by AFM revealed incompletely closed structures. This failure can be attributed either to an AFM artifact or to a design issue. For this reason, a second structure (E) was envisioned that, when bound to N would allow formation of a full hexameric hollow prism, termed NE.

Full-prism formation could successfully be proven by AFM, negative stain TEM, agarose gel and DLS. The kinetics of dimer formation was obtained by DLS at room temperature. The structure NE displays a higher amount of addressable sites, a lower flexibility[259,260] compared to the 6p120 prism. It had suitable dimensions for encapsulation of our target proteins, thus fulfilling the structural needs required for our purposes. The C6 symmetry of NE could be confirmed in negative stain TEM, with small deviations probably derived from staining artifacts (Figure 5-1 A). In particular, the size of the inner cavity was about 26 nm (wall-to-wall) in negative stain TEM, which is ca. 4 nm shorter than the expected distance from design. This empirical knowledge might be used in future similar designs.

During this work, the initial assembly procedure for the full prism was drastically shortened to approx. five hours, making sample preparation fast without oozing in assembly quality. However, the assembly process could potentially be further optimized with better knowledge about the melting behavior of N and E. This might be investigated in future projects by using fluorescence or UV spectroscopy to monitor thermal changes during the assembly.[147,166,261,262] Dimerization processes might also be shortened. For this a broader temperature range could be screened by DLS using different origamis concentrations.

Furthermore, Nemesis was successfully multimerized to form a superprism consisting of up to three NE subunits. Some structures showed small gaps between the subunits when analyzed by negative stain TEM

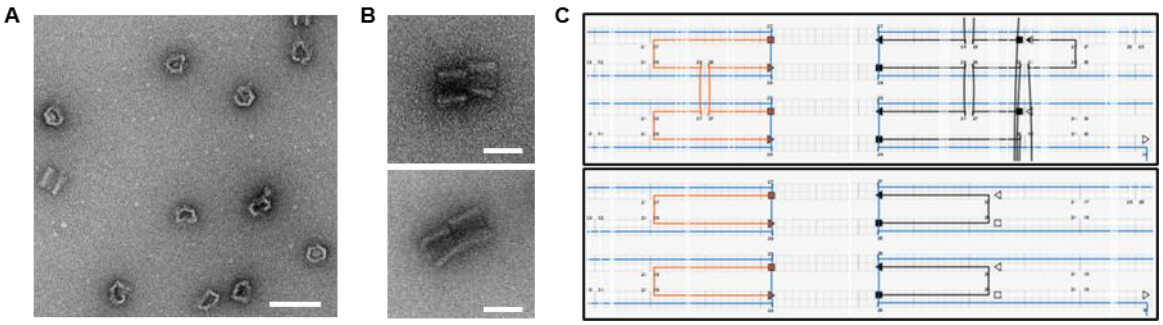

Figure 5-1: **A** Several NE B2 prism can be seen with parallel pore axis in this negative stain TEM image. Note, that the hexagonal shape seems to be distorted to some extent in most structures. Scale bar is 100 nm. **B** Exemplary negative stain TEM image of AB4 (top) and B4C (bottom) constructs. A gap/offset between two prisms can be seen in these constructs, however it could have been visualized for all dimers and trimers. **C** Current (upper) right (orange) and leftt (black) edge staple of a NE site. If one left staple with overhangs was used in the left edge it might have two corresponding right staples which would finally result in short free scaffold overhangs. By designing the staples pairwise this problem might be circumvented (lower).

(Figure 5-1 B). Despite this might be explained as a staining artefact, the same issue was reported by others as well[62,263]. Since the design was initially not planned for multimerization, troubles arose most likely due to unoptimized edge staples. When one staple was changed in one edge, in some cases two corresponding staples in the respective other edge had to be changed. The resulting four bases scaffold overhangs, similar to passivation in edge staple set 2, were seemingly insufficient to suppress helix blunt end stacking between origamis. This unspecific edge interaction made it more difficult to find the best ratio of hybridizing and passivated staples. A way to circumvent this in the future might be the redesign of the edges to contain pairwise edge staples (Figure 5-1 C). Newer designs should be less pseudo symmetric at edges to decrease simultaneous possible stacking interactions between edges.

One further drawback of the NE design was the lack of an internal topological marker. In negative stain TEM and AFM the structures appear symmetrical, due to the resolution limits of the techniques, which made it impossible to reliably assign the left and right side of the particles. The only exception were class averages of fully flattened Echo particles. Hence, additional structural features had to be introduced, as for example additional origami prisms or a DNA brick-based marker. Alternatively, information about the orientation of the DNA prism in microscopy techniques could be derived from the position of an encapsulated species such as p97H. In the future, topological markers should be included in the design of highly symmetric origamis.

In order to better control the flux of substrate within the nanochambers, so that translocation occurs along a defined direction, a DNA origami lid structure could be envisioned as an advanced version of the oligonucleotide PEG barrier (Figure 5-2 A). Such a DNA origami structure would hinder the entry of larger molecules from one side of the channel.[174] A lid could potentially also be used to enrich the amount of unfolded (or refolded) protein inside the channel, trapping the product of translocation between the lid and the encapsulated p97, as shown below (Figure 5-4 page 77).

Concerning the use of non-covalent and non-regioselective ligands for protein entrapment, a completely new DNA origami structure would be necessary if the purpose is to facilitate structural elucidation by EM. In this case, the formation of a lattice would be advantageous. An interesting property of this future design

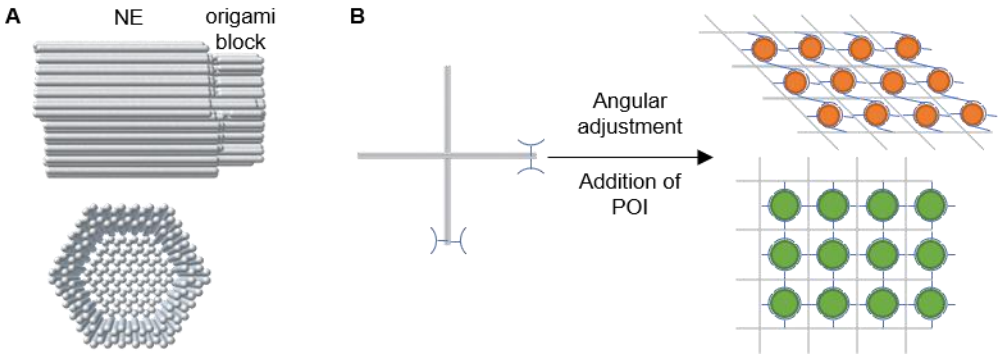

Figure 5-2: Potential future designs: **A** DNA origami block for the NE prism to hinder entry of particles from one side. The closed structure is shown as seen from the side (top) and from the prism pore (bottom). **B** DNA origami capable of forming 2D lattices (grey). Adjusting angles between the bundles would allow the change of the size of the inner cavity. Ligands (blue) might encapsulate different proteins (green and orange) depending on their size.

could be a switchable cavity size, potentially by angular adjustment (Figure 5-2 B). In this way, several protein sizes can be addressed with one design, enabling also easier automated screening of proteins in different orientations. While angular switches were reported for DNA origamis[87,92,264–269], switchable DNA origami lattices are difficult to obtain since small deviations might accumulate, leading to deficient lattice structures[87,92,269].

5.2. Encapsulation of p97 in forced orientation

In this work p97 could be encapsulated with high yields into a NE prism by using Halotag proteins at the C-termini of the ATPase. Other attempts, based on regioselective non-covalent interactions, failed most likely due to low binding constants or unforeseen undesired interactions.

Conjugation of the Halotags with DNA oligonucleotides was achieved with very good yield and the purified DNA-protein conjugates (p97H-DNA) maintained unfolding activity. Encapsulation of p97 was done using six handles protruding from the inner walls of the DNA origami. Encapsulation yield was as high as 75% for half-prisms with three protruding arms and up to over 95% for some NE prisms containing six protrusion arms.

DNA-encapsulated p97H was purified from excess free protein by SEC and showed a retained activity. When the protein was released by single-strand displacement, the measured unfolding reaction slowed down. This effect was proven to be related to the encapsulation of p97, as the presence of unbound origami or the release strand did not significantly influence the unfolding activity of free p97. It remains unknown if p97 is truly more active inside the prism or if p97 is protected by the origami shell to adverse effects in bulk solution, like binding to the wall of the reaction tube. Changed activity could alternatively explained by some effects described for proteins in nanoconfinements such as increased binding affinity for antibody-antigen pairs[270] and decreased structural fluctuations[271–273]. Even substrate or cofactor channeling might be an option.[181,185] Also, due to the dimension at play, proton and salt gradients near the origami walls might lead to different concentrations of those specimens from bulk and hence influence the activity as well[274,275]. Due to many factors potentially playing a role in the rather complex process of inhibitor3-Eos unfolding by an encapsulated p97, it would be difficult to address them separately and far beyond the scope of this work.

Activities were not compared between the constructs B1-B4 since the DNA origami concentration measurement might not be precise enough due to aberrations of extinction coefficients between the constructs and measurement variance. AB, BC and ABC constructs from one B construct however should be comparable as the same volume of B was pipetted for all.

The addition of a second prism to either side of the p97 containing chamber further increased the activity. This was also found for constructs in which one entrance was blocked with PEGylated oligonucleotides. This barrier hence was only effective in reducing the diffusion of p97 inside the prism but did not affect the diffusion of smaller molecules, such as the substrate and accessory proteins. The unfolding activity was not further increased by addition of a third prism on the other side of the encapsulated p97. One could speculate on several effects that might come into play for the addition of these extra prisms.

For example for a prism addition at the N-terminal/D1 site an increased effective substrate and cofactor binding due to molecular crowding effects in a confined space could be expected[270,276,277]. The complex formation step of ATPase, cofactor and substrate (or substrate commitment), is described as rate limiting step of unfolding for another AAA ATPase ClpX.[278,279] This might also be true for p97.[216,225] Note, that this effects might already be at play for single prism setups however more prone upon prism multimerization.

Furthermore, the addition of a prism at either side would lead to increased diffusion paths for adapter and substrate complex proteins as well as for the product. However, as mentioned above, movement of molecules in nanoconfinements is poorly understood to this day.

One possibility to investigate this would be to use fluorescently labelled origamis and fluorescently labelled parts of the unfolding complex and explore the colocalization lifetime in one, two and three prism setups via fluorescence microscopy. Additionally, ATP consumption assays could elucidate if the ATPase function p97 is also increased upon addition of a second or third prism.

Visualization and control of p97 orientation inside the prism remained a problem. Labelling with antibodies, p37-Snap and Ufd1-Npl4 either failed or did not result in any conclusive results. Manual counting of the orientation was mainly restricted due to resolution limits or potential unforeseen orientations inside the prism leaving most orientations unclear.

Counting of AuNP labels relied on the usage of a rather unstable Sp97H complex. The labelling efficiency with AuNP was quite low with only approx. 20% of the structures giving information about their orientation. The averages of the data obtained indicate a small preference for the N-out orientation except for construct B4 and B7/B8 derived thereof. AuNP counts were however not representative for the whole sample when resampled in groups of approx. 200 structures. See Figure 5-3 for collective orientation results.

Orientation counting and AuNP label were similarly indicating that p97 orientation was rather evenly distributed between the N-in and N-out configuration (Figure 5-3). The labelling technique with AuNPs confirmed the model of the p97 encapsulation process only to a certain extent: B4 constructs where p97 diffusion through the cavity should be impaired at one side of the prism led to a slightly increased N-in orientation, which was also reflected in the derived B7 and B8 constructs. Surprisingly, introduction of a second anchoring point in the constructs B5-B8 did not lead to a preferred orientation. Change of orientation after the initial binding event of p97 inside the prism could hence be considered as very unlikely since it would require several DNA melting events and/or considerable torsional strain on the DNA double helices. Therefore, p97 might simply not reach one of the additional anchoring points. The effect of the

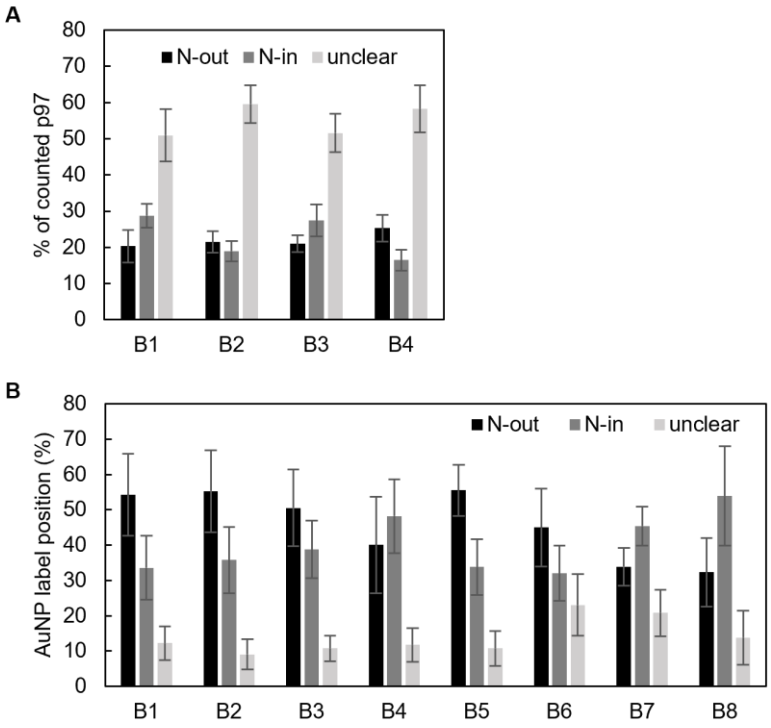

Figure 5-3: Summarized results for the p97H orientation inside the DNA origami prisms. Orientation as counted (**A**) and counted of Sp97H labelled with AuNP (**B**) as described in section4.2.6 and 4.2.8.

introduction of a blockage, a longer diffusion pathway through the prism and additional anchoring points to control the encapsulation pathways could hence be seen as insufficient.

Steering the p97 encapsulation process to achieve a certain orientation within the prism remains challenging. One could use other steric barriers, like long DNA strands spanning the entry or an origami lid as described before in section 5.1. As an alternative approach, pulling down one of the orientations by targeting either the N-terminal/D1 site or Halotags might be an option (Figure 5-4 A). If pull-down could be designed to be switchable, the two opposing orientations might be isolated independently.

To investigate the orientation by single molecule techniques new labelling methods would be necessary. The chosen ligands need to bind p97 strongly enough to enable labelling of samples in medium to low nM concentrations. Furthermore, they should be either modifiable or contain a marking moiety. Both topological and fluorescence marker might be of interest. If one orientation is strongly preferred over the other, bulk measurements like unfolding kinetics as well as orientation estimation by negative stain TEM might be helping but should be further supported by other techniques. For the latter, automated image analysis software could be of aid, avoiding personal bias. Finally, the structures might be possibly investigated by cryo EM. The *in silico* molecular modeling of the diffusion of p97H into a DNA origami might also give further insight how to optimize the DNA construct accordingly.

The current structure might already allow biophysical research on p97. The p97H conjugated to DNA oligonucleotides could be used to place the protein in a way that substrate unfolding could be monitored by optical tweezers or an AFM cantilever. In this way, molecular forces in action could be measured,

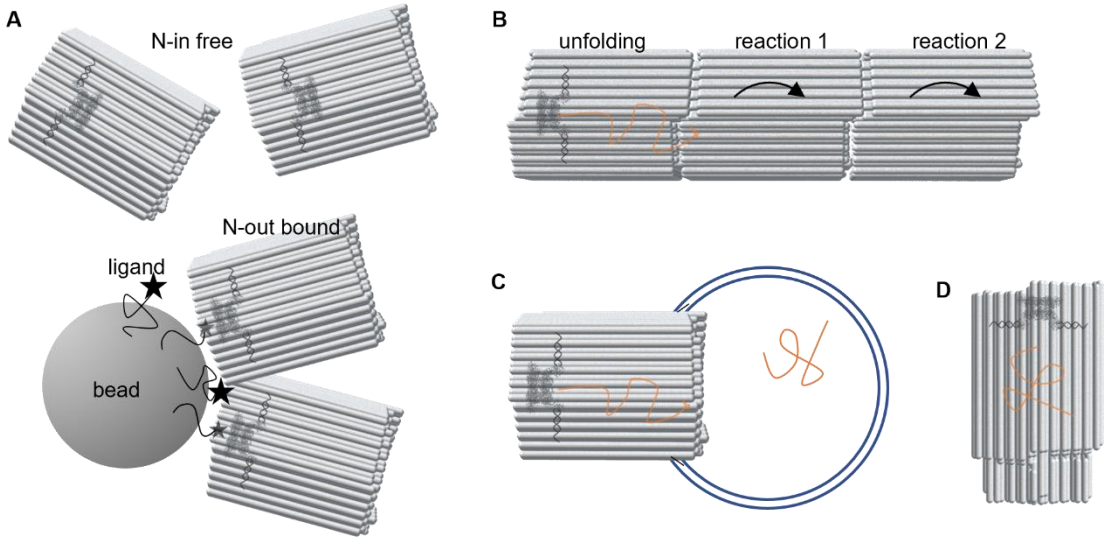

Figure 5-4: **A** Theoretical pulldown of N-in orientation. A bead displays ligands for the D1 ring of p97. While D1 is accessible for the ligand in N-out orientation it would be shielded in N-in orientation and hence the latter would stay in solution. **B** Three prism setup as a nanofactory. Unfolded substrate (orange) is further processed in following reaction chambers. These chambers could for example contain proteases or modifying enzymes. **C** DNA origami can be inserted in lipid double layers which would allow translocation of the substrate to the inner of a vesicle(blue). **D** By using a blocked Origami unfolded substrate might be contained.

understanding more about the role of the surrounding DNA shell on the activity of the encapsulated protein. Once the orientation issue can be overcome, it would be possible to develop a semiartificial protein translocation device. This construct could be theoretically used in a variety of advanced applications, like a nanofactory where unfolding of a protein is required for a downstream process (Figure 5-4 B). If the entry from the opposite side of the nanofactory can be fully closed, the purification of the correct p97orientation might become unnecessary, as wrongly oriented p97 would only lead to inactive nanofactories. Combined with proteases, this nanofactory could mimic p97 function upstream to the proteasome. Furthermore, the origami can be modified to insert into lipid vesicles[280,281], theoretically enabling pumping of proteins into them (Figure 5-4 C). The construct might also be interesting itself as a vessel if it can be developed such to contain the translocated protein. Additionally, the behavior of unfolded peptide chains in confined spaces could be studied as well (Figure 5-4 D).

5.3. Binding of thermophilic proteins to a DNA origami

Binding of a thermophilic Snaptag homolog (H^5*Ss*OGT) to a DNA origami during a one-pot thermal assembly was demonstrated for the first time to my knowledge., although further investigations are needed to clarify if the protein remained folded. Attachment of the H^5*Ss*OGT to other thermophilic proteins are currently investigated by our cooperation partners in Neaples.

DNA origamis are usually designed for applications at temperatures below 40°C and melt at elevated temperatures(55-65°C).[147,166,261] Hence, the current designs need to be adapted for higher temperatures to allow future investigation of thermophilic enzymatic reactions at high temperatures. Some design modifications, like staple strands with higher melting temperature or staple strand catenane formation are already reported in the literature to increase DNA origami thermostability.[282,283]

5.4. Encapsulation of proteins in random orientation

Binding of proteins inside a DNA origami cavity by low affinity ligands was successful for CLR01 tweezer and DegP hexamers. However, the precise binding affinity could not be determined. Due to the complexity of the system concerning the number of ligands and low concentration of prisms, analysis tools were limited. Generally, increased binding was confirmed by AGE, AFM and negative stain TEM.

In similar attempts, binding of p97 could not be visualized when using CLR01 or other ligands in AGE. When buffer was exchanged from TEMg to caco7Ca, some rare binding events could be visualized by AFM. Various conditions of pH, protrusion arm length, temperature and protein excess were also screened during other works outside this PhD project, but p97 binding was not evident. Therefore, distinct proteins may behave very differently within the same DNA environment.

The reasons for this effect are still unknown. One reason might be insufficient nominal binding affinities of the ligands, but also buffer substances, steric hinderance or unknown processes might contribute to change the effective affinity of the ligands for a certain protein surface. Additionally, the inner cavity of the DNA origami prism can be structurally affected by the large amount of protrusion arms, possibly increasing steric hinderance. This problem could be addressed in more adaptable and potentially more simplified systems where the DNA nanostructure is assembled after ligands are bound to the protein. As for pre-imprinted polymers,[284–286] those structures should have a higher affinity to the POI. Another possibility is to develop a library of DNA barcoded small molecules, whose attachment to the prism is weak. By screening DNA-encoded dynamic combinatorial libraries, optimal ligand/DNA sequence combinations might arise for each target protein[287–289].

Alternatively, the strategy could be changed to ligands that bind covalently, however reversibly. One example could be aldehyde-modified DNA oligonucleotides forming Schiff bases with protein amines as the lysin ε-NH_2 groups[290–292]. While this weak bond is readily hydrolyzed in bulk, the multivalency of an aldehyde-decorated DNA origami prism might result in overall entrapment of the protein. Similarly, cysteines thiol groups can be targeted[181] in very mild reductive conditions allowing reversible

oxidative/reductive reaction with thiol modified DNA oligonucleotides in DNA origami prism. In both cases the moieties would also be very small, decreasing the problem of steric hinderance.

As a further strategy, ligands can be used that address protein surface patches with high affinity such as protein dyes[293,294]. However, they are commercially not available for straight forward modification with DNA oligonucleotides, hence chemical synthesis methods need to be developed.

6. Summary

During this work an existing DNA origami structure was advanced and a new one was developed based on the hierarchical assembly of two distinct origami units. For the latter, so-called Nemesis prism, the assembly procedure and dimerization were optimized and multimerization along the central axis was developed. Both prisms were designed to allow a total of at least 54 attachment points, that were used in various ways to modify the inner of the DNA compartment.

The AAA+ ATPase p97 was successfully encapsulated within an origami prism. Unfolding assays showed that the DNA-encapsulated p97 has an increased activity when compared to free p97. The reason for this phenomenon is still under investigation. However, the resulting DNA/protein machinery is already a rare example of a molecular protein motor working efficiently inside a DNA origami cavity. The addition of more DNA origami prisms at either side of the p97-containing chamber increased the activity even further. This effect that could not be fully understood during this work, however it matches with previous findings for proteins in nanoconfinements. The orientation of p97 with respect to the DNA origami structure could neither be properly detected nor controlled, making the development of a bottom-up designed semi-artificial protein translocation device even more challenging.

Along the main goal of the project, that is the development of DNA origami compartments for proteins, encapsulation of a thermophilic tag protein in a one-pot assembly procedure was investigated and successfully performed. This novel approach would enable further encapsulation of thermostable proteins in DNA origamis.

The inactive form of the protease $DegP_6$ could also be successfully encapsulated into DNA origami hexaprisms using an inner decoration of lysine-selective molecular tweezers. A low binding yield was found also for p97; however, more studies are necessary to better understand and possibly quantify protein binding affinity to DNA origami cavities. This method might be further improved to allow protein encapsulation in DNA origami lattices for automated particle picking in TEM images and easier structural elucidation of proteins.

Overall, the toolbox of methods for binding proteins to a DNA nanostructure could successfully be extended to thermophilic tag proteins and for low-affinity protein ligands. A novel nanodevice was also developed for the encapsulation of an AAA protein motor which, if further developed, might lead to interesting DNA-based nanofactories.

7. Literature

(1) Ostwald, W. Die Welt der vernachlässigten Dimensionen: Eine Einführung in die Kolloidchemie: Mit besonderer Berücksichtigung ihrer Anwendungen, Nachdruck der 12von 1944.; Severus Verlag: Hamburg, 2015.

(2) Feynman, R. P. There's Plenty of Room at the Bottom. Eng. Sci. **1960**, 23 (5), 22–36.

(3) Drexler, K. E. Engines of Creation: The Coming Era of Nanotechnology, Reprint Edition.; Anchor: New York, 1987.

(4) NNI Budget | National Nanotechnology Initiative https://www.nano.gov/about-nni/what/funding (accessed 2021 -07 -06).

(5) Qiu, J. Nanotechnology Development in China: Challenges and Opportunities. Natl. Sci. Rev. **2016**, 3 (1), 148–152. https://doi.org/10.1093/nsr/nww007.

(6) Key nanotechnology indicators - OECD https://www.oecd.org/sti/emerging-tech/nanotechnology-indicators.htm (accessed 2021 -07 -06).

(7) Kelly, K. L.; Coronado, E.; Zhao, L. L.; Schatz, G. C. The Optical Properties of Metal Nanoparticles: The Influence of Size, Shape, and Dielectric Environment. J. Phys. Chem. B **2003**, 107 (3), 668–677. https://doi.org/10.1021/jp026731y.

(8) Ishida, T.; Murayama, T.; Taketoshi, A.; Haruta, M. Importance of Size and Contact Structure of Gold Nanoparticles for the Genesis of Unique Catalytic Processes. Chem. Rev. **2020**, 120 (2), 464–525. https://doi.org/10.1021/acs.chemrev.9b00551.

(9) Trindell, J. A.; Duan, Z.; Henkelman, G.; Crooks, R. M. Well-Defined Nanoparticle Electrocatalysts for the Refinement of Theory. Chem. Rev. **2020**, 120 (2), 814–850. https://doi.org/10.1021/acs.chemrev.9b00246.

(10) Zhu, J.; Hu, L.; Zhao, P.; Lee, L. Y. S.; Wong, K.-Y. Recent Advances in Electrocatalytic Hydrogen Evolution Using Nanoparticles. Chem. Rev. **2020**, 120 (2), 851–918. https://doi.org/10.1021/acs.chemrev.9b00248.

(11) Wang, Q.; Domen, K. Particulate Photocatalysts for Light-Driven Water Splitting: Mechanisms, Challenges, and Design Strategies. Chem. Rev. **2020**, 120 (2), 919–985. https://doi.org/10.1021/acs.chemrev.9b00201.

(12) Kastner, M. A. Artificial Atoms. Phys. Today **1993**, 46 (1), 24–31. https://doi.org/10.1063/1.881393.

(13) Kokarneswaran, M.; Selvaraj, P.; Ashokan, T.; Perumal, S.; Sellappan, P.; Murugan, K. D.; Ramalingam, S.; Mohan, N.; Chandrasekaran, V. Discovery of Carbon Nanotubes in Sixth Century BC Potteries from Keeladi, India. Sci. Rep. **2020**, 10 (1), 19786. https://doi.org/10.1038/s41598-020-76720-z.

(14) Reibold, M.; Paufler, P.; Levin, A. A.; Kochmann, W.; Pätzke, N.; Meyer, D. C. Carbon Nanotubes in an Ancient Damascus Sabre. Nature **2006**, 444 (7117), 286–286. https://doi.org/10.1038/444286a.

(15) Pradell, T.; Molera, J.; Pantos, E.; Smith, A. D.; Martin, C. M.; Labrador, A. Temperature Resolved Reproduction of Medieval Luster. Appl. Phys. A **2008**, 90 (1), 81–88. https://doi.org/10.1007/s00339-007-4226-z.

(16) Barber, D. J.; Freestone, I. C. An Investigation of the Origin of the Colour of the Lycurgus Cup by Analytical Transmission Electron Microscopy. Archaeometry **1990**, 32 (1), 33–45. https://doi.org/10.1111/j.1475-4754.1990.tb01079.x.

(17) Graham, T. Liquid Diffusion Applied to Analysis. Philos. Trans. R. Soc. Lond. **1861**, 151, 183–224. https://doi.org/10.1098/rstl.1861.0011.

(18) Faraday, M. The Bakerian Lecture. —Experimental Relations of Gold (and Other Metals) to Light. Philos. Trans. R. Soc. Lond. **1857**, 147, 145–181. https://doi.org/10.1098/rstl.1857.0011.

(19) F.R.S, L. R. On the Electromagnetic Theory of Light. Lond. Edinb. Dublin Philos. Mag. J. Sci. **1881**, 12 (73), 81–101. https://doi.org/10.1080/14786448108627074.

(20) Ruska, E. Das Elektronenmikroskop. Z. Für Phys. **1932**, 78, 318–339.

(21) Toumey, C. P. Reading Feynman Into Nanotechnology: A Text for a New Science. Techné Res. Philos. Technol. **2008**, 12 (3), 133–168. https://doi.org/techne20081231.

(22) Drexler, K. E. Molecular Engineering: An Approach to the Development of General Capabilities for Molecular Manipulation. Proc. Natl. Acad. Sci. **1981**, 78 (9), 5275–5278.

(23) Binnig, G.; Rohrer, H. Scanning Tunneling Microscopy. Surf. Sci. **1983**, 126 (1), 236–244. https://doi.org/10.1016/0039-6028(83)90716-1.
(24) Binnig, G.; Quate, C. F.; Gerber, Ch. Atomic Force Microscope. Phys. Rev. Lett. **1986**, 56 (9), 930–933. https://doi.org/10.1103/PhysRevLett.56.930.
(25) Kroto, H. W.; Heath, J. R.; O'Brien, S. C.; Curl, R. F.; Smalley, R. E. C 60 : Buckminsterfullerene. Nature **1985**, 318 (6042), 162–163. https://doi.org/10.1038/318162a0.
(26) Eigler, D. M.; Schweizer, E. K. Positioning Single Atoms with a Scanning Tunnelling Microscope. Nature **1990**, 344 (6266), 524–526. https://doi.org/10.1038/344524a0.
(27) Sun, T. Y.; Mitrano, D. M.; Bornhöft, N. A.; Scheringer, M.; Hungerbühler, K.; Nowack, B. Envisioning Nano Release Dynamics in a Changing World: Using Dynamic Probabilistic Modeling to Assess Future Environmental Emissions of Engineered Nanomaterials. Environ. Sci. Technol. **2017**, 51 (5), 2854–2863. https://doi.org/10.1021/acs.est.6b05702.
(28) Sun, T. Y.; Bornhöft, N. A.; Hungerbühler, K.; Nowack, B. Dynamic Probabilistic Modeling of Environmental Emissions of Engineered Nanomaterials. Environ. Sci. Technol. **2016**, 50 (9), 4701–4711. https://doi.org/10.1021/acs.est.5b05828.
(29) Gwyn, C. W.; Stulen, R.; Sweeney, D.; Attwood, D. Extreme Ultraviolet Lithography. J. Vac. Sci. Technol. B Microelectron. Nanometer Struct. Process. Meas. Phenom. **1998**, 16 (6), 3142–3149. https://doi.org/10.1116/1.590453.
(30) Fisslthaler, E.; Blümel, A.; Landfester, K.; Scherf, U.; W. List, E. J. Printing Functional Nanostructures : A Novel Route towards Nanostructuring of Organic Electronic Devices via Soft Embossing, Inkjet Printing and Colloidal Self Assembly of Semiconducting Polymer Nanospheres. Soft Matter **2008**, 4 (12), 2448–2453. https://doi.org/10.1039/B812235K.
(31) Yakovlev, A. V.; Milichko, V. A.; Vinogradov, V. V.; Vinogradov, A. V. Inkjet Color Printing by Interference Nanostructures. ACS Nano **2016**, 10 (3), 3078–3086. https://doi.org/10.1021/acsnano.5b06074.
(32) Venugopal, G.; Kim, S.-J. Nanolithography; IntechOpen, 2013. https://doi.org/10.5772/55527.
(33) Kumar, S.; Bhushan, P.; Bhattacharya, S. Fabrication of Nanostructures with Bottom-up Approach and Their Utility in Diagnostics, Therapeutics, and Others. In Environmental, Chemical and Medical Sensors; Bhattacharya, S., Agarwal, A. K., Chanda, N., Pandey, A., Sen, A. K., Eds.; Energy, Environment, and Sustainability; Springer: Singapore, 2018; pp 167–198. https://doi.org/10.1007/978-981-10-7751-7_8.
(34) Thiruvengadathan, R.; Korampally, V.; Ghosh, A.; Chanda, N.; Gangopadhyay, K.; Gangopadhyay, S. Nanomaterial Processing Using Self-Assembly-Bottom-up Chemical and Biological Approaches. Rep. Prog. Phys. **2013**, 76 (6), 066501. https://doi.org/10.1088/0034-4885/76/6/066501.
(35) Wong, T.-S.; Brough, B.; Ho, C.-M. Creation of Functional Micro/Nano Systems through Top-down and Bottom-up Approaches. Mol. Cell. Biomech. MCB **2009**, 6 (1), 1–55.
(36) Watson, J. D.; Crick, F. H. C. Molecular Structure of Nucleic Acids: A Structure for Deoxyribose Nucleic Acid. Nature **1953**, 171 (4356), 737–738. https://doi.org/10.1038/171737a0.
(37) Tiessen, A.; Pérez-Rodríguez, P.; Delaye-Arredondo, L. J. Mathematical Modeling and Comparison of Protein Size Distribution in Different Plant, Animal, Fungal and Microbial Species Reveals a Negative Correlation between Protein Size and Protein Number, Thus Providing Insight into the Evolution of Proteomes. BMC Res. Notes **2012**, 5 (1), 85. https://doi.org/10.1186/1756-0500-5-85.
(38) Erickson, H. P. Size and Shape of Protein Molecules at the Nanometer Level Determined by Sedimentation, Gel Filtration, and Electron Microscopy. Biol. Proced. Online **2009**, 11, 32–51. https://doi.org/10.1007/s12575-009-9008-x.
(39) Chan, W. C. W. Bionanotechnology Progress and Advances. Biol. Blood Marrow Transplant. **2006**, 12 (1, Supplement 1), 87–91. https://doi.org/10.1016/j.bbmt.2005.10.004.
(40) Nagamune, T. Biomolecular Engineering for Nanobio/Bionanotechnology. Nano Converg. **2017**, 4 (1), 9. https://doi.org/10.1186/s40580-017-0103-4.
(41) Hu, H.; Onyebueke, L.; Abatan, A. Characterizing and Modeling Mechanical Properties of Nanocomposites-Review and Evaluation. J. Miner. Mater. Charact. Eng. **2010**, 09 (04), 275.
(42) Howorka, S.; Cheley, S.; Bayley, H. Sequence-Specific Detection of Individual DNA Strands Using Engineered Nanopores. Nat. Biotechnol. **2001**, 19 (7), 636. https://doi.org/10.1038/90236.
(43) Manrao, E. A.; Derrington, I. M.; Laszlo, A. H.; Langford, K. W.; Hopper, M. K.; Gillgren, N.; Pavlenok, M.; Niederweis, M.; Gundlach, J. H. Reading DNA at Single-Nucleotide Resolution with

a Mutant MspA Nanopore and Phi29 DNA Polymerase. Nat. Biotechnol. **2012**, 30 (4), 349–353. https://doi.org/10.1038/nbt.2171.
(44) Diederichs, T.; Pugh, G.; Dorey, A.; Xing, Y.; Burns, J. R.; Nguyen, Q. H.; Tornow, M.; Tampé, R.; Howorka, S. Synthetic Protein-Conductive Membrane Nanopores Built with DNA. Nat. Commun. **2019**, 10 (1), 1–11. https://doi.org/10.1038/s41467-019-12639-y.
(45) Howorka, S.; Siwy, Z. S. Reading Amino Acids in a Nanopore. Nat. Biotechnol. **2020**, 38 (2), 159–160. https://doi.org/10.1038/s41587-019-0401-y.
(46) Neiman, M. S. Some fundamental issues of microminiaturization. Radiotekhnika **1964**, No. 1, 3–12.
(47) Organick, L.; Ang, S. D.; Chen, Y.-J.; Lopez, R.; Yekhanin, S.; Makarychev, K.; Racz, M. Z.; Kamath, G.; Gopalan, P.; Nguyen, B.; Takahashi, C. N.; Newman, S.; Parker, H.-Y.; Rashtchian, C.; Stewart, K.; Gupta, G.; Carlson, R.; Mulligan, J.; Carmean, D.; Seelig, G.; Ceze, L.; Strauss, K. Random Access in Large-Scale DNA Data Storage. Nat. Biotechnol. **2018**, 36 (3), 242–248. https://doi.org/10.1038/nbt.4079.
(48) Ceze, L.; Nivala, J.; Strauss, K. Molecular Digital Data Storage Using DNA. Nat. Rev. Genet. **2019**, 20 (8), 456–466. https://doi.org/10.1038/s41576-019-0125-3.
(49) Shankland, S. Startup Catalog has jammed all 16GB of Wikipedia's text onto DNA strands https://www.cnet.com/news/startup-packs-all-16gb-wikipedia-onto-dna-strands-demonstrate-new-storage-tech/ (accessed 2021 -06 -23).
(50) Valero, J.; Pal, N.; Dhakal, S.; Walter, N. G.; Famulok, M. A Bio-Hybrid DNA Rotor-Stator Nanoengine That Moves along Predefined Tracks. Nat. Nanotechnol. **2018**, 13 (6), 496–503. https://doi.org/10.1038/s41565-018-0109-z.
(51) Famulok, M.; Škugor, M.; Valero, J.; Murayama, K.; Centola, M.; Asanuma, H. Orthogonally Photocontrolled Non-Autonomous DNA Walker. Angew. Chem. Int. Ed. 0 (ja). https://doi.org/10.1002/anie.201901272.
(52) Yan, H.; Zhang, X.; Shen, Z.; Seeman, N. C. A Robust DNA Mechanical Device Controlled by Hybridization Topology. Nature **2002**, 415 (6867), 62–65. https://doi.org/10.1038/415062a.
(53) Krishnan, Y.; Simmel, F. C. Nucleic Acid Based Molecular Devices. Angew. Chem. Int. Ed. **2011**, 50 (14), 3124–3156. https://doi.org/10.1002/anie.200907223.
(54) Li, S.; Jiang, Q.; Liu, S.; Zhang, Y.; Tian, Y.; Song, C.; Wang, J.; Zou, Y.; Anderson, G. J.; Han, J.-Y.; Chang, Y.; Liu, Y.; Zhang, C.; Chen, L.; Zhou, G.; Nie, G.; Yan, H.; Ding, B.; Zhao, Y. A DNA Nanorobot Functions as a Cancer Therapeutic in Response to a Molecular Trigger in Vivo. Nat. Biotechnol. **2018**, 36 (3), 258–264. https://doi.org/10.1038/nbt.4071.
(55) Zhu, G.; Zheng, J.; Song, E.; Donovan, M.; Zhang, K.; Liu, C.; Tan, W. Self-Assembled, Aptamer-Tethered DNA Nanotrains for Targeted Transport of Molecular Drugs in Cancer Theranostics. Proc. Natl. Acad. Sci. **2013**, 110 (20), 7998–8003. https://doi.org/10.1073/pnas.1220817110.
(56) Lee, H.; Lytton-Jean, A. K. R.; Chen, Y.; Love, K. T.; Park, A. I.; Karagiannis, E. D.; Sehgal, A.; Querbes, W.; Zurenko, C. S.; Jayaraman, M.; Peng, C. G.; Charisse, K.; Borodovsky, A.; Manoharan, M.; Donahoe, J. S.; Truelove, J.; Nahrendorf, M.; Langer, R.; Anderson, D. G. Molecularly Self-Assembled Nucleic Acid Nanoparticles for Targeted in Vivo SiRNA Delivery. Nat. Nanotechnol. **2012**, 7 (6), 389–393. https://doi.org/10.1038/nnano.2012.73.
(57) Kuzyk, A.; Schreiber, R.; Zhang, H.; Govorov, A. O.; Liedl, T.; Liu, N. Reconfigurable 3D Plasmonic Metamolecules. Nat. Mater. **2014**, 13 (9), 862–866. https://doi.org/10.1038/nmat4031.
(58) Kuzyk, A.; Schreiber, R.; Fan, Z.; Pardatscher, G.; Roller, E.-M.; Högele, A.; Simmel, F. C.; Govorov, A. O.; Liedl, T. DNA-Based Self-Assembly of Chiral Plasmonic Nanostructures with Tailored Optical Response. Nature **2012**, 483 (7389), 311–314. https://doi.org/10.1038/nature10889.
(59) Woehrstein, J. B.; Strauss, M. T.; Ong, L. L.; Wei, B.; Zhang, D. Y.; Jungmann, R.; Yin, P. Sub–100-Nm Metafluorophores with Digitally Tunable Optical Properties Self-Assembled from DNA. Sci. Adv. **2017**, 3 (6), e1602128. https://doi.org/10.1126/sciadv.1602128.
(60) Gür, F. N.; Schwarz, F. W.; Ye, J.; Diez, S.; Schmidt, T. L. Toward Self-Assembled Plasmonic Devices: High-Yield Arrangement of Gold Nanoparticles on DNA Origami Templates. ACS Nano **2016**, 10 (5), 5374–5382. https://doi.org/10.1021/acsnano.6b01537.
(61) Liu, L.; Zheng, M.; Li, Z.; Li, Q.; Mao, C. Patterning Nanoparticles with DNA Molds. ACS Appl. Mater. Interfaces **2019**. https://doi.org/10.1021/acsami.8b22691.

(62) Bayrak, T.; Helmi, S.; Ye, J.; Kauert, D.; Kelling, J.; Schönherr, T.; Weichelt, R.; Erbe, A.; Seidel, R. DNA-Mold Templated Assembly of Conductive Gold Nanowires. Nano Lett. **2018**, 18 (3), 2116–2123. https://doi.org/10.1021/acs.nanolett.8b00344.
(63) Sun, W.; Boulais, E.; Hakobyan, Y.; Wang, W. L.; Guan, A.; Bathe, M.; Yin, P. Casting Inorganic Structures with DNA Molds. Science **2014**, 346 (6210), 1258361. https://doi.org/10.1126/science.1258361.
(64) Guo, M.; Hernández-Neuta, I.; Madaboosi, N.; Nilsson, M.; van der Wijngaart, W. Efficient DNA-Assisted Synthesis of Trans-Membrane Gold Nanowires. Microsyst. Nanoeng. **2018**, 4 (1), 1–8. https://doi.org/10.1038/micronano.2017.84.
(65) Wang, M.; Wang, M.-F.; Wang, Y.-M.; Shen, J.-W.; Wang, Z.-Y.; Gao, H.; Wang, L.-L.; Ouyang, X. DNA Assisted Synthesis of CeO2 Nanocrystals with Enhanced Peroxidase-like Activity. CrystEngComm **2018**, 20 (29), 4075–4079. https://doi.org/10.1039/C8CE00569A.
(66) He, Y.; Liu, D. R. Autonomous Multistep Organic Synthesis in a Single Isothermal Solution Mediated by a DNA Walker. Nat. Nanotechnol. **2010**, 5 (11), 778–782. https://doi.org/10.1038/nnano.2010.190.
(67) Lin, Y.-R.; Koga, N.; Vorobiev, S. M.; Baker, D. Cyclic Oligomer Design with de Novo Aβ-Proteins. Protein Sci. Publ. Protein Soc. **2017**, 26 (11), 2187–2194. https://doi.org/10.1002/pro.3270.
(68) Huang, P.-S.; Love, J. J.; Mayo, S. L. A de Novo Designed Protein–Protein Interface. Protein Sci. Publ. Protein Soc. **2007**, 16 (12), 2770–2774. https://doi.org/10.1110/ps.073125207.
(69) Modi, S.; Bhatia, D.; Simmel, F. C.; Krishnan, Y. Structural DNA Nanotechnology: From Bases to Bricks, From Structure to Function. J. Phys. Chem. Lett. **2010**, 1 (13), 1994–2005. https://doi.org/10.1021/jz1004957.
(70) Seeman, N. C. Structural DNA Nanotechnology, Illustrated Edition.; Cambridge University Press: Cambridge, United Kingdom, 2016.
(71) Doll, T. A. P. F.; Dey, R.; Burkhard, P. Design and Optimization of Peptide Nanoparticles. J. Nanobiotechnology **2015**, 13 (1), 73. https://doi.org/10.1186/s12951-015-0119-z.
(72) Lapenta, F.; Aupič, J.; Vezzoli, M.; Strmšek, Ž.; Da Vela, S.; Svergun, D. I.; Carazo, J. M.; Melero, R.; Jerala, R. Self-Assembly and Regulation of Protein Cages from Pre-Organised Coiled-Coil Modules. Nat. Commun. **2021**, 12 (1), 939. https://doi.org/10.1038/s41467-021-21184-6.
(73) Douglas, S. M.; Marblestone, A. H.; Teerapittayanon, S.; Vazquez, A.; Church, G. M.; Shih, W. M. Rapid Prototyping of 3D DNA-Origami Shapes with CaDNAno. Nucleic Acids Res. **2009**, 37 (15), 5001–5006. https://doi.org/10.1093/nar/gkp436.
(74) Huang, C.-M.; Kucinic, A.; Johnson, J. A.; Su, H.-J.; Castro, C. E. Integrated Computer-Aided Engineering and Design for DNA Assemblies. Nat. Mater. **2021**, 1–8. https://doi.org/10.1038/s41563-021-00978-5.
(75) Ljubetič, A.; Lapenta, F.; Gradišar, H.; Drobnak, I.; Aupič, J.; Strmšek, Ž.; Lainšček, D.; Hafner-Bratkovič, I.; Majerle, A.; Krivec, N.; Benčina, M.; Pisanski, T.; Veličković, T. Ć.; Round, A.; Carazo, J. M.; Melero, R.; Jerala, R. Design of Coiled-Coil Protein-Origami Cages That Self-Assemble in Vitro and in Vivo. Nat. Biotechnol. **2017**, nbt.3994. https://doi.org/10.1038/nbt.3994.
(76) Guo, P. The Emerging Field of RNA Nanotechnology. Nat. Nanotechnol. **2010**, 5 (12), 833–842. https://doi.org/10.1038/nnano.2010.231.
(77) Zhang, F.; Nangreave, J.; Liu, Y.; Yan, H. Structural DNA Nanotechnology: State of the Art and Future Perspective. J. Am. Chem. Soc. **2014**, 136 (32), 11198–11211. https://doi.org/10.1021/ja505101a.
(78) Kato, T.; Goodman, R. P.; Erben, C. M.; Turberfield, A. J.; Namba, K. High-Resolution Structural Analysis of a DNA Nanostructure by CryoEM. Nano Lett. **2009**, 9 (7), 2747–2750. https://doi.org/10.1021/nl901265n.
(79) Li, H.; Zhang, K.; Pi, F.; Guo, S.; Shlyakhtenko, L.; Chiu, W.; Shu, D.; Guo, P. Controllable Self-Assembly of RNA Tetrahedrons with Precise Shape and Size for Cancer Targeting. Adv. Mater. **2016**, 28 (34), 7501–7507. https://doi.org/10.1002/adma.201601976.
(80) Høiberg, H. C.; Sparvath, S. M.; Andersen, V. L.; Kjems, J.; Andersen, E. S. An RNA Origami Octahedron with Intrinsic SiRNAs for Potent Gene Knockdown. Biotechnol. J. 0 (ja), 1700634. https://doi.org/10.1002/biot.201700634.

(81) Stewart, J. M.; Subramanian, H. K. K.; Franco, E. Self-Assembly of Multi-Stranded RNA Motifs into Lattices and Tubular Structures. Nucleic Acids Res. **2017**, 45 (9), 5449–5457. https://doi.org/10.1093/nar/gkx063.
(82) Jasinski, D. L.; Li, H.; Guo, P. The Effect of Size and Shape of RNA Nanoparticles on Biodistribution. Mol. Ther. **2017**. https://doi.org/10.1016/j.ymthe.2017.12.018.
(83) Lapenta, F.; Aupič, J.; Strmšek, Ž.; Jerala, R. Coiled Coil Protein Origami: From Modular Design Principles towards Biotechnological Applications. Chem. Soc. Rev. **2018**. https://doi.org/10.1039/C7CS00822H.
(84) Ramakrishnan, S.; Ijäs, H.; Linko, V.; Keller, A. Structural Stability of DNA Origami Nanostructures under Application-Specific Conditions. Comput. Struct. Biotechnol. J. **2018**, 16, 342–349. https://doi.org/10.1016/j.csbj.2018.09.002.
(85) Kielar, C.; Xin, Y.; Shen, B.; Kostiainen, M. A.; Grundmeier, G.; Linko, V.; Keller, A. On the Stability of DNA Origami Nanostructures in Low-Magnesium Buffers. Angew. Chem. Int. Ed. **2018**, 57 (30), 9470–9474. https://doi.org/10.1002/anie.201802890.
(86) Martin, T. G.; Dietz, H. Magnesium-Free Self-Assembly of Multi-Layer DNA Objects. Nat. Commun. **2012**, 3, ncomms2095. https://doi.org/10.1038/ncomms2095.
(87) Wagenbauer, K. F.; Sigl, C.; Dietz, H. Gigadalton-Scale Shape-Programmable DNA Assemblies. Nature **2017**, 552 (7683), 78. https://doi.org/10.1038/nature24651.
(88) Ong, L. L.; Hanikel, N.; Yaghi, O. K.; Grun, C.; Strauss, M. T.; Bron, P.; Lai-Kee-Him, J.; Schueder, F.; Wang, B.; Wang, P.; Kishi, J. Y.; Myhrvold, C.; Zhu, A.; Jungmann, R.; Bellot, G.; Ke, Y.; Yin, P. Programmable Self-Assembly of Three-Dimensional Nanostructures from 10,000 Unique Components. Nature **2017**, 552 (7683), 72–77. https://doi.org/10.1038/nature24648.
(89) Kallenbach, N. R.; Ma, R.-I.; Seeman, N. C. An Immobile Nucleic Acid Junction Constructed from Oligonucleotides. Nature **1983**, 305 (5937), 829–831. https://doi.org/10.1038/305829a0.
(90) Ji, M.; Ma, N.; Tian, Y. 3D Lattice Engineering of Nanoparticles by DNA Shells. Small **2019**, 0 (0), 1805401. https://doi.org/10.1002/smll.201805401.
(91) Ke, Y.; Douglas, S. M.; Liu, M.; Sharma, J.; Cheng, A.; Leung, A.; Liu, Y.; Shih, W. M.; Yan, H. Multilayer DNA Origami Packed on a Square Lattice. J. Am. Chem. Soc. **2009**, 131 (43), 15903–15908. https://doi.org/10.1021/ja906381y.
(92) Wang, P.; Gaitanaros, S.; Lee, S.; Bathe, M.; Shih, W. M.; Ke, Y. Programming Self-Assembly of DNA Origami Honeycomb Two-Dimensional Lattices and Plasmonic Metamaterials. J. Am. Chem. Soc. **2016**, 138 (24), 7733–7740. https://doi.org/10.1021/jacs.6b03966.
(93) Woo, S.; Rothemund, P. W. K. Self-Assembly of Two-Dimensional DNA Origami Lattices Using Cation-Controlled Surface Diffusion. Nat. Commun. **2014**, 5, 4889. https://doi.org/10.1038/ncomms5889.
(94) He, Y.; Tian, Y.; Ribbe, A. E.; Mao, C. Highly Connected Two-Dimensional Crystals of DNA Six-Point-Stars. J. Am. Chem. Soc. **2006**, 128 (50), 15978–15979. https://doi.org/10.1021/ja0665141.
(95) Simmons, C. R.; Zhang, F.; Birktoft, J. J.; Qi, X.; Han, D.; Liu, Y.; Sha, R.; Abdallah, H. O.; Hernandez, C.; Ohayon, Y. P.; Seeman, N. C.; Yan, H. Construction and Structure Determination of a Three-Dimensional DNA Crystal. J. Am. Chem. Soc. **2016**, 138 (31), 10047–10054. https://doi.org/10.1021/jacs.6b06508.
(96) Kossel, A. Ueber Eine Neue Base Aus Dem Thierkörper. Berichte Dtsch. Chem. Ges. **1885**, 18 (1), 79–81. https://doi.org/10.1002/cber.18850180119.
(97) Kossel, A.; Neumann, A. Darstellung Und Spaltungsprodukte Der Nucleïnsäure (Adenylsäure). Berichte Dtsch. Chem. Ges. **1894**, 27 (2), 2215–2222. https://doi.org/10.1002/cber.189402702206.
(98) Levene, P. A.; London, E. J. On the Structure of Thymonucleic Acid. Science **1928**, 68 (1771), 572–573. https://doi.org/10.1126/science.68.1771.572-a.
(99) Watson, J. D.; Crick, F. H. C. Genetical Implications of the Structure of Deoxyribonucleic Acid. Nature **1953**, 171 (4361), 964–967. https://doi.org/10.1038/171964b0.
(100) Vologodskii, A. V.; Amirikyan, B. R.; Lyubchenko, Y. L.; Frank-Kamenetskii, M. D. Allowance for Heterogeneous Stacking in the DNA Helix-Coil Transition Theory. J. Biomol. Struct. Dyn. **1984**, 2 (1), 131–148. https://doi.org/10.1080/07391102.1984.10507552.
(101) Yakovchuk, P.; Protozanova, E.; Frank-Kamenetskii, M. D. Base-Stacking and Base-Pairing Contributions into Thermal Stability of the DNA Double Helix. Nucleic Acids Res. **2006**, 34 (2), 564–574. https://doi.org/10.1093/nar/gkj454.

(102) Mak, C. H. Unraveling Base Stacking Driving Forces in DNA. J. Phys. Chem. B **2016**, 120 (26), 6010–6020. https://doi.org/10.1021/acs.jpcb.6b01934.
(103) SantaLucia, J.; Hicks, D. The Thermodynamics of DNA Structural Motifs. Annu. Rev. Biophys. Biomol. Struct. **2004**, 33 (1), 415–440. https://doi.org/10.1146/annurev.biophys.32.110601.141800.
(104) SantaLucia, John; Allawi, H. T.; Seneviratne, P. A. Improved Nearest-Neighbor Parameters for Predicting DNA Duplex Stability. Biochemistry **1996**, 35 (11), 3555–3562. https://doi.org/10.1021/bi951907q.
(105) Schaller, H.; Weimann, G.; Lerch, B.; Khorana, H. G. Studies on Polynucleotides. XXIV.1 The Stepwise Synthesis of Specific Deoxyribopolynucleotides (4).2 Protected Derivatives of Deoxyribonucleosides and New Syntheses of Deoxyribonucleoside-3" Phosphates3. J. Am. Chem. Soc. **1963**, 85 (23), 3821–3827. https://doi.org/10.1021/ja00906a021.
(106) Letsinger, R. L.; Mahadevan, V. Oligonucleotide Synthesis on a Polymer Support1,2. J. Am. Chem. Soc. **1965**, 87 (15), 3526–3527. https://doi.org/10.1021/ja01093a058.
(107) Agarwal, K. L.; Büchi, H.; Caruthers, M. H.; Gupta, N.; Khorana, H. G.; Kleppe, K.; Kumar, A.; Ohtsuka, E.; Rajbhandary, U. L.; Van De Sande, J. H.; Sgaramella, V.; Weber, H.; Yamada, T. Total Synthesis of the Gene for an Alanine Transfer Ribonucleic Acid from Yeast. Nature **1970**, 227 (5253), 27–34. https://doi.org/10.1038/227027a0.
(108) Holliday, R. A Mechanism for Gene Conversion in Fungi. Genet. Res. **1964**, 5 (2), 282–304. https://doi.org/10.1017/S0016672300001233.
(109) Seeman, N. C.; Kallenbach, N. R. Design of Immobile Nucleic Acid Junctions. Biophys. J. **1983**, 44 (2), 201–209. https://doi.org/10.1016/S0006-3495(83)84292-1.
(110) Petrillo, M. L.; Newton, C. J.; Cunningham, R. P.; Ma, R.-I.; Kallenbach, N. R.; Seeman, N. C. The Ligation and Flexibility of Four-Arm DNA Junctions. Biopolymers **1988**, 27 (9), 1337–1352. https://doi.org/10.1002/bip.360270902.
(111) Ma, R.-I.; Kallenbach, N. R.; Sheardy, R. D.; Petrillo, M. L.; Seeman, N. C. Three-Arm Nucleic Acid Junctions Are Flexible. Nucleic Acids Res. **1986**, 14 (24), 9745–9753. https://doi.org/10.1093/nar/14.24.9745.
(112) Qi, J.; Li, X.; Yang, X.; Seeman, N. C. Ligation of Triangles Built from Bulged 3-Arm DNA Branched Junctions. J. Am. Chem. Soc. **1996**, 118 (26), 6121–6130. https://doi.org/10.1021/ja960161w.
(113) Du, S. M.; Zhang, S.; Seeman, N. C. DNA Junctions, Antijunctions, and Mesojunctions. Biochemistry **1992**, 31 (45), 10955–10963. https://doi.org/10.1021/bi00160a003.
(114) Wang, J. C. Helical Repeat of DNA in Solution. Proc. Natl. Acad. Sci. **1979**, 76 (1), 200–203. https://doi.org/10.1073/pnas.76.1.200.
(115) Fu, T. J.; Seeman, N. C. DNA Double-Crossover Molecules. Biochemistry **1993**, 32 (13), 3211–3220. https://doi.org/10.1021/bi00064a003.
(116) Winfree, E.; Liu, F.; Wenzler, L. A.; Seeman, N. C. Design and Self-Assembly of Two-Dimensional DNA Crystals. Nature **1998**, 394 (6693), 539–544. https://doi.org/10.1038/28998.
(117) He, Y.; Chen, Y.; Liu, H.; Ribbe, A. E.; Mao, C. Self-Assembly of Hexagonal DNA Two-Dimensional (2D) Arrays. J. Am. Chem. Soc. **2005**, 127 (35), 12202–12203. https://doi.org/10.1021/ja0541938.
(118) He, Y.; Tian, Y.; Ribbe, A. E.; Mao, C. Antibody Nanoarrays with a Pitch of ∼20 Nanometers. J. Am. Chem. Soc. **2006**, 128 (39), 12664–12665. https://doi.org/10.1021/ja065467+.
(119) LaBean, T. H.; Yan, H.; Kopatsch, J.; Liu, F.; Winfree, E.; Reif, J. H.; Seeman, N. C. Construction, Analysis, Ligation, and Self-Assembly of DNA Triple Crossover Complexes. J. Am. Chem. Soc. **2000**, 122 (9), 1848–1860. https://doi.org/10.1021/ja993393e.
(120) Yin, P.; Hariadi, R. F.; Sahu, S.; Choi, H. M. T.; Park, S. H.; LaBean, T. H.; Reif, J. H. Programming DNA Tube Circumferences. Science **2008**, 321 (5890), 824–826. https://doi.org/10.1126/science.1157312.
(121) Li, H.; LaBean, T. H.; Kenan, D. J. Single-Chain Antibodies against DNA Aptamers for Use as Adapter Molecules on DNA Tile Arrays in Nanoscale Materials Organization. Org. Biomol. Chem. **2006**, 4 (18), 3420–3426. https://doi.org/10.1039/B606391H.
(122) Lin, C.; Katilius, E.; Liu, Y.; Zhang, J.; Yan, H. Self-Assembled Signaling Aptamer DNA Arrays for Protein Detection. Angew. Chem. Int. Ed. **2006**, 45 (32), 5296–5301. https://doi.org/10.1002/anie.200600438.

(123) Park, S. H.; Yin, P.; Liu, Y.; Reif, J. H.; LaBean, T. H.; Yan, H. Programmable DNA Self-Assemblies for Nanoscale Organization of Ligands and Proteins. Nano Lett. **2005**, 5 (4), 729–733. https://doi.org/10.1021/nl050175c.
(124) Liu, D.; Park, S. H.; Reif, J. H.; LaBean, T. H. DNA Nanotubes Self-Assembled from Triple-Crossover Tiles as Templates for Conductive Nanowires. Proc. Natl. Acad. Sci. **2004**, 101 (3), 717–722.
(125) Yan, H.; Park, S. H.; Finkelstein, G.; Reif, J. H.; LaBean, T. H. DNA-Templated Self-Assembly of Protein Arrays and Highly Conductive Nanowires. Science **2003**, 301 (5641), 1882–1884. https://doi.org/10.1126/science.1089389.
(126) Agrawal, D. K.; Jiang, R.; Reinhart, S.; Mohammed, A. M.; Jorgenson, T. D.; Schulman, R. Terminating DNA Tile Assembly with Nanostructured Caps. ACS Nano **2017**. https://doi.org/10.1021/acsnano.7b02256.
(127) He, Y.; Ye, T.; Su, M.; Zhang, C.; Ribbe, A. E.; Jiang, W.; Mao, C. Hierarchical Self-Assembly of DNA into Symmetric Supramolecular Polyhedra. Nature **2008**, 452 (7184), 198–201. https://doi.org/10.1038/nature06597.
(128) Liu, Y.; Ke, Y.; Yan, H. Self-Assembly of Symmetric Finite-Size DNA Nanoarrays. J. Am. Chem. Soc. **2005**, 127 (49), 17140–17141. https://doi.org/10.1021/ja055614o.
(129) Lund, K.; Liu, Y.; Lindsay, S.; Yan, H. Self-Assembling a Molecular Pegboard. J. Am. Chem. Soc. **2005**, 127 (50), 17606–17607. https://doi.org/10.1021/ja0568446.
(130) Park, S. H.; Pistol, C.; Ahn, S. J.; Reif, J. H.; Lebeck, A. R.; Dwyer, C.; LaBean, T. H. Finite-Size, Fully Addressable DNA Tile Lattices Formed by Hierarchical Assembly Procedures. Angew. Chem. Int. Ed. **2006**, 45 (5), 735–739. https://doi.org/10.1002/anie.200503797.
(131) Evans, C. G.; Winfree, E. Physical Principles for DNA Tile Self-Assembly. Chem. Soc. Rev. **2017**, 46 (12), 3808–3829. https://doi.org/10.1039/C6CS00745G.
(132) Schulman, R.; Winfree, E. Synthesis of Crystals with a Programmable Kinetic Barrier to Nucleation. Proc. Natl. Acad. Sci. **2007**, 104 (39), 15236–15241. https://doi.org/10.1073/pnas.0701467104.
(133) Jorgenson, T. D.; Mohammed, A. M.; Agrawal, D. K.; Schulman, R. Self-Assembly of Hierarchical DNA Nanotube Architectures with Well-Defined Geometries. ACS Nano **2017**, 11 (2), 1927–1936. https://doi.org/10.1021/acsnano.6b08008.
(134) Shih, W. M.; Quispe, J. D.; Joyce, G. F. A 1.7-Kilobase Single-Stranded DNA That Folds into a Nanoscale Octahedron. Nature **2004**, 427 (6975), 618–621. https://doi.org/10.1038/nature02307.
(135) Yan, H.; LaBean, T. H.; Feng, L.; Reif, J. H. Directed Nucleation Assembly of DNA Tile Complexes for Barcode-Patterned Lattices. Proc. Natl. Acad. Sci. **2003**, 100 (14), 8103–8108. https://doi.org/10.1073/pnas.1032954100.
(136) Rothemund, P. W. K. Folding DNA to Create Nanoscale Shapes and Patterns. Nature **2006**, 440 (7082), 297–302. https://doi.org/10.1038/nature04586.
(137) Dietz, H.; Douglas, S. M.; Shih, W. M. Folding DNA into Twisted and Curved Nanoscale Shapes. Science **2009**, 325 (5941), 725–730. https://doi.org/10.1126/science.1174251.
(138) Han, D.; Pal, S.; Yang, Y.; Jiang, S.; Nangreave, J.; Liu, Y.; Yan, H. DNA Gridiron Nanostructures Based on Four-Arm Junctions. Science **2013**, 339 (6126), 1412–1415. https://doi.org/10.1126/science.1232252.
(139) Zhang, F.; Jiang, S.; Wu, S.; Li, Y.; Mao, C.; Liu, Y.; Yan, H. Complex Wireframe DNA Origami Nanostructures with Multi-Arm Junction Vertices. Nat. Nanotechnol. **2015**, 10 (9), 779–784. https://doi.org/10.1038/nnano.2015.162.
(140) Benson, E.; Mohammed, A.; Gardell, J.; Masich, S.; Czeizler, E.; Orponen, P.; Högberg, B. DNA Rendering of Polyhedral Meshes at the Nanoscale. Nature **2015**, 523 (7561), 441–444. https://doi.org/10.1038/nature14586.
(141) Wagenbauer, K. F.; Wachauf, C. H.; Dietz, H. Quantifying Quality in DNA Self-Assembly. Nat. Commun. **2014**, 5, 3691. https://doi.org/10.1038/ncomms4691.
(142) Veneziano, R.; Ratanalert, S.; Zhang, K.; Zhang, F.; Yan, H.; Chiu, W.; Bathe, M. Designer Nanoscale DNA Assemblies Programmed from the Top Down. Science **2016**, 352 (6293), 1534–1534. https://doi.org/10.1126/science.aaf4388.
(143) Jun, H.; Zhang, F.; Shepherd, T.; Ratanalert, S.; Qi, X.; Yan, H.; Bathe, M. Autonomously Designed Free-Form 2D DNA Origami. Sci. Adv. **2019**, 5 (1), eaav0655. https://doi.org/10.1126/sciadv.aav0655.

(144) Jun, H.; Shepherd, T. R.; Zhang, K.; Bricker, W. P.; Li, S.; Chiu, W.; Bathe, M. Automated Sequence Design of 3D Polyhedral Wireframe DNA Origami with Honeycomb Edges. ACS Nano **2019**, 13 (2), 2083–2093. https://doi.org/10.1021/acsnano.8b08671.
(145) Benson, E.; Mohammed, A.; Rayneau-Kirkhope, D.; Gådin, A.; Orponen, P.; Högberg, B. Effects of Design Choices on the Stiffness of Wireframe DNA Origami Structures. ACS Nano **2018**, 12 (9), 9291–9299. https://doi.org/10.1021/acsnano.8b04148.
(146) Niekamp, S.; Blumer, K.; Nafisi, P. M.; Tsui, K.; Garbutt, J.; Douglas, S. M. Folding Complex DNA Nanostructures from Limited Sets of Reusable Sequences. Nucleic Acids Res. **2016**, 44 (11), e102–e102. https://doi.org/10.1093/nar/gkw208.
(147) Sobczak, J.-P. J.; Martin, T. G.; Gerling, T.; Dietz, H. Rapid Folding of DNA into Nanoscale Shapes at Constant Temperature. Science **2012**, 338 (6113), 1458–1461. https://doi.org/10.1126/science.1229919.
(148) Jungmann, R.; Liedl, T.; Sobey, T. L.; Shih, W.; Simmel, F. C. Isothermal Assembly of DNA Origami Structures Using Denaturing Agents. J. Am. Chem. Soc. **2008**, 130 (31), 10062–10063. https://doi.org/10.1021/ja8030196.
(149) Shaw, A.; Benson, E.; Högberg, B. Purification of Functionalized DNA Origami Nanostructures. ACS Nano **2015**, 9 (5), 4968–4975. https://doi.org/10.1021/nn507035g.
(150) Lin, C.; Perrault, S. D.; Kwak, M.; Graf, F.; Shih, W. M. Purification of DNA-Origami Nanostructures by Rate-Zonal Centrifugation. Nucleic Acids Res. **2013**, 41 (2), e40–e40. https://doi.org/10.1093/nar/gks1070.
(151) Timm, C.; Niemeyer, C. M. Assembly and Purification of Enzyme-Functionalized DNA Origami Structures. Angew. Chem. Int. Ed. **2015**, 54 (23), 6745–6750. https://doi.org/10.1002/anie.201500175.
(152) Wagenbauer, K. F.; Engelhardt, F. A. S.; Stahl, E.; Hechtl, V. K.; Stömmer, P.; Seebacher, F.; Meregalli, L.; Ketterer, P.; Gerling, T.; Dietz, H. How We Make DNA Origami. ChemBioChem n/a-n/a. https://doi.org/10.1002/cbic.201700377.
(153) Yao, G.; Zhang, F.; Wang, F.; Peng, T.; Liu, H.; Poppleton, E.; Šulc, P.; Jiang, S.; Liu, L.; Gong, C.; Jing, X.; Liu, X.; Wang, L.; Liu, Y.; Fan, C.; Yan, H. Meta-DNA Structures. Nat. Chem. **2020**, 1–9. https://doi.org/10.1038/s41557-020-0539-8.
(154) Pfeifer, W.; Lill, P.; Gatsogiannis, C.; Saccà, B. Hierarchical Assembly of DNA Filaments with Designer Elastic Properties. ACS Nano **2018**, 12 (1), 44–55. https://doi.org/10.1021/acsnano.7b06012.
(155) Franquelim, H. G.; Khmelinskaia, A.; Sobczak, J.-P.; Dietz, H.; Schwille, P. Membrane Sculpting by Curved DNA Origami Scaffolds. Nat. Commun. **2018**, 9 (1), 811. https://doi.org/10.1038/s41467-018-03198-9.
(156) Zhang, T. DNA Origami-Based Microtubule Analogue. Nanotechnology **2020**, 31 (50), 50LT01. https://doi.org/10.1088/1361-6528/abb395.
(157) Derr, N. D.; Goodman, B. S.; Jungmann, R.; Leschziner, A. E.; Shih, W. M.; Reck-Peterson, S. L. Tug-of-War in Motor Protein Ensembles Revealed with a Programmable DNA Origami Scaffold. Science **2012**, 338 (6107), 662–665. https://doi.org/10.1126/science.1226734.
(158) Rangnekar, A.; Gothelf, K. V.; LaBean, T. H. Design and Synthesis of DNA Four-Helix Bundles. Nanotechnology **2011**, 22 (23), 235601. https://doi.org/10.1088/0957-4484/22/23/235601.
(159) Woo, S.; Rothemund, P. W. K. Programmable Molecular Recognition Based on the Geometry of DNA Nanostructures. Nat. Chem. **2011**, 3 (8), 620–627. https://doi.org/10.1038/nchem.1070.
(160) Tikhomirov, G.; Petersen, P.; Qian, L. Triangular DNA Origami Tilings. J. Am. Chem. Soc. **2018**, 140 (50), 17361–17364. https://doi.org/10.1021/jacs.8b10609.
(161) Liu, W.; Zhong, H.; Wang, R.; Seeman, N. C. Crystalline Two-Dimensional DNA-Origami Arrays. Angew. Chem. Int. Ed. **2011**, 50 (1), 264–267. https://doi.org/10.1002/anie.201005911.
(162) Zhang, T.; Hartl, C.; Frank, K.; Heuer-Jungemann, A.; Fischer, S.; Nickels, P. C.; Nickel, B.; Liedl, T. 3D DNA Origami Crystals. Adv. Mater. **2018**, 30 (28), 1800273. https://doi.org/10.1002/adma.201800273.
(163) Ke, Y.; Ong, L. L.; Shih, W. M.; Yin, P. Three-Dimensional Structures Self-Assembled from DNA Bricks. Science **2012**, 338 (6111), 1177–1183. https://doi.org/10.1126/science.1227268.
(164) Myhrvold, C.; Dai, M.; Silver, P. A.; Yin, P. Isothermal Self-Assembly of Complex DNA Structures under Diverse and Biocompatible Conditions. Nano Lett. **2013**, 13 (9), 4242–4248. https://doi.org/10.1021/nl4019512.

(165) Wei, B.; Dai, M.; Yin, P. Complex Shapes Self-Assembled from Single-Stranded DNA Tiles. Nature **2012**, 485 (7400), 623–626. https://doi.org/10.1038/nature11075.
(166) Wei, X.; Nangreave, J.; Jiang, S.; Yan, H.; Liu, Y. Mapping the Thermal Behavior of DNA Origami Nanostructures. J. Am. Chem. Soc. **2013**, 135 (16), 6165–6176. https://doi.org/10.1021/ja4000728.
(167) Jacobs, W. M.; Reinhardt, A.; Frenkel, D. Rational Design of Self-Assembly Pathways for Complex Multicomponent Structures. Proc. Natl. Acad. Sci. **2015**, 112 (20), 6313–6318. https://doi.org/10.1073/pnas.1502210112.
(168) Reinhardt, A.; Frenkel, D. Numerical Evidence for Nucleated Self-Assembly of DNA Brick Structures. Phys. Rev. Lett. **2014**, 112 (23), 238103. https://doi.org/10.1103/PhysRevLett.112.238103.
(169) Fonseca, P.; Romano, F.; Schreck, J. S.; Ouldridge, T. E.; Doye, J. P. K.; Louis, A. A. Multi-Scale Coarse-Graining for the Study of Assembly Pathways in DNA-Brick Self-Assembly. J. Chem. Phys. **2018**, 148 (13), 134910. https://doi.org/10.1063/1.5019344.
(170) Zhang, Y.; Reinhardt, A.; Wang, P.; Song, J.; Ke, Y. Programming the Nucleation of DNA Brick Self-Assembly with a Seeding Strand. Angew. Chem. **2020**, 132 (22), 8672–8678. https://doi.org/10.1002/ange.201915063.
(171) Funke, J. J.; Ketterer, P.; Lieleg, C.; Schunter, S.; Korber, P.; Dietz, H. Uncovering the Forces between Nucleosomes Using DNA Origami. Sci. Adv. **2016**, 2 (11), e1600974. https://doi.org/10.1126/sciadv.1600974.
(172) Douglas, S. M.; Bachelet, I.; Church, G. M. A Logic-Gated Nanorobot for Targeted Transport of Molecular Payloads. Science **2012**, 335 (6070), 831–834. https://doi.org/10.1126/science.1214081.
(173) Bazrafshan, A.; Meyer, T. A.; Su, H.; Brockman, J. M.; Blanchard, A. T.; Piranej, S.; Duan, Y.; Ke, Y.; Salaita, K. Tunable DNA Origami Motors Translocate Ballistically Over Mm Distances at Nm/s Speeds. Angew. Chem. Int. Ed. **2020**, 59 (24), 9514–9521. https://doi.org/10.1002/anie.201916281.
(174) Grossi, G.; Jepsen, M. D. E.; Kjems, J.; Andersen, E. S. Control of Enzyme Reactions by a Reconfigurable DNA Nanovault. Nat. Commun. **2017**, 8 (1), 992. https://doi.org/10.1038/s41467-017-01072-8.
(175) Tan, S. J.; Campolongo, M. J.; Luo, D.; Cheng, W. Building Plasmonic Nanostructures with DNA. Nat. Nanotechnol. **2011**, 6 (5), 268–276. https://doi.org/10.1038/nnano.2011.49.
(176) Grome, M. W.; Zhang, Z.; Pincet, F.; Lin, C. Vesicle Tubulation with Self-assembling DNA Nanosprings. Angew. Chem. Int. Ed. https://doi.org/10.1002/anie.201800141.
(177) Shen, Q.; Grome, M. W.; Yang, Y.; Lin, C. Engineering Lipid Membranes with Programmable DNA Nanostructures. Adv. Biosyst. **2020**, 4 (1), 1900215. https://doi.org/10.1002/adbi.201900215.
(178) Madsen, M.; Gothelf, K. V. Chemistries for DNA Nanotechnology. Chem. Rev. **2019**. https://doi.org/10.1021/acs.chemrev.8b00570.
(179) Liu, M.; Fu, J.; Hejesen, C.; Yang, Y.; Woodbury, N. W.; Gothelf, K.; Liu, Y.; Yan, H. A DNA Tweezer-Actuated Enzyme Nanoreactor. Nat. Commun. **2013**, 4, 2127. https://doi.org/10.1038/ncomms3127.
(180) Zhao, Z.; Fu, J.; Dhakal, S.; Johnson-Buck, A.; Liu, M.; Zhang, T.; Woodbury, N. W.; Liu, Y.; Walter, N. G.; Yan, H. Nanocaged Enzymes with Enhanced Catalytic Activity and Increased Stability against Protease Digestion. Nat. Commun. **2016**, 7, 10619. https://doi.org/10.1038/ncomms10619.
(181) Fu, J.; Liu, M.; Liu, Y.; Woodbury, N. W.; Yan, H. Interenzyme Substrate Diffusion for an Enzyme Cascade Organized on Spatially Addressable DNA Nanostructures. J. Am. Chem. Soc. **2012**, 134 (12), 5516–5519. https://doi.org/10.1021/ja300897h.
(182) Conrado, R. J.; Wu, G. C.; Boock, J. T.; Xu, H.; Chen, S. Y.; Lebar, T.; Turnšek, J.; Tomšič, N.; Avbelj, M.; Gaber, R.; Koprivnjak, T.; Mori, J.; Glavnik, V.; Vovk, I.; Benčina, M.; Hodnik, V.; Anderluh, G.; Dueber, J. E.; Jerala, R.; DeLisa, M. P. DNA-Guided Assembly of Biosynthetic Pathways Promotes Improved Catalytic Efficiency. Nucleic Acids Res. **2012**, 40 (4), 1879–1889. https://doi.org/10.1093/nar/gkr888.
(183) Glettenberg, M.; Niemeyer, C. M. Tuning of Peroxidase Activity by Covalently Tethered DNA Oligonucleotides. Bioconjug. Chem. **2009**, 20 (5), 969–975. https://doi.org/10.1021/bc800558g.

(184) Gao, Y.; Roberts, C. C.; Zhu, J.; Lin, J.-L.; Chang, C. A.; Wheeldon, I. Tuning Enzyme Kinetics through Designed Intermolecular Interactions Far from the Active Site. ACS Catal. **2015**, 5 (4), 2149–2153. https://doi.org/10.1021/acscatal.5b00130.
(185) Müller, J.; Niemeyer, C. M. DNA-Directed Assembly of Artificial Multienzyme Complexes. Biochem. Biophys. Res. Commun. **2008**, 377 (1), 62–67. https://doi.org/10.1016/j.bbrc.2008.09.078.
(186) Hahn, J.; Chou, L. Y. T.; Sørensen, R. S.; Guerra, R. M.; Shih, W. M. Extrusion of RNA from a DNA-Origami-Based Nanofactory. ACS Nano **2020**. https://doi.org/10.1021/acsnano.9b06466.
(187) Ke, G.; Liu, M.; Jiang, S.; Qi, X.; Yang, Y. R.; Wootten, S.; Zhang, F.; Zhu, Z.; Liu, Y.; Yang, C. J.; Yan, H. Directional Regulation of Enzyme Pathways through the Control of Substrate Channeling on a DNA Origami Scaffold. Angew. Chem. Int. Ed. **2016**, 55 (26), 7483–7486. https://doi.org/10.1002/anie.201603183.
(188) Jaekel, A.; Stegemann, P.; Saccà, B. Manipulating Enzymes Properties with DNA Nanostructures. Molecules **2019**, 24 (20), 3694. https://doi.org/10.3390/molecules24203694.
(189) Corey, D. R.; Schultz, P. G. Generation of a Hybrid Sequence-Specific Single-Stranded Deoxyribonuclease. Science **1987**, 238 (4832), 1401–1403. https://doi.org/10.1126/science.3685986.
(190) Rosen, C. B.; Kodal, A. L. B.; Nielsen, J. S.; Schaffert, D. H.; Scavenius, C.; Okholm, A. H.; Voigt, N. V.; Enghild, J. J.; Kjems, J.; Tørring, T.; Gothelf, K. V. Template-Directed Covalent Conjugation of DNA to Native Antibodies, Transferrin and Other Metal-Binding Proteins. Nat. Chem. **2014**, 6 (9), 804–809. https://doi.org/10.1038/nchem.2003.
(191) Cui, C.; Zhang, H.; Wang, R.; Cansiz, S.; Pan, X.; Wan, S.; Hou, W.; Li, L.; Chen, M.; Liu, Y.; Chen, X.; Liu, Q.; Tan, W. Recognition-Then-Reaction Enables Site-Selective Bioconjugation to Proteins on Live-Cell Surfaces. Angew. Chem. Int. Ed. **2017**, 56 (39), 11954–11957. https://doi.org/10.1002/anie.201706285.
(192) Hermanson, G. T. Chapter23 - Nucleic Acid and Oligonucleotide Modification and Conjugation. In Bioconjugate Techniques (Third edition); Academic Press: Boston, 2013; pp 959–987.
(193) Lieser, R. M.; Yur, D.; Sullivan, M. O.; Chen, W. Site-Specific Bioconjugation Approaches for Enhanced Delivery of Protein Therapeutics and Protein Drug Carriers. Bioconjug. Chem. **2020**, 31 (10), 2272–2282. https://doi.org/10.1021/acs.bioconjchem.0c00456.
(194) Saccà, B.; Meyer, R.; Erkelenz, M.; Kiko, K.; Arndt, A.; Schroeder, H.; Rabe, K. S.; Niemeyer, C. M. Orthogonal Protein Decoration of DNA Origami. Angew. Chem. Int. Ed. **2010**, 49 (49), 9378–9383. https://doi.org/10.1002/anie.201005931.
(195) Li, H.; Park, S. H.; Reif, J. H.; LaBean, T. H.; Yan, H. DNA-Templated Self-Assembly of Protein and Nanoparticle Linear Arrays. J. Am. Chem. Soc. **2004**, 126 (2), 418–419. https://doi.org/10.1021/ja0383367.
(196) Hager, R.; Burns, J. R.; Grydlik, M. J.; Halilovic, A.; Haselgrübler, T.; Schäffler, F.; Howorka, S. Co-Immobilization of Proteins and DNA Origami Nanoplates to Produce High-Contrast Biomolecular Nanoarrays. Small **2016**, 12 (21), 2877–2884. https://doi.org/10.1002/smll.201600311.
(197) Niemeyer, C. M.; Sano, T.; Smith, C. L.; Cantor, C. R. Oligonucleotide-Directed Self-Assembly of Proteins: Semisynthetic DNA—Streptavidin Hybrid Molecules as Connectors for the Generation of Macroscopic Arrays and the Construction of Supramolecular Bioconjugates. Nucleic Acids Res. **1994**, 22 (25), 5530–5539. https://doi.org/10.1093/nar/22.25.5530.
(198) Wacker, R.; Niemeyer, C. M. DDI-MFIA—A Readily Configurable Microarray-Fluorescence Immunoassay Based on DNA-Directed Immobilization of Proteins. ChemBioChem **2004**, 5 (4), 453–459. https://doi.org/10.1002/cbic.200300788.
(199) Kuzuya, A.; Kimura, M.; Numajiri, K.; Koshi, N.; Ohnishi, T.; Okada, F.; Komiyama, M. Precisely Programmed and Robust 2D Streptavidin Nanoarrays by Using Periodical Nanometer-Scale Wells Embedded in DNA Origami Assembly. ChemBioChem **2009**, 10 (11), 1811–1815. https://doi.org/10.1002/cbic.200900229.
(200) Fruk, L.; Müller, J.; Niemeyer, C. M. Kinetic Analysis of Semisynthetic Peroxidase Enzymes Containing a Covalent DNA–Heme Adduct as the Cofactor. Chem. – Eur. J. **2006**, 12 (28), 7448–7457. https://doi.org/10.1002/chem.200501613.
(201) Fruk, L.; Niemeyer, C. M. Covalent Hemin–DNA Adducts for Generating a Novel Class of Artificial Heme Enzymes. Angew. Chem. Int. Ed. **2005**, 44 (17), 2603–2606. https://doi.org/10.1002/anie.200462567.

(202) Nakata, E.; Liew, F. F.; Uwatoko, C.; Kiyonaka, S.; Mori, Y.; Katsuda, Y.; Endo, M.; Sugiyama, H.; Morii, T. Zinc-Finger Proteins for Site-Specific Protein Positioning on DNA-Origami Structures. Angew. Chem. Int. Ed. **2012**, 51 (10), 2421–2424. https://doi.org/10.1002/anie.201108199.
(203) Kramm, K.; Schröder, T.; Gouge, J.; Vera, A. M.; Gupta, K.; Heiss, F. B.; Liedl, T.; Engel, C.; Berger, I.; Vannini, A.; Tinnefeld, P.; Grohmann, D. DNA Origami-Based Single-Molecule Force Spectroscopy Elucidates RNA Polymerase III Pre-Initiation Complex Stability. Nat. Commun. **2020**, 11 (1), 2828. https://doi.org/10.1038/s41467-020-16702-x.
(204) Sprengel, A.; Lill, P.; Stegemann, P.; Bravo-Rodriguez, K.; Schöneweiß, E.-C.; Merdanovic, M.; Gudnason, D.; Aznauryan, M.; Gamrad, L.; Barcikowski, S.; Sanchez-Garcia, E.; Birkedal, V.; Gatsogiannis, C.; Ehrmann, M.; Saccà, B. Tailored Protein Encapsulation into a DNA Host Using Geometrically Organized Supramolecular Interactions. Nat. Commun. **2017**, 8, 14472. https://doi.org/10.1038/ncomms14472.
(205) Zhao, Z.; Zhang, M.; Hogle, J. M.; Shih, W. M.; Wagner, G.; Nasr, M. L. DNA-Corralled Nanodiscs for the Structural and Functional Characterization of Membrane Proteins and Viral Entry. J. Am. Chem. Soc. **2018**, 140 (34), 10639–10643. https://doi.org/10.1021/jacs.8b04638.
(206) Dong, Y.; Chen, S.; Zhang, S.; Sodroski, J.; Yang, Z.; Liu, D.; Mao, Y. Folding DNA into a Lipid-Conjugated Nanobarrel for Controlled Reconstitution of Membrane Proteins. Angew. Chem. Int. Ed. **2018**, 57 (8), 2072–2076. https://doi.org/10.1002/anie.201710147.
(207) Fu, J.; Yang, Y. R.; Johnson-Buck, A.; Liu, M.; Liu, Y.; Walter, N. G.; Woodbury, N. W.; Yan, H. Multi-Enzyme Complexes on DNA Scaffolds Capable of Substrate Channelling with an Artificial Swinging Arm. Nat. Nanotechnol. **2014**, 9 (7), 531–536. https://doi.org/10.1038/nnano.2014.100.
(208) Linko, V.; Eerikäinen, M.; Kostiainen, M. A. A Modular DNA Origami-Based Enzyme Cascade Nanoreactor. Chem. Commun. **2015**, 51 (25), 5351–5354. https://doi.org/10.1039/C4CC08472A.
(209) Bellot, G.; McClintock, M. A.; Chou, J. J.; Shih, W. M. DNA Nanotubes for NMR Structure Determination of Membrane Proteins. Nat. Protoc. **2013**, 8 (4), 755–770. https://doi.org/10.1038/nprot.2013.037.
(210) Iric, K.; Subramanian, M.; Oertel, J.; Agarwal, N. P.; Matthies, M.; Periole, X.; Sakmar, T. P.; Huber, T.; Fahmy, K.; Schmidt, T. L. DNA-Encircled Lipid Bilayers. Nanoscale **2018**, 10 (39), 18463–18467. https://doi.org/10.1039/C8NR06505E.
(211) Meyer, H.; Bug, M.; Bremer, S. Emerging Functions of the VCP/P97 AAA-ATPase in the Ubiquitin System. Nat. Cell Biol. **2012**, 14 (2), 117–123. https://doi.org/10.1038/ncb2407.
(212) Ye, Y.; Tang, W. K.; Zhang, T.; Xia, D. A Mighty "Protein Extractor" of the Cell: Structure and Function of the P97/CDC48 ATPase. Front. Mol. Biosci. **2017**, 4, 39. https://doi.org/10.3389/fmolb.2017.00039.
(213) Meyer, H.; Weihl, C. C. The VCP/P97 System at a Glance: Connecting Cellular Function to Disease Pathogenesis. J. Cell Sci. **2014**, 127 (18), 3877–3883. https://doi.org/10.1242/jcs.093831.
(214) Stach, L.; Freemont, P. S. The AAA+ ATPase P97, a Cellular Multitool. Biochem. J. **2017**, 474 (17), 2953–2976. https://doi.org/10.1042/BCJ20160783.
(215) Hänzelmann, P.; Schindelin, H. The Interplay of Cofactor Interactions and Post-Translational Modifications in the Regulation of the AAA+ ATPase P97. Front. Mol. Biosci. **2017**, 4. https://doi.org/10.3389/fmolb.2017.00021.
(216) van den Boom, J.; Meyer, H. VCP/P97-Mediated Unfolding as a Principle in Protein Homeostasis and Signaling. Mol. Cell **2018**, 69 (2), 182–194. https://doi.org/10.1016/j.molcel.2017.10.028.
(217) Snider, J.; Thibault, G.; Houry, W. A. The AAA+ Superfamily of Functionally Diverse Proteins. Genome Biol. **2008**, 9 (4), 216. https://doi.org/10.1186/gb-2008-9-4-216.
(218) Zhang, S.; Mao, Y. AAA+ ATPases in Protein Degradation: Structures, Functions and Mechanisms. Biomolecules **2020**, 10 (4), 629. https://doi.org/10.3390/biom10040629.
(219) DeLaBarre, B.; Brunger, A. T. Complete Structure of P97/Valosin-Containing Protein Reveals Communication between Nucleotide Domains. Nat. Struct. Mol. Biol. **2003**, 10 (10), 856–863. https://doi.org/10.1038/nsb972.
(220) Davies, J. M.; Brunger, A. T.; Weis, W. I. Improved Structures of Full-Length P97, an AAA ATPase: Implications for Mechanisms of Nucleotide-Dependent Conformational Change. Structure **2008**, 16 (5), 715–726. https://doi.org/10.1016/j.str.2008.02.010.
(221) Banerjee, S.; Bartesaghi, A.; Merk, A.; Rao, P.; Bulfer, S. L.; Yan, Y.; Green, N.; Mroczkowski, B.; Neitz, R. J.; Wipf, P.; Falconieri, V.; Deshaies, R. J.; Milne, J. L. S.; Huryn, D.; Arkin, M.; Subramaniam, S. 2.3 Å Resolution Cryo-EM Structure of Human P97 and Mechanism of

Allosteric Inhibition. Science **2016**, 351 (6275), 871–875. https://doi.org/10.1126/science.aad7974.
(222) Bodnar, N. O.; Rapoport, T. A. Molecular Mechanism of Substrate Processing by the Cdc48 ATPase Complex. Cell **2017**, 169 (4), 722-735.e9. https://doi.org/10.1016/j.cell.2017.04.020.
(223) Barthelme, D.; Sauer, R. T. Origin and Functional Evolution of the Cdc48/P97/VCP AAA+ Protein Unfolding and Remodeling Machine. J. Mol. Biol. **2016**, 428 (9, Part B), 1861–1869. https://doi.org/10.1016/j.jmb.2015.11.015.
(224) Zhang, X.; Gui, L.; Zhang, X.; Bulfer, S. L.; Sanghez, V.; Wong, D. E.; Lee, Y.; Lehmann, L.; Lee, J. S.; Shih, P.-Y.; Lin, H. J.; Iacovino, M.; Weihl, C. C.; Arkin, M. R.; Wang, Y.; Chou, T.-F. Altered Cofactor Regulation with Disease-Associated P97/VCP Mutations. Proc. Natl. Acad. Sci. **2015**, 112 (14), E1705–E1714. https://doi.org/10.1073/pnas.1418820112.
(225) Blythe, E. E.; Olson, K. C.; Chau, V.; Deshaies, R. J. Ubiquitin- and ATP-Dependent Unfoldase Activity of P97/VCP•NPLOC4•UFD1L Is Enhanced by a Mutation That Causes Multisystem Proteinopathy. Proc. Natl. Acad. Sci. **2017**, 114 (22), E4380–E4388. https://doi.org/10.1073/pnas.1706205114.
(226) Cooney, I.; Han, H.; Stewart, M. G.; Carson, R. H.; Hansen, D. T.; Iwasa, J. H.; Price, J. C.; Hill, C. P.; Shen, P. S. Structure of the Cdc48 Segregase in the Act of Unfolding an Authentic Substrate. Science **2019**, 365 (6452), 502–505. https://doi.org/10.1126/science.aax0486.
(227) Pan, M.; Zheng, Q.; Yu, Y.; Ai, H.; Xie, Y.; Zeng, X.; Wang, C.; Liu, L.; Zhao, M. Seesaw Conformations of Npl4 in the Human P97 Complex and the Inhibitory Mechanism of a Disulfiram Derivative. Nat. Commun. **2021**, 12 (1), 121. https://doi.org/10.1038/s41467-020-20359-x.
(228) Weith, M.; Seiler, J.; van den Boom, J.; Kracht, M.; Hülsmann, J.; Primorac, I.; del Pino Garcia, J.; Kaschani, F.; Kaiser, M.; Musacchio, A.; Bollen, M.; Meyer, H. Ubiquitin-Independent Disassembly by a P97 AAA-ATPase Complex Drives PP1 Holoenzyme Formation. Mol. Cell **2018**, 72 (4), 766-777.e6. https://doi.org/10.1016/j.molcel.2018.09.020.
(229) Kracht, M.; van den Boom, J.; Seiler, J.; Kröning, A.; Kaschani, F.; Kaiser, M.; Meyer, H. Protein Phosphatase-1 Complex Disassembly by P97 Is Initiated through Multivalent Recognition of Catalytic and Regulatory Subunits by the P97 SEP-Domain Adapters. J. Mol. Biol. **2020**, 432 (23), 6061–6074. https://doi.org/10.1016/j.jmb.2020.10.001.
(230) Ando, R.; Hama, H.; Yamamoto-Hino, M.; Mizuno, H.; Miyawaki, A. An Optical Marker Based on the UV-Induced Green-to-Red Photoconversion of a Fluorescent Protein. Proc. Natl. Acad. Sci. **2002**, 99 (20), 12651–12656. https://doi.org/10.1073/pnas.202320599.
(231) Mizuno, H.; Mal, T. K.; Tong, K. I.; Ando, R.; Furuta, T.; Ikura, M.; Miyawaki, A. Photo-Induced Peptide Cleavage in the Green-to-Red Conversion of a Fluorescent Protein. Mol. Cell **2003**, 12 (4), 1051–1058. https://doi.org/10.1016/S1097-2765(03)00393-9.
(232) Zhang, M.; Chang, H.; Zhang, Y.; Yu, J.; Wu, L.; Ji, W.; Chen, J.; Liu, B.; Lu, J.; Liu, Y.; Zhang, J.; Xu, P.; Xu, T. Rational Design of True Monomeric and Bright Photoactivatable Fluorescent Proteins. Nat. Methods **2012**, 9 (7), 727–729. https://doi.org/10.1038/nmeth.2021.
(233) Twomey, E. C.; Ji, Z.; Wales, T. E.; Bodnar, N. O.; Ficarro, S. B.; Marto, J. A.; Engen, J. R.; Rapoport, T. A. Substrate Processing by the Cdc48 ATPase Complex Is Initiated by Ubiquitin Unfolding. Science **2019**, 365 (6452). https://doi.org/10.1126/science.aax1033.
(234) Cabrera, Ma. Á.; Blamey, J. M. Biotechnological Applications of Archaeal Enzymes from Extreme Environments. Biol. Res. **2018**, 51 (1), 37. https://doi.org/10.1186/s40659-018-0186-3.
(235) Turner, P.; Mamo, G.; Karlsson, E. N. Potential and Utilization of Thermophiles and Thermostable Enzymes in Biorefining. Microb. Cell Factories **2007**, 6 (1), 9. https://doi.org/10.1186/1475-2859-6-9.
(236) Perugino, G.; Miggiano, R.; Serpe, M.; Vettone, A.; Valenti, A.; Lahiri, S.; Rossi, F.; Rossi, M.; Rizzi, M.; Ciaramella, M. Structure-Function Relationships Governing Activity and Stability of a DNA Alkylation Damage Repair Thermostable Protein. Nucleic Acids Res. **2015**, 43 (18), 8801–8816. https://doi.org/10.1093/nar/gkv774.
(237) Perugino, G.; Vettone, A.; Illiano, G.; Valenti, A.; Ferrara, M. C.; Rossi, M.; Ciaramella, M. Activity and Regulation of Archaeal DNA Alkyltransferase. J. Biol. Chem. **2012**, 287 (6), 4222–4231. https://doi.org/10.1074/jbc.M111.308320.
(238) Vettone, A.; Serpe, M.; Hidalgo, A.; Berenguer, J.; Monaco, G. del; Valenti, A.; Rossi, M.; Ciaramella, M.; Perugino, G. A Novel Thermostable Protein-Tag: Optimization of the Sulfolobus

Solfataricus DNA- Alkyl-Transferase by Protein Engineering. Extremophiles **2016**, 20 (1), 1–13. https://doi.org/10.1007/s00792-015-0791-9.
(239) Fokkens, M.; Schrader, T.; Klärner, F.-G. A Molecular Tweezer for Lysine and Arginine. J. Am. Chem. Soc. **2005**, 127 (41), 14415–14421. https://doi.org/10.1021/ja052806a.
(240) Klärner, F.-G.; Kahlert, B.; Nellesen, A.; Zienau, J.; Ochsenfeld, C.; Schrader, T. Molecular Tweezer and Clip in Aqueous Solution: Unexpected Self-Assembly, Powerful Host−Guest Complex Formation, Quantum Chemical 1H NMR Shift Calculation. J. Am. Chem. Soc. **2006**, 128 (14), 4831–4841. https://doi.org/10.1021/ja058410g.
(241) Meiners, A.; Bäcker, S.; Hadrović, I.; Heid, C.; Beuck, C.; Ruiz-Blanco, Y. B.; Mieres-Perez, J.; Pörschke, M.; Grad, J.-N.; Vallet, C.; Hoffmann, D.; Bayer, P.; Sánchez-García, E.; Schrader, T.; Knauer, S. K. Specific Inhibition of the Survivin–CRM1 Interaction by Peptide-Modified Molecular Tweezers. Nat. Commun. **2021**, 12 (1), 1505. https://doi.org/10.1038/s41467-021-21753-9.
(242) Bier, D.; Rose, R.; Bravo-Rodriguez, K.; Bartel, M.; Ramirez-Anguita, J. M.; Dutt, S.; Wilch, C.; Klärner, F.-G.; Sanchez-Garcia, E.; Schrader, T.; Ottmann, C. Molecular Tweezers Modulate 14-3-3 Protein–Protein Interactions. Nat. Chem. **2013**, 5 (3), 234–239. https://doi.org/10.1038/nchem.1570.
(243) Trusch, F.; Kowski, K.; Bravo-Rodriguez, K.; Beuck, C.; Sowislok, A.; Wettig, B.; Matena, A.; Sanchez-Garcia, E.; Meyer, H.; Schrader, T.; Bayer, P. Molecular Tweezers Target a Protein–Protein Interface and Thereby Modulate Complex Formation. Chem. Commun. **2016**, 52 (98), 14141–14144. https://doi.org/10.1039/C6CC08039A.
(244) Stahl, E.; Martin, T. G.; Praetorius, F.; Dietz, H. Facile and Scalable Preparation of Pure and Dense DNA Origami Solutions. Angew. Chem. Int. Ed. **2014**, 53 (47), 12735–12740. https://doi.org/10.1002/anie.201405991.
(245) Efiok, B. J. S. Basic Calculations for Chemical and Biological Analysis; AOAC International: Arlington, Va., 1993.
(246) Gerstein, A. S. Nucleotides, Oligonucleotides,and Polynucleotides. In Molecular Biology Problem Solver; John Wiley & Sons, Ltd, 2001; pp 267–289. https://doi.org/10.1002/0471223905.ch10.
(247) Sprengel, A. Tailored Protein Encapsulation into a DNA Host Using Geometrically Organized Supramolecular Interactions, Universität Duisburg-Essen, Essen, 2017.
(248) Kim, D.-N.; Kilchherr, F.; Dietz, H.; Bathe, M. Quantitative Prediction of 3D Solution Shape and Flexibility of Nucleic Acid Nanostructures. Nucleic Acids Res. **2012**, 40 (7), 2862–2868. https://doi.org/10.1093/nar/gkr1173.
(249) Ovid; Kline, A. S. Metamorphoses; Borders Classics: Ann Arbor, MI, 2004.
(250) Schneider, F.; Möritz, N.; Dietz, H. The Sequence of Events during Folding of a DNA Origami. Sci. Adv. **2019**, 5 (5), eaaw1412. https://doi.org/10.1126/sciadv.aaw1412.
(251) Allen, M. D.; Buchberger, A.; Bycroft, M. The PUB Domain Functions as a P97 Binding Module in Human Peptide N-Glycanase. J. Biol. Chem. **2006**, 281 (35), 25502–25508. https://doi.org/10.1074/jbc.M601173200.
(252) Blueggel, M.; van den Boom, J.; Meyer, H.; Bayer, P.; Beuck, C. Structure of the PUB Domain from Ubiquitin Regulatory X Domain Protein 1 (UBXD1) and Its Interaction with the P97 AAA+ ATPase. Biomolecules **2019**, 9 (12), 876. https://doi.org/10.3390/biom9120876.
(253) Keefe, A. D.; Wilson, D. S.; Seelig, B.; Szostak, J. W. One-Step Purification of Recombinant Proteins Using a Nanomolar-Affinity Streptavidin-Binding Peptide, the SBP-Tag. Protein Expr. Purif. **2001**, 23 (3), 440–446. https://doi.org/10.1006/prep.2001.1515.
(254) Chaiet, L.; Wolf, F. J. The Properties of Streptavidin, a Biotin-Binding Protein Produced by Streptomycetes. Arch. Biochem. Biophys. **1964**, 106, 1–5. https://doi.org/10.1016/0003-9861(64)90150-X.
(255) Southern, E. M. Detection of Specific Sequences among DNA Fragments Separated by Gel Electrophoresis. J. Mol. Biol. **1975**, 98 (3), 503–517. https://doi.org/10.1016/S0022-2836(75)80083-0.
(256) Heid, C.; Sowislok, A.; Schaller, T.; Niemeyer, F.; Klärner, F.-G.; Schrader, T. Molecular Tweezers with Additional Recognition Sites. Chem. – Eur. J. **2018**, 24 (44), 11332–11343. https://doi.org/10.1002/chem.201801508.
(257) Mason, A. J.; Hurst, I.; Malik, R.; Siddique, I.; Solomonov, I.; Sagi, I.; Klärner, F.-G.; Schrader, T.; Bitan, G. Different Inhibitors of Aβ42-Induced Toxicity Have Distinct Metal-Ion Dependency. ACS Chem. Neurosci. **2020**, 11 (15), 2243–2255. https://doi.org/10.1021/acschemneuro.0c00192.

(258) Ouyang, X.; De Stefano, M.; Krissanaprasit, A.; Kodal, A. L. B.; Rosen, C. B.; Liu, T.; Helmig, S.; Fan, C.; Gothelf, K. V. Docking of Antibodies into Cavities in DNA Origami. Angew. Chem. Int. Ed. n/a-n/a. https://doi.org/10.1002/anie.201706765.
(259) Kube, M.; Kohler, F.; Feigl, E.; Nagel-Yüksel, B.; Willner, E. M.; Funke, J. J.; Gerling, T.; Stömmer, P.; Honemann, M. N.; Martin, T. G.; Scheres, S. H. W.; Dietz, H. Revealing the Structures of Megadalton-Scale DNA Complexes with Nucleotide Resolution. Nat. Commun. **2020**, 11 (1), 6229. https://doi.org/10.1038/s41467-020-20020-7.
(260) Mallik, L.; Dhakal, S.; Nichols, J.; Mahoney, J.; Dosey, A. M.; Jiang, S.; Sunahara, R. K.; Skiniotis, G.; Walter, N. G. Electron Microscopic Visualization of Protein Assemblies on Flattened DNA Origami. ACS Nano **2015**, 9 (7), 7133–7141. https://doi.org/10.1021/acsnano.5b01841.
(261) Arbona, J.-M.; Aimé, J.-P.; Elezgaray, J. Cooperativity in the Annealing of DNA Origamis. J. Chem. Phys. **2013**, 138 (1), 015105. https://doi.org/10.1063/1.4773405.
(262) Majikes, J. M.; Nash, J. A.; LaBean, T. H. Competitive Annealing of Multiple DNA Origami: Formation of Chimeric Origami. New J. Phys. **2016**, 18 (11), 115001. https://doi.org/10.1088/1367-2630/18/11/115001.
(263) Groeer, S.; Walther, A. Switchable Supracolloidal 3D DNA Origami Nanotubes Mediated through Fuel/Antifuel Reactions. Nanoscale **2020**, 12 (32), 16995–17004. https://doi.org/10.1039/D0NR04209A.
(264) Ketterer, P.; Willner, E. M.; Dietz, H. Nanoscale Rotary Apparatus Formed from Tight-Fitting 3D DNA Components. Sci. Adv. **2016**, 2 (2), e1501209. https://doi.org/10.1126/sciadv.1501209.
(265) Marras, A. E.; Shi, Z.; Lindell, M. G.; Patton, R. A.; Huang, C.-M.; Zhou, L.; Su, H.-J.; Arya, G.; Castro, C. E. Cation-Activated Avidity for Rapid Reconfiguration of DNA Nanodevices. ACS Nano **2018**, 12 (9), 9484–9494. https://doi.org/10.1021/acsnano.8b04817.
(266) Liu, Y.; Cheng, J.; Fan, S.; Ge, H.; Luo, T.; Tang, L.; Ji, B.; Zhang, C.; Cui, D.; Ke, Y.; Song, J. Modular Reconfigurable DNA Origami: From Two-Dimensional to Three-Dimensional Structures. Angew. Chem. Int. Ed. **2020**, 59 (51), 23277–23282. https://doi.org/10.1002/anie.202010433.
(267) Kuzyk, A.; Yang, Y.; Duan, X.; Stoll, S.; Govorov, A. O.; Sugiyama, H.; Endo, M.; Liu, N. A Light-Driven Three-Dimensional Plasmonic Nanosystem That Translates Molecular Motion into Reversible Chiroptical Function. Nat. Commun. **2016**, 7 (1), 10591. https://doi.org/10.1038/ncomms10591.
(268) Marras, A. E.; Zhou, L.; Su, H.-J.; Castro, C. E. Programmable Motion of DNA Origami Mechanisms. Proc. Natl. Acad. Sci. **2015**, 112 (3), 713–718.
(269) Lee, C.; Lee, J. Y.; Kim, D.-N. Polymorphic Design of DNA Origami Structures through Mechanical Control of Modular Components. Nat. Commun. **2017**, 8 (1), 2067. https://doi.org/10.1038/s41467-017-02127-6.
(270) Galvin, C. J.; Shirai, K.; Rahmani, A.; Masaya, K.; Shen, A. Q. Total Capture, Convection-Limited Nanofluidic Immunoassays Exhibiting Nanoconfinement Effects. Anal. Chem. **2018**, 90 (5), 3211–3219. https://doi.org/10.1021/acs.analchem.7b04664.
(271) Hayer-Hartl, M.; Minton, A. P. A Simple Semiempirical Model for the Effect of Molecular Confinement upon the Rate of Protein Folding. Biochemistry **2006**, 45 (44), 13356–13360. https://doi.org/10.1021/bi061597j.
(272) Siefker, J.; Biehl, R.; Kruteva, M.; Feoktystov, A.; Coppens, M.-O. Confinement Facilitated Protein Stabilization As Investigated by Small-Angle Neutron Scattering. J. Am. Chem. Soc. **2018**, 140 (40), 12720–12723. https://doi.org/10.1021/jacs.8b08454.
(273) Sang, L.-C.; Coppens, M.-O. Effects of Surface Curvature and Surface Chemistry on the Structure and Activity of Proteins Adsorbed in Nanopores. Phys. Chem. Chem. Phys. **2011**, 13 (14), 6689–6698. https://doi.org/10.1039/C0CP02273J.
(274) Zhang, Y.; Tsitkov, S.; Hess, H. Proximity Does Not Contribute to Activity Enhancement in the Glucose Oxidase–Horseradish Peroxidase Cascade. Nat. Commun. **2016**, 7, ncomms13982. https://doi.org/10.1038/ncomms13982.
(275) Roodhuizen, J. A. L.; Hendrikx, P. J. T. M.; Hilbers, P. A. J.; de Greef, T. F. A.; Markvoort, A. J. Counterion-Dependent Mechanisms of DNA Origami Nanostructure Stabilization Revealed by Atomistic Molecular Simulation. ACS Nano **2019**, 13 (9), 10798–10809. https://doi.org/10.1021/acsnano.9b05650.

(276) Zhou, H.-X. Influence of Crowded Cellular Environments on Protein Folding, Binding, and Oligomerization: Biological Consequences and Potentials of Atomistic Modeling. FEBS Lett. **2013**, 587 (8), 1053–1061. https://doi.org/10.1016/j.febslet.2013.01.064.
(277) Wang, W.; Xu, W.-X.; Levy, Y.; Trizac, E.; Wolynes, P. G. Confinement Effects on the Kinetics and Thermodynamics of Protein Dimerization. Proc. Natl. Acad. Sci. **2009**, 106 (14), 5517–5522. https://doi.org/10.1073/pnas.0809649106.
(278) Cordova, J. C.; Olivares, A. O.; Shin, Y.; Stinson, B. M.; Calmat, S.; Schmitz, K. R.; Aubin-Tam, M.-E.; Baker, T. A.; Lang, M. J.; Sauer, R. T. Stochastic but Highly Coordinated Protein Unfolding and Translocation by the ClpXP Proteolytic Machine. Cell **2014**, 158 (3), 647–658. https://doi.org/10.1016/j.cell.2014.05.043.
(279) Kenniston, J. A.; Baker, T. A.; Sauer, R. T. Partitioning between Unfolding and Release of Native Domains during ClpXP Degradation Determines Substrate Selectivity and Partial Processing. Proc. Natl. Acad. Sci. **2005**, 102 (5), 1390–1395. https://doi.org/10.1073/pnas.0409634102.
(280) Göpfrich, K.; Li, C.-Y.; Ricci, M.; Bhamidimarri, S. P.; Yoo, J.; Gyenes, B.; Ohmann, A.; Winterhalter, M.; Aksimentiev, A.; Keyser, U. F. Large-Conductance Transmembrane Porin Made from DNA Origami. ACS Nano **2016**, 10 (9), 8207–8214. https://doi.org/10.1021/acsnano.6b03759.
(281) Langecker, M.; Arnaut, V.; Martin, T. G.; List, J.; Renner, S.; Mayer, M.; Dietz, H.; Simmel, F. C. Synthetic Lipid Membrane Channels Formed by Designed DNA Nanostructures. Science **2012**, 338 (6109), 932–936. https://doi.org/10.1126/science.1225624.
(282) Cassinelli, V.; Oberleitner, B.; Sobotta, J.; Nickels, P.; Grossi, G.; Kempter, S.; Frischmuth, T.; Liedl, T.; Manetto, A. One-Step Formation of "Chain-Armor"-Stabilized DNA Nanostructures. Angew. Chem. Int. Ed. **2015**, 54 (27), 7795–7798. https://doi.org/10.1002/anie.201500561.
(283) Song, J.; Arbona, J.-M.; Zhang, Z.; Liu, L.; Xie, E.; Elezgaray, J.; Aime, J.-P.; Gothelf, K. V.; Besenbacher, F.; Dong, M. Direct Visualization of Transient Thermal Response of a DNA Origami. J. Am. Chem. Soc. **2012**, 134 (24), 9844–9847. https://doi.org/10.1021/ja3017939.
(284) Baggiani, C.; Giovannoli, C.; Anfossi, L.; Passini, C.; Baravalle, P.; Giraudi, G. A Connection between the Binding Properties of Imprinted and Nonimprinted Polymers: A Change of Perspective in Molecular Imprinting. J. Am. Chem. Soc. **2012**, 134 (3), 1513–1518. https://doi.org/10.1021/ja205632t.
(285) Smolin, D.; Tötsch, N.; Grad, J.-N.; Linders, J.; Kaschani, F.; Kaiser, M.; Kirsch, M.; Hoffmann, D.; Schrader, T. Accelerated Trypsin Autolysis by Affinity Polymer Templates. RSC Adv. **2020**, 10 (48), 28711–28719. https://doi.org/10.1039/D0RA05827K.
(286) Gilles, P.; Wenck, K.; Stratmann, I.; Kirsch, M.; Smolin, D. A.; Schaller, T.; de Groot, H.; Kraft, A.; Schrader, T. High-Affinity Copolymers Inhibit Digestive Enzymes by Surface Recognition. Biomacromolecules **2017**, 18 (6), 1772–1784. https://doi.org/10.1021/acs.biomac.7b00162.
(287) Li, G.; Zheng, W.; Chen, Z.; Zhou, Y.; Liu, Y.; Yang, J.; Huang, Y.; Li, X. Design, Preparation, and Selection of DNA-Encoded Dynamic Libraries. Chem. Sci. **2015**, 6 (12), 7097–7104. https://doi.org/10.1039/C5SC02467F.
(288) Reddavide, F. V.; Lin, W.; Lehnert, S.; Zhang, Y. DNA-Encoded Dynamic Combinatorial Chemical Libraries. Angew. Chem. Int. Ed. **2015**, 54 (27), 7924–7928. https://doi.org/10.1002/anie.201501775.
(289) Reddavide, F. V.; Cui, M.; Lin, W.; Fu, N.; Heiden, S.; Andrade, H.; Thompson, M.; Zhang, Y. Second Generation DNA-Encoded Dynamic Combinatorial Chemical Libraries. Chem. Commun. **2019**, 55 (26), 3753–3756. https://doi.org/10.1039/C9CC01429B.
(290) Viguera, A. R.; Villa, M. J.; Goñi, F. M. A Water-Soluble Polylysine-Retinaldehyde Schiff Base. Stability in Aqueous and Nonaqueous Environments. J. Biol. Chem. **1990**, 265 (5), 2527–2532.
(291) Cai, X.; Li, Y.; Yue, D.; Yi, Q.; Li, S.; Shi, D.; Gu, Z. Reversible PEGylation and Schiff-Base Linked Imidazole Modification of Polylysine for High-Performance Gene Delivery. J. Mater. Chem. B **2015**, 3 (8), 1507–1517. https://doi.org/10.1039/C4TB01724B.
(292) Kodal, A. L. B.; Rosen, C. B.; Mortensen, M. R.; Tørring, T.; Gothelf, K. V. DNA-Templated Introduction of an Aldehyde Handle in Proteins. ChemBioChem **2016**, 17 (14), 1338–1342. https://doi.org/10.1002/cbic.201600254.
(293) Panda, D.; Datta, A. Evidence for Covalent Binding of Epicocconone with Proteins from Synchronous Fluorescence Spectra and Fluorescence Lifetimes. J. Chem. Sci. **2007**, 119 (2), 99–104. https://doi.org/10.1007/s12039-007-0016-6.

(294) Georgiou, C. D.; Grintzalis, K.; Zervoudakis, G.; Papapostolou, I. Mechanism of Coomassie Brilliant Blue G-250 Binding to Proteins: A Hydrophobic Assay for Nanogram Quantities of Proteins. Anal. Bioanal. Chem. **2008**, 391 (1), 391–403. https://doi.org/10.1007/s00216-008-1996-x.
(295) de Llano, E.; Miao, H.; Ahmadi, Y.; Wilson, A. J.; Beeby, M.; Viola, I.; Barisic, I. Adenita: Interactive 3D Modelling and Visualization of DNA Nanostructures. Nucleic Acids Res. https://doi.org/10.1093/nar/gkaa593.
(296) Yoo, J.; Aksimentiev, A. In Situ Structure and Dynamics of DNA Origami Determined through Molecular Dynamics Simulations. Proc. Natl. Acad. Sci. **2013**, 110 (50), 20099–20104.
(297) Castro, C. E.; Kilchherr, F.; Kim, D.-N.; Shiao, E. L.; Wauer, T.; Wortmann, P.; Bathe, M.; Dietz, H. A Primer to Scaffolded DNA Origami. Nat. Methods **2011**, 8 (3), 221–229. https://doi.org/10.1038/nmeth.1570.
(298) Tang, G.; Peng, L.; Baldwin, P. R.; Mann, D. S.; Jiang, W.; Rees, I.; Ludtke, S. J. EMAN2: An Extensible Image Processing Suite for Electron Microscopy. J. Struct. Biol. **2007**, 157 (1), 38–46. https://doi.org/10.1016/j.jsb.2006.05.009.
(299) Random DNA Generator http://www.faculty.ucr.edu/~mmaduro/random.htm (accessed 2021 -07 -08).
(300) Schindelin, J.; Arganda-Carreras, I.; Frise, E.; Kaynig, V.; Longair, M.; Pietzsch, T.; Preibisch, S.; Rueden, C.; Saalfeld, S.; Schmid, B.; Tinevez, J.-Y.; White, D. J.; Hartenstein, V.; Eliceiri, K.; Tomancak, P.; Cardona, A. Fiji: An Open-Source Platform for Biological-Image Analysis. Nat. Methods **2012**, 9 (7), 676–682. https://doi.org/10.1038/nmeth.2019.
(301) Barrette-Ng, I. H.; Wu, S.-C.; Tjia, W.-M.; Wong, S.-L.; Ng, K. K. S. The Structure of the SBP-Tag–Streptavidin Complex Reveals a Novel Helical Scaffold Bridging Binding Pockets on Separate Subunits. Acta Crystallogr. D Biol. Crystallogr. **2013**, 69 (5), 879–887. https://doi.org/10.1107/S0907444913002576.
(302) Abe, H.; Abe, N.; Shibata, A.; Ito, K.; Tanaka, Y.; Ito, M.; Saneyoshi, H.; Shuto, S.; Ito, Y. Structure Formation and Catalytic Activity of DNA Dissolved in Organic Solvents. Angew. Chem. Int. Ed. **2012**, 51 (26), 6475–6479. https://doi.org/10.1002/anie.201201111.
(303) Mok, H.; Park, T. G. PEG-Assisted DNA Solubilization in Organic Solvents for Preparing Cytosol Specifically Degradable PEG/DNA Nanogels. Bioconjug. Chem. **2006**, 17 (6), 1369–1372. https://doi.org/10.1021/bc060119i.
(304) Renart, J.; Reiser, J.; Stark, G. R. Transfer of Proteins from Gels to Diazobenzyloxymethyl-Paper and Detection with Antisera: A Method for Studying Antibody Specificity and Antigen Structure. Proc. Natl. Acad. Sci. U. S. A. **1979**, 76 (7), 3116–3120.
(305) Bebeacua, C.; Förster, A.; McKeown, C.; Meyer, H. H.; Zhang, X.; Freemont, P. S. Distinct Conformations of the Protein Complex P97-Ufd1-Npl4 Revealed by Electron Cryomicroscopy. Proc. Natl. Acad. Sci. **2012**, 109 (4), 1098–1103. https://doi.org/10.1073/pnas.1114341109.
(306) Le, L. T. M.; Kang, W.; Kim, J.-Y.; Le, O. T. T.; Lee, S. Y.; Yang, J. K. Structural Details of Ufd1 Binding to P97 and Their Functional Implications in ER-Associated Degradation. PLoS ONE **2016**, 11 (9), e0163394. https://doi.org/10.1371/journal.pone.0163394.
(307) Swierczewska, M.; Lee, S.; Chen, X. The Design and Application of Fluorophore–Gold Nanoparticle Activatable Probes. Phys. Chem. Chem. Phys. PCCP **2011**, 13 (21), 9929–9941. https://doi.org/10.1039/c0cp02967j.
(308) Teschome, B.; Facsko, S.; Gothelf, K. V.; Keller, A. Alignment of Gold Nanoparticle-Decorated DNA Origami Nanotubes: Substrate Prepatterning versus Molecular Combing. Langmuir **2015**, 31 (46), 12823–12829. https://doi.org/10.1021/acs.langmuir.5b02569.
(309) Hartl, C.; Frank, K.; Amenitsch, H.; Fischer, S.; Liedl, T.; Nickel, B. Position Accuracy of Gold Nanoparticles on DNA Origami Structures Studied with Small-Angle X-Ray Scattering. Nano Lett. **2018**, 18 (4), 2609–2615. https://doi.org/10.1021/acs.nanolett.8b00412.
(310) Schmuck, C.; Rupprecht, D.; Junkers, M.; Schrader, T. Artificial Ditopic Arg-Gly-Asp (RGD) Receptors. Chem. – Eur. J. **2007**, 13 (24), 6864–6873. https://doi.org/10.1002/chem.200601821.
(311) Schmuck, C.; Schwegmann, M. A Naked-Eye Sensing Ensemble for the Selective Detection of Citrate—but Not Tartrate or Malate—in Water Based on a Tris-Cationic Receptor. Org. Biomol. Chem. **2006**, 4 (5), 836–838. https://doi.org/10.1039/B516019G.
(312) Schmuck, C. Side Chain Selective Binding of N-Acetyl-α-Amino Acid Carboxylates by a 2-(Guanidiniocarbonyl)Pyrrole Receptor in Aqueous Solvents. Chem. Commun. **1999**, No. 9, 843–844. https://doi.org/10.1039/A901126I.

(313) Rensing, S.; Arendt, M.; Springer, A.; Grawe, T.; Schrader, T. Optimization of a Synthetic Arginine Receptor. Systematic Tuning of Noncovalent Interactions. J. Org. Chem. **2001**, 66 (17), 5814–5821. https://doi.org/10.1021/jo0156161.

Appendix

I. Materials and equipment used in this work

a. Kits and Chemicals

Table 0-1: Commercially obtained kits and chemicals for this work

Name	Vendor	Notes
1000 bp ladder + loading dye	New England Biolabs	
acetic acid	Fisher Chemicals	
acrylamide/bis solution (19:1; 40% w/v)	Merck	for SDS and nat. PAGE
acrylamide/bis solution (37.5:1; 30% w/v)	Merck	for den. PAGE
ammonium acetate	VWR	
APS	Carl Roth GmbH + Co. KG	
bacto tryptone	Becton, Dickinson and company	
bacto yeast extract	Merck	
BG GLA NHS	Promega	Snaptag ligand
boric acid	Carl Roth GmbH + Co. KG	
bromophenol blue sodium salt	Merck	
cacodylate	Merck	
calcium chloride	Merck	
Coomassie R250	Thermo Fisher scientific	
$CuSO_4$	Merck	
dodecyne	Acros Organics	
DyLight Maleimide (Alexa650)	Thermo Fisher scientific	
EDC	Fluoro Chem	
ethanol	VWR	
ethidium bromide	Merck	
glycerol	Merck	
glycine	VWR	
Halotag Succinimidyl Ester (O4) Ligand	Promega	Halotag ligand
HCl	Merck	for pH adjustment
HEPES	Merck	
imidazole	Merck	
isopropanol	VWR	
LE agarose	Affymetrix	
lysis-Buffer (0.2 M NaOH, 1% SDS)	Macherey-Nagel	
magnesiumchlorid hexahydrate	Merck	
Na_2EDTA	Merck	
n-butanol	VWR	
Neutralization-Buffer (3 M KOAc pH 5.5)	Macherey-Nagel	
N-Z-Amine (NZA)	Merck	
PEG8000	Merck	
potassium chloride	Carl Roth GmbH + Co. KG	
sodium acetate	VWR	
sodium ascorbate	Merck	
Sodium chloride	Carl Roth GmbH + Co. KG	

sodium dihydrogenphosphate	Merck
Sodium dodecyl sulfate (SDS)	Merck
sodium hydrogenhosphate	Merck
Spectra™ Multicolor Broad range protein ladder	Thermo Fisher Scientific
Spectra™ Multicolor low range protein ladder	Thermo Fisher Scientific
SYBR Gold nucleic acid gel staining	Thermo Fisher Scientific
SYBR green	Thermo Fisher Scientific
TBTA	Merck
TCEP	Merck
TEMED	Carl Roth GmbH + Co. KG
Tetracycline	Merck
Tris base	Merck
Tris-HCl	Merck
urea	Merck
NHS-PEG5000	Nanocs

b. ssDNA strands

Scaffold sequences were purchased from tilibit nanosystems GmbH, Munich, Germany and amplified as described in (section 3.4, page 18).

M13mp18 (p7249) scaffold sequence:

AATGCTACTACTATTAGTAGAATTGATGCCACCTTTTCAGCTCGCGCCCCAAATGAAAATATAGCTAAACAGGTTATTGACCATTTGCGAAATGTATCTAATGGTCAAACTAA
ATCTACTCGTTCGCAGAATTGGGAATCAACTGTTATATGGAATGAAACTTCCAGACACCGTACTTTAGTTGCATATTTAAAACATGTTGAGCTACAGCATTATATTCAGCAAT
TAAGCTCTAAGCCATCCGCAAAAATGACCTCTTATCAAAAGGAGCAATTAAAGGTACTCTCTAATCCTGACCTGTTGGAGTTTGCTTCCGGTCTGGTTCGCTTTGAAGCTCGA
ATTAAAACGCGATATTTGAAGTCTTTCGGGCTTCCTCTTAATCTTTTTGATGCAATCCGCTTTGCTTCTGACTATAATAGTCAGGGTAAAGACCTGATTTTTGATTTATGGTCA
TTCTCGTTTTCTGAACTGTTTAAAGCATTTGAGGGGGATTCAATGAATATTTATGACGATTCCGCAGTATTGGACGCTATCCAGTCTAAACATTTTACTATTACCCCCTCTGG
CAAAACTTCTTTTGCAAAAGCCTCTCGCTATTTTGGTTTTTATCGTCGTCTGGTAAACGAGGGTTATGATAGTGTTGCTCTTACTATGCCTCGTAATTCCTTTTGGCGTTATGT
ATCTGCATTAGTTGAATGTGGTATTCCTAAATCTCAACTGATGAATCTTTCTACCTGTAATAATGTTGTTCCGTTAGTTCGTTTTATTAACGTAGATTTTTCTTCCCAACGTCCT
GACTGGTATAATGAGCCAGTTCTTAAAATCGCATAAGGTAATTCACAATGATTAAAGTTGAAATTAAACCATCTCAAGCCCAATTTACTACTCGTTCTGGTGTTTCTCGTCAG
GGCAAGCCTTATTCACTGAATGAGCAGCTTTGTTACGTTGATTTGGGTAATGAATATCCGGTTCTTGTCAAGATTACTCTTGATGAAGGTCAGCCAGCCTATGCGCCTGGTC
TGTACACCGTTCATCTGTCCTCTTTCAAAGTTGGTCAGTTCGGTTCCCTTATGATTGACCGTCTGCGCCTCGTTCCGGCTAAGTAACATGGAGCAGGTCGCGGATTTCGACAC
AATTTATCAGGCGATGATACAAATCTCCGTTGTACTTTGTTTCGCGCTTGGTATAATCGCTGGGGGTCAAAGATGAGTGTTTTAGTGTATTCTTTTGCCTCTTTCGTTTTAGG
TTGGTGCCTTCGTAGTGGCATTACGTATTTTACCCGTTTAATGGAAACTTCCTCATGAAAAAGTCTTTAGTCCTCAAAGCCTCTGTAGCCGTTGCTACCCTCGTTCCGATGCT
GTCTTTCGCTGCTGAGGGTGACGATCCCGCAAAAGCGGCCTTTAACTCCCTGCAAGCCTCAGCGACCGAATATATCGGTTATGCGTGGGCGATGGTTGTTGTCATTGTCGG
CGCAACTATCGGTATCAAGCTGTTTAAGAAATTCACCTCGAAAGCAAGCTGATAAACCGATACAATTAAAGGCTCCTTTTGGAGCCTTTTTTTTGGAGATTTTCAACGTGAAA
AAATTATTATTCGCAATTCCTTTAGTTGTTCCTTTCTATTCTCACTCCGCTGAAACTGTTGAAAGTTGTTTAGCAAAATCCCATACAGAAAATTCATTTACTAACGTCTGGAAA
GACGACAAAACTTTAGATCGTTACGCTAACTATGAGGGCTGTCTGTGGAATGCTACAGGCGTTGTAGTTTGTACTGGTGACGAAACTCAGTGTTACGGTACATGGGTTCCT
ATTGGGCTTGCTATCCCTGAAAATGAGGGTGGTGGCTCTGAGGGTGGCGGTTCTGAGGGTGGCGGTTCTGAGGGTGGCGGTACTAAACCTCCTGAGTACGGTGATACAC
CTATTCCGGGCTATACTTATATCAACCCTCTCGACGGCACTTATCCGCCTGGTACTGAGCAAAACCCCGCTAATCCTAATCCTTCTCTTGAGGAGTCTCAGCCTCTTAATACTT
TCATGTTTCAGAATAATAGGTTCCGAAATAGGCAGGGGGCATTAACTGTTTATACGGGCACTGTTACTCAAGGCACTGACCCCGTTAAAACTTATTACCAGTACACTCCTGT
ATCATCAAAAGCCATGTATGACGCTTACTGGAACGGTAAATTCAGAGACTGCGCTTTCCATTCTGGCTTTAATGAGGATTTATTTGTTTGTGAATATCAAGGCCAATCGTCTG
ACCTGCCTCAACCTCCTGTCAATGCTGGCGGCGGCTCTGGTGGTGGTTCTGGTGGCGGCTCTGAGGGTGGTGGCTCTGAGGGTGGCGGTTCTGAGGGTGGCGGCTCTGA
GGGAGGCGGTTCCGGTGGTGGCTCTGGTTCCGGTGATTTTGATTATGAAAAGATGGCAAACGCTAATAAGGGGGCTATGACCGAAAATGCCGATGAAAACGCGCTACAG
TCTGACGCTAAAGGCAAACTTGATTCTGTCGCTACTGATTACGGTGCTGCTATCGATGGTTTCATTGGTGACGTTTCCGGCCTTGCTAATGGTAATGGTGCTACTGGTGATT
TTGCTGGCTCTAATTCCCAAATGGCTCAAGTCGGTGACGGTGATAATTCACCTTTAATGAATAATTTCCGTCAATATTTACCTTCCCTCCCTCAATCGGTTGAATGTCGCCCTT
TTGTCTTTGGCGCTGGTAAACCATATGAATTTTCTATTGATTGTGACAAAATAAACTTATTCCGTGGTGTCTTTGCGTTTCTTTTATATGTTGCCACCTTTATGTATGTATTTT
CTACGTTTGCTAACATACTGCGTAATAAGGAGTCTTAATCATGCCAGTTCTTTTGGGTATTCCGTTATTATTGCGTTTCCTCGGTTTCCTTCTGGTAACTTTGTTCGGCTATCT
GCTTACTTTTCTTAAAAAGGGCTTCGGTAAGATAGCTATTGCTATTTCATTGTTTCTTGCTCTTATTATTGGGCTTAACTCAATTCTTGTGGGTTATCTCTCTGATATTAGCGC
TCAATTACCCTCTGACTTTGTTCAGGGTGTTCAGTTAATTCTCCCGTCTAATGCGCTTCCCTGTTTTTATGTTATTCTCTCTGTAAAGGCTGCTATTTTCATTTTTGACGTTAAA
CAAAAAATCGTTTCTTATTTGGATTGGGATAAATAATATGGCTGTTTATTTTGTAACTGGCAAATTAGGCTCTGGAAAGACGCTCGTTAGCGTTGGTAAGATTCAGGATAAA
ATTGTAGCTGGGTGCAAAATAGCAACTAATCTTGATTTAAGGCTTCAAAACCTCCCGCAAGTCGGGAGGTTCGCTAAAACGCCTCGCGTTCTTAGAATACCGGATAAGCCTT
CTATATCTGATTTGCTTGCTATTGGGCGCGGTAATGATTCCTACGATGAAAATAAAAACGGCTTGCTTGTTCTCGATGAGTGCGGTACTTGGTTTAATACCCGTTCTTGGAA
TGATAAGGAAAGACAGCCGATTATTGATTGGTTTCTACATGCTCGTAAATTAGGATGGGATATTATTTTTCTTGTTCAGGACTTATCTATTGTTGATAAACAGGCGCGTTCT
GCATTAGCTGAACATGTTGTTTATTGTCGTCGTCTGGACAGAATTACTTTACCTTTTGTCGGTACTTTATATTCTCTTATTACTGGCTCGAAAATGCCTCTGCCTAAATTACAT
GTTGGCGTTGTTAAATATGGCGATTCTCAATTAAGCCCTACTGTTGAGCGTTGGCTTTATACTGGTAAGAATTTGTATAACGCATATGATACTAAACAGGCTTTTTCTAGTAA
TTATGATTCCGGTGTTTATTCTTATTTAACGCCTTATTTATCACACGGTCGGTATTTCAAACCATTAAATTTAGGTCAGAAGATGAAATTAACTAAAATATATTTGAAAAAGTT
TTCTCGCGTTCTTTGTCTTGCGATTGGATTTGCATCAGCATTTACATATAGTTATATAACCCAACCTAAGCCGGAGGTTAAAAAGGTAGTCTCTCAGACCTATGATTTTGATA
AATTCACTATTGACTCTTCTCAGCGTCTTAATCTAAGCTATCGCTATGTTTTCAAGGATTCTAAGGGAAAATTAATTAATAGCGACGATTTACAGAAGCAAGGTTATTCACTC

ACATATATTGATTTATGTACTGTTTCCATTAAAAAAGGTAATTCAAATGAAATTGTTAAATGTAATTAATTTTGTTTTCTTGATGTTTGTTTCATCATCTTCTTTTGCTCAGGTA
ATTGAAATGAATAATTCGCCTCTGCGCGATTTTGTAACTTGGTATTCAAAGCAATCAGGCGAATCCGTTATTGTTTCTCCCGATGTAAAAGGTACTGTTACTGTATATTCATC
TGACGTTAAACCTGAAAATCTACGCAATTTCTTTATTTCTGTTTTACGTGCAAATAATTTTGATATGGTAGGTTCTAACCCTTCCATTATTCAGAAGTATAATCCAAACAATCA
GGATTATATTGATGAATTGCCATCATCTGATAATCAGGAATATGATGATAATTCCGCTCCTTCTGGTGGTTTCTTTGTTCCGCAAAATGATAATGTTACTCAAACTTTTAAAAT
TAATAACGTTCGGGCAAAGGATTTAATACGAGTTGTCGAATTGTTTGTAAAGTCTAATACTTCTAAATCCTCAAATGTATTATCTATTGACGGCTCTAATCTATTAGTTGTTA
GTGCTCCTAAAGATATTTTAGATAACCTTCCTCAATTCCTTTCAACTGTTGATTTGCCAACTGACCAGATATTGATTGAGGGTTTGATATTTGAGGTTCAGCAAGGTGATGCT
TTAGATTTTTCATTTGCTGCTGGCTCTCAGCGTGGCACTGTTGCAGGCGGTGTTAATACTGACCGCCTCACCTCTGTTTTATCTTCTGCTGGTGGTTCGTTCGGTATTTTTAA
TGGCGATGTTTTAGGGCTATCAGTTCGCGCATTAAAGACTAATAGCCATTCAAAAATATTGTCTGTGCCACGTATTCTTACGCTTTCAGGTCAGAAGGGTTCTATCTCTGTTG
GCCAGAATGTCCCTTTTATTACTGGTCGTGTGACTGGTGAATCTGCCAATGTAAATAATCCATTTCAGACGATTGAGCGTCAAAATGTAGGTATTTCCATGAGCGTTTTTCCT
GTTGCAATGGCTGGCGGTAATATTGTTCTGGATATTACCAGCAAGGCCGATAGTTTGAGTTCTTCTACTCAGGCAAGTGATGTTATTACTAATCAAAGAAGTATTGCTACAA
CGGTTAATTTGCGTGATGGACAGACTCTTTTACTCGGTGGCCTCACTGATTATAAAAACACTTCTCAGGATTCTGGCGTACCGTTCCTGTCTAAAATCCCTTTAATCGGCCTC
CTGTTTAGCTCCCGCTCTGATTCTAACGAGGAAAGCACGTTATACGTGCTCGTCAAAGCAACCATAGTACGCGCCCTGTAGCGGCGCATTAAGCGCGGCGGGTGTGGTGGT
TACGCGCAGCGTGACCGCTACACTTGCCAGCGCCCTAGCGCCCGCTCCTTTCGCTTTCTTCCCTTCCTTTCTCGCCACGTTCGCCGGCTTTCCCCGTCAAGCTCTAAATCGGG
GGCTCCCTTTAGGGTTCCGATTTAGTGCTTTACGGCACCTCGACCCCAAAAAACTTGATTTGGGTGATGGTTCACGTAGTGGGCCATCGCCCTGATAGACGGTTTTTCGCCC
TTTGACGTTGGAGTCCACGTTCTTTAATAGTGGACTCTTGTTCCAAACTGGAACAACACTCAACCCTATCTCGGGCTATTCTTTTGATTTATAAGGGATTTTGCCGATTTCGG
AACCACCATCAAACAGGATTTTCGCCTGCTGGGGCAAACCAGCGTGGACCGCTTGCTGCAACTCTCTCAGGGCCAGGCGGTGAAGGGCAATCAGCTGTTGCCCGTCTCACT
GGTGAAAAGAAAAACCACCCTGGCGCCCAATACGCAAACCGCCTCTCCCCGCGCGTTGGCCGATTCATTAATGCAGCTGGCACGACAGGTTTCCCGACTGGAAAGCGGGCA
GTGAGCGCAACGCAATTAATGTGAGTTAGCTCACTCATTAGGCACCCCAGGCTTTACACTTTATGCTTCCGGCTCGTATGTTGTGTGGAATTGTGAGCGGATAACAATTTCA
CACAGGAAACAGCTATGACCATGATTACGAATTCGAGCTCGGTACCCGGGGATCCTCTAGAGTCGACCTGCAGGCATGCAAGCTTGGCACTGGCCGTCGTTTTACAACGTC
GTGACTGGGAAAACCCTGGCGTTACCCAACTTAATCGCCTTGCAGCACATCCCCCTTTCGCCAGCTGGCGTAATAGCGAAGAGGCCCGCACCGATCGCCCTTCCCAACAGTT
GCGCAGCCTGAATGGCGAATGGCGCTTTGCCTGGTTTCCGGCACCAGAAGCGGTGCCGGAAAGCTGGCTGGAGTGCGATCTTCCTGAGGCCGATACTGTCGTCGTCCCCT
CAAACTGGCAGATGCACGGTTACGATGCGCCCATCTACACCAACGTGACCTATCCCATTACGGTCAATCCGCCGTTTGTTCCCACGGAGAATCCGACGGGTTGTTACTCGCT
CACATTTAATGTTGATGAAAGCTGGCTACAGGAAGGCCAGACGCGAATTATTTTTGATGGCGTTCCTATTGGTTAAAAAATGAGCTGATTTAACAAAAATTTAATGCGAATT
TTAACAAAATATTAACGTTTACAATTTAAATATTTGCTTATACAATCTTCCTGTTTTTGGGGCTTTTCTGATTATCAACCGGGGTACATATGATTGACATGCTAGTTTTACGAT
TACCGTTCATCGATTCTCTTGTTTGCTCCAGACTCTCAGGCAATGACCTGATAGCCTTTGTAGATCTCTCAAAAATAGCTACCCTCTCCGGCATTAATTTATCAGCTAGAACGG
TTGAATATCATATTGATGGTGATTTGACTGTCTCCGGCCTTTCTCACCCTTTTGAATCTTTACCTACACATTACTCAGGCATTGCATTTAAAATATATGAGGGTTCTAAAAATT
TTTATCCTTGCGTTGAAATAAAGGCTTCTCCCGCAAAAGTATTACAGGGTCATAATGTTTTTGGTACAACCGATTTAGCTTTATGCTCTGAGGCTTTATTGCTTAATTTTGCTA
ATTCTTTGCCTTGCCTGTATGATTTATTGGATGTT

p7560 scaffold sequence:

AGCTTGGCACTGGCCGTCGTTTTACAACGTCGTGACTGGGAAAACCCTGGCGTTACCCAACTTAATCGCCTTGCAGCACATCCCCCTTTCGCCAGCTGGCGTAATAGCGAAG
AGGCCCGCACCGATCGCCCTTCCCAACAGTTGCGCAGCCTGAATGGCGAATGGCGCTTTGCCTGGTTTCCGGCACCAGAAGCGGTGCCGGAAAGCTGGCTGGAGTGCGAT
CTTCCTGAGGCCGATACTGTCGTCGTCCCCTCAAACTGGCAGATGCACGGTTACGATGCGCCCATCTACACCAACGTGACCTATCCCATTACGGTCAATCCGCCGTTTGTTCC
CACGGAGAATCCGACGGGTTGTTACTCGCTCACATTTAATGTTGATGAAAGCTGGCTACAGGAAGGCCAGACGCGAATTATTTTTGATGGCGTTCCTATTGGTTAAAAAAT
GAGCTGATTTAACAAAAATTTAATGCGAATTTTAACAAAATATTAACGTTTACAATTTAAATATTTGCTTATACAATCTTCCTGTTTTTGGGGCTTTTCTGATTATCAACCGGG
GTACATATGATTGACATGCTAGTTTTACGATTACCGTTCATCGATTCTCTTGTTTGCTCCAGACTCTCAGGCAATGACCTGATAGCCTTTGTAGATCTCTCAAAAATAGCTACC
CTCTCCGGCATTAATTTATCAGCTAGAACGGTTGAATATCATATTGATGGTGATTTGACTGTCTCCGGCCTTTCTCACCCTTTTGAATCTTTACCTACACATTACTCAGGCATT
GCATTTAAAATATATGAGGGTTCTAAAAATTTTTATCCTTGCGTTGAAATAAAGGCTTCTCCCGCAAAAGTATTACAGGGTCATAATGTTTTTGGTACAACCGATTTAGCTTT
ATGCTCTGAGGCTTTATTGCTTAATTTTGCTAATTCTTTGCCTTGCCTGTATGATTTATTGGATGTTAATGCTACTACTATTAGTAGAATTGATGCCACCTTTTCAGCTCGCGC
CCCAAATGAAAATATAGCTAAACAGGTTATTGACCATTTGCGAAATGTATCTAATGGTCAAACTAAATCTACTCGTTCGCAGAATTGGGAATCAACTGTTATATGGAATGAA
ACTTCCAGACACCGTACTTTAGTTGCATATTTAAAACATGTTGAGCTACAGCATTATATTCAGCAATTAAGCTCTAAGCCATCCGCAAAAATGACCTCTTATCAAAAGGAGCA
ATTAAAGGTACTCTCTAATCCTGACCTGTTGGAGTTTGCTTCCGGTCTGGTTCGCTTTGAAGCTCGAATTAAAACGCGATATTTGAAGTCTTTCGGGCTTCCTCTTAATCTTT
TTGATGCAATCCGCTTTGCTTCTGACTATAATAGTCAGGGTAAAGACCTGATTTTTGATTTATGGTCATTCTCGTTTTCTGAACTGTTTAAAGCATTTGAGGGGGATTCAATG
AATATTTATGACGATTCCGCAGTATTGGACGCTATCCAGTCTAAACATTTTACTATTACCCCCTCTGGCAAAACTTCTTTTGCAAAAGCCTCTCGCTATTTTGGTTTTTATCGTC
GTCTGGTAAACGAGGGTTATGATAGTGTTGCTCTTACTATGCCTCGTAATTCCTTTTGGCGTTATGTATCTGCATTAGTTGAATGTGGTATTCCTAAATCTCAACTGATGAAT
CTTTCTACCTGTAATAATGTTGTTCCGTTAGTTCGTTTTATTAACGTAGATTTTTCTTCCCAACGTCCTGACTGGTATAATGAGCCAGTTCTTAAAATCGCATAAGGTAATTCA
CAATGATTAAAGTTGAAATTAAACCATCTCAAGCCCAATTTACTACTCGTTCTGGTGTTTCTCGTCAGGGCAAGCCTTATTCACTGAATGAGCAGCTTTGTTACGTTGATTTG
GGTAATGAATATCCGGTTCTTGTCAAGATTACTCTTGATGAAGGTCAGCCAGCCTATGCGCCTGGTCTGTACACCGTTCATCTGTCCTCTTTCAAAGTTGGTCAGTTCGGTTC
CCTTATGATTGACCGTCTGCGCCTCGTTCCGGCTAAGTAACATGGAGCAGGTCGCGGATTTCGACACAATTTATCAGGCGATGATACAAATCTCCGTTGTACTTTGTTTCGC
GCTTGGTATAATCGCTGGGGGTCAAAGATGAGTGTTTTAGTGTATTCTTTTGCCTCTTTCGTTTTAGGTTGGTGCCTTCGTAGTGGCATTACGTATTTTACCCGTTTAATGG
AAACTTCCTCATGAAAAAGTCTTTAGTCCTCAAAGCCTCTGTAGCCGTTGCTACCCTCGTTCCGATGCTGTCTTTCGCTGCTGAGGGTGACGATCCCGCAAAAGCGGCCTTTA
ACTCCCTGCAAGCCTCAGCGACCGAATATATCGGTTATGCGTGGGCGATGGTTGTTGTCATTGTCGGCGCAACTATCGGTATCAAGCTGTTTAAGAAATTCACCTCGAAAGC
AAGCTGATAAACCGATACAATTAAAGGCTCCTTTTGGAGCCTTTTTTTTGGAGATTTTCAACGTGAAAAAATTATTATTCGCAATTCCTTTAGTTGTTCCTTTCTATTCTCACTC
CGCTGAAACTGTTGAAAGTTGTTTAGCAAAATCCCATACAGAAAATTCATTTACTAACGTCTGGAAAGACGACAAAACTTTAGATCGTTACGCTAACTATGAGGGCTGTCTG
TGGAATGCTACAGGCGTTGTAGTTTGTACTGGTGACGAAACTCAGTGTTACGGTACATGGGTTCCTATTGGGCTTGCTATCCCTGAAAATGAGGGTGGTGGCTCTGAGGG
TGGCGGTTCTGAGGGTGGCGGTTCTGAGGGTGGCGGTACTAAACCTCCTGAGTACGGTGATACACCTATTCCGGGCTATACTTATATCAACCCTCTCGACGGCACTTATCC
GCCTGGTACTGAGCAAAACCCCGCTAATCCTAATCCTTCTCTTGAGGAGTCTCAGCCTCTTAATACTTTCATGTTTCAGAATAATAGGTTCCGAAATAGGCAGGGGGCATTAA
CTGTTTATACGGGCACTGTTACTCAAGGCACTGACCCCGTTAAAACTTATTACCAGTACACTCCTGTATCATCAAAAGCCATGTATGACGCTTACTGGAACGGTAAATTCAGA
GACTGCGCTTTCCATTCTGGCTTTAATGAGGATTTATTTGTTTGTGAATATCAAGGCCAATCGTCTGACCTGCCTCAACCTCCTGTCAATGCTGGCGGCGGCTCTGGTGGTG
GTTCTGGTGGCGGCTCTGAGGGTGGTGGCTCTGAGGGTGGCGGCTCTGAGGGTGGCGGCTCTGAGGGAGGCGGTTCCGGTGGTGGCTCTGGTTCCGGTGATTTTGATT
ATGAAAAGATGGCAAACGCTAATAAGGGGGCTATGACCGAAAATGCCGATGAAAACGCGCTACAGTCTGACGCTAAAGGCAAACTTGATTCTGTCGCTACTGATTACGGTG
CTGCTATCGATGGTTTCATTGGTGACGTTTCCGGCCTTGCTAATGGTAATGGTGCTACTGGTGATTTTGCTGGCTCTAATTCCCAAATGGCTCAAGTCGGTGACGGTGATAA
TTCACCTTTAATGAATAATTTCCGTCAATATTTACCTTCCCTCCCTCAATCGGTTGAATGTCGCCCTTTTGTCTTTGGCGCTGGTAAACCATATGAATTTTCTATTGATTGTGAC
AAAATAAACTTATTCCGTGGTGTCTTTGCGTTTCTTTTATATGTTGCCACCTTTATGTATGTATTTTCTACGTTTGCTAACATACTGCGTAATAAGGAGTCTTAATCATGCCAG
TTCTTTTGGGTATTCCGTTATTATTGCGTTTCCTCGGTTTCCTTCTGGTAACTTTGTTCGGCTATCTGCTTACTTTTCTTAAAAAGGGCTTCGGTAAGATAGCTATTGCTATTT
CATTGTTTCTTGCTCTTATTATTGGGCTTAACTCAATTCTTGTGGGTTATCTCTCTGATATTAGCGCTCAATTACCCTCTGACTTTGTTCAGGGTGTTCAGTTAATTCTCCCGTC
TAATGCGCTTCCCTGTTTTTATGTTATTCTCTCTGTAAAGGCTGCTATTTTCATTTTTGACGTTAAACAAAAAATCGTTTCTTATTTGGATTGGGATAAATAATATGGCTGTTT
ATTTTGTAACTGGCAAATTAGGCTCTGGAAAGACGCTCGTTAGCGTTGGTAAGATTCAGGATAAAATTGTAGCTGGGTGCAAAATAGCAACTAATCTTGATTTAAGGCTTCA
AAACCTCCCGCAAGTCGGGAGGTTCGCTAAAACGCCTCGCGTTCTTAGAATACCGGATAAGCCTTCTATATCTGATTTGCTTGCTATTGGGCGCGGTAATGATTCCTACGAT

GAAAATAAAAACGGCTTGCTTGTTCTCGATGAGTGCGGTACTTGGTTTAATACCCGTTCTTGGAATGATAAGGAAAGACAGCCGATTATTGATTGGTTTCTACATGCTCGTA
AATTAGGATGGGATATTATTTTTCTTGTTCAGGACTTATCTATTGTTGATAAACAGGCGCGTTCTGCATTAGCTGAACATGTTGTTTATTGTCGTCGTCTGGACAGAATTACT
TTACCTTTTGTCGGTACTTTATATTCTCTTATTACTGGCTCGAAAATGCCTCTGCCTAAATTACATGTTGGCGTTGTTAAATATGGCGATTCTCAATTAAGCCCTACTGTTGAG
CGTTGGCTTTATACTGGTAAGAATTTGTATAACGCATATGATACTAAACAGGCTTTTTCTAGTAATTATGATTCCGGTGTTTATTCTTATTTAACGCCTTATTTATCACACGGT
CGGTATTTCAAACCATTAAATTTAGGTCAGAAGATGAAATTAACTAAAATATATTTGAAAAAGTTTTCTCGCGTTCTTTGTCTTGCGATTGGATTTGCATCAGCATTTACATAT
AGTTATATAACCCAACCTAAGCCGGAGGTTAAAAAGGTAGTCTCTCAGACCTATGATTTTGATAAATTCACTATTGACTCTTCTCAGCGTCTTAATCTAAGCTATCGCTATGTT
TTCAAGGATTCTAAGGGAAAATTAATTAATAGCGACGATTTACAGAAGCAAGGTTATTCACTCACATATATTGATTTATGTACTGTTTCCATTAAAAAAGGTAATTCAAATGA
AATTGTTAAATGTAATTAATTTTGTTTTCTTGATGTTTGTTTCATCATCTTCTTTTGCTCAGGTAATTGAAATGAATAATTCGCCTCTGCGCGATTTTGTAACTTGGTATTCAA
AGCAATCAGGCGAATCCGTTATTGTTTCTCCCGATGTAAAAGGTACTGTTACTGTATATTCATCTGACGTTAAACCTGAAAATCTACGCAATTTCTTTATTTCTGTTTTACGTG
CAAATAATTTTGATATGGTAGGTTCTAACCCTTCCATTATTCAGAAGTATAATCCAAACAATCAGGATTATATTGATGAATTGCCATCATCTGATAATCAGGAATATGATGAT
AATTCCGCTCCTTCTGGTGGTTTCTTTGTTCCGCAAAATGATAATGTTACTCAAACTTTTAAAATTAATAACGTTCGGGCAAAGGATTTAATACGAGTTGTCGAATTGTTTGT
AAAGTCTAATACTTCTAAATCCTCAAATGTATTATCTATTGACGGCTCTAATCTATTAGTTGTTAGTGCTCCTAAAGATATTTTAGATAACCTTCCTCAATTCCTTTCAACTGTT
GATTTGCCAACTGACCAGATATTGATTGAGGGTTTGATATTTGAGGTTCAGCAAGGTGATGCTTTAGATTTTTCATTTGCTGCTGGCTCTCAGCGTGGCACTGTTGCAGGC
GGTGTTAATACTGACCGCCTCACCTCTGTTTTATCTTCTGCTGGTGGTTCGTTCGGTATTTTTAATGGCGATGTTTTAGGGCTATCAGTTCGCGCATTAAAGACTAATAGCCA
TTCAAAAATATTGTCTGTGCCACGTATTCTTACGCTTTCAGGTCAGAAGGGTTCTATCTCTGTTGGCCAGAATGTCCCTTTTATTACTGGTCGTGTGACTGGTGAATCTGCCA
ATGTAAATAATCCATTTCAGACGATTGAGCGTCAAAATGTAGGTATTTCCATGAGCGTTTTTCCTGTTGCAATGGCTGGCGGTAATATTGTTCTGGATATTACCAGCAAGGC
CGATAGTTTGAGTTCTTCTACTCAGGCAAGTGATGTTATTACTAATCAAAGAAGTATTGCTACAACGGTTAATTTGCGTGATGGACAGACTCTTTTACTCGGTGGCCTCACT
GATTATAAAAACACTTCTCAGGATTCTGGCGTACCGTTCCTGTCTAAAATCCCTTTAATCGGCCTCCTGTTTAGCTCCCGCTCTGATTCTAACGAGGAAAGCACGTTATACGT
GCTCGTCAAAGCAACCATAGTACGCGCCCTGTAGCGGCGCATTAAGCGCGGCGGGTGTGGTGGTTACGCGCAGCGTGACCGCTACACTTGCCAGCGCCCTAGCGCCCGCT
CCTTTCGCTTTCTTCCCTTCCTTTCTCGCCACGTTCGCCGGCTTTCCCCGTCAAGCTCTAAATCGGGGGCTCCCTTTAGGGTTCCGATTTAGTGCTTTACGGCACCTCGACCCC
AAAAAACTTGATTTGGGTGATGGTTCACGTAGTGGGCCATCGCCCTGATAGACGGTTTTTCGCCCTTTGACGTTGGAGTCCACGTTCTTTAATAGTGGACTCTTGTTCCAAA
CTGGAACAACACTCAACCCTATCTCGGGCTATTCTTTTGATTTATAAGGGATTTTGCCGATTTCGGAACCACCATCAAACAGGATTTTCGCCTGCTGGGGCAAACCAGCGTG
GACCGCTTGCTGCAACTCTCTCAGGGCCAGGCGGTGAAGGGCAATCAGCTGTTGCCCGTCTCACTGGTGAAAAGAAAAACCACCCTGGCGCCCAATACGCAAACCGCCTCT
CCCCGCGCGTTGGCCGATTCATTAATGCAGCTGGCACGACAGGTTTCCCGACTGGAAAGCGGGCAGTGAGCGCAACGCAATTAATGTGAGTTAGCTCACTCATTAGGCACC
CCAGGCTTTACACTTTATGCTTCCGGCTCGTATGTTGTGTGGAATTGTGAGCGGATAACAATTTCACACAGGAAACAGCTATGACCATGATTACGAATTCGAGCTCGGTACC
CGGGGATCCTCCGTCTTTATCGAGGTAACAAGCACCACGTAGCTTAAGCCCTGTTTACTCATTACACCAACCAGGAGGTCAGAGTTCGGAGAAATGATTTATGTGAAATGCG
TCAGCCGATTCAAGGCCCCTATATTCGTGCCCACCGACGAGTTGCTTACAGATGGCAGGGCCGCACTGTCGGTATCATAGAGTCACTCCAGGGCGAGCGTAAATAGATTAG
AAGCGGGGTTATTTTGGCGGGACATTGTCATAAGGTTGACAATTCAGCACTAAGGACACTTAAGTCGTGCGCATGAATTCACAACCACTTAGAAGAACATCCACCCTGGCTT
CTCCTGAGAA

Staple sequences were ordered from former Sigma-Aldrich Chemie GmbH, Steinheim, Germany, now part of the Merck group. Following tables contain the DNA staple sequences used for the DNA origami production in this work. Start and End mark the respective base position in the cadnano design file.

Table 0-2: 6p120 core staples

Start	End	Sequence	total length (base)
0[159]	2[160]	CACTACGTAAACCGTCTATCAGGGTTTTTCGGTTTGC	37
0[31]	2[32]	GAAGGGAATTTTTTGGTGGTTCCGAAATCCGAAAATC	37
1[112]	47[110]	CCACTATTGAGGTGCCGTAAAGGCGCCG	28
1[144]	47[142]	AGGGCGAAGAACCATCACCCAATGACGA	28
1[48]	47[47]	CCCTTATAAAGCCGGCGAACGTCGCTAGG	29
1[80]	47[79]	GGTTGAGTAAGGGAGCCCCCGATGCGCGT	29
10[159]	12[160]	CAAAAACAAGCATAAAGCTAAATCTTTTTCTGTAGCT	37
10[31]	12[32]	GGGTGAGATTTTTAGCTATATTTTCATTTGGTCAATA	37
11[112]	9[111]	CAAGGCAACTTTATTTCAACGCAATTTTTGAG	32
11[144]	9[143]	AGCCTCAGTTATGACCCTGTAATATTGCCTGA	32
11[48]	9[47]	AGCTGAAATAATGTGTAGGTAAAGAAATCACC	32
11[80]	9[79]	TAGTAGCAAACCCTCATATATTTTAGCTGATA	32
12[159]	14[160]	CAACATGTATTGCTGAATATAATGTTTTTCATTGAAT	37
12[31]	14[32]	ACCTGTTTTTTTTATATCGCGTTTTAATTGCCCGAAA	37
13[112]	11[111]	TTTTGATAAGTTTCATTCCATATACATACAGG	32
13[144]	11[143]	AGAGCTTATTTAAATATGCAACTAAGCAATAA	32
13[48]	11[47]	AAAGCGAAGATACATTTCGCAAATGGGGCGCG	32
13[80]	11[79]	GGTCAGGATCTGCGAACGAGTAGAACTAATAG	32
14[127]	16[128]	GAGAATGAATGTTTAGACTGGATAGTAACGGAACA	35
14[159]	16[160]	CCCCCTCAAATCGTCATAAATATTTTGGGAAGAAA	35
14[31]	16[32]	GACTTCAATTTTTAACACTATCATAACCCTACGAGGCATA	40
14[63]	16[64]	TTGCATCAGATAAAAACCAAAATAGACTAATGCAG	35
14[95]	16[96]	ACCCTGACAAAGAAGTTTTGCCAGATCATCAGTTG	35
15[112]	13[111]	ATAGTAAACCATAAATCAAAAATCATTGCTCC	32
15[144]	13[143]	TACTGCGGAATGCTTTAAACAGTTGATGGCTT	32
15[48]	13[47]	CAGACGACAAAAGATTAAGAGGAACGAGCTTC	32
15[80]	13[79]	CTTTTGCATATTATAGTCAGAAGCCTCCAACA	32
16[159]	18[160]	AATCTACGATTGTGAATTACCTTACTGCTCCA	32

16[190]	17[190]	TTATTATGGCTCTT	14
16[31]	18[32]	GTAAGAGCTTTTTGAACCGGATATTCATTAGAGTAAT	37
17[112]	15[111]	AGTAAATTACAGGTAGAAAGATGGGGGTA	29
17[144]	15[143]	CTTTAATCTTAATAAAACGAACCGTCCAA	29
17[176]	16[170]	TAAGAACTACCAGTCAGGACGT	22
17[48]	15[47]	CAACGTAACGCCAAAAGGAATTCGTTTAC	29
17[80]	15[79]	GGCTTGCCGAATACCACATTCACGAGAGG	29
18[159]	20[160]	TGTTACTTAACAAAGTACAACGGACACGCATA	32
18[190]	19[190]	TTAATTGTGATATT	14
18[31]	20[32]	CTTGACAATTTTTATGAGGAAGTTTCCATGACTAAAG	37
19[112]	17[111]	AACACTCAGGGAACCGAACTGACCGAACGAGT	32
19[144]	17[143]	AAGCGCGAAGCCGGAACGAGGCGCAATTTCAA	32
19[176]	17[175]	TCATCGCCTGTCGAAATCCGCGACTGCGATTT	32
19[48]	17[47]	TAAAATACTGGCTGACCTTCATCAACCCAAAT	32
19[80]	17[79]	CCTAAAACAGATGAACGGTGTACAGTGAATAA	32
2[159]	4[160]	GTATTGGGAACGCGCGGGGAGAGGTTTTTTGTAAAAC	37
2[31]	4[32]	CTGTTTGATTTTTAGCCGGAAGCATAAAGTTCCACAC	37
20[159]	22[160]	ACCGATATGAATTTCTTAAACAGCCACCAGTA	32
20[190]	21[190]	TTACAATCGCCGTT	14
20[31]	22[32]	ACTTTTTCTTTTTCGGAGTGAGAATAGAACTTTCAAC	37
21[112]	19[111]	AGCCTTTAGCCGCTTTTGCGGGATTACACTAA	32
21[144]	19[143]	TTCGAGGTATTCGGTCGCTGAGGCATTATACC	32
21[176]	19[175]	GATAGTTGGACAACAACCATCGCCGATTTGTA	32
21[48]	19[47]	CTAAAGGACTACAGAGGCTTTGAGTAAACGGG	32
21[80]	19[79]	TTGAAAATGAAAGACAGCATCGGAGGCACCAA	32
22[127]	24[128]	GCCCTCATCCTCAGAACCGCCACCCTTAATGCCCC	35
22[159]	24[160]	CAAACTACTCATTTTCAGGGATAGCTTTGCCTTGA	35
22[190]	23[190]	TTTACCGCCATGTT	14
22[31]	24[32]	AGTTTCAGTTTTTGATAAGTGCCGTCGAGATTTGCTCAGT	40
22[63]	24[64]	TCTGTATGTAGCCCGGAATAGGTGTCTCCTCAAGA	35
22[95]	24[96]	TGTCGTCTAGGTTTAGTACCGCCACTTCTGAAACA	35
23[112]	21[111]	ACCGCCACAGTTAGCGTAACGATCCCAAAAGG	32
23[144]	21[143]	CACCACCCAACGCCTGTAGCATTCAGCTTGCT	32
23[169]	21[175]	AAGCCCAATAGGAACTAACACTGAGTTTCGTTTGATACC	39
23[48]	21[47]	TATAAGTAGGATTTTGCTAAACAAAGGAACAA	32
23[80]	21[79]	TACTCAGGTTCCAGACGTTAGTAATTTTCACG	32
24[159]	26[160]	GTAACAGTGTTTTAACGGGGTCAGTTTTTAACCAGAG	37
24[31]	26[32]	ACCAGGCGTTTTTATTGGCCTTGATATTCTGAGGCAG	37
25[112]	23[111]	ATACATGGTTCGGAACCTATTACCTCAGA	29
25[144]	23[143]	GGTAATAAGCCCGTATAAACAGTCAGAGC	29
25[48]	23[47]	ATAAATCCAGGATTAGCGGGGTGGGTTGA	29
25[80]	23[79]	CAGTCTCTTTAAGAGGCTGAGAATCACCG	29
26[159]	28[160]	CCACCACCTAATCAAAATCACCGGTTTTTATTGAGGG	37
26[31]	28[32]	GTCAGACGTTTTTTGAAACCATCGATAGCCCGGAAAC	37
27[112]	25[111]	TTCGGTCAAACCGCCACCCTCAGATAAGCGTC	32
27[144]	25[143]	TCTTTTCAGGAACCGCCTCCCTCAAGTGTACT	32
27[48]	25[47]	AATCAGTAAGCATTGACAGGAGGTACAAACAA	32
27[80]	25[79]	GCGTCAGACCGCCACCAGAACCACGGAAAGCG	32
28[159]	30[160]	AGGGAAGGGGGCGACATTCAACCGTTTTTGCAATAGC	37
28[31]	30[32]	GTCACCAATTTTTTAGCAAACGTAGAAAATTATTACG	37
29[112]	27[111]	AATAGAAAAATTATCACCGTCACCTCGGCATT	32
29[144]	27[143]	AGACAAAATAAATATTGACGGAAAGTTTGCCA	32
29[48]	27[47]	TAAAGGTGATTACCATTAGCAAGGAGCACCGT	32
29[80]	27[79]	ACACCACGGAATTAGAGCCAGCAATGCCTTTA	32
3[112]	1[111]	TCGGGAAACGGGCAACAGCTGATTACAAGAGT	32
3[144]	1[143]	AATCGGCCCGCCAGGGTGGTTTTTAACGTCAA	32
3[48]	1[47]	CTGGGGTGGGTTTGCCCCAGCAGGGGCAAAAT	32
3[80]	1[79]	TAATTGCGCCCTGAGAGAGTTGCACGAGATAG	32
30[127]	32[128]	GCAGATAGACAAGAATTGAGTTAAGAGCCTAATTT	35
30[159]	32[160]	TATCTTACAAGAAACAATGAAATATTTTCTTACCA	35
30[31]	32[32]	CAGTATGTTTTTTACATAAAAACAGGGAAGGCCTTTACAG	40
30[63]	32[64]	AAGAACTGAATTAACTGAACACCCTTTTTTTGTTT	35
30[95]	32[96]	CCGAGGAAGTAATTGAGCGCTAATAATATTATTTA	35
31[112]	29[111]	GATAACCCCCGAACAAAGTTACCATCACAATC	32
31[144]	29[143]	ATAAGAGCCGAAGCCCTTTTTAAGAGCGCCAA	32
31[48]	29[47]	GACGGGAGGCATGATTAAGACTCCTACATACA	32
31[80]	29[79]	GTCAGAGGACGCAATAATAACGGAACGCAAAG	32
32[159]	34[160]	ACGCTAACACAATTTTATCCTGAATTTTTCTAATTTA	37
32[31]	34[32]	AGAGAATATTTTTTAGCAAGCAAATCAGATCATTACC	37
33[112]	31[111]	AAGCCTTACAAAATAAACAGCCTCAGAGA	29

33[144]	31[143]	ACCCAGCTGAGCGTCTTTCCAGCCCAATA	29
33[48]	31[47]	GCTTATCCAAATGAAAATAGCACGCATTA	29
33[80]	31[79]	TTAGCGAACAAATAAGAAACGAGAACAAA	29
34[159]	36[160]	CGAGCATGAAAATAATATCCCATCTTTTTAATTACTA	37
34[31]	36[32]	GCGCCCAATTTTTCAGTAATAAGAGAATAAGAGGCAT	37
35[112]	33[111]	ACGCGCCTTATCATTCCAAGAACGAGGTTTTG	32
35[144]	33[143]	GAACAAGATAGAAACCAATCAATATATTTTGC	32
35[48]	33[47]	CGACAAAAATTTTCATCGTAGGAATATAGAAG	32
35[80]	33[79]	CGACAATACCGCACTCATCGAGAAGAGGCGTT	32
36[159]	38[160]	GAAAAAGCTAAACACCGGAATCATTTTTTTAGAATCC	37
36[31]	38[32]	TTTCGAGCTTTTTCAAATCCAATCGCAAGTATGTAAA	37
37[112]	35[111]	GAAATACCTACCAGTATAAAGCCAAATGCAGA	32
37[144]	35[143]	AATAAGAACTGTTTAGTATCATATTAAGTCCT	32
37[48]	35[47]	CGCGAGAAAACATGTAATTTAGGCTAAAGTAC	32
37[80]	35[79]	AATTTCATCTTAATTGAGAATCGCCCAGACGA	32
38[127]	40[128]	CTGAGAAGGTGAATAACCTTGCTTCACCTTTTACA	35
38[159]	40[160]	TTGAAAACTTAATTAATTTTCCCTTGGTTTAACGT	35
38[31]	40[32]	TGCTGATGTTTTTTGAAACAAACATCAAGACTGAGCAAAA	40
38[63]	40[64]	GGCTTAGGCATTTAACAATTTCATTTCGCGCAGAG	35
38[95]	40[96]	CATAGGTCAATGGAAACAGTACATACGCCTGATTG	35
39[112]	37[111]	ATATGTGAAGTCAATAGTGAATTTAATGGTTT	32
39[144]	37[143]	CGTCGCTAATAGCGATAGCTTAGAAGGCGTTA	32
39[48]	37[47]	ATTAATTATTGGGTTATATAACTAACAAAGAA	32
39[80]	37[79]	CCTTTTTTTGAGAGACTACCTTTTTTTTAGTT	32
4[159]	6[160]	GACGGCCATTCCCAGTCACGACGTTTTTTGTAATGGG	37
4[31]	6[32]	AACATACGTTTTTAAGCGCCATTCGCCATTGCCGGAA	37
40[159]	42[160]	CAGATGAACCATATCAAAATTATTAACAACTA	32
40[190]	41[190]	TTGAAATATAAATT	14
40[31]	42[32]	GAAGATGATTTTTCGGAACAAAGAAACCATAACATTA	37
41[112]	39[111]	TTTGGATTAACAATAACGGATTAATCAAT	29
41[144]	39[143]	AGAACCTATATACAGTAACAGTTGTAAAT	29
41[176]	40[170]	AAACAGAATGCGTAGATTTTCA	22
41[48]	39[47]	AGCGGAATTTCATTTCAATTACAAACAAA	29
41[80]	39[79]	ATGATGGCACCAAGTTACAAAATGAATTA	29
42[159]	44[160]	ATAGATTAGCAAATCAACAGTTGAAGAACCCT	32
42[190]	43[190]	TTTAAAATTATCTT	14
42[31]	44[32]	TCATTTTGTTTTTGGTGAGGCGGTCAGTACAGAAGAT	37
43[112]	41[111]	ACCTCAAAAGAAGTATTAGACTTTCCTGATTG	32
43[144]	41[143]	GTCAGTTGGAGCCGTCAATAGATAGAAGGGTT	32
43[176]	41[175]	GAGGAAGGTATCTTTAGGAGCACTTGCACGTA	32
43[48]	41[47]	GCCTGCAAATTTTAAAAGTTTGAGCCAGAAGG	32
43[80]	41[79]	CAAATGAACTCGTATTAAATCCTTATTATCAG	32
44[159]	46[160]	TCTGACCTTGGCAGATTCACCAGTTTTAGACA	32
44[190]	45[190]	TTGACATAAAGGTT	14
44[31]	46[32]	AAAACAGATTTTTAGAACTCAAACTATCGCACTTGCC	37
45[112]	43[111]	ACATTTTGTTTTGAATGGCTATTACTTGCTGA	32
45[144]	43[143]	ATTTACATGAAAGCGTAAGAATACAATATCTG	32
45[176]	43[175]	CAGTAATATCTGGCCAACAGAGATAAGGAATT	32
45[48]	43[47]	GGTAATATCCGAACGAACCACCAGTTAACACC	32
45[80]	43[79]	TTGCAACACTGATAGCCCTAAAACGCCAGCAG	32
46[127]	0[128]	TTATAATCGCGTACTATGGTTGCTTATCAAGTTTT	35
46[159]	0[160]	GGAACGGTACGTGCTTTCCTCGTTATTCGATGGCC	35
46[190]	47[190]	TTCAGGACTAAATT	14
46[31]	0[32]	TGAGTAGATTTTTAAAGCGAAAGGAGCGGGGGCGAGAAAG	40
46[63]	0[64]	TACTTCTTAAGTGTAGCGGTCACGCTTTAGAGCTT	35
46[95]	0[96]	CTGTCCATCACCCGCCGCGCTTAATCACTAAATCG	35
47[111]	45[111]	CTACAGGGCAGTGAGGCCACCGAGTAAATACCT	33
47[143]	45[143]	GCACGTATAACGCCAGAATCCTGAGAATGGATT	33
47[169]	45[175]	GAATCAGAGCGGGAGGGCCGATTAAAGGGATCACACGAC	39
47[48]	45[47]	GCGCTGGCTGATTAGTAATAACATGCCTTGCT	32
47[80]	45[79]	AACCACCACACGCAAATTAACCGTGCCAGCCA	32
5[112]	3[111]	GATGTGCTAGAGGATCCCCGGGTACTTTCCAG	32
5[144]	3[143]	CCAGGGTTGTGCCAAGCTTGCATGCATTAATG	32
5[48]	3[47]	CGCAACTGTGTTATCCGCTCACAATGTAAAGC	32
5[80]	3[79]	CTCTTCGCAATCATGGTCATAGCTACTCACAT	32
6[127]	8[128]	AACCGTGCGAGTAACAACCCGTCGGAATCATATGT	35
6[159]	8[160]	ATAGGTCAAAACGGCGGATTGACCTTTGATGAACG	35
6[31]	8[32]	ACCAGGCATTTTTTTAAATCAGCTCATTTTATTCGCATTA	40
6[63]	8[64]	CCAGCTTTGCCATCAAAAATAATTCATTTAAATTG	35
6[95]	8[96]	ACAGTATCGTAGCCAGCTTTCATCAGCCCCAAAAA	35

7[112]	5[111]	ATGTGAGCATCTGCCAGTTTGAGGGAAAGGGG	32
7[144]	5[143]	GTGGGAACCGTTGGTGTAGATGGGGGGTAACG	32
7[48]	5[47]	ATAGGAACCCGGCACCGCTTCTGGTCAGGCTG	32
7[80]	5[79]	GCCTTCCTGGCCTCAGGAAGATCGGTGCGGGC	32
8[159]	10[160]	GTAATCGTAGCAAACAAGAGAATCTTTTTGGTTGTAC	37
8[31]	10[32]	AATTTTTGTTTTTAAGGCCGGAGACAGTCATTCAAAA	37
9[112]	7[111]	AGATCTACTGATAATCAGAAAAACATTAA	29
9[144]	7[143]	GAGTCTGGAAAACTAGCATGTCATTCTCC	29
9[48]	7[47]	ATCAATATAATATTTTGTTAAATTAACCA	29
9[80]	7[79]	AATTAATGTTGTATAAGCAAATGCGTCTG	29

Table 0-3: 6p120 P_0 staples

Start	End	Sequence	total length (base)
0[127]	49[149]	TTGGGGTCAAAGAACGTGGACTCCCTTTTCAC	32
0[63]	49[85]	GACGGGGAAATCAAAAGAATAGCCGCAAGCGG	32
0[95]	49[117]	GAACCCTAGTTGTTCCAGTTTGGAGCCCTTCA	32
10[127]	57[149]	GGAGAAGCAGAATTAGCAAAATTAAAGTACGG	32
10[63]	57[85]	TGCCTGAGAGGTGGCATCAATTCTTTTAGTTT	32
10[95]	57[117]	ATTTTTAGTTAACATCCAATAAATACAGTTGA	32
12[127]	59[149]	TGTCTGGAAGAGGTCATTTTTGCGCAGAAAAC	32
12[63]	59[85]	GACCATTACCAGACCGGAAGCAAAAAAGCGGA	32
12[95]	59[117]	TTCCCAATTTAGAGAGTACCTTTAAGGTCTTT	32
16[127]	61[149]	ACATTATTGGGCTTGAGATGGTTTAGACGGTC	32
16[63]	61[85]	ATACATAACAAAGCTGCTCATTCAGACCAGGC	32
16[95]	61[117]	AGATTTAGCTGACGAGAAACACCAAACTTTGA	32
18[127]	63[149]	AATCATAATCTTTGACCCCCAGCGTTGCAGGG	32
18[63]	63[85]	GCATAGGCGTAATGCCACTACGAAACGAGGGT	32
18[95]	63[117]	AAGAGGACGAAAGAGGCAAAAGAACGTCACCC	32
2[127]	51[149]	CAGTGAGACCTGTCGTGCCAGCTGCCTGCAGG	32
2[63]	51[85]	TCCACGCTCCTAATGAGTGAGCTAGTTTCCTG	32
2[95]	51[117]	CCGCCTGGTTGCGCTCACTGCCCGCCGAGCTC	32
20[127]	65[149]	AGTTAAAGATTGTATCGGTTTATCCACAGACA	32
20[63]	65[85]	AGCAACGGATTGCGAATAATAATTATGAATTT	32
20[95]	65[117]	TCAGCAGCCTCCAAAAAAAAGGCTTAAAGTTT	32
24[127]	67[149]	CTGCCTATCTTTTGATGATACAGGGAGCCGCC	32
24[63]	67[85]	GAAGGATTTCATTAAAGCCAGAATCACCAGAG	32
24[95]	67[117]	TGAAAGTAGAATTTACCGTTCCAGGCCACCAC	32
26[127]	69[149]	ACCCTCAGTAGCCCCCTTATTAGCTTATTCAT	32
26[63]	69[85]	CCGCCGCCGCGACAGAATCAAGTTAATCACCA	32
26[95]	69[117]	CCTCAGAGCTGTAGCGCGTTTTCAGACTTGAG	32
28[127]	71[149]	TAAAGGTGATTCATATGGTTTACCAAAAGTAA	32
28[63]	71[85]	GTAGCACCGCAACATATAAAAGAAATACCCAA	32
28[95]	71[117]	CCATTTGGGAATAAGTTTATTTTGGAAGGAAA	32
32[127]	73[149]	GCCAGTTAAATCAAGATTAGTTGCATCGGCTG	32
32[63]	73[85]	AACGTCAAGGTATTCTAAGAACGCCAAGCAAG	32
32[95]	73[117]	TCCCAATCCCTCCCGACTTGCGGGGGTATTAA	32
34[127]	75[149]	TCTTTCCTGTTTATCAACAATAGAGCGTTATA	32
34[63]	75[85]	CCGTTTTTGGTAAAGTAATTCTGTCATATTTA	32
34[95]	75[117]	ACCAAGTAAACAACATGTTCAGCTACGCTCAA	32
36[127]	77[149]	CAAATTCTGACCGTGTGATAAATATTAAGACG	32
36[63]	77[85]	ACAACGCCAACTTTTTCAAATATATAACCTCC	32
36[95]	77[117]	CAGTAGGGCTTCTGACCTAAATTTATCAAAAT	32
4[127]	53[149]	TCGACTCTGCAAGGCGATTAAGTTCGCATCGT	32
4[63]	53[85]	TGTGAAATTTGGGAAGGGCGATCGCACTCCAG	32
4[95]	53[117]	GAATTCGTTATTACGCCAGCTGGCGGACGACG	32
40[127]	79[149]	TCGGGAGAATACTTCTGAATAATGATACATTT	32
40[63]	79[85]	GCGAATTATATCATCATATTCCTGTGCCCGAA	32
40[95]	79[117]	CTTTGAATAATTCATCAATATAATACAAACAA	32
42[127]	81[149]	GAGGATTTTATCAAACCCTCAATCGTGGCACA	32
42[63]	81[85]	CGTTATTACAGTGCCACGCTGAGAATCGCCAT	32
42[95]	81[117]	TTCGACAAAAATCTAAAGCATCACGTCTTTAA	32
44[127]	83[149]	GACAATATACGCTCAATCGTCTGAAAGTGTTT	32
44[63]	83[85]	TAAAAATACCAGAACAATATTACCTGTAGCAA	32
44[95]	83[117]	TGCGCGAAGGAAAAACGCTCATGGAAAAGAGT	32
8[127]	55[149]	ACCCCGGTAAAGGCTATCAGGTCACTTTTGCG	32
8[63]	55[85]	TAAACGTTGATATTCAACCGTTCTAAATGCAA	32
8[95]	55[117]	CAGGAAGACCGGAGAGGGTAGCTAGGATAAAA	32

Table 0-4: 6p120 cF9(22) modification staples

Start	End	Sequence	total length (base)
0[127]	49[149]	TTGGGGTCAAAGAACGTGGACTCCCTTTTCACCTTCACGATTGCCACTTTCCAC	54
0[63]	49[85]	GACGGGGAAATCAAAAGAATAGCCGCAAGCGGCTTCACGATTGCCACTTTCCAC	54
0[95]	49[117]	GAACCCTAGTTGTTCCAGTTTGGAGCCCTTCACTTCACGATTGCCACTTTCCAC	54
10[127]	57[149]	GGAGAAGCAGAATTAGCAAAATTAAAGTACGGCTTCACGATTGCCACTTTCCAC	54
10[63]	57[85]	TGCCTGAGAGGTGGCATCAATTCTTTTAGTTTCTTCACGATTGCCACTTTCCAC	54
10[95]	57[117]	ATTTTTAGTTAACATCCAATAAATACAGTTGACTTCACGATTGCCACTTTCCAC	54
12[127]	59[149]	TGTCTGGAAGAGGTCATTTTTGCGCAGAAAACCTTCACGATTGCCACTTTCCAC	54
12[63]	59[85]	GACCATTACCAGACCGGAAGCAAAAAAGCGGACTTCACGATTGCCACTTTCCAC	54
12[95]	59[117]	TTCCCAATTTAGAGAGTACCTTTAAGGTCTTTCTTCACGATTGCCACTTTCCAC	54
16[127]	61[149]	ACATTATTGGGCTTGAGATGGTTTAGACGGTCCTTCACGATTGCCACTTTCCAC	54
16[63]	61[85]	ATACATAACAAAGCTGCTCATTCAGACCAGGCCTTCACGATTGCCACTTTCCAC	54
16[95]	61[117]	AGATTTAGCTGACGAGAAACACCAAACTTTGACTTCACGATTGCCACTTTCCAC	54
18[127]	63[149]	AATCATAATCTTTGACCCCCAGCGTTGCAGGGCTTCACGATTGCCACTTTCCAC	54
18[63]	63[85]	GCATAGGCGTAATGCCACTACGAAACGAGGGTCTTCACGATTGCCACTTTCCAC	54
18[95]	63[117]	AAGAGGACGAAAGAGGCAAAAGAACGTCACCCCTTCACGATTGCCACTTTCCAC	54
2[127]	51[149]	CAGTGAGACCTGTCGTGCCAGCTGCCTGCAGGCTTCACGATTGCCACTTTCCAC	54
2[63]	51[85]	TCCACGCTCCTAATGAGTGAGCTAGTTTCCTGCTTCACGATTGCCACTTTCCAC	54
2[95]	51[117]	CCGCCTGGTTGCGCTCACTGCCCGCCGAGCTCCTTCACGATTGCCACTTTCCAC	54
20[127]	65[149]	AGTTAAAGATTGTATCGGTTTATCCACAGACACTTCACGATTGCCACTTTCCAC	54
20[63]	65[85]	AGCAACGGATTGCGAATAATAATTATGAATTTCTTCACGATTGCCACTTTCCAC	54
20[95]	65[117]	TCAGCAGCCTCCAAAAAAAAGGCTTAAAGTTTCTTCACGATTGCCACTTTCCAC	54
24[127]	67[149]	CTGCCTATCTTTTGATGATACAGGGAGCCGCCCTTCACGATTGCCACTTTCCAC	54
24[63]	67[85]	GAAGGATTTCATTAAAGCCAGAATCACCAGAGCTTCACGATTGCCACTTTCCAC	54
24[95]	67[117]	TGAAAGTAGAATTTACCGTTCCAGGCCACCACCTTCACGATTGCCACTTTCCAC	54
26[127]	69[149]	ACCCTCAGTAGCCCCCTTATTAGCTTATTCATCTTCACGATTGCCACTTTCCAC	54
26[63]	69[85]	CCGCCGCCGCGACAGAATCAAGTTAATCACCACTTCACGATTGCCACTTTCCAC	54
26[95]	69[117]	CCTCAGAGCTGTAGCGCGTTTTCAGACTTGAGCTTCACGATTGCCACTTTCCAC	54
28[127]	71[149]	TAAAGGTGATTCATATGGTTTACCAAAAGTAACTTCACGATTGCCACTTTCCAC	54
28[63]	71[85]	GTAGCACCGCAACATATAAAAGAAATACCCAACTTCACGATTGCCACTTTCCAC	54
28[95]	71[117]	CCATTTGGGAATAAGTTTATTTTGGAAGGAAACTTCACGATTGCCACTTTCCAC	54
32[127]	73[149]	GCCAGTTAAATCAAGATTAGTTGCATCGGCTGCTTCACGATTGCCACTTTCCAC	54
32[63]	73[85]	AACGTCAAGGTATTCTAAGAACGCCAAGCAAGCTTCACGATTGCCACTTTCCAC	54
32[95]	73[117]	TCCCAATCCCTCCCGACTTGCGGGGGTATTAACTTCACGATTGCCACTTTCCAC	54
34[127]	75[149]	TCTTTCCTGTTTATCAACAATAGAGCGTTATACTTCACGATTGCCACTTTCCAC	54
34[63]	75[85]	CCGTTTTTGGTAAAGTAATTCTGTCATATTTACTTCACGATTGCCACTTTCCAC	54
34[95]	75[117]	ACCAAGTAAACAACATGTTCAGCTACGCTCAACTTCACGATTGCCACTTTCCAC	54
36[127]	77[149]	CAAATTCTGACCGTGTGATAAATATTAAGACGCTTCACGATTGCCACTTTCCAC	54
36[63]	77[85]	ACAACGCCAACTTTTTCAAATATATAACCTCCCTTCACGATTGCCACTTTCCAC	54
36[95]	77[117]	CAGTAGGGCTTCTGACCTAAATTTATCAAAATCTTCACGATTGCCACTTTCCAC	54
4[127]	53[149]	TCGACTCTGCAAGGCGATTAAGTTCGCATCGTCTTCACGATTGCCACTTTCCAC	54
4[63]	53[85]	TGTGAAATTTGGGAAGGGCGATCGCACTCCAGCTTCACGATTGCCACTTTCCAC	54
4[95]	53[117]	GAATTCGTTATTACGCCAGCTGGCGGACGACGCTTCACGATTGCCACTTTCCAC	54
40[127]	79[149]	TCGGGAGAATACTTCTGAATAATGATACATTTCTTCACGATTGCCACTTTCCAC	54
40[63]	79[85]	GCGAATTATATCATCATATTCCTGTGCCCGAACTTCACGATTGCCACTTTCCAC	54
40[95]	79[117]	CTTTGAATAATTCATCAATATAATACAAACAACTTCACGATTGCCACTTTCCAC	54
42[127]	81[149]	GAGGATTTTATCAAACCCTCAATCGTGGCACACTTCACGATTGCCACTTTCCAC	54
42[63]	81[85]	CGTTATTACAGTGCCACGCTGAGAATCGCCATCTTCACGATTGCCACTTTCCAC	54
42[95]	81[117]	TTCGACAAAAATCTAAAGCATCACGTCTTTAACTTCACGATTGCCACTTTCCAC	54
44[127]	83[149]	GACAATATACGCTCAATCGTCTGAAAGTGTTTCTTCACGATTGCCACTTTCCAC	54
44[63]	83[85]	TAAAAATACCAGAACAATATTACCTGTAGCAACTTCACGATTGCCACTTTCCAC	54
44[95]	83[117]	TGCGCGAAGGAAAAACGCTCATGGAAAAGAGTCTTCACGATTGCCACTTTCCAC	54
8[127]	55[149]	ACCCCGGTAAAGGCTATCAGGTCACTTTTGCGCTTCACGATTGCCACTTTCCAC	54
8[63]	55[85]	TAAACGTTGATATTCAACCGTTCTAAATGCAACTTCACGATTGCCACTTTCCAC	54
8[95]	55[117]	CAGGAAGACCGGAGAGGGTAGCTAGGATAAAACTTCACGATTGCCACTTTCCAC	54

Table 0-5: Narcissus core staples

Start	End	Sequence	total length (bases)
0[107]	61[101]	TGTTGCGGGAGATATATTCGGTCGCATCGCCCTTAAACATCA	42
10[116]	48[118]	CTTTATGATGGCAATTCATTGAATAAAATCGTCTAGTCAGA	41
10[93]	49[113]	GTAATCATATTCCTGATCCTACCACACAAACAACCAATAC	40
11[151]	7[156]	CGAAGCCCGAAGTGTTGTTCCAGTACTCCAACGTCAAAGTGCCGTAAA	48

11[88]	52[76]	ATCTTAAATCTCTAAAATAAGTATAGCCCGGTTAGGATCCTATTTC	46
13[119]	45[114]	CCCTTCACAGTGAGGATTAAGTTAGCGTCAGACTGCAT	38
13[130]	10[117]	CTGATACTTCCAATATAATTTAGAAGTATTAGA	33
13[140]	46[129]	GAGAGTTCAGGGTGACTTCAAGCGACAGAATCAAGTTTG	39
13[77]	45[72]	CTTTTACAAATCGCAACCGCCATAGCCCCCTTATTTTT	38
15[119]	43[114]	CGGGAAATTGCGCTAAGGCCGCAAAGACAAAAGGGATA	38
15[140]	46[150]	TGCATTAAGCTAACGAAACCATCGATAGATCA	32
15[98]	46[97]	ATTTCATTTTTTTAAGTAGCACCATTACTAGCGCGTTTTCATC	43
17[144]	41[136]	CATAGCTCGAAATAAGTTGCGGATGGCTTAGTAAA	35
17[87]	44[76]	AGCGCAGTACATAAATCAATTAGAGGTAAATAT	33
18[100]	44[97]	TCAATAAAGGTGGCAACCGACATTCAACCGAT	32
19[108]	18[122]	CCTCTGTGAGAGACGCTGTGAAATTGTTATCCTCAT	36
2[118]	63[107]	CGGTACGCCTCACTTAACAAGTGAATTTCAC	31
2[143]	57[143]	CGATATGGTTGAATGCGCAGCGGGCGCTAGGGCCGCGACCTGCTCCAGAA	50
2[79]	59[90]	TCGAAACGCTTTCTGGCCAATATTTTTGAATAACTGACCTGTATG	45
20[125]	17[129]	TCACATAGTGTAATGAGTAAAATCATGGGCTC	32
20[146]	40[130]	CCTTGAATAAGCTAGACCATTAGATACATTT	31
20[72]	39[83]	AGTAAATAAGGCGTTAAAGAGAGAAGTAGTA	31
20[83]	39[73]	AAATATAGATGCAAGAGCTGAAAAGGTGTACT	32
22[125]	37[115]	AAAGCCAAAGCCTGCAAGGATAAAAATTTCAT	32
22[136]	25[122]	CTTAAAATAACTGAATTCTGTAAAAGGCGAAAGGGGGATGTGCTGCCCCA	50
24[104]	24[115]	TGGACGACAGACAATTGTCAACCTTATGAGTG	32
24[114]	26[98]	TCCGGGTTTTAAGGCGATTAAGTTGGAATAA	31
24[125]	37[125]	CGACTTAACAATGTATTAATGTTTTAAA	28
24[145]	21[152]	TGGTTGCCCGCTTCTAATCTCCGACAGTGTACAACGTTACGGCCCTG	47
24[83]	37[94]	TTCAGCTAAAAGGTGGCTATCAGAATTAACTGAACACCC	39
32[149]	24[146]	TCGCGCAACTCTATTACGCCAGCTCGACGGCCAGTGCCCTTCTAAG	46
34[108]	37[104]	TCATTATTTATGGTAATCGTAAAACGGGTAGCTATTTTTACAAAGT	46
34[150]	36[151]	AATATTTTGTTGATAATCAGAAAAGTAT	28
34[87]	23[92]	ATAAGAAACGACAAACAAGAGAATCCTACAAAAAAGTAATT	41
37[105]	19[107]	CAAACCCTTTAGGAGGGTAATTAAATCATACAGGCTGTTTAGTGA	45
37[116]	33[125]	ATACCGGAGATAGCATGTTAAATCTTAACCAATAGGAA	38
37[126]	22[137]	TGCAATGTTCAACGTTTAGTATCATATGATT	31
37[95]	34[109]	TGAGAGAGATGATGAACCCCAATCCAAAATAAACAGCCATATTTTAGC	48
38[150]	17[150]	TGCGGGAGAAGTAAAGCCTCAGAGCTTAGTTTCGTGGTGGGTACCGACGA	50
39[126]	36[136]	GCAAAATTAAGCAACCTTTATCCTGAGTGTTC	32
39[84]	42[76]	GCATTAAGGGGCGCATCCAATATTTATCAAAATCAGCAAACGAACGCAAT	50
40[129]	44[129]	CGCAAATGGTCTTTAAATATGCAACAGCTTAACAAAGACCCAG	43
41[105]	39[125]	AAAGCTCAACATGTAATAACCAAGGCAAAGAATTA	35
41[137]	44[139]	GTACGGTGTCTGGAAGTTCATTTTTTATTTTATAGAAAATTCATAT	46
42[75]	44[87]	AATAACAGCCCTTTTTAAGAAAAGTAACCGAGGATAGAAAAAGGG	45
43[115]	41[94]	TAAAAGAAACGTTGCTGAATATAATGCTGTAGTTACCAGAAGGAAAGCAG	50
44[128]	17[143]	CGCGAAACGTCACCAATTCACATTATTCCACACAA	35
44[75]	48[66]	TGACGGAAATTATTGAGCCAAGCGTTTAGAGCCAACCA	38
44[86]	18[101]	AAGCCAGCAAAATCACCATGGAAAATAGCTTAGATTAAAGAG	42
44[96]	41[104]	TGAGGGTACATACATAGTGACGCAAGACAAAGTCCTATATTGCCGAAC	48
45[73]	17[86]	GGGAATATATGAGAATCCTTGAAAACAT	28
46[128]	50[108]	CCTAGGAAGCACTATTAATAAATAAGTAAAATGTTTAGACTGGATAGCG	49
46[96]	50[76]	GGCATTTTCGGTCTCCCTCAGCCACCATTGGCCTGCCAGAATGGAAAGC	49
48[138]	13[129]	ACCCTGCCGAAAGGTTTTTCTTTTCACCCGC	31
48[75]	14[62]	GCCGCCCCACCGGGCAGAGGCGAATTAT	28
48[96]	48[97]	CTCAGAGAGCCGCCACCCTCAGTTGCAGCGGAAACCGCCACC	42
49[114]	9[108]	TGCGGTGGAAGGGTTAGAATATCAGACAAACAACTAA	37
50[107]	11[87]	TATAAATCCTCATTAAATGATATTTATCAAAATTATTTAATT	42
50[75]	48[76]	GCAGTCGGCAGGTCAGACGACCCTCAGA	28
51[124]	11[150]	ACACTATCATAACCCTTTTGAGGATCCTGATTTGGTGGTTC	41
51[151]	55[153]	CGACAGATACAAAGATTCATCAGTCTCATTATACCAGTAATCATT	45
51[61]	9[66]	TTTGATGATACAGGAGCGAACGTTATTAATGAAA	34
52[107]	10[94]	CGTATAAACAGTTAATGGTTTTAAACTC	28
53[102]	51[123]	TACCAGGCGGATAACGAACTAACGAGGCATAGTAACAGTGAGTAAGAGCA	50
53[144]	54[137]	TAGATAACGCCAAAAGGAATTACGGAACAACATTATTATTG	41
55[154]	53[143]	GTGAATTTTCAGTGAATAAGGCTTGCCCCAACTTTCAGGACGCAGG	46
56[115]	58[116]	GTGGGATAGCAAGGCTGGCTGACCTGCG	28
57[144]	4[151]	CCGGATATTCATTACCCTCGAAATCGCTGGCCACCCGCCGC	41
57[81]	56[95]	GAACCGTAACAGAACCGCCACCCTCAGAGCCTAG	34
57[91]	53[101]	CAGACCAGGCGCATAGCCCAAACCACCCCGAGAGGTCAG	39
58[115]	8[122]	CAGAGAACTGATAAAGGGAAAGGGCCACCCAAGGCG	36
59[144]	2[144]	AAAGTACAACGGAGATTAACCTAAGAGCACGGGAGCTAAACAGGAGGC	48
59[70]	61[80]	AGTAAATAGGAATTGCGAATAAAGGCTCCAAAAGGAGCC	39
6[111]	60[116]	CATCGCCAATGCGCCGGTCAAAACTTTCAAGACCCTCT	38

6[132]	60[137]	TGGCGAGAAGAAAGTTAGCCGTTATACCAAGCGCGAAG	38
6[90]	57[90]	ACGAACCACCAGCACACGCTGAGAGCCACCATGTACGGTGTA	42
60[107]	0[108]	CAGTGCTTTCGAGGACTTTTGAGGAATCCTGGTAAAAGAGTC	42
60[136]	56[116]	AATACACTAAAACACTCACCAGCGAGAACGAGTCATCAAAGAACGAGTA	49
61[102]	2[80]	GCTCGGAGTGAGAATAGATACCTAGTAGAAGAACTCAAACTA	42
8[111]	52[108]	ACAAGCATCACCTTAGGAGCATTCGACACGGGGTCAGTGCCTTGCC	46
8[121]	51[143]	ATGATTAGAGCCGTCAATAGATAATAGGTTGGATAGCACGTT	42
8[69]	57[80]	CAATATCGCCTGCATTCGTCACAGACAGCCAGGACAGAT	39
8[90]	52[87]	CTCAAATATCAAACAAGGTTACTTTGCCTGTACTGGTAATAACCCC	46
9[109]	55[122]	CAAGTGCCGTTCATTTTCAAAATTGGGC	28

Table 0-6: Narcissus $P_{cF^{9(22)}}$ staples

Start	End	Sequence	total length (bases)
11[67]	120[57]	ACCACCAGAAGGAGCGGGCACGTAAAACAGAACAGTACCTTCACGATTGCCACTTTCCAC	60
13[98]	122[78]	TAACGGATGCTTTGAATACCATTTAACACTTCACGATTGCCACTTTCCAC	50
15[77]	120[78]	CAAAATTAATTACAAGTTACAATCGGGAGAAACAACTTCACGATTGCCACTTTCCAC	57
17[130]	122[120]	ACAAATTGCGCCTGTCGTGCCAGCCTTCACGATTGCCACTTTCCAC	46
18[121]	129[124]	AGCTGTTTCCCTGGTTGAATCATTCTAGAAAACGCTCAACAGTAGCTTCACGATTGCCACTTTCCAC	67
20[104]	129[103]	ACAACGCGAGAAAATAAACACTTGAGAATCGCCATCTTCACGATTGCCACTTTCCAC	57
22[104]	127[124]	GGCTTAACGGAATCATAATTATCTCCGACTTCACGATTGCCACTTTCCAC	50
22[62]	127[82]	ATTTAGGACCGACCGTGTGATTAATTTCCTTCACGATTGCCACTTTCCAC	50
22[83]	131[82]	ATTTAACAACGCCATACCGACAATGCAGAACGCGCCTTCACGATTGCCACTTTCCAC	57
23[93]	131[124]	CTGTCCAATAAATAGAAACCAATCGTAACGCCATTAGTGCCTTCACGATTGCCACTTTCCAC	62
24[62]	129[82]	CTGTTTAAAGAGAATATAAAGACATGTACTTCACGATTGCCACTTTCCAC	50
25[123]	129[145]	GTCATTTTTGTCAATCATATGTACCTGATAACCCGCCACCAGTATCTTCACGATTGCCACTTTCCAC	67
26[97]	131[103]	TCGGCTGTCTTTCCTTATCATAATTTACGAGCATGCAACATGCTTCACGATTGCCACTTTCCAC	64
36[135]	131[145]	TAGCCCGGTTAAAATTCGCATTAAACGACGTATGCGCACTTCACGATTGCCACTTTCCAC	60
4[111]	123[110]	AGTCACACGACCAGAGTCTTTATTAAAAATACCGACTTCACGATTGCCACTTTCCAC	57
41[95]	127[103]	ATATTCATTTCATCCAATGAGCGCTAATATCATAAGAACTTTTTCCTTCACGATTGCCACTTTCCAC	67
43[72]	122[57]	TGTTATAGGTCTGAGAGACTTCCCTTTGAGTGAAAACATCAAGAAAACTTCACGATTGCCACTTTCCAC	69
44[138]	127[145]	GGTTTAACCACGGATTCGTACAGGGCTTCGGCTGACGCATTCTTCACGATTGCCACTTTCCAC	63
45[115]	122[99]	TAGCCACTGCCCGTTACCTTGAACTTTCCAGTCTTCACGATTGCCACTTTCCAC	54
48[117]	120[99]	AGCAAATCAAAAAACGGGCAACCTGATTTCGCAGCTGATTGCTTCACGATTGCCACTTTCCAC	63
51[144]	120[120]	TACCCAGAGGGGGTAATTTCATTGTTGGATTGCCCTGACTTCACGATTGCCACTTTCCAC	60
52[75]	125[89]	GGAACCTATTATTCCTCAAGAGAAGGAAATAGGTATTGAGGCCTCAATCTTCACGATTGCCACTTTCCAC	70
52[86]	125[110]	CTGTAGCGGGGTTTTGCGTTGATATATCTTTGCTGAACCTTCACGATTGCCACTTTCCAC	60
54[136]	123[152]	GGAAGAAAAATAGATGGTTTAATTTTGACGAGTTTTTGGGCGAACGCTTCACGATTGCCACTTTCCAC	68
55[123]	125[131]	TTGCTACGTTAATAAAACTAATAGGCCCACTCTTCACGATTGCCACTTTCCAC	53
56[94]	123[131]	GAACGCAGCAAATGAAAAATCTAGTGAACCATCCTAAAACTTCACGATTGCCACTTTCCAC	61
59[91]	121[110]	GGATTTTGCTAAACTCATAAGGGAACCGGGCTATTTAATAAACTTCACGATTGCCACTTTCCAC	64
60[115]	121[131]	TTCAATCGTCTGAAATGGTTGGCAGATTCACCCTTCACGATTGCCACTTTCCAC	54
61[81]	121[89]	TTTCAACTAAGAATTTTCAACTTTGAAAGCTGCACAGACAACAGACTTCACGATTGCCACTTTCCAC	67
7[157]	125[152]	GCACAGAGCTTGACGGGGAAAGCCGGGTCGAGGGGCGAAAAACCGTCTTCACGATTGCCACTTTCCAC	68
8[132]	121[152]	CTATCAGATCAAGTAAACACCGAGTAATCTTGACAATGTTACCGAAAGGCGCTACACTTCACGATTGCCACTTTCCAC	78
9[67]	123[89]	GGAGTATCACGAACCGCCACCCTCACTGAGTACAGTGCGAAGATACTTCACGATTGCCACTTTCCAC	67

Table 0-7: Narcissus self-dimer staples

Start	End	Sequence	total length (bases)
0[134]	2[119]	TCAGTGAGGCCACCGAAGAAGTGACAGGAA	30
1[82]	60[108]	AGCAATACTTCTTTGATTAGTAATGCCTGACATTTTGACGCTCAGTTT	48
27[135]	34[151]	CCATTCAGGCTGGATTCTCATTCGCGTCTGGCCGTT	36
28[81]	29[78]	GAATCATTACCGCGCGAGGCG	21
29[131]	32[150]	CCTCAGGAAGATCGCAACGACGACGTAATGGGATAGGCCCG	41
30[78]	28[63]	TTTTAGCGAACCTCCCCTAAGAACGCCCAA	30
31[128]	30[131]	CGGCGGATTGACCAGTATCGG	21
31[158]	28[135]	GTTGCCAGTTTGAGGGGCTCCAGCCCAGGCAAAGCGCCATTCG	43
32[85]	34[88]	TGCACCCAGTAATTTGCCAGTTACAA	26
33[126]	32[128]	CGCCATCAAAAATACGTGGGAACAAA	26
33[74]	31[85]	GCCCTACAATAGATTAGTTGCTATTT	26
34[66]	27[81]	AACGTAATATCCCATCCTTCCAAGATTTTCATCGTAG	37
4[132]	1[134]	GGTTACAATTATGCGCGTACTTAAAGGGATTTTAGTTTTTATAA	44
4[90]	62[79]	AGGGACACATGGAAAAAGGAAAATTGTATCGGTTTAGCTTGATACCGATAGTTG	54
62[130]	59[143]	GGCTACAGAGGCAAAGACTTTTTCATGAGGAAGTTTCCATGAGGCAAAAAC	51

63[108]	65[127]	GCATAAGGAACGCATCCCTCGTCACCCTCAGCAG	34
63[79]	64[86]	CGCCGACAATGACAACAACCTGAGGCTTGCA	31
64[127]	63[130]	CGAAAGACAGAGGGTAGCAAC	21
65[86]	0[82]	GGGAGTTAAAGGCCGCTTTCCATCACGCAAATTAACCGTTGT	42

Table 0-8: Narcissus left passivation set1

Start	End	Sequence	total length (bases)
11[48]	48[51]	CATTTTGCGGAACAAAAATTGCTGACAGGCCACCACCAGAG	41
13[40]	11[66]	TTTTGTTTAACGTCAGATGAATATACAGTAAATAAAGAGAA	41
14[61]	46[51]	TCATTTCGGAACCGCCATCTTTTCA	25
15[48]	44[51]	AGAAGATGATGAAACATAACCTACCGACTTCATTAAAGGTG	41
17[48]	18[48]	CGCTATTAATTAATTTACCTTTTTAACCTC	30
19[40]	20[40]	TTTTTTAGGTTGGGTTGACCTAAATTTATTTT	32
20[62]	40[55]	ATCTTCTATATAACAACAATGA	22
21[40]	22[40]	TTTTATGGTTTGAAATCAGAGGCATTTTTTTT	32
23[40]	24[40]	TTTTCGAGCCAGTAATTCAACAATAGATTTTT	32
25[40]	26[40]	TTTTAAGTCCTGAACAAAGTACCGCACTTTTT	32
26[62]	34[47]	TTAAACCAGAAAAATCAAAAATGAAATTTT	30
27[40]	28[40]	TTTTCATCGAGAACAACAAATCAGATATTTTT	32
28[62]	32[47]	TAGCAAGGCAAGCCTGAATCTTACCATTTT	30
29[48]	30[47]	GGCTTATCCGGTATTGACTTGCGGGAGTTTT	31
3[47]	4[47]	TTTTATTACCGCCAGCCCCTTCTGACCTTTTT	32
31[47]	26[63]	TTTTGTTTTGAAGCCTTAAATCATTTATCCGTTTTTAACGGGTA	44
33[47]	33[73]	TTTTACGCTAACGAGCGTCTTTCCAGA	27
35[47]	34[67]	TTTTATAGCAGCCTTTACGAGAGTCTGGAGTTTTTTGTTT	40
37[47]	38[55]	TTTTAAAAACAGGGAAGCGCATTCAAGAATTGAGTTAA	38
39[55]	20[73]	ATAAGAGCAAAATTCGCATCGATATATGTAAATGCTTTTT	40
39[74]	36[47]	AATTAACCCAAGACGGGAGGTCATTGCCTAGAGAGAATAACATTTTT	47
4[69]	2[55]	GATAGAACATTGCAACAGGAAGCCTTGCTGGTAATATCCAGAA	43
41[55]	43[71]	TAGCTATCTTACCGAGGAATACTACGCAGTA	31
43[51]	42[51]	AAGACTCCTTATCCAAAAGAACTG	24
45[43]	16[40]	TTTTATCACCGTCTGCTTCTGTAAATTTT	29
47[43]	14[40]	TTTTCAAAATCACCAATTACCTGAGTTTT	29
48[65]	50[51]	GAAAGGTTGATCTGAATTTACCGTTCCAG	29
49[43]	12[40]	TTTTCGCCAGCATGTAGATTTTCAGTTTT	29
5[47]	6[47]	TTTTGAAAGCGTAAGAGGTGAGGCGGTCTTTT	32
51[43]	10[40]	TTTTCGTCATACAGTTTGAGTAACATTTT	29
53[51]	52[51]	GAGGCTGAGACTCTGAAACATGAA	24
55[51]	54[51]	CCGCCACCCTCACGTACTCAGGAG	24
6[69]	56[51]	AAACAGAATACGTGCATAGTTAGCGTAACATTCCACCAGTACAAACT	47
61[43]	59[69]	TTTTGAAAATCTCCAAAAAAATAATTTTCTTTCCAGACGTT	41
7[47]	8[47]	TTTTAGTATTAACACCTGGTCAGTTGGCTTTT	32
9[47]	51[60]	TTTTAAATCAACAGTTTTTAAAATGGCT	28

Table 0-9: Narcissus right passivation set1

Start	End	Sequence	total length (bases)
12[165]	48[139]	CCAGCAGGCGAAAATCCTGTTTGAGTAATCCCCAGGTCTTT	41
16[165]	17[165]	CTGGGGTGCCTAGGAAGCATAAAG	24
17[151]	13[165]	GCCATGAGTGATGAATCTGGGCGCGCAGCAAGCGGTCCACGCT	43
18[165]	20[147]	GGAGGATCCCCGCTTGTTACACGAATATAGGGG	33
2[180]	6[165]	TTTTCGTTAGAATCAGAGCGTATAACGACCACCAAAGTGTACCG	44
21[153]	25[169]	CCATCTGTTATGATAATTTACGGGATGTTAAGCTTTCTCAGGAGA	45
26[165]	29[165]	CGGGCCTCTTCGGTTGGGACCGGAAACAGCTTTCCGGC	38
30[172]	31[172]	AACCGTGCATCTGGTGTAGATGGG	24
32[172]	33[172]	AAATGTGAGCGAAGCCAGCTTTCA	24
34[172]	31[157]	AAATATTTAAATTGTAAACTTCCTGTGTAACAATCAC	37
36[150]	37[172]	GATATTCAACCAATGTGTAGGTAAAGATTCAAAAGGGTGAGAAA	44
36[172]	35[172]	ACAGTCAAATCACCATCAACCCCAAAAACAGGAAGATT	38
38[172]	39[172]	CATTATGACCCTTAAATCGGTTGT	24
4[150]	61[176]	GCTTCTTTGACAACGAAATAAACGGGTAAAATACGTAATGCCACTTTT	48
40[172]	41[172]	ATTCTGCGAACGCATATAACAGTT	24

42[168]	38[151]	CCTTTTGATAAGAGGTTCATTCAGTAGATATAAAGCGTAATACTTT	46
44[168]	43[168]	TCAGGATTAGAATCAGTCACAGAGTACCTT	30
46[149]	15[165]	GTAATATCGCGTTTTAATGCGTATGGCCAACGCGCG	36
46[168]	45[168]	AACCAGACCGCCGTACAGCAGAAGCAAACT	30
48[168]	51[150]	GAATGACCATAAATCAAAAATCCTCAAATAGTTTTGCAGA	40
50[168]	49[168]	GGCTTTTGCAAAAGAGCTTTAAACAGTTCA	30
52[168]	11[165]	CACATTCAACTAATGCGATAAAAAAGAATAATCGGCAAAAT	41
54[176]	53[176]	TTTTTTTAAGAACTGGTGAGATTTAGGATTTT	32
56[176]	55[176]	TTTTCAAAGCTGCTCAACCTTATGCGATTTTT	32
58[176]	57[176]	TTTTTGATAAATTGTGAAATCAACGTAATTTT	32
6[164]	9[180]	ATTTTAAATCGAACGTGGTTGGAACAAGAGTCCATTTT	38
6[180]	5[180]	TTTTAGGGAGCCCGCGGTCACGTTTT	26
60[176]	59[176]	TTTTTACGAAGGCACCTGTATCATCGCCTTTT	32

Table 0-10: Narcissus P_0 staples

Start	End	Sequence	total length (bases)
11[67]	13[76]	ACCACCAGAAGGAGCGGGCACGTAAAACAGAACAGTAC	38
13[98]	15[97]	TAACGGATGCTTTGAATACCATTTAACA	28
15[77]	13[97]	CAAAATTAATTACAAGTTACAATCGGGAGAAACAA	35
17[130]	15[139]	ACAAATTGCGCCTGTCGTGCCAGC	24
18[121]	22[105]	AGCTGTTTCCCTGGTTGAATCATTCTAGAAAACGCTCAACAGTAG	45
20[104]	22[84]	ACAACGCGAGAAAATAAACACTTGAGAATCGCCAT	35
22[104]	20[105]	GGCTTAACGGAATCATAATTATCTCCGA	28
22[62]	20[63]	ATTTAGGACCGACCGTGTGATTAATTTC	28
22[83]	24[63]	ATTTAACAACGCCATACCGACAATGCAGAACGCGC	35
23[93]	24[105]	CTGTCCAATAAATAGAAACCAATCGTAACGCCATTAGTGC	40
24[62]	22[63]	CTGTTTAAAGAGAATATAAAGACATGTA	28
25[123]	22[126]	GTCATTTTTGTCAATCATATGTACCTGATAACCCGCCACCAGTAT	45
26[97]	24[84]	TCGGCTGTCTTTCCTTATCATAATTTACGAGCATGCAACATG	42
36[135]	24[126]	TAGCCCGGTTAAAATTCGCATTAAACGACGTATGCGCA	38
4[111]	6[91]	AGTCACACGACCAGAGTCTTTATTAAAAATACCGA	35
41[95]	20[84]	ATATTCATTTCATCCAATGAGCGCTAATATCATAAGAACTTTTTC	45
43[72]	15[76]	TGTTATAGGTCTGAGAGACTTCCCTTTGAGTGAAAACATCAAGAAAA	47
44[138]	20[126]	GGTTTAACCACGGATTCGTACAGGGCTTCGGCTGACGCATT	41
45[115]	15[118]	TAGCCACTGCCCGTTACCTTGAACTTTCCAGT	32
48[117]	13[118]	AGCAAATCAAAAAACGGGCAACCTGATTTCGCAGCTGATTG	41
51[144]	13[139]	TACCCAGAGGGGGTAATTTCATTGTTGGATTGCCCTGA	38
52[75]	8[70]	GGAACCTATTATTCCTCAAGAGAAGGAAATAGGTATTGAGGCCTCAAT	48
52[86]	8[91]	CTGTAGCGGGGTTTTGCGTTGATATATCTTTGCTGAAC	38
54[136]	6[133]	GGAAGAAAAATAGATGGTTTAATTTTGACGAGTTTTTGGGCGAACG	46
55[123]	8[112]	TTGCTACGTTAATAAAACTAATAGGCCCACT	31
56[94]	6[112]	GAACGCAGCAAATGAAAAATCTAGTGAACCATCCTAAAA	39
59[91]	4[91]	GGATTTTGCTAAACTCATAAGGGAACCGGGCTATTTAATAAA	42
60[115]	4[112]	TTCAATCGTCTGAAATGGTTGGCAGATTCACC	32
61[81]	4[70]	TTTCAACTAAGAATTTTCAACTTTGAAAGCTGCACAGACAACAGA	45
7[157]	8[133]	GCACAGAGCTTGACGGGGAAAGCCGGGTCGAGGGGCGAAAAACCGT	46
8[132]	4[133]	CTATCAGATCAAGTAAACACCGAGTAATCTTGACAATGTTACCGAAAGGCGCTACA	56
9[67]	6[70]	GGAGTATCACGAACCGCCACCCTCACTGAGTACAGTGCGAAGATA	45

Table 0-11: Narcissus passivated six helix protrusion staples

Start	End	Sequence	total length (bases)
0[138]	2[119]	TTTTTCAGTGAGGCCACCGAAGAAGTGACAGGAA	34
1[86]	60[108]	ATACTTCTTTGATTAGTAATGCCTGACATTTTGACGCTCAGTTT	44
27[131]	34[151]	TTTTCCATTCAGGCTGGATTCTCATTCGCGTCTGGCCGTT	40
28[85]	29[82]	TTTTGAATCATTACCGCGCGAGGCGTTTT	29
29[127]	32[150]	TTTTCCTCAGGAAGATCGCAACGACGACGTAATGGGATAGGCCCG	45
30[82]	28[63]	TTTTTTTTAGCGAACCTCCCCTAAGAACGCCCAA	34
31[124]	30[127]	TTTTCGGCGGATTGACCAGTATCGGTTTT	29
31[158]	28[131]	GTTGCCAGTTTGAGGGGCTCCAGCCCAGGCAAAGCGCCATTCGTTTT	47
32[89]	34[88]	TTTTTGCACCCAGTAATTTGCCAGTTACAA	30
33[126]	32[124]	CGCCATCAAAAATACGTGGGAACAAATTTT	30
33[74]	31[89]	GCCCTACAATAGATTAGTTGCTATTTTTTT	30
34[66]	27[85]	AACGTAATATCCCATCCTTCCAAGATTTTCATCGTAGTTTT	41

4[132]	1[138]	GGTTACAATTATGCGCGTACTTAAAGGGATTTTAGTTTTTATAATTTT	48
4[90]	62[83]	AGGGACACATGGAAAAAGGAAAATTGTATCGGTTTAGCTTGATACCGATA	50
62[126]	59[143]	ACAGAGGCAAAGACTTTTTCATGAGGAAGTTTCCATGAGGCAAAAAC	47
63[108]	65[131]	GCATAAGGAACGCATCCCTCGTCACCCTCAGCAGTTTT	38
63[83]	64[90]	GACAATGACAACAACCTGAGGCT	23
64[131]	63[134]	TTTTCGAAAGACAGAGGGTAGCAACTTTT	29
65[90]	0[86]	GTTAAAGGCCGCTTTCCATCACGCAAATTAACCG	34

Table 0-12: Narcissus left stacking staples

Start	End	Sequence	total length (bases)
11[44]	48[47]	TTATCATTTTGCGGAACAAAAATTGCTGACAGGCCACCACCAGAGCCGC	49
13[44]	11[66]	GTTTAACGTCAGATGAATATACAGTAAATAAAGAGAA	37
14[61]	46[47]	TCATTTCGGAACCGCCATCTTTTCATAAT	29
15[44]	44[47]	CAAAAGAAGATGATGAAACATAACCTACCGACTTCATTAAAGGTGAATT	49
17[44]	18[44]	TCGTCGCTATTAATTAATTTACCTTTTTAACCTCCGGC	38
19[44]	20[44]	TTAGGTTGGGTTGACCTAAATTTA	24
20[62]	40[51]	ATCTTCTATATAACAACAATGAAATA	26
21[44]	22[44]	ATGGTTTGAAATCAGAGGCATTTT	24
23[44]	24[44]	CGAGCCAGTAATTCAACAATAGAT	24
25[44]	26[44]	AAGTCCTGAACAAAGTACCGCACT	24
26[62]	34[51]	TTAAACCAGAAAAATCAAAAATGAAA	26
27[44]	28[44]	CATCGAGAACAACAAATCAGATAT	24
28[62]	32[51]	TAGCAAGGCAAGCCTGAATCTTACCA	26
29[44]	30[51]	AGAAGGCTTATCCGGTATTGACTTGCGGGAG	31
3[51]	4[51]	ATTACCGCCAGCCCCTTCTGACCT	24
31[51]	26[63]	GTTTTGAAGCCTTAAATCATTTATCCGTTTTTAACGGGTA	40
33[51]	33[73]	ACGCTAACGAGCGTCTTTCCAGA	23
35[51]	34[67]	ATAGCAGCCTTTACGAGAGTCTGGAGTTTTTTGTTT	36
37[51]	38[51]	AAAAACAGGGAAGCGCATTCAAGAATTGAGTTAAGCCC	38
39[51]	20[73]	AATAATAAGAGCAAAATTCGCATCGATATATGTAAATGCTTTTT	44
39[74]	36[51]	AATTAACCCAAGACGGGAGGTCATTGCCTAGAGAGAATAACAT	43
4[69]	2[51]	GATAGAACATTGCAACAGGAAGCCTTGCTGGTAATATCCAGAACAAT	47
41[51]	43[71]	GCAATAGCTATCTTACCGAGGAATACTACGCAGTA	35
43[47]	42[47]	GATTAAGACTCCTTATCCAAAAGAACTGGCAT	32
45[47]	16[44]	ATCACCGTCTGCTTCTGTAAA	21
47[47]	14[44]	CAAAATCACCAATTACCTGAG	21
48[65]	50[47]	GAAAGGTTGATCTGAATTTACCGTTCCAGTAAG	33
49[47]	12[44]	CGCCAGCATGTAGATTTTCAG	21
5[51]	6[51]	GAAAGCGTAAGAGGTGAGGCGGTC	24
51[47]	10[44]	CGTCATACAGTTTGAGTAACA	21
53[47]	52[47]	TTAAGAGGCTGAGACTCTGAAACATGAAAGTA	32
55[47]	54[47]	AGTACCGCCACCCTCACGTACTCAGGAGGTTT	32
6[69]	56[47]	AAACAGAATACGTGCATAGTTAGCGTAACATTCCACCAGTACAAACTACAA	51
61[47]	59[69]	GAAAATCTCCAAAAAAATAATTTTCTTTCCAGACGTT	37
7[51]	8[51]	AGTATTAACACCTGGTCAGTTGGC	24
9[51]	51[60]	AAATCAACAGTTTTTAAAATGGCT	24
59[47]	60[47]	GTTTTGTCGTTTCACGTT	18
8[176]	7[176]	CTATTAAAGGAACCCTAA	18

Table 0-13: Narcissus right stacking staples

Start	End	Sequence	total length (bases)
12[169]	48[139]	TGCCCCAGCAGGCGAAAATCCTGTTTGAGTAATCCCCAGGTCTTT	45
16[169]	17[169]	AAGCCTGGGGTGCCTAGGAAGCATAAAGTGTA	32
17[151]	13[169]	GCCATGAGTGATGAATCTGGGCGCGCAGCAAGCGGTCCACGCTGGTT	47
18[169]	20[147]	AGACGGAGGATCCCCGCTTGTTACACGAATATAGGGG	37
2[176]	6[165]	CGTTAGAATCAGAGCGTATAACGACCACCAAAGTGTACCG	40
21[153]	25[169]	CCATCTGTTATGATAATTTACGGGATGTTAAGCTTTCTCAGGAGA	45
26[169]	29[169]	GGTGCGGGCCTCTTCGGTTGGGACCGGAAACAGCTTTCCGGCACCG	46
30[176]	31[176]	TCGTAACCGTGCATCTGGTGTAGATGGGCGCA	32
32[176]	33[176]	CATTAAATGTGAGCGAAGCCAGCTTTCATCAA	32
34[176]	31[157]	AAGCAAATATTTAAATTGTAAACTTCCTGTGTAACAATCAC	41
36[150]	37[176]	GATATTCAACCAATGTGTAGGTAAAGATTCAAAAGGGTGAGAAAGGCC	48
36[176]	35[176]	GGAGACAGTCAAATCACCATCAACCCCAAAAACAGGAAGATTGTAT	46
38[176]	39[176]	AAAACATTATGACCCTTAAATCGGTTGTACCA	32
4[150]	61[172]	GCTTCTTTGACAACGAAATAAACGGGTAAAATACGTAATGCCAC	44
40[176]	41[176]	CCCAATTCTGCGAACGCATATAACAGTTGATT	32
42[172]	38[151]	TGCTCCTTTTGATAAGAGGTTCATTCAGTAGATATAAAGCGTAATACTTT	50
44[172]	43[172]	CAGGTCAGGATTAGAATCAGTCACAGAGTACCTTTAAT	38
46[149]	15[169]	GTAATATCGCGTTTTAATGCGTATGGCCAACGCGCGGGGA	40
46[172]	45[172]	AGCGAACCAGACCGCCGTACAGCAGAAGCAAACTCCAA	38
48[172]	51[150]	ACGAGAATGACCATAAATCAAAAATCCTCAAATAGTTTTGCAGA	44
50[172]	49[172]	GAGAGGCTTTTGCAAAAGAGCTTTAAACAGTTCAGAAA	38
52[172]	11[169]	ATACCACATTCAACTAATGCGATAAAAAAGAATAATCGGCAAAATCCCT	49
54[172]	53[172]	TTTAAGAACTGGTGAGATTTAGGA	24
56[172]	55[172]	CAAAGCTGCTCAACCTTATGCGAT	24
58[172]	57[172]	TGATAAATTGTGAAATCAACGTAA	24
6[164]	9[176]	ATTTTAAATCGAACGTGGTTGGAACAAGAGTCCA	34
6[176]	5[176]	AGGGAGCCCGCGGTCACG	18
60[172]	59[172]	TACGAAGGCACCTGTATCATCGCC	24
10[169]	51[172]	TATAAATCAAACCAAAATAGC	21
14[169]	47[172]	GAGGCGGTTTTCGAGCTTCAA	21
20[169]	19[169]	GTCGGTGGGCCTCGATAA	18
22[169]	21[169]	GAGTGACTCAAGCAACTC	18
24[169]	23[169]	AGCCAGGGTCTCGCCCTG	18
28[169]	27[169]	CTTCTGGTGAGGGCGATC	18
4[176]	3[176]	CTGCGCGTATGCTTTCCT	18
57[47]	58[47]	CGCCTGTAGCGATCTAAA	18

Table 0-14: Narcissus left passivation set2

Start	End	Sequence	total length (bases)
41[55]	43[71]	TAGCTATCTTACCGAGGAATACTACGCAGTA	31
48[65]	50[51]	GAAAGGTTGATCTGAATTTACCGTTCCAG	29
6[69]	56[51]	AAACAGAATACGTGCATAGTTAGCGTAACATTCCACCAGTACAAACT	47
4[69]	2[55]	GATAGAACATTGCAACAGGAAGCCTTGCTGGTAATATCCAGAA	43
28[62]	32[55]	TAGCAAGGCAAGCCTGAATCTT	22
11[48]	48[51]	CATTTTGCGGAACAAAAATTGCTGACAGGCCACCACCAGAG	41
61[51]	59[69]	ATCTCCAAAAAAATAATTTTCTTTCCAGACGTT	33
55[51]	54[51]	CCGCCACCCTCACGTACTCAGGAG	24
35[55]	34[67]	CAGCCTTTACGAGAGTCTGGAGTTTTTTGTTT	32
14[61]	46[51]	TCATTTCGGAACCGCCATCTTTTCA	25
33[55]	33[73]	TAACGAGCGTCTTTCCAGA	19
26[62]	34[55]	TTAAACCAGAAAAATCAAAAAT	22
37[55]	38[55]	ACAGGGAAGCGCATTCAAGAATTGAGTTAA	30
39[55]	20[73]	ATAAGAGCAAAATTCGCATCGATATATGTAAATGCTTTTT	40
15[48]	44[51]	AGAAGATGATGAAACATAACCTACCGACTTCATTAAAGGTG	41
17[48]	18[48]	CGCTATTAATTAATTTACCTTTTTAACCTC	30
39[74]	36[55]	AATTAACCCAAGACGGGAGGTCATTGCCTAGAGAGAATA	39
31[55]	26[63]	TGAAGCCTTAAATCATTTATCCGTTTTTAACGGGTA	36
43[51]	42[51]	AAGACTCCTTATCCAAAAGAACTG	24
9[55]	51[60]	CAACAGTTTTTAAAATGGCT	20
20[62]	40[55]	ATCTTCTATATAACAACAATGA	22
53[51]	52[51]	GAGGCTGAGACTCTGAAACATGAA	24
29[48]	30[55]	GGCTTATCCGGTATTGACTTGCG	23
13[48]	11[66]	AACGTCAGATGAATATACAGTAAATAAAGAGAA	33

Table 0-15: Narcissus right passivation set2

Start	End	Sequence	total length (bases)
2[172]	6[165]	AGAATCAGAGCGTATAACGACCACCAAAGTGTACCG	36
36[150]	37[172]	GATATTCAACCAATGTGTAGGTAAAGATTCAAAAGGGTGAGAAA	44
17[151]	13[165]	GCCATGAGTGATGAATCTGGGCGCGCAGCAAGCGGTCCACGCT	43
21[153]	25[165]	CCATCTGTTATGATAATTTACGGGATGTTAAGCTTTCTCAG	41
4[150]	61[168]	GCTTCTTTGACAACGAAATAAACGGGTAAAATACGTAATG	40
48[168]	51[150]	GAATGACCATAAATCAAAAATCCTCAAATAGTTTTGCAGA	40
54[168]	53[168]	AGAACTGGTGAGATTT	16
6[164]	9[172]	ATTTTAAATCGAACGTGGTTGGAACAAGAG	30
26[165]	29[165]	CGGGCCTCTTCGGTTGGGACCGGAAACAGCTTTCCGGC	38
52[168]	11[165]	CACATTCAACTAATGCGATAAAAAAGAATAATCGGCAAAAT	41
12[165]	48[139]	CCAGCAGGCGAAAATCCTGTTTGAGTAATCCCCAGGTCTTT	41
46[168]	45[168]	AACCAGACCGCCGTACAGCAGAAGCAAACT	30
40[172]	41[172]	ATTCTGCGAACGCATATAACAGTT	24
56[168]	55[168]	GCTGCTCAACCTTATG	16
42[168]	38[151]	CCTTTTGATAAGAGGTTCATTCAGTAGATATAAAGCGTAATACTTT	46
58[168]	57[168]	AAATTGTGAAATCAAC	16
36[172]	35[172]	ACAGTCAAATCACCATCAACCCCAAAAACAGGAAGATT	38
30[172]	31[172]	AACCGTGCATCTGGTGTAGATGGG	24
38[172]	39[172]	CATTATGACCCTTAAATCGGTTGT	24
50[168]	49[168]	GGCTTTTGCAAAAGAGCTTTAAACAGTTCA	30
34[172]	31[157]	AAATATTTAAATTGTAAACTTCCTGTGTAACAATCAC	37
46[149]	15[165]	GTAATATCGCGTTTTAATGCGTATGGCCAACGCGCG	36
60[168]	59[168]	AAGGCACCTGTATCAT	16
16[165]	17[165]	CTGGGGTGCCTAGGAAGCATAAAG	24
32[172]	33[172]	AAATGTGAGCGAAGCCAGCTTTCA	24
44[168]	43[168]	TCAGGATTAGAATCAGTCACAGAGTACCTT	30
18[165]	20[147]	GGAGGATCCCCGCTTGTTACACGAATATAGGGG	33

Table 0-16: Narcissus 6T passivated left staples (set3)

Start	End	Sequence	total length (bases)
11[38]	48[41]	TTTTTTTTATCATTTTGCGGAACAAAAATTGCTGACAGGCCACCACCAGAGCCGCTTTTTT	61
13[38]	11[66]	TTTTTTGTTTAACGTCAGATGAATATACAGTAAATAAAGAGAA	43
14[61]	46[41]	TCATTTCGGAACCGCCATCTTTTCATAATTTTTTT	35
15[38]	44[41]	TTTTTTCAAAAGAAGATGATGAAACATAACCTACCGACTTCATTAAAGGTGAATTTTTTTT	61
17[38]	18[38]	TTTTTTTCGTCGCTATTAATTAATTTACCTTTTTAACCTCCGGCTTTTTT	50
19[38]	20[38]	TTTTTTTTAGGTTGGGTTGACCTAAATTTATTTTTT	36
20[62]	40[45]	ATCTTCTATATAACAACAATGAAATATTTTTT	32
21[38]	22[38]	TTTTTTATGGTTTGAAATCAGAGGCATTTTTTTTTT	36
23[38]	24[38]	TTTTTTCGAGCCAGTAATTCAACAATAGATTTTTTT	36
25[38]	26[38]	TTTTTTAAGTCCTGAACAAAGTACCGCACTTTTTTT	36
26[62]	34[45]	TTAAACCAGAAAAATCAAAAATGAAATTTTTT	32
27[38]	28[38]	TTTTTTCATCGAGAACAACAAATCAGATATTTTTTT	36
28[62]	32[45]	TAGCAAGGCAAGCCTGAATCTTACCATTTTTT	32
29[38]	30[45]	TTTTTTAGAAGGCTTATCCGGTATTGACTTGCGGGAGTTTTTT	43
3[45]	4[45]	TTTTTTATTACCGCCAGCCCCTTCTGACCTTTTTTT	36
31[45]	26[63]	TTTTTTGTTTTGAAGCCTTAAATCATTTATCCGTTTTTAACGGGTA	46
33[45]	33[73]	TTTTTTACGCTAACGAGCGTCTTTCCAGA	29
35[45]	34[67]	TTTTTTATAGCAGCCTTTACGAGAGTCTGGAGTTTTTTGTTT	42
37[45]	38[45]	TTTTTTAAAAACAGGGAAGCGCATTCAAGAATTGAGTTAAGCCCTTTTTT	50
39[45]	20[73]	TTTTTTAATAATAAGAGCAAAATTCGCATCGATATATGTAAATGCTTTTT	50
39[74]	36[45]	AATTAACCCAAGACGGGAGGTCATTGCCTAGAGAGAATAACATTTTTTT	49
4[69]	2[45]	GATAGAACATTGCAACAGGAAGCCTTGCTGGTAATATCCAGAACAATTTTTTT	53
41[45]	43[71]	TTTTTTGCAATAGCTATCTTACCGAGGAATACTACGCAGTA	41
43[41]	42[41]	TTTTTTGATTAAGACTCCTTATCCAAAAGAACTGGCATTTTTTT	44
45[41]	16[38]	TTTTTTATCACCGTCTGCTTCTGTAAATTTTTT	33
47[41]	14[38]	TTTTTTCAAAATCACCAATTACCTGAGTTTTTT	33
48[65]	50[41]	GAAAGGTTGATCTGAATTTACCGTTCCAGTAAGTTTTTT	39
49[41]	12[38]	TTTTTTCGCCAGCATGTAGATTTTCAGTTTTTT	33
5[45]	6[45]	TTTTTTGAAAGCGTAAGAGGTGAGGCGGTCTTTTTT	36
51[41]	10[38]	TTTTTTCGTCATACAGTTTGAGTAACATTTTTT	33
53[41]	52[41]	TTTTTTTTAAGAGGCTGAGACTCTGAAACATGAAAGTATTTTTT	44
55[41]	54[41]	TTTTTTAGTACCGCCACCCTCACGTACTCAGGAGGTTTTTTTTT	44
57[41]	58[41]	TTTTTTCGCCTGTAGCGATCTAAATTTTTT	30
59[41]	60[41]	TTTTTTGTTTTGTCGTTTCACGTTTTTTT	30
6[69]	56[41]	AAACAGAATACGTGCATAGTTAGCGTAACATTCCACCAGTACAAACTACAATTTTTT	57
61[41]	59[69]	TTTTTTGAAAATCTCCAAAAAAATAATTTTCTTTCCAGACGTT	43
7[45]	8[45]	TTTTTTAGTATTAACACCTGGTCAGTTGGCTTTTTT	36
9[45]	51[60]	TTTTTTAAATCAACAGTTTTTAAAATGGCT	30

Table 0-17: Narcissus 6T passivated right staples (set3)

Start	End	Sequence	total length (bases)
10[175]	51[178]	TTTTTTTATAAATCAAACCAAAATAGCTTTTTT	33
12[175]	48[139]	TTTTTTTGCCCCAGCAGGCGAAAATCCTGTTTGAGTAATCCCCAGGTCTTT	51
14[175]	47[178]	TTTTTTGAGGCGGTTTTCGAGCTTCAATTTTTT	33
16[175]	17[175]	TTTTTTAAGCCTGGGGTGCCTAGGAAGCATAAAGTGTATTTTTT	44
17[151]	13[175]	GCCATGAGTGATGAATCTGGGCGCGCAGCAAGCGGTCCACGCTGGTTTTTTTT	53
18[175]	20[147]	TTTTTTAGACGGAGGATCCCCGCTTGTTACACGAATATAGGGG	43
2[182]	6[165]	TTTTTTCGTTAGAATCAGAGCGTATAACGACCACCAAAGTGTACCG	46
20[175]	19[175]	TTTTTTGTCGGTGGGCCTCGATAATTTTTT	30
21[153]	25[175]	CCATCTGTTATGATAATTTACGGGATGTTAAGCTTTCTCAGGAGATTTTTT	51
22[175]	21[175]	TTTTTTGAGTGACTCAAGCAACTCTTTTTT	30
24[175]	23[175]	TTTTTTAGCCAGGGTCTCGCCCTGTTTTTT	30
26[175]	29[175]	TTTTTTGGTGCGGGCCTCTTCGGTTGGGACCGGAAACAGCTTTCCGGCACCGTTTTTT	58
28[175]	27[175]	TTTTTTCTTCTGGTGAGGGCGATCTTTTTT	30
30[182]	31[182]	TTTTTTTCGTAACCGTGCATCTGGTGTAGATGGGCGCATTTTTT	44
32[182]	33[182]	TTTTTTCATTAAATGTGAGCGAAGCCAGCTTTCATCAATTTTTT	44
34[182]	31[157]	TTTTTTAAGCAAATATTTAAATTGTAAACTTCCTGTGTAACAATCAC	47
36[150]	37[182]	GATATTCAACCAATGTGTAGGTAAAGATTCAAAAGGGTGAGAAAGGCCTTTTTT	54
36[182]	35[182]	TTTTTTGGAGACAGTCAAATCACCATCAACCCCAAAAACAGGAAGATTGTATTTTTTT	58
38[182]	39[182]	TTTTTTAAAACATTATGACCCTTAAATCGGTTGTACCATTTTTT	44
4[150]	61[178]	GCTTCTTTGACAACGAAATAAACGGGTAAAATACGTAATGCCACTTTTTT	50
4[182]	3[182]	TTTTTTCTGCGCGTATGCTTTCCTTTTTTT	30
40[182]	41[182]	TTTTTTCCCAATTCTGCGAACGCATATAACAGTTGATTTTTTTT	44

42[178]	38[151]	TTTTTTTGCTCCTTTTGATAAGAGGTTCATTCAGTAGATATAAAGCGTAATACTTT	56
44[178]	43[178]	TTTTTTCAGGTCAGGATTAGAATCAGTCACAGAGTACCTTTAATTTTTTT	50
46[149]	15[175]	GTAATATCGCGTTTTAATGCGTATGGCCAACGCGCGGGGATTTTTT	46
46[178]	45[178]	TTTTTTAGCGAACCAGACCGCCGTACAGCAGAAGCAAACTCCAATTTTTT	50
48[178]	51[150]	TTTTTTACGAGAATGACCATAAATCAAAAATCCTCAAATAGTTTTGCAGA	50
50[178]	49[178]	TTTTTTGAGAGGCTTTTGCAAAAGAGCTTTAAACAGTTCAGAAATTTTTT	50
52[178]	11[175]	TTTTTTATACCACATTCAACTAATGCGATAAAAAAGAATAATCGGCAAAATCCCTTTTTTT	61
54[178]	53[178]	TTTTTTTTTAAGAACTGGTGAGATTTAGGATTTTTT	36
56[178]	55[178]	TTTTTTCAAAGCTGCTCAACCTTATGCGATTTTTTT	36
58[178]	57[178]	TTTTTTTGATAAATTGTGAAATCAACGTAATTTTTT	36
6[164]	9[182]	ATTTTAAATCGAACGTGGTTGGAACAAGAGTCCATTTTTT	40
6[182]	5[182]	TTTTTTAGGGAGCCCGCGGTCACGTTTTTT	30
60[178]	59[178]	TTTTTTTACGAAGGCACCTGTATCATCGCCTTTTTT	36
8[182]	7[182]	TTTTTTCTATTAAAGGAACCCTAATTTTTT	30

Table 0-18: Narcissus staples hybridizing with Echo

Start	End	Sequence	total length (base)
0[130]	2[119]	TGAGGCCACCGAAGAAGTGACAGGAA	26
1[86]	60[108]	ATACTTCTTTGATTAGTAATGCCTGACATTTTGACGCTCAGTTT	44
27[131]	34[151]	CGTACCATTCAGGCTGGATTCTCATTCGCGTCTGGCCGTT	40
28[85]	29[74]	ATTAGAATCATTACCGCGCGA	21
29[135]	32[150]	AGGAAGATCGCAACGACGACGTAATGGGATAGGCCCG	37
30[82]	28[63]	CTGTTTTTAGCGAACCTCCCCTAAGAACGCCCAA	34
31[124]	30[135]	AAAACGGCGGATTGACCAGTA	21
31[158]	28[139]	GTTGCCAGTTTGAGGGGCTCCAGCCCAGGCAAAGCGCCA	39
32[89]	34[88]	TGTATGCACCCAGTAATTTGCCAGTTACAA	30
33[126]	32[124]	CGCCATCAAAAATACGTGGGAACAAATTAA	30
33[74]	31[81]	GCCCTACAATAGATTAGTTGCT	22
34[66]	27[85]	AACGTAATATCCCATCCTTCCAAGATTTTCATCGTAGAACC	41
4[132]	1[138]	GGTTACAATTATGCGCGTACTTAAAGGGATTTTAGTTTTTATAAGATT	48
4[90]	62[83]	AGGGACACATGGAAAAAGGAAAATTGTATCGGTTTAGCTTGATACCGATA	50
62[126]	59[143]	ACAGAGGCAAAGACTTTTTCATGAGGAAGTTTCCATGAGGCAAAAAC	47
63[108]	65[125]	GCATAAGGAACGCATCCCTCGTCACCCTCAGC	32
63[83]	64[90]	GACAATGACAACAACCTGAGGCT	23
64[123]	63[134]	AGACAGAGGGTAGCAACGGTG	21
65[90]	0[86]	GTTAAAGGCCGCTTTCCATCACGCAAATTAACCG	34

Table 0-19: Narcissus P_{lblock}

Start	End	Sequence	total length (bases)
11[67]	13[76]	ACCACCAGAAGGAGCGGGCACGTAAAACAGAACAGTACGACTTCTGGTAAACGCTCGTTG	38
22[62]	20[63]	ATTTAGGACCGACCGTGTGATTAATTTCGACTTCTGGTAAACGCTCGTTG	28
22[83]	24[63]	ATTTAACAACGCCATACCGACAATGCAGAACGCGCGACTTCTGGTAAACGCTCGTTG	35
24[62]	22[63]	CTGTTTAAAGAGAATATAAAGACATGTAGACTTCTGGTAAACGCTCGTTG	28
43[72]	15[76]	TGTTATAGGTCTGAGAGACTTCCCTTTGAGTGAAAACATCAAGAAAAGACTTCTGGTAAACGCTCGTTG	47
52[75]	8[70]	GGAACCTATTATTCCTCAAGAGAAGGAAATAGGTATTGAGGCCTCAATGACTTCTGGTAAACGCTCGTTG	48
61[81]	4[70]	TTTCAACTAAGAATTTTCAACTTTGAAAGCTGCACAGACAACAGAGACTTCTGGTAAACGCTCGTTG	45
9[67]	6[70]	GGAGTATCACGAACCGCCACCCTCACTGAGTACAGTGCGAAGATAGACTTCTGGTAAACGCTCGTTG	45

Table 0-20: Narcissus P_{rblock}

Start	End	Sequence	total length (bases)
17[130]	122[120]	ACAAATTGCGCCTGTCGTGCCAGCGACTTCTGGTAAACGCTCGTTG	46
25[123]	129[145]	GTCATTTTTGTCAATCATATGTACCTGATAACCCGCCACCAGTATGACTTCTGGTAAACGCTCGTTG	67
36[135]	131[145]	TAGCCCGGTTAAAATTCGCATTAAACGACGTATGCGCAGACTTCTGGTAAACGCTCGTTG	60
44[138]	127[145]	GGTTTAACCACGGATTCGTACAGGGCTTCGGCTGACGCATTGACTTCTGGTAAACGCTCGTTG	63
51[144]	120[120]	TACCCAGAGGGGGTAATTTCATTGTTGGATTGCCCTGAGACTTCTGGTAAACGCTCGTTG	60
54[136]	123[152]	GGAAGAAAAATAGATGGTTTAATTTTGACGAGTTTTTGGGCGAACGGACTTCTGGTAAACGCTCGTTG	68
7[157]	125[152]	GCACAGAGCTTGACGGGGAAAGCCGGGTCGAGGGGCGAAAAACCGTGACTTCTGGTAAACGCTCGTTG	68
8[132]	121[152]	CTATCAGATCAAGTAAACACCGAGTAATCTTGACAATGTTACCGAAAGGCGCTACAGACTTCTGGTAAACGCTCGTTG	78

Table 0-21: Narcissus left shortened staples

Start	End	Sequence	total length (bases)
11[48]	48[51]	CATTTTGCGGAACAAAAATTGCTGACAGGCCACCACCAGAG	41
13[48]	11[66]	AACGTCAGATGAATATACAGTAAATAAAGAGAA	33
14[61]	46[51]	TCATTTCGGAACCGCCATCTTTTCA	25
15[48]	44[51]	AGAAGATGATGAAACATAACCTACCGACTTCATTAAAGGTG	41
17[48]	18[48]	CGCTATTAATTAATTTACCTTTTTAACCTC	30
19[48]	20[48]	GTTGGGTTGACCTAAA	16
20[62]	40[55]	ATCTTCTATATAACAACAATGA	22
21[48]	22[48]	TTTGAAATCAGAGGCA	16
23[48]	24[48]	CCAGTAATTCAACAAT	16
25[48]	26[48]	CCTGAACAAAGTACCG	16
26[62]	34[55]	TTAAACCAGAAAAATCAAAAAT	22
27[48]	28[48]	GAGAACAACAAATCAG	16
28[62]	32[55]	TAGCAAGGCAAGCCTGAATCTT	22
29[48]	30[55]	GGCTTATCCGGTATTGACTTGCG	23
3[55]	4[55]	CCGCCAGCCCCTTCTG	16
31[55]	26[63]	TGAAGCCTTAAATCATTTATCCGTTTTTAACGGGTA	36
33[55]	33[73]	TAACGAGCGTCTTTCCAGA	19
35[55]	34[67]	CAGCCTTTACGAGAGTCTGGAGTTTTTTGTTT	32
37[55]	38[55]	ACAGGGAAGCGCATTCAAGAATTGAGTTAA	30
39[55]	20[73]	ATAAGAGCAAAATTCGCATCGATATATGTAAATGCTTTTT	40
39[74]	36[55]	AATTAACCCAAGACGGGAGGTCATTGCCTAGAGAGAATA	39
4[69]	2[55]	GATAGAACATTGCAACAGGAAGCCTTGCTGGTAATATCCAGAA	43
41[55]	43[71]	TAGCTATCTTACCGAGGAATACTACGCAGTA	31
43[51]	42[51]	AAGACTCCTTATCCAAAAGAACTG	24
45[51]	16[48]	CCGTCTGCTTCTG	13
47[51]	14[48]	ATCACCAATTACC	13
48[65]	50[51]	GAAAGGTTGATCTGAATTTACCGTTCCAG	29
49[51]	12[48]	AGCATGTAGATTT	13
5[55]	6[55]	GCGTAAGAGGTGAGGC	16
51[51]	10[48]	ATACAGTTTGAGT	13
53[51]	52[51]	GAGGCTGAGACTCTGAAACATGAA	24
55[51]	54[51]	CCGCCACCCTCACGTACTCAGGAG	24
57[51]	58[51]	TGTAGCGATC	10
59[51]	60[51]	TGTCGTTTCA	10
6[69]	56[51]	AAACAGAATACGTGCATAGTTAGCGTAACATTCCACCAGTACAAACT	47
61[51]	59[69]	ATCTCCAAAAAAATAATTTTCTTTCCAGACGTT	33
7[55]	8[55]	TTAACACCTGGTCAGT	16
9[55]	51[60]	CAACAGTTTTTAAAATGGCT	20

Table 0-22: Narcissus right extruding staples

Start	End	Sequence	total length (bases)
10[47]	51[50]	AACATATAAATCAAACCAAAATAGCCGTC	29
12[47]	48[139]	TCAGTGCCCCAGCAGGCGAAAATCCTGTTTGAGTAATCCCCAGGTCTTT	49
14[47]	47[50]	TGAGGAGGCGGTTTTCGAGCTTCAACAAA	29
16[47]	17[47]	TAAAAAGCCTGGGGTGCCTAGGAAGCATAAAGTGTATCGT	40
17[151]	13[47]	GCCATGAGTGATGAATCTGGGCGCGCAGCAAGCGGTCCACGCTGGTTGTTT	51
18[47]	20[147]	CGGCAGACGGAGGATCCCCGCTTGTTACACGAATATAGGGG	41
2[54]	6[163]	CAATCGTTAGAATCAGAGCGTATAACGACCACCAAAGTGTACCGAT	46
20[47]	19[47]	TTTAGTCGGTGGGCCTCGATAATTAG	26
21[153]	25[47]	CCATCTGTTATGATAATTTACGGGATGTTAAGCTTTCTCAGGAGAAAGT	49
22[47]	21[47]	TTTTGAGTGACTCAAGCAACTCATGG	26
24[47]	23[47]	AGATAGCCAGGGTCTCGCCCTGCGAG	26
26[47]	29[47]	CACTGGTGCGGGCCTCTTCGGTTGGGACCGGAAACAGCTTTCCGGCACCGAGAA	54
28[47]	27[47]	ATATCTTCTGGTGAGGGCGATCCATC	26
30[54]	31[54]	GGAGTCGTAACCGTGCATCTGGTGTAGATGGGCGCAGTTT	40
32[54]	33[54]	ACCACATTAAATGTGAGCGAAGCCAGCTTTCATCAAACGC	40
34[54]	31[157]	GAAAAAGCAAATATTTAAATTGTAAACTTCCTGTGTAACAATCAC	45
36[150]	37[54]	GATATTCAACCAATGTGTAGGTAAAGATTCAAAAGGGTGAGAAAGGCCAAAA	52
36[54]	35[54]	ACATGGAGACAGTCAAATCACCATCAACCCCAAAAACAGGAAGATTGTATATAG	54
38[54]	39[54]	GCCCAAAACATTATGACCCTTAAATCGGTTGTACCAAATA	40
4[150]	61[50]	GCTTCTTTGACAACGAAATAAACGGGTAAAATACGTAATGCCACGAAA	48
4[54]	3[54]	ACCTCTGCGCGTATGCTTTCCTATTA	26
40[54]	41[54]	AATACCCAATTCTGCGAACGCATATAACAGTTGATTGCAA	40
42[50]	38[151]	GCATTGCTCCTTTTGATAAGAGGTTCATTCAGTAGATATAAAGCGTAATACTTT	54
44[50]	43[50]	AATTCAGGTCAGGATTAGAATCAGTCACAGAGTACCTTTAATGATT	46
46[149]	15[47]	GTAATATCGCGTTTTAATGCGTATGGCCAACGCGCGGGGACAAA	44
46[50]	45[50]	TAATAGCGAACCAGACCGCCGTACAGCAGAAGCAAACTCCAAATCA	46
48[50]	51[150]	CCGCACGAGAATGACCATAAATCAAAAATCCTCAAATAGTTTTGCAGA	48
50[50]	49[50]	TAAGGAGAGGCTTTTGCAAAAGAGCTTTAAACAGTTCAGAAACGCC	46
52[50]	11[47]	AGTAATACCACATTCAACTAATGCGATAAAAAAGAATAATCGGCAAAATCCCTTTAT	57
54[50]	53[50]	GTTTTTTAAGAACTGGTGAGATTTAGGATTAA	32
56[50]	55[50]	ACAACAAAGCTGCTCAACCTTATGCGATAGTA	32
58[50]	57[50]	TAAATGATAAATTGTGAAATCAACGTAACGCC	32
6[162]	9[54]	TTTAAATCGAACGTGGTTGGAACAAGAGTCCAAAAT	36
6[54]	5[54]	GGTCAGGGAGCCCGCGGTCACGGAAA	26
60[50]	59[50]	CGTTTACGAAGGCACCTGTATCATCGCCGTTT	32
8[54]	7[54]	TGGCCTATTAAAGGAACCCTAAAGTA	26

Table 0-23: Narcissus left extruding staples

Start	End	Sequence	total length (bases)
11[166]	48[169]	CCCTTTATCATTTTGCGGAACAAAAATTGCTGACAGGCCACCACCAGAGCCGCACGA	57
13[166]	11[66]	GGTTGTTTAACGTCAGATGAATATACAGTAAATAAAGAGAA	41
14[61]	46[169]	TCATTTCGGAACCGCCATCTTTTCATAATAGCG	33
15[166]	44[169]	GGGACAAAAGAAGATGATGAAACATAACCTACCGACTTCATTAAAGGTGAATTCAGG	57
17[166]	18[166]	TGTATCGTCGCTATTAATTAATTTACCTTTTTAACCTCCGGCAGAC	46
19[166]	20[166]	ATAATTAGGTTGGGTTGACCTAAATTTAGTCG	32
20[62]	40[173]	ATCTTCTATATAACAACAATGAAATACCCA	30
21[166]	22[166]	ACTCATGGTTTGAAATCAGAGGCATTTTGAGT	32
23[166]	24[166]	CCTGCGAGCCAGTAATTCAACAATAGATAGCC	32
25[166]	26[166]	GAGAAAGTCCTGAACAAAGTACCGCACTGGTG	32
26[62]	34[173]	TTAAACCAGAAAAATCAAAAATGAAAAAGC	30
27[166]	28[166]	GATCCATCGAGAACAACAAATCAGATATCTTC	32
28[62]	32[173]	TAGCAAGGCAAGCCTGAATCTTACCACATT	30
29[166]	30[173]	ACCGAGAAGGCTTATCCGGTATTGACTTGCGGGAGTCGT	39
3[173]	4[173]	TCCTATTACCGCCAGCCCCTTCTGACCTCTGC	32
31[173]	26[63]	CGCAGTTTTGAAGCCTTAAATCATTTATCCGTTTTTAACGGGTA	44
33[173]	33[73]	TCAAACGCTAACGAGCGTCTTTCCAGA	27
35[173]	34[67]	GTATATAGCAGCCTTTACGAGAGTCTGGAGTTTTTTGTTT	40
37[173]	38[173]	GGCCAAAAACAGGGAAGCGCATTCAAGAATTGAGTTAAGCCCAAAA	46
39[173]	20[73]	ACCAAATAATAAGAGCAAAATTCGCATCGATATATGTAAATGCTTTTT	48
39[74]	36[173]	AATTAACCCAAGACGGGAGGTCATTGCCTAGAGAGAATAACATGGAG	47
4[69]	2[173]	GATAGAACATTGCAACAGGAAGCCTTGCTGGTAATATCCAGAACAATCGTT	51
41[173]	43[71]	GATTGCAATAGCTATCTTACCGAGGAATACTACGCAGTA	39
43[169]	42[169]	TAATGATTAAGACTCCTTATCCAAAAGAACTGGCATTGCT	40
45[169]	16[166]	CCAAATCACCGTCTGCTTCTGTAAAAAGC	29
47[169]	14[166]	TCAACAAAATCACCAATTACCTGAGGAGG	29
48[65]	50[169]	GAAAGGTTGATCTGAATTTACCGTTCCAGTAAGGAGA	37
49[169]	12[166]	GAAACGCCAGCATGTAGATTTTCAGTGCC	29
5[173]	6[173]	CACGGAAAGCGTAAGAGGTGAGGCGGTCAGGG	32
51[169]	10[166]	TAGCCGTCATACAGTTTGAGTAACATATA	29
53[169]	52[169]	AGGATTAAGAGGCTGAGACTCTGAAACATGAAAGTAATAC	40
55[169]	54[169]	CGATAGTACCGCCACCCTCACGTACTCAGGAGGTTTTTTA	40
57[169]	58[169]	GTAACGCCTGTAGCGATCTAAATGAT	26
59[169]	60[169]	CGCCGTTTTGTCGTTTCACGTTTACG	26
6[69]	56[169]	AAACAGAATACGTGCATAGTTAGCGTAACATTCCACCAGTACAAACTACAACAAA	55
61[169]	59[69]	CCACGAAAATCTCCAAAAAAATAATTTTCTTTCCAGACGTT	41
7[173]	8[173]	CTAAAGTATTAACACCTGGTCAGTTGGCCTAT	32
9[173]	51[60]	TCCAAAATCAACAGTTTTTAAAATGGCT	28

Table 0-24: Narcissus right shortened staples

Start	End	Sequence	total length (bases)
10[165]	51[168]	AATCAAACCAAAA	13
12[165]	48[139]	CCAGCAGGCGAAAATCCTGTTTGAGTAATCCCCAGGTCTTT	41
14[165]	47[168]	CGGTTTTCGAGCT	13
16[165]	17[165]	CTGGGGTGCCTAGGAAGCATAAAG	24
17[151]	13[165]	GCCATGAGTGATGAATCTGGGCGCGCAGCAAGCGGTCCACGCT	43
18[165]	20[147]	GGAGGATCCCCGCTTGTTACACGAATATAGGGG	33
2[172]	6[163]	AGAATCAGAGCGTATAACGACCACCAAAGTGTACCGAT	38
20[165]	19[165]	GTGGGCCTCG	10
21[153]	25[165]	CCATCTGTTATGATAATTTACGGGATGTTAAGCTTTCTCAG	41
22[165]	21[165]	GACTCAAGCA	10
24[165]	23[165]	AGGGTCTCGC	10
26[165]	29[165]	CGGGCCTCTTCGGTTGGGACCGGAAACAGCTTTCCGGC	38
28[165]	27[165]	TGGTGAGGGC	10
30[172]	31[172]	AACCGTGCATCTGGTGTAGATGGG	24
32[172]	33[172]	AAATGTGAGCGAAGCCAGCTTTCA	24
34[172]	31[157]	AAATATTTAAATTGTAAACTTCCTGTGTAACAATCAC	37
36[150]	37[172]	GATATTCAACCAATGTGTAGGTAAAGATTCAAAAGGGTGAGAAA	44
36[172]	35[172]	ACAGTCAAATCACCATCAACCCCAAAAACAGGAAGATT	38
38[172]	39[172]	CATTATGACCCTTAAATCGGTTGT	24
4[150]	61[168]	GCTTCTTTGACAACGAAATAAACGGGTAAAATACGTAATG	40
4[172]	3[172]	GCGTATGCTT	10
40[172]	41[172]	ATTCTGCGAACGCATATAACAGTT	24
42[168]	38[151]	CCTTTTGATAAGAGGTTCATTCAGTAGATATAAAGCGTAATACTTT	46
44[168]	43[168]	TCAGGATTAGAATCAGTCACAGAGTACCTT	30
46[149]	15[165]	GTAATATCGCGTTTTAATGCGTATGGCCAACGCGCG	36
46[168]	45[168]	AACCAGACCGCCGTACAGCAGAAGCAAACT	30
48[168]	51[150]	GAATGACCATAAATCAAAAATCCTCAAATAGTTTTGCAGA	40
50[168]	49[168]	GGCTTTTGCAAAAGAGCTTTAAACAGTTCA	30
52[168]	11[165]	CACATTCAACTAATGCGATAAAAAAGAATAATCGGCAAAAT	41
54[168]	53[168]	AGAACTGGTGAGATTT	16
56[168]	55[168]	GCTGCTCAACCTTATG	16
58[168]	57[168]	AAATTGTGAAATCAAC	16
6[162]	9[172]	TTTAAATCGAACGTGGTTGGAACAAGAG	28
6[172]	5[172]	AGCCCGCGGT	10
60[168]	59[168]	AAGGCACCTGTATCAT	16
8[172]	7[172]	TAAAGGAACC	10

Table 0-25: Narcisuss top topological marker

Start	End	Sequence	length (bases)
136[150]	138[149]	GACATTATTGAGGTTCAAAGGCGGGAGCTGGTCATG	36
137[124]	138[129]	TTTTTTCGGAGAGGGGTCAGCCGCCTCAGCTCACGGCCAAATTTTTT	47
137[144]	136[144]	TTGAACCTCAATGGGGGTTCTAACCGTA	28
137[174]	136[167]	TTTTTTTGAGATCATGTCCCCCCCCTAGAATAGTAGGTTTTTT	43
138[129]	136[149]	TTTTTTTTTGGCCGTCTGACCCCTCTCCGGCTGCGTGTCAGTTCGTCACTACGGT	55
138[150]	141[138]	TCCACAGACAATATAATCCGTTGTAGCGGAAGCTTTAAATTTACCG	46
139[157]	138[157]	GGATTAAGGAAATACCTATTGT	22
139[168]	140[154]	GCGGTGGGGCCTACACGGTGACTTCGTATACCAGGCCCAGAA	42
139[181]	138[174]	TTTTTTGTAGGCCCCACCGCTTCCTGGTATCTGAGTCTTTTTT	43
140[129]	139[129]	TTTTTTTACTTGTATAGACAATGGTTGGTACCGAATGGTTTTTT	44
140[137]	138[144]	ATACAAGTACCATTCGGTACCAACCTTCCGCTACAACCTGTGGACATGAC	50
141[124]	140[138]	TTTTTTCTTTCCTGTGGGTACGGTAAATTTAATGATTCCGAAAGCATTGTCT	52
141[137]	142[171]	TACCCACAGGAAAGCTCCGGGTCGGCGCCCCGCAGTGTGGCGTGGAGCCGGTATCCGGTCCATTTTTT	68
141[154]	138[168]	TCGCCCGTCACCCCCCTACTAGGGACATGATCTCAGACTCAG	42
141[168]	142[144]	TGCCTGGACCGGATACCGGCTCCACGCCACAC	32
141[171	140[181]	TTTTTTGGCAGGGGTGACGGGCGAATCATTCGGATTCTGGGCCTGGTATACGAAGTCACCGTTTTTTT	68
2[143]	136[124]	CGATATGGTTGAATGCGCAGCGGGCGCTAGGGCCGCGACCTGCTCCAGAAGTGACGAACTGACACGCAGCTTTTTT	76
62[130]	142[124]	ACAGAGGCAAAGACTTTTTCATGAGGAAGTTTCCATGAGGCAAAAACTGCGGGGCGCCGACCCGGAGTTTTTT	73

Table 0-26: Narcissus right topological marker

Start	End	Sequence	length (bases)
21[179]	38[179]	GAATGACTTGTGGCCAACAGTGTGTGACCAGGCGTGCTCACG	42
21[200]	38[200]	TACTGTCGAATGGTATACACGGGGGAGTCTCTTACGGACT	40
21[220]	38[220]	AGATGCGTCTTTTTTTTTTTTTTTTTTTTTTGTATCTTTAGAGA	44
22[170]	21[170]	TGACAAAGTGGGACCAAAGTCATTCAGCAGACTA	34
22[174]	39[182]	TGTCAGAGTGACTCAAGCAACTCTAGTCTGCTCGAAAACATTATGACCCTTAAATCGGTTGTACCATTTTTT	72
22[187]	21[187]	TCCCCCCCTAAACTATGCCATCGACAGTAACTGTTGGCCACA	42
22[195]	23[195]	AGGGGGGGATTGGTCCCACTTAGGCCCCCATCAGGAACGTGT	42
22[208]	21[208]	CTGGGGAGAACCGTTCCGTACGACGCATCTGTGTATACCATT	42
22[216]	23[216]	TCTCCCCAGATGGCATAGTTTCACGCAATATCCGAGGTAAAT	42
22[237]	23[237]	TTTTTTTTTGTACGGAACGGTGCGTCCCGTCCGAACACTATT	42
24[175]	23[174]	TTTTTTAGCCAGGGTCTCGCCCTGGAATC	29
36[150]	36[173]	GATATTCAACCAATGTGTAGGTAAAGATTCAAAAGGGTGAGAAAGGCCGGTAATTCCAGGAG	62
36[172]	35[182]	ACAGTCAAATCACCATCAACCCCAAAAACAGGAAGATTGTATTTTTTT	48
36[177]	23[170]	TGGAAACTCTAGTTCTTACGTTCCTGATGGGGGCCTGATTC	41
36[194]	23[194]	TGGGCTATATCGACACCTTACTTACCTCGGATATTGCGTGAC	42
36[215]	23[215]	GTCTGACCGTCCGGTCTCCAATAGTGTTCGGACGGGACGCAT	42
37[182]	36[182]	GGTATGACCAAGGAACTCATGTATAGCCCAAAGAACTAGAGT	42
37[203]	36[203]	GGTGCGCTTCTTCTTACGAACCGGTCAGACGTAAGGTGTCGA	42
37[224]	36[224]	TCTCTGATGTTTTTTTTTTTTTTTTTTTTTTGGAGACCGGA	42
38[177]	37[177]	CGCGTGAGCACGCCGGTCATACCTTACC	28
38[191]	37[191]	TGGTCACACAGTCCGTAAGAGAAGCGCACCCATGAGTTCCTT	42
38[212]	37[212]	ACTCCCCCTCTCTAAAGATACCATCAGAGAGTTCGTAAGAAG	42

Table 0-27: Narcissus left topological marker

Start	End	Sequence	length (bases)
17[38]	18[35]	TTTTTTTCGTCGCTATTAATTAATTTACCTTTTTAACCTCCGGCAGTAGGCCC	53
18[2]	19[2]	GTAGGAGTAACACGTGCTTACCAGTGTCCCAGGGGAGCATTA	42
18[23]	19[23]	TGGCGCCACCTGGGGCCTACTAAATTGCCTAGATCAGTAAGC	42
19[21]	40[21]	TGGCTTACTGATCTAGGCAATCTGTCTGCCATTGCGATTCTG	42
19[3]	40[8]	AATGCTCCCCTGGGACACCGACCACAGGTATTTTTT	36
19[42]	20[38]	TTTTAGGTTGGGTTGACCTAAATTTATTTTTT	32
20[62]	40[42]	ATCTTCTATATAACAACAATGAAATATCGACTTGT	35
40[30]	41[30]	AATGGCAGACAGACAAGTCGATTTTACTTAGTTCTTGGGGAT	42
40[9]	41[9]	TACCTGTGGTCGCAGAATCGCTATACTCTAGCGTAGTGAGCA	42
41[17]	42[17]	ACGCTAGAGTATAATCCCCAAATCTTGAAATCCCACCCTCGG	42
41[38]	43[71]	GAACTAAGTAAAAGCAATAGCTATCTTACCGAGGAATACTACGCAGTA	48
41[8]	42[4]	TTTTTTTGCTCACTTGAGACGGAAGGTTTTTT	32
42[26]	43[26]	GGATTTCAAGATTGCTTCCTTCAATCATCTCCGCTTGGACAC	42
42[5]	43[5]	CCTTCCGTCTCACCGAGGGTGTTCACCGTAACACAGGGCAGA	42
43[14]	18[14]	TGTTACGGTGAAGTGTCCAAGCAGGTGGCGCCAGTAAGCACG	42
43[35]	42[38]	CGGAGATGATTGGATTAAGACTCCTTATCCAAAAGAACTGGCATAAGGAAGCA	53
43[4]	18[1]	TTTTTTTCTGCCCTGTGTTACTCCTACTTTTTT	33

Table 0-28: Narcissus $P_{mrAumod}$

Start	End	Sequence	total length (bases)
18[121]	22[105]	AGCTGTTTCCCTGGTTGAATCATTCTAGAAAACGCTCAACAGTAGGCCTCTGGTTTTCGCCTATG	45
22[104]	20[105]	GGCTTAACGGAATCATAATTATCTCCGAGCCTCTGGTTTTCGCCTATG	28
23[93]	24[105]	CTGTCCAATAAATAGAAACCAATCGTAACGCCATTAGTGCGCCTCTGGTTTTCGCCTATG	40
45[115]	15[118]	TAGCCACTGCCCGTTACCTTGAACTTTCCAGTGCCTCTGGTTTTCGCCTATG	32
48[117]	13[118]	AGCAAATCAAAAAACGGGCAACCTGATTTCGCAGCTGATTGGCCTCTGGTTTTCGCCTATG	41
55[123]	8[112]	TTGCTACGTTAATAAAACTAATAGGCCCACTGCCTCTGGTTTTCGCCTATG	31
56[94]	6[112]	GAACGCAGCAAATGAAAAATCTAGTGAACCATCCTAAAAGCCTCTGGTTTTCGCCTATG	39
60[115]	4[112]	TTCAATCGTCTGAAATGGTTGGCAGATTCACCGCCTCTGGTTTTCGCCTATG	32

Table 0-29: Echo $P_{mrAumod}$

Start	End	Sequence	total length (bases)
105[144]	106[119]	AGATTTTGTTTAACGTCAAAAATGAAAACAGGAGATAACCCACAAGCCTCTGGTTTTCGCCTATG	45
113[126]	115[125]	TCAAAATCCACCCTCAGAGCCCCACCACGCCTCTGGTTTTCGCCTATG	28
119[102]	117[125]	TCCAGAACAATATAAACCCGTATTGAGCAGTCTCTGAAGCCTCTGGTTTTCGCCTATG	38
75[130]	113[125]	TAAGGATCGTCACCCTCCTGTCGTTTAGCGTTTCATAAGCCTCTGGTTTTCGCCTATG	38
79[119]	108[119]	TGATACCGATAAGGAATCACAGTGCGGCAAAGACATAGAAAAGCCTCTGGTTTTCGCCTATG	42
99[112]	101[111]	TTTAGTTGAGAAGAGTCAATATTGCTTCGCCTCTGGTTTTCGCCTATG	28
99[123]	99[111]	TCACGTTAAATAAGAATAAACACCAATATATGCCTCTGGTTTTCGCCTATG	31
99[91]	97[111]	AGAAAACTTTTTCAGGAATCAATGTAATTTAGGCAGCCTCTGGTTTTCGCCTATG	35

Table 0-30: Echo core staples

Start	End	Sequence	total length (base)
101[112]	101[101]	TGTAAATGAATTATTCATTTCAATTACCAATA	32
101[133]	99[143]	AATTTTCCCTTAGAACATAGCTTTA	25
101[70]	85[66]	ACAGTACACAAACAAGTAACACATCGTAACCGTGCCCAG	39
101[91]	85[87]	GTGAGTGTGAGCAACCGTGGGTCACGTTGGTGTAGGCCA	39
102[135]	85[129]	CAACCAATACTTTTGCCAGAGGGGAACC	28
103[137]	88[143]	ATAAACATTAGTTTACCAGACGACAAAGAAGTGCGGAATGCT	42
103[95]	88[101]	TACAATACCAGGAATTACGAGGCAGGATAGGAACAAACAATC	42
105[101]	108[129]	ATACTTCTGCAGTTAAGCATAGCCGAACAAAGTTACCAGAAGGAAAGCAA	50
106[118]	84[123]	GAATTGAGAGAGAAAATTGGGTTAAGAACTGGCTCTAG	38
106[139]	84[144]	TATCAGAGGAAGCGGAAACACCAGTCAGGACGTTGACG	38
106[76]	103[73]	TAGCAATATTCATCAATATAATATCAAAATTATTTATGA	39
106[97]	79[87]	TAAGAGCTGTTTGGATTTCAACTTTACCCGACGGCGGATGTTTCTA	46
108[118]	111[121]	TACATACATAAAGGGGTTTACTTAGAGCAATGAAACCATCGATAG	45
108[128]	80[144]	ACGAAAGGGCGACATTCGACGGTCGAACCGAACTGACCGAC	41
108[76]	81[55]	ACCACGGATCTTACGTGGTTGTGAATTCATGCGCACGACTTAAACGCCA	49
108[97]	110[66]	ATATAAAAGAAACGCAATCAAGTAGCACCATTAGTATTAGACTTTA	46
109[95]	77[108]	AAAGTCGGTGTATTTACGCTCGCCCTGGAGTTCTGTAAAACG	42
110[149]	71[143]	GTGATCAAGTATCGGCAACCGATAACCGATAGTTGCGCTTCC	42
110[65]	74[73]	CAAATTTGAGAGGAGCATGAGCTAACTCACACAAT	35
111[122]	79[118]	CAGCGAGCCATTTGGGAACAGCGCCCCTGCCAGACTCTA	39
111[74]	72[83]	TAGAACCATTAGCAAGGAAGGTTACGTTGCGGCGGTTTG	39
112[128]	76[144]	TTAGCCAACCATCGCCCTTTTGCGAGACTTTTTCATGATGC	41
112[135]	112[129]	AGCTCAGTAGCGACAGAAATTATCACCGTCACCGACTTACCGTAACCCC	49
112[58]	71[66]	CAAATCACCTTGCTGAACCACGCTCGCC	28
112[93]	109[94]	AGGCCGGAAACGTCACCCAGCAAAATCACCATAGA	35
113[105]	112[94]	GTTGGCAAAATCTTTTGCCTCAACAGTTGAAAGGAATTG	39
113[84]	72[94]	CCCTCAATTAACACCAGCAAGCGGTCCAGGGA	32
115[105]	114[108]	CAGAAGATACAGAAGCCACAAACAG	25
115[126]	68[115]	CAGAGCCTAAAGCCTCTCCAAGAACAACTAAAGGAATTG	39
115[60]	117[73]	ATAGCCCTAAACAATATTTTTGAACATTGGCAGATTCACCAG	42
116[108]	72[115]	AACCGTAATTTTTTCACGGCCCGAGAGCAGGCTAAT	36
117[105]	66[94]	GCCAACAACCGCCAGTTTTGTGTAGCATTCCACAGACAG	39
117[126]	119[136]	TTTACCGTTGAGTAACAGTGCAGTTAATGCCCCCTGCCT	39
117[147]	68[146]	ATACATGGCTTTTGTGATATTCACAAACAAGGAGCCAGCGGAG	43
117[84]	118[94]	AGTAATAAAAAACGCTCATGGCAAACTATCGGCCTTGCTGGTCAAC	46
118[93]	68[83]	AGGAAAGGGACCTGAAAGCGTAAGACCCAAAACTAAATC	39
29[109]	96[101]	ACGCATTCCTTGTCTAGCAAATCAGTAATTCTGTCCAGACGA	42
32[107]	94[111]	GCAAACAAGCAAGCCGTCCAATAGCAGCGCGTTGGGAGG	39
67[121]	67[120]	AGACGTTAGTAACCAGTACAAACTACAACGCCTCGTCTTTCC	42
67[67]	1[66]	GAACAAGTGTAGCGGTCTAATGCGTAGCAATGGCCACCGAGT	42
68[114]	119[101]	CGAATAATCGAGGTGCCATCTAAAGCCATTGAATA	35
68[145]	0[150]	TGAGAATTCTGTAACGGGGTTCGGAACCTATTATTCCT	38
68[61]	65[66]	GATTTAAGAAAGGTGACGCTACTTGCCTGAGTAGACCGTTGCCGC	45
68[82]	70[94]	GGAACCAAAGGAGCGGTTAGCGTAACGGTAAAGCTCAAGTTTGTT	45
69[144]	112[136]	CAAAAATAAATCCTCATGCCGCCAAGAGCCACACCGGATCAT	42
70[124]	116[109]	AGAATATTGAAAAAGAATGGAAAGCGATAG	30
71[67]	68[62]	TGGTTAAAGAACGTGGAAGGGCGATGGCCCAGAGCCCCC	39
72[136]	70[125]	CAATGACAACAGCTGCATGAAAATCCTGTTTGAAATCAAA	40
72[82]	115[59]	CGTATTGGGCGCCAGGGTGGTTTTTCTCCTTCACGAGAGCCACTG	45
72[93]	75[118]	GAGCTCACTGCCCGCTTTCCAGTCGGGAAACAGCAGCGTACAGAG	45
74[51]	77[55]	AAGGGGTACCGAGCTCGCGTGGTGCTTGTTACTCCTGG	38
74[72]	77[87]	TCCAATCATGGTCATAGTTGACCCCCGGGCTAAACAAGCGATTATACCA	49

74[82]	111[73]	CGCTCATTAATTGTCTAAAATATCTTTGATT	31
75[109]	74[83]	GGCAAAGACAGCATCGGAATGAAATTGTTATC	32
75[119]	75[108]	GCTTTGACTAAAACGAAAGAGGCAAAAGCAAC	32
77[109]	75[129]	GAGATTTGTATCATCGCCTGATAACACCAACGGAC	35
77[56]	79[76]	TTGGTGTTGACGCACCGAACGTTATTTAAGTTTATGGCCTTGAAAATAA	49
77[88]	76[102]	AGCCTCATCTCTGTTTCCTGTGCGAGGGTAGAAT	34
79[67]	74[52]	GCCAATCGGCAATGAGTTAAGCTAAATTCGTACACAACATACGAGCCGG	49
79[77]	81[97]	CCCCGCTCTTCTAACGAAGCCCTTTTTAAGAAAAGCCAGGGTCAGTGCC	49
80[143]	82[123]	CAGGCGCATAGGCTGGCTGACCTTCATCAAGACAAGAACCGGATATAGT	49
82[122]	103[115]	AGTATAACATAAAAATAGCAGCCTTTAAC	29
82[80]	84[102]	TCGCTATTACGGGGCGATCGGTGCGGGATCATTGTGAATTACCTTAATT	49
84[101]	103[94]	TAGGATCGGGAGAAACAATAAATAATGGAAGGGTTAGAACTTT	43
84[122]	105[100]	AAAGATTCATCAGTTGAGTGCGATTCTTGAGATGGTTTAATT	42
84[143]	105[150]	GAACCCTTACAAAATAAAAACGATTCGGG	29
84[149]	105[143]	CTAGGAAGAAGCTTGCCCTGACGACATT	28
85[108]	85[107]	TAAGAGCAACACTATCATGTAATAGTAAAAACCGTAATGTAG	42
85[130]	81[149]	CTCTTACAGGATTATACCAGAACGTCATTACCCAAATCAACGTAACAA	48
85[67]	82[81]	CCAACCGCTTTTGGGAACCAGCTGCCCAGTCACGACGTTGTAAAATCT	48
85[81]	88[69]	AACATGGGCGACCCGTCTTAACCAATAGGAAC	32
85[88]	85[80]	AAACATTCAACTAATGCAGCCGGCGCTTTATACAT	35
86[58]	104[66]	GCCATTAAATGTGAGCGTCAAGAAACGTCAGGCAC	35
87[117]	103[136]	TTAGACTGGATAGCGTAATCGCGGATTGCTTTGA	34
88[100]	103[87]	AGGTCTTTGCTCATTTTGGATTCTAAGAAGAACAG	35
88[131]	92[122]	AGAAAACGAGAATAGCGGATGACCGGAAACAGGTTGAA	38
88[68]	92[59]	GCCATCAAAAATAATTTTGTAACAGGACAGGTCAAATG	38
89[107]	87[116]	AGTCAGAAGCAAGACCATAAATCAAAGGCGGATTGTGT	38
90[131]	88[132]	GAACCATGCATCAAAAAGATAACAGTTC	28
90[68]	90[80]	CCCAAATAAAATTCGCATTAAATTTTTGATA	31
90[79]	90[90]	ATCGGAGCAAACAAGAGAATCGATTATGTACC	32
90[89]	89[106]	CCGGTTGTTAAATCAACCCTGACTATTAT	29
91[117]	92[101]	CCAGCAAACTAGCATGTCAATCAGAACGGTACAT	34
92[100]	32[108]	GTTGTTTCATATTTTTACCTTTATCATTAACTCATACAGGCAAGGCAGA	49
92[121]	91[116]	TATAATGCTGTAGCTCAAATCGTAAAACT	29
92[136]	90[132]	AGCTTAATTGCCAGGATTAGAGAGTTTCAAAGC	33
92[78]	90[69]	TTCTAGCTGATAAATTTTGCCTGAGAGTCTAGAAAAGC	38
95[74]	96[94]	ACGAGCATGTAGAAACCAATCAATCAAT	28
96[93]	92[79]	AAATCTGGAATTAAATATGCAACTAACCG	29
97[91]	96[80]	CGCCAACTAATTACTAGAAAAAGCCTGTGCCATATTTCA	39
98[58]	95[73]	TACAGTAGGGCTGTTTAAATATCCCATCCTAATTT	35
99[133]	99[122]	ACCTAAAGATAGCTTAGATTAAGACGCTAATT	32
99[70]	98[59]	AATCGCAAGACTACCTTTTTAACCTCCGGCTGATGGTTA	39

Table 0-31: Echo $P_{cF9(22)}$ staples

Start	End	Sequence	total length (base)
101[102]	128[70]	ACCGTGAATTTATCAAAATCATAGAATATATCTTCACGATTGCCACTTTCCAC	52
103[116]	128[112]	GGATTCGCCTCAGAGGCCGTCGCTATTAATTCTTCACGATTGCCACTTTCCAC	52
103[74]	126[70]	ATATACAGTATGATGAAATAAATCGTCTGAGAGACAAAGAACGCGCTTCACGATTGCCACTTTCCAC	66
103[88]	133[97]	TACCCTACCATCCTGATAAGAAACAATGAAACTTCACGATTGCCACTTTCCAC	52
105[144]	133[139]	AGATTTTGTTTAACGTCAAAAATGAAAACAGGAGATAACCCACAACTTCACGATTGCCACTTTCCAC	66
108[139]	133[160]	TATGTTACCGAGGAAACGCAAGCGCTAACTTCACGATTGCCACTTTCCAC	49
113[126]	132[105]	TCAAAATCCACCCTCAGAGCCCCACCACCTTCACGATTGCCACTTTCCAC	49
113[147]	132[126]	CCACCACGAACCGCCACCCTCGCATTGACTTCACGATTGCCACTTTCCAC	49
114[107]	134[84]	AGGTTGCCCCATAGGGTTGAGTGTTTTTGGGCTTCTGACATTCTGCTTCACGATTGCCACTTTCCAC	66
115[84]	130[84]	AAATACCGAACGAAGTCAGTATCAATATCTGGTCACTTCACGATTGCCACTTTCCAC	56
117[74]	130[63]	TCAGGCACAGAACATCGAACAGTGCCTCAAATATCAAACTTCACGATTGCCACTTTCCAC	59
119[102]	134[105]	TCCAGAACAATATAAACCCGTATTGAGCAGTCTCTGAACTTCACGATTGCCACTTTCCAC	59
119[137]	134[126]	ATTCAGTGCCTTCCAGTAAGCGTCCTTCACGATTGCCACTTTCCAC	45
68[72]	132[63]	AGGCTACGTGTCCACTACCCTGAGAGAGTTGCGCCTGCCCATTAACTTCACGATTGCCACTTTCCAC	66
70[93]	134[63]	CCAGTTTGGAACAAGAGAACCATCAATACGTCACGACCCTTCACGATTGCCACTTTCCAC	59
72[114]	132[84]	GAATCGGCCAACGCGCGCGCTGGTTGAGGCGCCACCAGCTTCACGATTGCCACTTTCCAC	59
75[130]	130[105]	TAAGGATCGTCACCCTCCTGTCGTTTAGCGTTTCATAACTTCACGATTGCCACTTTCCAC	59
75[151]	130[126]	GTTGAGTTAAAGGCCGCACGCATATTTTCGGACCAGAGCTTCACGATTGCCACTTTCCAC	59
76[101]	135[118]	ACACTAAAACAGCGAAACAAAGTACGCAACTCTTCATATTGGCAACCTTCACGATTGCCACTTTCCAC	67
76[143]	135[160]	CACTACGAAGGATTGTGTCGAAATCAGGCGCAAACCGATTACGCAGCTTCACGATTGCCACTTTCCAC	67
79[119]	135[139]	TGATACCGATAAGGAATCACAGTGCGGCAAAGACATAGAAAACTTCACGATTGCCACTTTCCAC	63
79[88]	135[97]	ATCGGCACGAATATAGGTTTGTCACAAAGACCTTCACGATTGCCACTTTCCAC	52

81[98]	133[118]	AAGCTTTCTCTTGAGTAATCAGGAGAAGTAAGCAGCCAATAACTTCACGATTGCCACTTTCCAC	63
84[59]	128[49]	GTGCAGGTTTAAACAAAACTTTTTTAATGGAACTTCACGATTGCCACTTTCCAC	53
94[142]	124[112]	TAACCTGTTTAGCTATAAATTCTGCGACAAACCAGTAACTTCACGATTGCCACTTTCCAC	59
94[79]	124[49]	AATGCAATGCCTGAGTACCATCAAAACGCGCCTTAATTCTTCACGATTGCCACTTTCCAC	59
96[79]	124[70]	GCTAATGCAGTATGATATTCAAAGTACGGTGCAACATGTTAACAACTTCACGATTGCCACTTTCCAC	66
97[133]	126[112]	TAAGAGATGTGATAAATAAGGTCTTCTGCTTCACGATTGCCACTTTCCAC	49
97[70]	126[49]	GAGAATCTTAGTATCATATGCCAAATCCCTTCACGATTGCCACTTTCCAC	49
99[112]	128[91]	TTTAGTTGAGAAGAGTCAATATTGCTTCCTTCACGATTGCCACTTTCCAC	49
99[123]	126[91]	TCACGTTAAATAAGAATAAACACCAATATATCTTCACGATTGCCACTTTCCAC	52
99[91]	124[91]	AGAAAACTTTTTCAGGAATCAATGTAATTTAGGCACTTCACGATTGCCACTTTCCAC	56

Table 0-32: Echo self-dimer staples

Start	End	Sequence	total length (base)
0[149]	62[131]	CAAAGGGATAGCCACCCTCAGAACCCGTACTAGTATAGCCCGGAATA	47
0[81]	67[66]	TCACGCAAATTAAAGAACTAAATACCTACATTTAAGG	37
1[135]	63[150]	GATTAGCGGGGTTTTGCTCTGATATACAGG	30
1[67]	63[78]	AAATACGCCATTAAAGGGATTTTAGA	26
27[82]	94[80]	AACCAAGTACCGCACTCCAAGAAGGAGAAGGAACCCTCATATATTTTA	48
28[134]	92[137]	GGAATCATTAAGGCTTATCCGGTAAAGTACCGAACGATAG	40
29[79]	28[82]	AATACTTTTGCGCGGGTATTA	21
30[130]	31[127]	GGCATCAATTCTTTAGCAAAA	21
31[86]	30[79]	CCAAAAAATAAAATCCACATTATGACCCTGT	31
32[127]	29[108]	TTAAGCAATAAAGCCTCAAAGAAACTAATAGTAGTAGTTCA	41
62[78]	1[81]	CAGGAACGGAGAGTCTGTCCA	21
63[131]	64[128]	GGTGTATCACGCCACCCTCAG	21
64[85]	68[73]	TTGCTTTGACGAGCACAGGGCGCGCGCTGGGAAAGCGCTAA	41
65[128]	69[143]	AGCCACCACCCTTTCGTCAATGAATTTAGAAAGAAAAAAGGCTC	44
66[145]	0[135]	CTGAGTCATTTTCGAGAAGGATTAG	25
66[93]	65[85]	CCCTCATAGGCGCTAGGGTACTATGG	26
94[110]	29[130]	ATAAAATCCATATAACAGTTGATTCCCTTTTCATAGCTGAAAAGGT	46
96[100]	32[86]	CGAAATCGGCTATCATTCATCGAGTAAAGCTAAATCGGTTGTA	43
97[112]	27[134]	GAGGCATTTTCGAGAGGTAAAGATATAGACCGCGCTTTTATTTTCATCGTA	51

Table 0-33: Echo left passivation set1

Start	End	Sequence	total length (base)
101[44]	86[40]	CATTTGAATTACTTAATTACATCAACAGTTTGAGGGGACGAC	42
103[48]	86[59]	AGATTTTCCGGAAACAGGAAGATCGCACTATCT	33
104[65]	108[48]	GTAGATGGCAAGACCAGAAACCCTAAAATTTTAAAAGTTTGAGTAA	46
105[48]	82[40]	TCCTGATTGGGGATGTGCTGCAAG	24
107[48]	106[48]	TTTTGCGGAACAAAGAAGGAGCGGAATTAT	30
109[48]	79[66]	TCCTTTGCTTTCACAACCTTATGACAATGTCCC	33
111[48]	110[48]	GTCAATAGATAATACACAATTCGACAACTC	30
63[44]	66[52]	GAGCTAAACAGGCCTCGTTCCGCGCTACGC	30
65[67]	62[48]	TACGTATAACGTGCTTTAGGCCGAGAATCCTGAGAAGTG	39
66[51]	70[44]	TGCCGTGGCGGAGCTTGGTCTATCCTCCAACGTCAA	36
71[44]	112[59]	ACAGCTGATTGCTTTCACCGGGTGCCTAATGAGCTAA	37
77[40]	76[40]	AACTCTGACCCTCGATAA	18
79[40]	78[40]	GAATTGTCATAAATCATT	18
81[40]	80[40]	AAGTTGGGTAGTGTCCTT	18
81[56]	104[48]	GGGTTTTGCGAAAGATCAGATAAACAGAAATAAAGA	36
83[40]	84[60]	TCGCCATTCAGGCTGCGCAACTGCTG	26
85[40]	84[40]	ATCGGCCTCCAGGCAAAG	18
91[40]	90[40]	GATCTACAAAGGCTATAGATTGTATAAGCAAA	32
92[58]	94[40]	CCGCAAATCAATGTGTAGGTAAAGATTCAAAAG	33
93[40]	92[40]	AAAGGCCGGAGACAGTGAGAGGGTAGCTATTT	32
95[44]	96[44]	AACAAGAAAAATTCAACAATAGAT	24
97[44]	98[44]	CCAACGCTCAACAAATTCTTACCA	24
99[44]	88[40]	CTATATGTAAATGCTTAGGCGTTAATATTCGCGTCTGGCCTT	42

Table 0-34: Echo right passivation set1

Start	End	Sequence	total length (base)
1[158]	67[161]	CCACTGAGACTCTGAAAGGTAATAAGTTTTATGGGATTTTGCTAAA	46
104[165]	103[165]	ATCCAAATAAGACAGCCATATTAT	24
105[151]	107[165]	AGATAATTGATAATAACGGAATACCCAAA	29
106[165]	105[165]	AAAGTCAGAGGGATTAACTGAACA	24
108[165]	110[150]	CATGATTAAGACTCCTTATTGAGGGAAAAG	30
110[165]	109[165]	AAATTATTCATTGGGAAGGTAAAT	24
112[165]	111[165]	TAGCGCGTTTTCTTGCCTTTAGCG	24
115[147]	113[165]	CAGGAGGTTGAGGCACCCTCACGGAACCGCCTC	33
62[165]	1[157]	CGTCGAGAGGGTAGTA	16
70[161]	72[137]	TTATCAGCTTGCTCGGCAAAATCCCTTATATGGTGGCGA	39
71[144]	71[161]	GAAATTTCGAGGTGAATT	18
78[158]	75[150]	TTAGCCGGAACGCGCGACCTACGTAAGGAA	30
81[150]	79[158]	AGCTGTGTACAAACTTTGAAAGA	23
86[158]	84[150]	GAGGCTTTTGCAGATAAAACGAA	23
88[142]	101[161]	TTATAAGAGGAAGCCCGCCTGAAAATCCTAACGCTAACG	39
88[158]	102[136]	ATCCCCCTCAAATCGTCATCTAATTTGCCAGAAGTTA	37
90[158]	94[143]	ATCGCGTTTTAATTCGAGCACCTTTAGATGGCTGTAGATTTCAA	44
92[158]	91[158]	GTCATTTTTGCGATTGCTCCTTTT	24
94[158]	96[150]	TTTCGCAAATGGTAGTTTGTTGC	23
96[149]	95[161]	GGGAGGTTATATTCTAAGAACGCGAGGCGTTT	32
98[161]	99[161]	ATTTTGCACCAAATAGTTTGCAGCTACAAT	30
99[144]	97[161]	ATGCCGACCGATTTGAAGCCTTAAATCAAGAT	32

Table 0-35: Echo P_0 staples

Start	End	Sequence	total length (base)
101[102]	101[90]	ACCGTGAATTTATCAAAATCATAGAATATAT	31
103[116]	101[132]	GGATTCGCCTCAGAGGCCGTCGCTATTAATT	31
103[74]	99[90]	ATATACAGTATGATGAAATAAATCGTCTGAGAGACAAAGAACGCG	45
103[88]	106[77]	TACCCTACCATCCTGATAAGAAACAATGAAA	31
105[144]	106[119]	AGATTTTGTTTAACGTCAAAAATGAAAACAGGAGATAACCCACAA	45
108[139]	106[140]	TATGTTACCGAGGAAACGCAAGCGCTAA	28
113[126]	115[125]	TCAAAATCCACCCTCAGAGCCCCACCAC	28
113[147]	115[146]	CCACCACGAACCGCCACCCTCGCATTGA	28
114[107]	117[104]	AGGTTGCCCCATAGGGTTGAGTGTTTTTGGGCTTCTGACATTCTG	45
115[84]	113[104]	AAATACCGAACGAAGTCAGTATCAATATCTGGTCA	35
117[74]	113[83]	TCAGGCACAGAACATCGAACAGTGCCTCAAATATCAAA	38
119[102]	117[125]	TCCAGAACAATATAAACCCGTATTGAGCAGTCTCTGAA	38
119[137]	117[146]	ATTCAGTGCCTTCCAGTAAGCGTC	24
68[72]	115[83]	AGGCTACGTGTCCACTACCCTGAGAGAGTTGCGCCTGCCCATTAA	45
70[93]	117[83]	CCAGTTTGGAACAAGAGAACCATCAATACGTCACGACC	38
72[114]	115[104]	GAATCGGCCAACGCGCGCGCTGGTTGAGGCGCCACCAG	38
75[130]	113[125]	TAAGGATCGTCACCCTCCTGTCGTTTAGCGTTTCATAA	38
75[151]	113[146]	GTTGAGTTAAAGGCCGCACGCATATTTTCGGACCAGAG	38
76[101]	108[98]	ACACTAAAACAGCGAAACAAAGTACGCAACTCTTCATATTGGCAAC	46
76[143]	108[140]	CACTACGAAGGATTGTGTCGAAATCAGGCGCAAACCGATTACGCAG	46
79[119]	108[119]	TGATACCGATAAGGAATCACAGTGCGGCAAAGACATAGAAAA	42
79[88]	108[77]	ATCGGCACGAATATAGGTTTGTCACAAAGAC	31
81[98]	106[98]	AAGCTTTCTCTTGAGTAATCAGGAGAAGTAAGCAGCCAATAA	42
84[59]	101[69]	GTGCAGGTTTAAACAAAACTTTTTTAATGGAA	32
94[142]	97[132]	TAACCTGTTTAGCTATAAATTCTGCGACAAACCAGTAA	38
94[79]	97[69]	AATGCAATGCCTGAGTACCATCAAAACGCGCCTTAATT	38
96[79]	97[90]	GCTAATGCAGTATGATATTCAAAGTACGGTGCAACATGTTAACAA	45
97[133]	99[132]	TAAGAGATGTGATAAATAAGGTCTTCTG	28
97[70]	99[69]	GAGAATCTTAGTATCATATGCCAAATCC	28
99[112]	101[111]	TTTAGTTGAGAAGAGTCAATATTGCTTC	28
99[123]	99[111]	TCACGTTAAATAAGAATAAACACCAATATAT	31
99[91]	97[111]	AGAAAACTTTTTCAGGAATCAATGTAATTTAGGCA	35

Table 0-36: Echo passivated six helix protrusion staples

Start	End	Sequence	total length (base)
0[149]	62[135]	CAAAGGGATAGCCACCCTCAGAACCCGTACTAGTATAGCCCGG	43
0[77]	67[66]	GCAAATTAAAGAACTAAATACCTACATTTAAGG	33
1[139]	63[150]	AGCGGGGTTTTGCTCTGATATACAGG	26
1[67]	63[74]	AAATACGCCATTAAAGGGATTT	22
27[86]	94[80]	AAGTACCGCACTCCAAGAAGGAGAAGGAACCCTCATATATTTTA	44
28[130]	92[137]	TCATTAAGGCTTATCCGGTAAAGTACCGAACGATAG	36
31[90]	30[83]	AAAATAAAATCCACATTATGACC	23
32[123]	29[108]	GCAATAAAGCCTCAAAGAAACTAATAGTAGTAGTTCA	37
64[81]	68[73]	TTTGACGAGCACAGGGCGCGCGCTGGGAAAGCGCTAA	37
65[132]	69[143]	ACCACCCTTTCGTCAATGAATTTAGAAAGAAAAAAGGCTC	40
66[145]	0[139]	CTGAGTCATTTTCGAGAAGGA	21
66[93]	65[81]	CCCTCATAGGCGCTAGGGTACT	22
94[110]	29[126]	ATAAAATCCATATAACAGTTGATTCCCTTTTCATAGCTGAAA	42
96[100]	32[90]	CGAAATCGGCTATCATTCATCGAGTAAAGCTAAATCGGT	39
97[112]	27[130]	GAGGCATTTTCGAGAGGTAAAGATATAGACCGCGCTTTTATTTTCAT	47

Table 0-37: Echo left stacking staples

Start	End	Sequence	total length (base)
1[44]	0[44]	TATAATCAGTGAACTTCTTTGATT	24
101[40]	86[37]	ATTTCATTTGAATTACTTAATTACATCAACAGTTTGAGGGGACGACGAC	49
103[44]	86[59]	GCGTAGATTTTCCGGAAACAGGAAGATCGCACTATCT	37
104[65]	108[44]	GTAGATGGCAAGACCAGAAACCCTAAAATTTTAAAAGTTTGAGTAACATT	50
105[44]	82[37]	ATATTCCTGATTGGGGATGTGCTGCAAGGCG	31
107[44]	106[44]	ATCATTTTGCGGAACAAAGAAGGAGCGGAATTATCATC	38
109[44]	79[66]	TAAATCCTTTGCTTTCACAACCTTATGACAATGTCCC	37
111[44]	110[44]	AGCCGTCAATAGATAATACACAATTCGACAACTCGTAT	38
113[44]	112[44]	AAAATCTAAAGCCTAATAGATTAG	24
115[44]	114[44]	TTTAATGCGCGAAGCAGCAAATGA	24
117[44]	116[44]	ATGGATTATTTATGGCTATTAGTC	24
119[44]	118[44]	AGTAATAACATCCAATCGTCTGAA	24
63[40]	66[52]	GCGGGAGCTAAACAGGCCTCGTTCCGCGCTACGC	34
65[40]	64[40]	CCACACCCGAGAATCAGA	18
65[67]	62[44]	TACGTATAACGTGCTTTAGGCCGAGAATCCTGAGAAGTGTTTT	43
66[51]	70[40]	TGCCGTGGCGGAGCTTGGTCTATCCTCCAACGTCAAAGGG	40
67[40]	66[40]	GCCGGCGAAGCGTAACCA	18
69[40]	68[40]	CGAAAAACCACGGGGAAA	18
71[40]	112[59]	GGCAACAGCTGATTGCTTTCACCGGGTGCCTAATGAGCTAA	41
73[40]	72[40]	TAAAGCCTGAGTGAGACG	18
75[37]	74[40]	CGGAGGATCCCCCATAAAGTG	21
77[37]	76[37]	CCGAACTCTGACCCTCGATAAAGA	24
79[37]	78[37]	GCTGAATTGTCATAAATCATTTCT	24
81[37]	80[37]	ATTAAGTTGGGTAGTGTCCTTAGT	24
81[56]	104[44]	GGGTTTTGCGAAAGATCAGATAAACAGAAATAAAGAAATT	40
83[37]	84[60]	CATTCGCCATTCAGGCTGCGCAACTGCTG	29
85[37]	84[37]	AGTATCGGCCTCCAGGCAAAGCGC	24
87[37]	102[40]	GTAGCCAGCTTTCATTTAACA	21
89[37]	100[40]	TTAAATTGTAAATTGGGTTAT	21
91[37]	90[37]	AGAGATCTACAAAGGCTATAGATTGTATAAGCAAATAT	38
92[58]	94[37]	CCGCAAATCAATGTGTAGGTAAAGATTCAAAAGGGT	36
93[37]	92[37]	GAGAAAGGCCGGAGACAGTGAGAGGGTAGCTATTTTTG	38
95[40]	96[40]	CCTGAACAAGAAAAATTCAACAATAGATAAGT	32
97[40]	98[40]	AAAGCCAACGCTCAACAAATTCTTACCAGTAT	32
99[40]	88[37]	ATAACTATATGTAAATGCTTAGGCGTTAATATTCGCGTCTGGCCTTCCT	49

Table 0-38: Echo right stacking staples

Start	End	Sequence	total length (base)
0[169]	1[169]	ATTAAGAGGGGCGGATAA	18
1[158]	67[165]	CCACTGAGACTCTGAAAGGTAATAAGTTTTATGGGATTTTGCTAAACAAC	50
100[165]	89[162]	TCCTGAATCTTAAAAGACTTC	21
102[165]	87[162]	TCTTTCCAGAGCAAATATTCA	21

104[169]	103[169]	CCCAATCCAAATAAGACAGCCATATTATTTAT	32
105[151]	107[169]	AGATAATTGATAATAACGGAATACCCAAAAGAA	33
106[169]	105[169]	GAACAAAGTCAGAGGGATTAACTGAACACCCT	32
108[169]	110[150]	CTGGCATGATTAAGACTCCTTATTGAGGGAAAAG	34
110[169]	109[169]	ACGGAAATTATTCATTGGGAAGGTAAATATTG	32
112[169]	111[169]	ACTGTAGCGCGTTTTCTTGCCTTTAGCGTCAG	32
114[169]	115[169]	AGAGCCGCCAGGTCAGAC	18
115[147]	113[169]	CAGGAGGTTGAGGCACCCTCACGGAACCGCCTCCCTC	37
116[169]	117[169]	GATTGGCCTATGATACAG	18
118[169]	119[169]	GAGTGTACTCATGAAAGT	18
62[169]	1[157]	GTGCCGTCGAGAGGGTAGTA	20
63[151]	63[165]	AGGTTTAGTACCGCC	15
64[165]	65[165]	ACCCTCAGAACCGCAAGCCCAATA	24
66[165]	66[146]	GGAACCCATGTACCGTAACA	20
68[165]	69[165]	TTTCAACAGTTTCTTTAATTGTAT	24
70[165]	72[137]	CGGTTTATCAGCTTGCTCGGCAAAATCCCTTATATGGTGGCGA	43
71[144]	71[165]	GAAATTTCGAGGTGAATTTCTT	22
72[165]	73[165]	AAACAGCTTGATTATTCGGTCGCT	24
74[165]	75[162]	GAGGCTTGCAGGTCCATTAAA	21
76[162]	77[162]	CGGGTAAAATGCTCCATG	18
78[162]	75[150]	TTACTTAGCCGGAACGCGCGACCTACGTAAGGAA	34
80[162]	81[162]	AGATGAACGGCTCATTCA	18
81[150]	79[162]	AGCTGTGTACAAACTTTGAAAGAGGAC	27
82[162]	83[162]	GTGAATAAGAAATCTACG	18
84[162]	85[162]	TTAATAAAAACCAAAATA	18
86[162]	84[150]	GCGAGAGGCTTTTGCAGATAAAACGAA	27
88[142]	101[165]	TTATAAGAGGAAGCCCGCCTGAAAATCCTAACGCTAACGAGCG	43
88[162]	102[136]	TTGAATCCCCCTCAAATCGTCATCTAATTTGCCAGAAGTTA	41
90[162]	94[143]	AAATATCGCGTTTTAATTCGAGCACCTTTAGATGGCTGTAGATTTCAA	48
92[162]	91[162]	AGAGGTCATTTTTGCGATTGCTCCTTTTGATA	32
94[162]	96[150]	TACATTTCGCAAATGGTAGTTTGTTGC	27
96[149]	95[165]	GGGAGGTTATATTCTAAGAACGCGAGGCGTTTTAGC	36
96[165]	93[162]	GAACCTCCCGACACCATTAGA	21
98[165]	99[165]	TGCTATTTTGCACCAAATAGTTTGCAGCTACAATTTTA	38
99[144]	97[165]	ATGCCGACCGATTTGAAGCCTTAAATCAAGATTAGT	36

Table 0-39: Echo staples hybridizing with Narcissus

Start	End	Sequence	total length (base)
0[149]	62[127]	CAAAGGGATAGCCACCCTCAGAACCCGTACTAGTATAGCCCGGAATAGGCT	51
0[85]	67[66]	TTGTTCACGCAAATTAAAGAACTAAATACCTACATTTAAGG	41
1[139]	63[150]	AGCGGGGTTTTGCTCTGATATACAGG	26
1[67]	63[82]	AAATACGCCATTAAAGGGATTTTAGACGCC	30
27[86]	94[80]	AAGTACCGCACTCCAAGAAGGAGAAGGAACCCTCATATATTTTA	44
28[138]	92[137]	TTCGGGAATCATTAAGGCTTATCCGGTAAAGTACCGAACGATAG	44
29[75]	28[86]	GGCGAATACTTTTGCGCGGGT	21
30[134]	31[123]	TCGGGGCATCAATTCTTTAGC	21
31[82]	30[83]	ATTTCCAAAAAATAAAATCCACATTATGACC	31
32[123]	29[108]	GCAATAAAGCCTCAAAGAAACTAATAGTAGTAGTTCA	37
62[82]	1[85]	GTTGCAGGAACGGAGAGTCTGTCCAAGCA	29
63[135]	64[124]	TATCACGCCACCCTCAGCGAA	21
64[89]	68[73]	TGCATTGCTTTGACGAGCACAGGGCGCGCGCTGGGAAAGCGCTAA	45
65[126]	69[143]	AGAGCCACCACCCTTTCGTCAATGAATTTAGAAAGAAAAAAGGCTC	46
66[145]	0[131]	CTGAGTCATTTTCGAGAAGGATTAGTCAG	29
66[93]	65[89]	CCCTCATAGGCGCTAGGGTACTATGGGGGA	30
94[110]	29[134]	ATAAAATCCATATAACAGTTGATTCCCTTTTCATAGCTGAAAAGGTCCTC	50
96[100]	32[90]	CGAAATCGGCTATCATTCATCGAGTAAAGCTAAATCGGT	39
97[112]	27[130]	GAGGCATTTTCGAGAGGTAAAGATATAGACCGCGCTTTTATTTTCAT	47

Table 0-40: Echo P_{lblock}

Start	End	Sequence	total length (bases)
103[88]	106[77]	TACCCTACCATCCTGATAAGAAACAATGAAAGACTTCTGGTAAACGCTCGTTG	31
117[74]	113[83]	TCAGGCACAGAACATCGAACAGTGCCTCAAATATCAAAGACTTCTGGTAAACGCTCGTTG	38
68[72]	115[83]	AGGCTACGTGTCCACTACCCTGAGAGAGTTGCGCCTGCCCATTAAGACTTCTGGTAAACGCTCGTTG	45
70[93]	117[83]	CCAGTTTGGAACAAGAGAACCATCAATACGTCACGACCGACTTCTGGTAAACGCTCGTTG	38
79[88]	108[77]	ATCGGCACGAATATAGGTTTGTCACAAAGACGACTTCTGGTAAACGCTCGTTG	31
84[59]	101[69]	GTGCAGGTTTAAACAAAACTTTTTTAATGGAAGACTTCTGGTAAACGCTCGTTG	32
94[79]	97[69]	AATGCAATGCCTGAGTACCATCAAAACGCGCCTTAATTGACTTCTGGTAAACGCTCGTTG	38
97[70]	99[69]	GAGAATCTTAGTATCATATGCCAAATCCGACTTCTGGTAAACGCTCGTTG	28

Table 0-41: Echo P_{rblock}

Start	End	Sequence	total length (bases)
103[116]	128[112]	GGATTCGCCTCAGAGGCCGTCGCTATTAATTGACTTCTGGTAAACGCTCGTTG	53
108[139]	133[160]	TATGTTACCGAGGAAACGCAAGCGCTAAGACTTCTGGTAAACGCTCGTTG	50
113[147]	132[126]	CCACCACGAACCGCCACCCTCGCATTGAGACTTCTGGTAAACGCTCGTTG	50
119[137]	134[126]	ATTCAGTGCCTTCCAGTAAGCGTCGACTTCTGGTAAACGCTCGTTG	46
75[151]	130[126]	GTTGAGTTAAAGGCCGCACGCATATTTTCGGACCAGAGGACTTCTGGTAAACGCTCGTTG	60
76[143]	135[160]	CACTACGAAGGATTGTGTCGAAATCAGGCGCAAACCGATTACGCAGGACTTCTGGTAAACGCTCGTTG	68
94[142]	124[112]	TAACCTGTTTAGCTATAAATTCTGCGACAAACCAGTAAGACTTCTGGTAAACGCTCGTTG	60
97[133]	126[112]	TAAGAGATGTGATAAATAAGGTCTTCTGGACTTCTGGTAAACGCTCGTTG	50

Table 0-42: Echo 6T passivated left staples

Start	End	Sequence	total length (base)
1[38]	0[38]	TTTTTTTATAATCAGTGAACTTCTTTGATTTTTTTT	36
101[34]	86[31]	TTTTTTATTTCATTTGAATTACTTAATTACATCAACAGTTTGAGGGGACGACGACTTTTTT	61
103[38]	86[59]	TTTTTTGCGTAGATTTTCCGGAAACAGGAAGATCGCACTATCT	43
104[65]	108[38]	GTAGATGGCAAGACCAGAAACCCTAAAATTTTAAAAGTTTGAGTAACATTTTTTTT	56
105[38]	82[31]	TTTTTTATATTCCTGATTGGGGATGTGCTGCAAGGCGTTTTTT	43
107[38]	106[38]	TTTTTTATCATTTTGCGGAACAAAGAAGGAGCGGAATTATCATCTTTTTT	50
109[38]	79[66]	TTTTTTTAAATCCTTTGCTTTCACAACCTTATGACAATGTCCC	43
111[38]	110[38]	TTTTTTAGCCGTCAATAGATAATACACAATTCGACAACTCGTATTTTTTT	50
113[38]	112[38]	TTTTTTAAAATCTAAAGCCTAATAGATTAGTTTTTT	36
115[38]	114[38]	TTTTTTTTTAATGCGCGAAGCAGCAAATGATTTTTT	36
117[38]	116[38]	TTTTTTATGGATTATTTATGGCTATTAGTCTTTTTT	36
119[38]	118[38]	TTTTTTAGTAATAACATCCAATCGTCTGAATTTTTT	36
63[34]	66[52]	TTTTTTGCGGGAGCTAAACAGGCCTCGTTCCGCGCTACGC	40
65[34]	64[34]	TTTTTTCCACACCCGAGAATCAGATTTTTT	30
65[67]	62[38]	TACGTATAACGTGCTTTAGGCCGAGAATCCTGAGAAGTGTTTTTTTTTT	49
66[51]	70[34]	TGCCGTGGCGGAGCTTGGTCTATCCTCCAACGTCAAAGGGTTTTTT	46
67[34]	66[34]	TTTTTTGCCGGCGAAGCGTAACCATTTTTT	30
69[34]	68[34]	TTTTTTCGAAAAACCACGGGGAAATTTTTT	30
71[34]	112[59]	TTTTTTGGCAACAGCTGATTGCTTTCACCGGGTGCCTAATGAGCTAA	47
73[34]	72[34]	TTTTTTTAAAGCCTGAGTGAGACGTTTTTT	30
75[31]	74[34]	TTTTTTCGGAGGATCCCCCATAAAGTGTTTTTT	33
77[31]	76[31]	TTTTTTCCGAACTCTGACCCTCGATAAAGATTTTTT	36
79[31]	78[31]	TTTTTTGCTGAATTGTCATAAATCATTTCTTTTTTT	36
81[31]	80[31]	TTTTTTATTAAGTTGGGTAGTGTCCTTAGTTTTTTT	36
81[56]	104[38]	GGGTTTTGCGAAAGATCAGATAAACAGAAATAAAGAAATTTTTTTT	46
83[31]	84[60]	TTTTTTCATTCGCCATTCAGGCTGCGCAACTGCTG	35
85[31]	84[31]	TTTTTTAGTATCGGCCTCCAGGCAAAGCGCTTTTTT	36
87[31]	102[34]	TTTTTTGTAGCCAGCTTTCATTTAACATTTTTT	33
89[31]	100[34]	TTTTTTTTAAATTGTAAATTGGGTTATTTTTTT	33
91[31]	90[31]	TTTTTTAGAGATCTACAAAGGCTATAGATTGTATAAGCAAATATTTTTTT	50
92[58]	94[31]	CCGCAAATCAATGTGTAGGTAAAGATTCAAAAGGGTTTTTTT	42
93[31]	92[31]	TTTTTTGAGAAAGGCCGGAGACAGTGAGAGGGTAGCTATTTTTGTTTTTT	50
95[34]	96[34]	TTTTTTCCTGAACAAGAAAAATTCAACAATAGATAAGTTTTTTT	44
97[34]	98[34]	TTTTTTAAAGCCAACGCTCAACAAATTCTTACCAGTATTTTTTT	44
99[34]	88[31]	TTTTTTATAACTATATGTAAATGCTTAGGCGTTAATATTCGCGTCTGGCCTTCCTTTTTTT	61

Table 0-43: Echo 6T passivated right staples

Start	End	Sequence	total length (base)
0[175]	1[175]	TTTTTTATTAAGAGGGGCGGATAATTTTTT	30
1[158]	67[171]	CCACTGAGACTCTGAAAGGTAATAAGTTTTATGGGATTTTGCTAAACAACTTTTTT	56
100[171]	89[168]	TTTTTTTCCTGAATCTTAAAAGACTTCTTTTTT	33
102[171]	87[168]	TTTTTTTCTTTCCAGAGCAAATATTCATTTTTT	33
104[175]	103[175]	TTTTTTCCCAATCCAAATAAGACAGCCATATTATTTATTTTTTT	44
105[151]	107[175]	AGATAATTGATAATAACGGAATACCCAAAAGAATTTTTT	39
106[175]	105[175]	TTTTTTGAACAAAGTCAGAGGGATTAACTGAACACCCTTTTTTT	44
108[175]	110[150]	TTTTTTCTGGCATGATTAAGACTCCTTATTGAGGGAAAAG	40
110[175]	109[175]	TTTTTTACGGAAATTATTCATTGGGAAGGTAAATATTGTTTTTT	44
112[175]	111[175]	TTTTTTACTGTAGCGCGTTTTCTTGCCTTTAGCGTCAGTTTTTT	44
114[175]	115[175]	TTTTTTAGAGCCGCCAGGTCAGACTTTTTT	30
115[147]	113[175]	CAGGAGGTTGAGGCACCCTCACGGAACCGCCTCCCTCTTTTTT	43
116[175]	117[175]	TTTTTTGATTGGCCTATGATACAGTTTTTT	30
118[175]	119[175]	TTTTTTGAGTGTACTCATGAAAGTTTTTTT	30
62[175]	1[157]	TTTTTTGTGCCGTCGAGAGGGTAGTA	26
63[151]	63[171]	AGGTTTAGTACCGCCTTTTTT	21
64[171]	65[171]	TTTTTTACCCTCAGAACCGCAAGCCCAATATTTTTT	36
66[171]	66[146]	TTTTTTGGAACCCATGTACCGTAACA	26
68[171]	69[171]	TTTTTTTTTCAACAGTTTCTTTAATTGTATTTTTTT	36
70[171]	72[137]	TTTTTTCGGTTTATCAGCTTGCTCGGCAAAATCCCTTATATGGTGGCGA	49
71[144]	71[171]	GAAATTTCGAGGTGAATTTCTTTTTTTT	28
72[171]	73[171]	TTTTTTAAACAGCTTGATTATTCGGTCGCTTTTTTT	36
74[171]	75[168]	TTTTTTGAGGCTTGCAGGTCCATTAAATTTTTT	33
76[168]	77[168]	TTTTTTCGGGTAAAATGCTCCATGTTTTTT	30
78[168]	75[150]	TTTTTTTTACTTAGCCGGAACGCGCGACCTACGTAAGGAA	40
80[168]	81[168]	TTTTTTAGATGAACGGCTCATTCATTTTTT	30
81[150]	79[168]	AGCTGTGTACAAACTTTGAAAGAGGACTTTTTT	33
82[168]	83[168]	TTTTTTGTGAATAAGAAATCTACGTTTTTT	30
84[168]	85[168]	TTTTTTTTAATAAAAACCAAAATATTTTTT	30
86[168]	84[150]	TTTTTTGCGAGAGGCTTTTGCAGATAAAACGAA	33
88[142]	101[171]	TTATAAGAGGAAGCCCGCCTGAAAATCCTAACGCTAACGAGCGTTTTTT	49
88[168]	102[136]	TTTTTTTTGAATCCCCCTCAAATCGTCATCTAATTTGCCAGAAGTTA	47
90[168]	94[143]	TTTTTTAAATATCGCGTTTTAATTCGAGCACCTTTAGATGGCTGTAGATTTCAA	54
92[168]	91[168]	TTTTTTAGAGGTCATTTTTGCGATTGCTCCTTTTGATATTTTTT	44
94[168]	96[150]	TTTTTTTACATTTCGCAAATGGTAGTTTGTTGC	33
96[149]	95[171]	GGGAGGTTATATTCTAAGAACGCGAGGCGTTTTAGCTTTTTT	42
96[171]	93[168]	TTTTTTGAACCTCCCGACACCATTAGATTTTTT	33
98[171]	99[171]	TTTTTTTGCTATTTTGCACCAAATAGTTTGCAGCTACAATTTTATTTTTT	50
99[144]	97[171]	ATGCCGACCGATTTGAAGCCTTAAATCAAGATTAGTTTTTTT	42

Table 0-44: Echo left shortened staples

Start	End	Sequence	total length (base)
1[48]	0[48]	ATCAGTGAACTTCTTT	16
101[44]	86[41]	CATTTGAATTACTTAATTACATCAACAGTTTGAGGGGACGA	41
103[48]	86[59]	AGATTTTCCGGAAACAGGAAGATCGCACTATCT	33
104[65]	108[48]	GTAGATGGCAAGACCAGAAACCCTAAAATTTTAAAAGTTTGAGTAA	46
105[48]	82[41]	TCCTGATTGGGGATGTGCTGCAA	23
107[48]	106[48]	TTTTGCGGAACAAAGAAGGAGCGGAATTAT	30
109[48]	79[66]	TCCTTTGCTTTCACAACCTTATGACAATGTCCC	33
111[48]	110[48]	GTCAATAGATAATACACAATTCGACAACTC	30
113[48]	112[48]	TCTAAAGCCTAATAGA	16
115[48]	114[48]	ATGCGCGAAGCAGCAA	16
117[48]	116[48]	ATTATTTATGGCTATT	16
119[48]	118[48]	ATAACATCCAATCGTC	16
63[44]	66[52]	GAGCTAAACAGGCCTCGTTCCGCGCTACGC	30
65[44]	64[44]	ACCCGAGAAT	10
65[67]	62[48]	TACGTATAACGTGCTTTAGGCCGAGAATCCTGAGAAGTG	39
66[51]	70[44]	TGCCGTGGCGGAGCTTGGTCTATCCTCCAACGTCAA	36
67[44]	66[44]	GCGAAGCGTA	10
69[44]	68[44]	AAACCACGGG	10
71[44]	112[59]	ACAGCTGATTGCTTTCACCGGGTGCCTAATGAGCTAA	37
73[44]	72[44]	GCCTGAGTGA	10
75[41]	74[44]	GGATCCCCCATAA	13

77[41]	76[41]	ACTCTGACCCTCGATA	16
79[41]	78[41]	AATTGTCATAAATCAT	16
81[41]	80[41]	AGTTGGGTAGTGTCCT	16
81[56]	104[48]	GGGTTTTGCGAAAGATCAGATAAACAGAAATAAAGA	36
83[41]	84[60]	CGCCATTCAGGCTGCGCAACTGCTG	25
85[41]	84[41]	TCGGCCTCCAGGCAAA	16
87[41]	102[44]	CCAGCTTTCATTT	13
89[41]	100[44]	ATTGTAAATTGGG	13
91[41]	90[41]	ATCTACAAAGGCTATAGATTGTATAAGCAA	30
92[58]	94[41]	CCGCAAATCAATGTGTAGGTAAAGATTCAAAA	32
93[41]	92[41]	AAGGCCGGAGACAGTGAGAGGGTAGCTATT	30
95[44]	96[44]	AACAAGAAAAATTCAACAATAGAT	24
97[44]	98[44]	CCAACGCTCAACAAATTCTTACCA	24
99[44]	88[41]	CTATATGTAAATGCTTAGGCGTTAATATTCGCGTCTGGCCT	41

Table 0-45: Echo right extruding staples

Start	End	Sequence	total length (base)
0[47]	1[47]	GATTATTAAGAGGGGCGGATAATATA	26
1[158]	67[43]	CCACTGAGACTCTGAAAGGTAATAAGTTTTATGGGATTTTGCTAAACAACGCCG	54
100[43]	89[40]	TTATTCCTGAATCTTAAAAGACTTCTTAA	29
102[43]	87[40]	AACATCTTTCCAGAGCAAATATTCAGTAG	29
104[47]	103[47]	AATTCCCAATCCAAATAAGACAGCCATATTATTTATGCGT	40
105[151]	107[47]	AGATAATTGATAATAACGGAATACCCAAAAGAAATCA	37
106[47]	105[47]	CATCGAACAAAGTCAGAGGGATTAACTGAACACCCTATAT	40
108[47]	110[150]	CATTCTGGCATGATTAAGACTCCTTATTGAGGGAAAAG	38
110[47]	109[47]	GTATACGGAAATTATTCATTGGGAAGGTAAATATTGTAAA	40
112[47]	111[47]	TTAGACTGTAGCGCGTTTTCTTGCCTTTAGCGTCAGAGCC	40
114[47]	115[47]	ATGAAGAGCCGCCAGGTCAGACTTTA	26
115[147]	113[47]	CAGGAGGTTGAGGCACCCTCACGGAACCGCCTCCCTCAAAA	41
116[47]	117[47]	AGTCGATTGGCCTATGATACAGATGG	26
118[47]	119[47]	TGAAGAGTGTACTCATGAAAGTAGTA	26
62[47]	1[157]	TTTTGTGCCGTCGAGAGGGTAGTA	24
63[151]	63[43]	AGGTTTAGTACCGCCGCGG	19
64[43]	65[43]	CAGAACCCTCAGAACCGCAAGCCCAATACCAC	32
66[43]	66[146]	ACCAGGAACCCATGTACCGTAACA	24
68[43]	69[43]	GAAATTTCAACAGTTTCTTTAATTGTATCGAA	32
70[43]	72[137]	AGGGCGGTTTATCAGCTTGCTCGGCAAAATCCCTTATATGGTGGCGA	47
71[144]	71[43]	GAAATTTCGAGGTGAATTTCTTGGCA	26
72[43]	73[43]	GACGAAACAGCTTGATTATTCGGTCGCTTAAA	32
74[43]	75[40]	AGTGGAGGCTTGCAGGTCCATTAAACGGA	29
76[40]	77[40]	AAGACGGGTAAAATGCTCCATGCCGA	26
78[40]	75[150]	TTCTTTACTTAGCCGGAACGCGCGACCTACGTAAGGAA	38
80[40]	81[40]	TAGTAGATGAACGGCTCATTCAATTA	26
81[150]	79[40]	AGCTGTGTACAAACTTTGAAAGAGGACGCTG	31
82[40]	83[40]	GGCGGTGAATAAGAAATCTACGCATT	26
84[40]	85[40]	GCGCTTAATAAAAACCAAAATAAGTA	26
86[40]	84[150]	CGACGCGAGAGGCTTTTGCAGATAAAACGAA	31
88[142]	101[43]	TTATAAGAGGAAGCCCGCCTGAAAATCCTAACGCTAACGAGCGATTT	47
88[40]	102[136]	TCCTTTGAATCCCCCTCAAATCGTCATCTAATTTGCCAGAAGTTA	45
90[40]	94[143]	ATATAAATATCGCGTTTTAATTCGAGCACCTTTAGATGGCTGTAGATTTCAA	52
92[40]	91[40]	TTTGAGAGGTCATTTTTGCGATTGCTCCTTTTGATAAGAG	40
94[40]	96[150]	GGGTTACATTTCGCAAATGGTAGTTTGTTGC	31
96[149]	95[43]	GGGAGGTTATATTCTAAGAACGCGAGGCGTTTTAGCCCTG	40
96[43]	93[40]	AAGTGAACCTCCCGACACCATTAGAGAGA	29
98[43]	99[43]	GTATTGCTATTTTGCACCAAATAGTTTGCAGCTACAATTTTAATAA	46
99[144]	97[43]	ATGCCGACCGATTTGAAGCCTTAAATCAAGATTAGTAAAG	40

Table 0-46: Echo left extruding staples

Start	End	Sequence	total length (base)
1[166]	0[166]	ATAATATAATCAGTGAACTTCTTTGATTATTA	32
101[162]	86[159]	AGCGATTTCATTTGAATTACTTAATTACATCAACAGTTTGAGGGGACGACGACGCGA	57
103[166]	86[59]	TTATGCGTAGATTTTCCGGAAACAGGAAGATCGCACTATCT	41
104[65]	108[166]	GTAGATGGCAAGACCAGAAACCCTAAAATTTTAAAAGTTTGAGTAACATTCTGG	54

105[166]	82[159]	CCCTATATTCCTGATTGGGGATGTGCTGCAAGGCGGTGA	39
107[166]	106[166]	AGAAATCATTTTGCGGAACAAAGAAGGAGCGGAATTATCATCGAAC	46
109[166]	79[66]	ATTGTAAATCCTTTGCTTTCACAACCTTATGACAATGTCCC	41
111[166]	110[166]	TCAGAGCCGTCAATAGATAATACACAATTCGACAACTCGTATACGG	46
113[166]	112[166]	CCTCAAAATCTAAAGCCTAATAGATTAGACTG	32
115[166]	114[166]	AGACTTTAATGCGCGAAGCAGCAAATGAAGAG	32
117[166]	116[166]	ACAGATGGATTATTTATGGCTATTAGTCGATT	32
119[166]	118[166]	AAGTAGTAATAACATCCAATCGTCTGAAGAGT	32
63[162]	66[52]	CGCCGCGGGAGCTAAACAGGCCTCGTTCCGCGCTACGC	38
65[162]	64[162]	AATACCACACCCGAGAATCAGAACCC	26
65[67]	62[166]	TACGTATAACGTGCTTTAGGCCGAGAATCCTGAGAAGTGTTTTGTGC	47
66[51]	70[162]	TGCCGTGGCGGAGCTTGGTCTATCCTCCAACGTCAAAGGGCGGT	44
67[162]	66[162]	CAACGCCGGCGAAGCGTAACCAGGAA	26
69[162]	68[162]	GTATCGAAAAACCACGGGGAAATTTC	26
71[162]	112[59]	TCTTGGCAACAGCTGATTGCTTTCACCGGGTGCCTAATGAGCTAA	45
73[162]	72[162]	CGCTTAAAGCCTGAGTGAGACGAAAC	26
75[159]	74[162]	TAAACGGAGGATCCCCCATAAAGTGGAGG	29
77[159]	76[159]	CATGCCGAACTCTGACCCTCGATAAAGACGGG	32
79[159]	78[159]	GGACGCTGAATTGTCATAAATCATTTCTTTAC	32
81[159]	80[159]	TTCAATTAAGTTGGGTAGTGTCCTTAGTAGAT	32
81[56]	104[166]	GGGTTTTGCGAAAGATCAGATAAACAGAAATAAAGAAATTCCCA	44
83[159]	84[60]	TACGCATTCGCCATTCAGGCTGCGCAACTGCTG	33
85[159]	84[159]	AATAAGTATCGGCCTCCAGGCAAAGCGCTTAA	32
87[159]	102[162]	TTCAGTAGCCAGCTTTCATTTAACATCTT	29
89[159]	100[162]	CTTCTTAAATTGTAAATTGGGTTATTCCT	29
91[159]	90[159]	GATAAGAGATCTACAAAGGCTATAGATTGTATAAGCAAATATAAAT	46
92[58]	94[159]	CCGCAAATCAATGTGTAGGTAAAGATTCAAAAGGGTTACA	40
93[159]	92[159]	TAGAGAGAAAGGCCGGAGACAGTGAGAGGGTAGCTATTTTTGAGAG	46
95[162]	96[162]	TAGCCCTGAACAAGAAAAATTCAACAATAGATAAGTGAAC	40
97[162]	98[162]	TAGTAAAGCCAACGCTCAACAAATTCTTACCAGTATTGCT	40
99[162]	88[159]	TTTAATAACTATATGTAAATGCTTAGGCGTTAATATTCGCGTCTGGCCTTCCTTTGA	57

Table 0-47: Echo right shortened staples

Start	End	Sequence	total length (base)
0[165]	1[165]	AGAGGGGCGG	10
1[158]	67[161]	CCACTGAGACTCTGAAAGGTAATAAGTTTTATGGGATTTTGCTAAA	46
100[161]	89[158]	GAATCTTAAAAGA	13
102[161]	87[158]	TCCAGAGCAAATA	13
104[165]	103[165]	ATCCAAATAAGACAGCCATATTAT	24
105[151]	107[165]	AGATAATTGATAATAACGGAATACCCAAA	29
106[165]	105[165]	AAAGTCAGAGGGATTAACTGAACA	24
108[165]	110[150]	CATGATTAAGACTCCTTATTGAGGGAAAAG	30
110[165]	109[165]	AAATTATTCATTGGGAAGGTAAAT	24
112[165]	111[165]	TAGCGCGTTTTCTTGCCTTTAGCG	24
114[165]	115[165]	CCGCCAGGTC	10
115[147]	113[165]	CAGGAGGTTGAGGCACCCTCACGGAACCGCCTC	33
116[165]	117[165]	GGCCTATGAT	10
118[165]	119[165]	GTACTCATGA	10
62[165]	1[157]	CGTCGAGAGGGTAGTA	16
63[151]	63[161]	AGGTTTAGTAC	11
64[161]	65[161]	TCAGAACCGCAAGCCC	16
66[161]	66[146]	CCCATGTACCGTAACA	16
68[161]	69[161]	AACAGTTTCTTTAATT	16
70[161]	72[137]	TTATCAGCTTGCTCGGCAAAATCCCTTATATGGTGGCGA	39
71[144]	71[161]	GAAATTTCGAGGTGAATT	18
72[161]	73[161]	AGCTTGATTATTCGGT	16
74[161]	75[158]	CTTGCAGGTCCAT	13
76[158]	77[158]	TAAAATGCTC	10
78[158]	75[150]	TTAGCCGGAACGCGCGACCTACGTAAGGAA	30
80[158]	81[158]	GAACGGCTCA	10
81[150]	79[158]	AGCTGTGTACAAACTTTGAAAGA	23
82[158]	83[158]	ATAAGAAATC	10
84[158]	85[158]	TAAAAACCAA	10
86[158]	84[150]	GAGGCTTTTGCAGATAAAACGAA	23
88[142]	101[161]	TTATAAGAGGAAGCCCGCCTGAAAATCCTAACGCTAACG	39
88[158]	102[136]	ATCCCCCTCAAATCGTCATCTAATTTGCCAGAAGTTA	37

90[158]	94[143]	ATCGCGTTTTAATTCGAGCACCTTTAGATGGCTGTAGATTTCAA	44
92[158]	91[158]	GTCATTTTTGCGATTGCTCCTTTT	24
94[158]	96[150]	TTTCGCAAATGGTAGTTTGTTGC	23
96[149]	95[161]	GGGAGGTTATATTCTAAGAACGCGAGGCGTTT	32
96[161]	93[158]	CTCCCGACACCAT	13
98[161]	99[161]	ATTTTGCACCAAATAGTTTGCAGCTACAAT	30
99[144]	97[161]	ATGCCGACCGATTTGAAGCCTTAAATCAAGAT	32

Other single-stranded DNA oligonucleotides were purchased depending on their modification, price and yield from various vendors as listed below:

Table 0-48: Other used oligonucleotides

Name	Sequence	Vendor
P1	CGTAAAGCACTAAATCGGAACCCT	Merck/IDT
P2	TCACTGCCCGCTTTCCA	Merck/IDT
P3	GTTTTCCCAGTCACGACGTTGTAA	Merck/IDT
P4	GAAAAGCCCCAAAAACAGGAAGAT	Merck/IDT
P5	ATCATACAGGCAAGGCAAAGAATT	Merck/IDT
P6	AAAAAGATTAAGAGGAAGCCCGAA	Merck/IDT
P7	CGATAAAAACCAAAATAGCGAGAG	Merck/IDT
P8	TTGACCCCCAGCGATTATACCA	Merck/IDT
P9	TGACAACAACCATCGCCCAC	Merck/IDT
P10	ATAAGTGCCGTCGAGAGGGTTG	Merck/IDT
P11	CATAATCAAAATCACCGGAACCAG	Merck/IDT
P12	GAAACCGAGGAAACGCAATAATAA	Merck/IDT
P13	GACTTGCGGGAGGTTTTGAA	Merck/IDT
P14	CAAGACAAAGAACGCGAGAAAACT	Merck/IDT
P15	CCTGAGCAAAAGAAGATGATGAAA	Merck/IDT
P16	ACCTCAAATATCAAACCCTCAATC	Merck/IDT
P17	GTCCATCACGCAAATTAACCG	Merck/IDT
P18	ATAGGGGCCTTGAATCGGCT	Merck/IDT
F9(22)	GTGGAAAGTGGCAATCGTGAAG	Merck/IDT
bt-T10-cF9(22)	biotin-TTTTTTTTTTCTTCACGATTGCCACTTTCCAC	Merck/IDT
NH_2-L-block	amino-TAATCGGAGGTCGCTTTCAGTGGTACAGATTATTATAGAGGTGGTCAACGAGCGTTTACCA	Merck/IDT
NH_2-L-block Cy5	amino-TAATCGGAGGTCGCTTTCAGTGGTACAGATTATTATAGAGGTGGTCAACGAGCGTTTACCA-Cy5	Merck/IDT
NH_2-M-block	amino-TTCAGTGGTACAGATTATTATAGAGGTGGTCAACGAGCGTTTACCA	Merck/IDT
NH_2-M-block Cy5	amino-TTCAGTGGTACAGATTATTATAGAGGTGGTCAACGAGCGTTTACCA-Cy5	Merck/IDT
NH_2-S-block	amino-TTATTATAGAGGTGGTCAACGAGCGTTTACCA	Merck/IDT
NH_2-S-block Cy5	amino-TTATTATAGAGGTGGTCAACGAGCGTTTACCA-Cy5	Merck/IDT
NH_2-Aubind-FAM	amino-CATAGGCGAAAACCAG	Merck/IDT
F9(16)-FAM	GTGGAAAGTGGCAATC-FAM	Merck/IDT
block release	TGGTAAACGCTCGTTGACCACCTCTATAATAA	Merck/IDT
Aumod	thiol-TTTTTTTTTTGCCTCTGGTTTTCGCCTATG	Merck/IDT
F9(16)-TAMRA	GTGGAAAGTGGCAATC-TAMRA	Merck/IDT

NH_2-F9(16)-FAM	amino-GTGGAAAGTGGCAATC-FAM	Merck/IDT
NH_2-F9(16)-TAMRA	amino-GTGGAAAGTGGCAATC-TAMRA	Merck/IDT
N_3-F9(16)	azide-GTGGAAAGTGGCAATC	Baseclick
N_3-F9(16)-TAMRA	azide-GTGGAAAGTGGCAATC-TAMRA	Baseclick
phoshate-F9(16)	phosphate-F9(16)	Merck

c. Buffer

Table 0-49: Buffers used in this work and their composition

Name	Composition
TEMg	20 mM tris base, 2 mM Na_2EDTA, 12.5 mM $MgCl_2$, pH8
TEMg20	5 mM tris base, 1 mM Na_2EDTA, 20 mM $MgCl_2$, pH8
caco7Ca	50 mM sodium cacodylate, 7 mM $CaCl_2$, pH6
PBS pH6.5	41.8 mM NaH_2PO4, 8.2 mM Na_2HPO4, pH 6.5
PBS pH7.6	14.5 mM NaH_2PO4, 35.5 mM Na_2HPO4, pH 6.5
FluoReaction buffer	41.8 mM NaH_2PO4, 8.2 mM Na_2HPO4, 100 mM NaCl, 1 mM DTT pH 6.5
HEPESMg	50 mM HEPES, 11 mM $MgCl_2$, pH 7.4
p97 storage buffer	50 mM HEPES, 130 mM KCl, 5 mM $MgCl_2$, 5% glycerol, pH7.4
p97 unfolding buffer	25 mM HEPES, 100 mM KCl, 5 mM $MgCl_2$, pH7.4
TBEMg	40 mM tris base, 20 mM boric acid, 2 mM Na_2EDTA, 12.5 mM $MgCl_2$
TBEMg11	45 mM tris base, 45 mM boric acid, 11 mM $MgCl_2$
TE	20 mM tris base, 2 mM Na_2EDTA, pH8
TEN100	10 mM tris base, 1 mM Na_2EDTA, 100 mM NaCl, pH7.5
Native AGE buffer	125 mM trisbase, 950 mM glycine, pH6.8
Native AGE loading dye	250 mM tris-HCl, 40% glycerol, pH6.8
AGE loading dye	70% 5XTBEMg, 30% glycerol
TBE	89 mM tris base, 89 mM boric acid, 2 mM Na_2EDTA, pH8
Denaturating DNA PAGE buffer	TBE buffer, 7 M urea
SDS PAGE lower gel buffer	375 mM tris base, 1 g/l SDS pH 8.8
SDS PAGE upper gel buffer	125 mM tris-HCl, 1 g/l SDS, pH6.8
5X SDS PAGE loading dye	125 mM tris-HCl, 2.5 g/l SDS, 10% glycerol, pH6.8
Coomassie R staining solution	25% isopropanol, 10% acetic acid, 0.5 g/l Coomassie R250
SDS PAGE running buffer	192 mM glycine, 33 mM tris base, 1 g/l SDS
Native PAGE lower gel buffer	375 mM tris base pH 8.8
Native PAGE upper gel buffer	125 mM tris-HCl, pH6.8
Native PAGE loading dye	250 mM tris-HCl, 40% glycerol, pH6.8
Native PAGE running buffer	125 mM tris base, 950 mM glycine, pH6.8
Uranyl formate staining solution	1% uranyl formate
NZA medium	10 g/l NZA, 5 g/l bacto yeast extract, 10 g/l NaCl, 12.5 mg/l tetracycline
PEG precipitation buffer	5 mM tris base, 1 mM Na_2EDTA, 505 mM NaCl, 15% PEG8000
2xYT medium	16 g/l bacto tryptone, 10g/l bacto yeast extract, 5 g NaCl, 5 mM $MgCl_2$, 12.5 mg/l tetracycline, pH7
20X E-Mix	200 mM creatin phosphate, 40 mM ATP, 100 mM HEPES, 20 mM DTT, 0.2 mg/ml creatine kinase in 6.15 mM K_2HPO_4 and 3.85 mM KH_2PO_4 (pH 7)

d. Consumables

Table 0-50: Consumables used in this work

Name	Vendor
384 well plate, black, transparent F-bottom	Greiner Bio-One
96-well plates	Sarstedt AG & Co.
AFM metal specimen disk	Ted Pella Inc.
AFM tips ScanAsyst air/liquid	Bruker Nano Inc.
beaker/flasks	Schott
dye removal column	Thermo Fisher Scientific
Formvar/coal coated copper grids S-162	Plano GmbH
mica (V1&V3)	Plano GmbH
MWCO filter	Sartorius/Millipore
NAP™5, NAP™10 columns	GE Healthcare
PCR tubes (0.2 ml)	VWR
pipetting tips (20 µl, 200 µl,1000 µl, 2 ml, 5 ml)	Eppendorf AG
protein low binding reaction tubes (1.5 ml)	Eppendorf AG
Quantum Prep Freeze 'N Squeeze DNA Gel extraction spin columns	Bio-Rad Laboratories Inc.
reaction tubes (1.5 ml, 2 ml, 5 ml)	Sarstedt AG & Co.
reaction tubes (15 ml, 50 ml)	VWR
SNAP-Capture Pull-Down Resin	New England BioLabs
streptavidin magnetic particles	Merck
XL1-Blue *E .coli* bacteria	Agilent technologies

e. Equipment

Table 0-51: Equipment used during this work

Name	Vendor
Agarose gel system	VWR International GmbH/Bio-Rad Laboratories Inc.
Analytical balance	Sartorius AG
Atomic force microscope, MultiMode8	Bruker
Autoflex-2	Bruker
Centrifuge 5424R, 5430R, 5810R	Eppendorf AG
DS11 Spectrophotometer	DeNovix
Gel documentation system	Intas
Glow discharger	Pelco easiGlow
incubater (37°C)	New Brunswick scientific
JEM 1400Plus	JEOL
Pipettes: Eppendorf Research Plus	Eppendorf AG
poly acrylamide gel system	VWR International GmbH/Bio-Rad Laboratories Inc.
Precision balance	Sartorius AG
Tecan Spark 10 M	Tecan
Typhoon FLA9000	GE Healthcare Life sciences
Zetasizer	Malvern Analytics

f. Software

Cadnano2: All DNA origamis were designed using this software both as Maya 2015 plugin as well as standalone version.[73] Color coding was used for sorting oligonucleotides in .csv output files. The generated .json files were used for graphical representation in Maya, Adenita plugin for SAMSON[295] and Cadnano2pdb webtool provided by the Aksimentev group[296] as well as modelling in online tool Cando[73,248,297].

Eman2: This program was installed on a Ubuntu operation system in order to obtain 2D class averages of particles from negative stain TEM images.[298]

design_analyzer.app: This tool was used to estimate melting behavior of the staples in an origami depending on the base sequence of their segments.[86]

UCR Random sequence generator: This webtool was used to generate random sequences. Only the length was changed while desired GC content was remained at around 50%.[299]

FiJi: Beside of graphical representations, band intensities were estimated using FiJis respective gel analysis program. Similarly, for counting structures in microscopy images the cell-counter plug-in was used. For some negative stain TEM images, fast four transformation (FFT) bandpass filter was applied, generally filtering out image frequencies below 1 nm and above 70 px.[300]

Nanoscope 1.9: AFM images were flattened and analyzed using this software.

Zeta Analyzer Software: Build-in software to analyze obtained data by dynamic light scattering.

II. Additional data for section 4.1

a. Origami design files

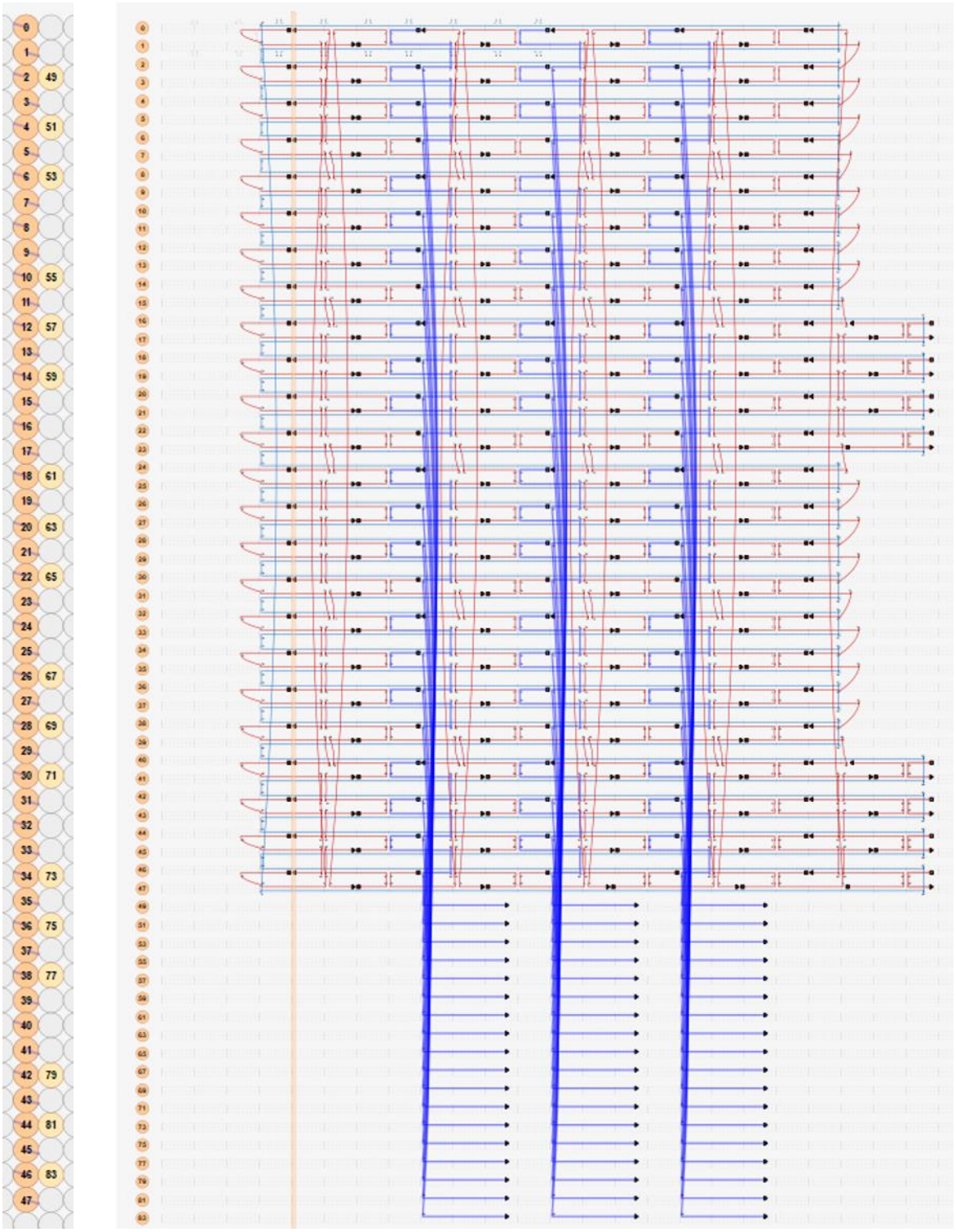

Figure 0-1: Cadnano design of the 6p120_54cF9. Protrusion arm staples are colored dark blue

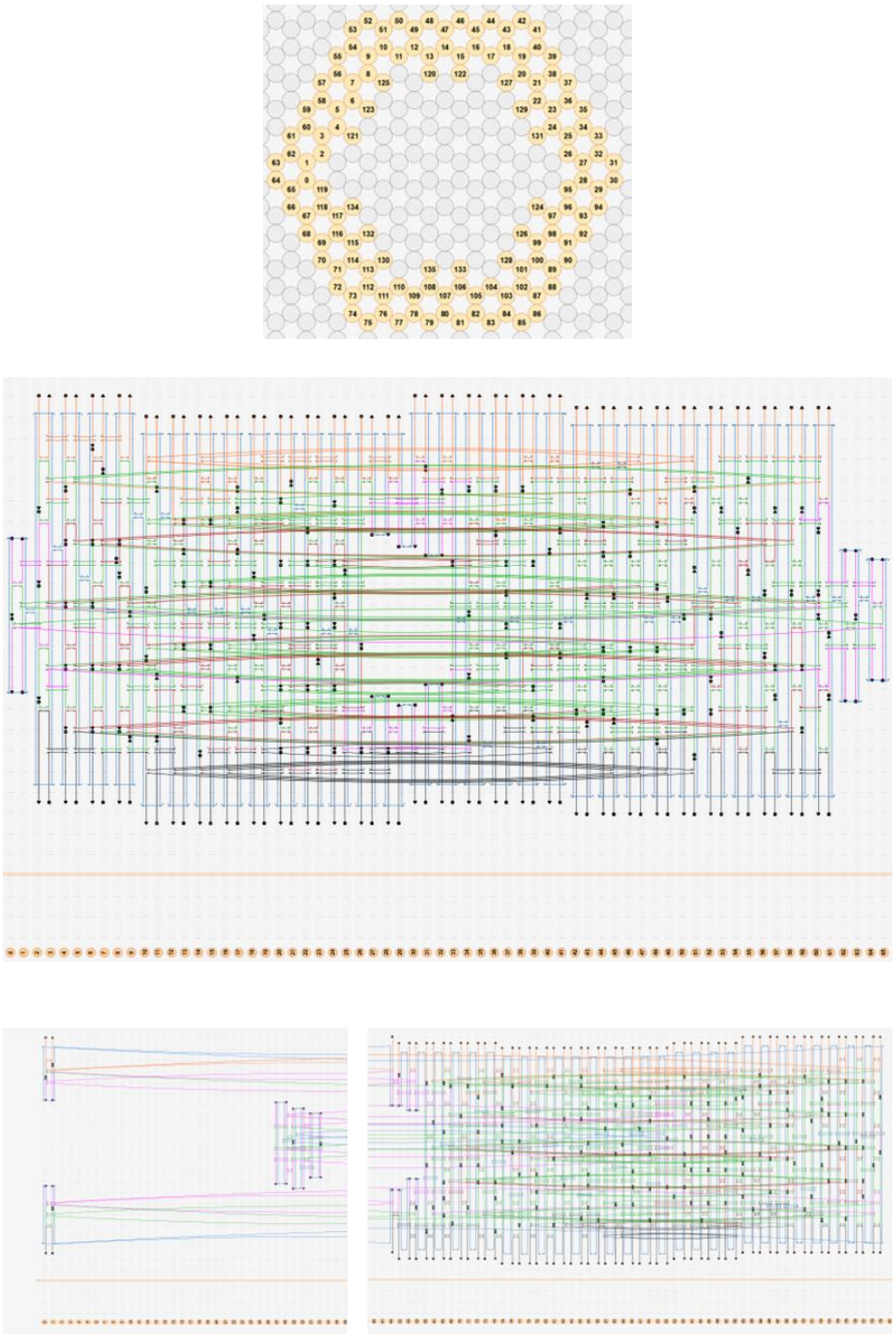

Figure 0-2: Cadnano design file of hexamprism with basic helix layout (upper) and the helix side view of Narcissus (middle) and Echo (lower) with staple sets cs$P_0L_{6T}R_{6T}$stack. Staple sets are color coded: Core green, P red, left edge black, right edge orange and interaction site pink.

b. Assembly at high scaffold concentration

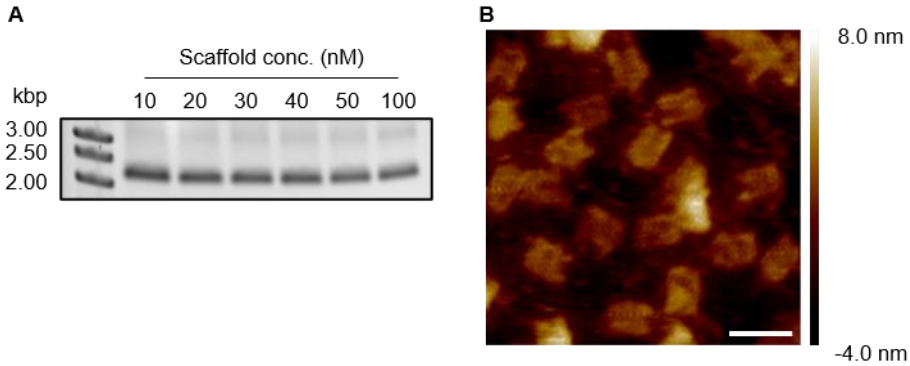

Figure 0-3: **A** AGE of Narcissus assembled in various concentrations. Staple excess was fivefold for scaffold concentrations up to 50 nM. For 100 nM threefold excess was used. **B** Successful formation in higher concentrations can be confirmed by AFM, here assembly with 100 nM scaffold. Scale bar is 100 nm.

The range of scaffold concentration where correct monomers were formed was found to be at least up to 100 nM with only threefold excess of staple strands over scaffold (Figure 0-3). However, full-prism formation from the half-prism at these concentrations led to some extent of clustering, hence the assembly was kept at scaffold concentration of 5 or 10 nM.

c. Additional data for NE multimerization

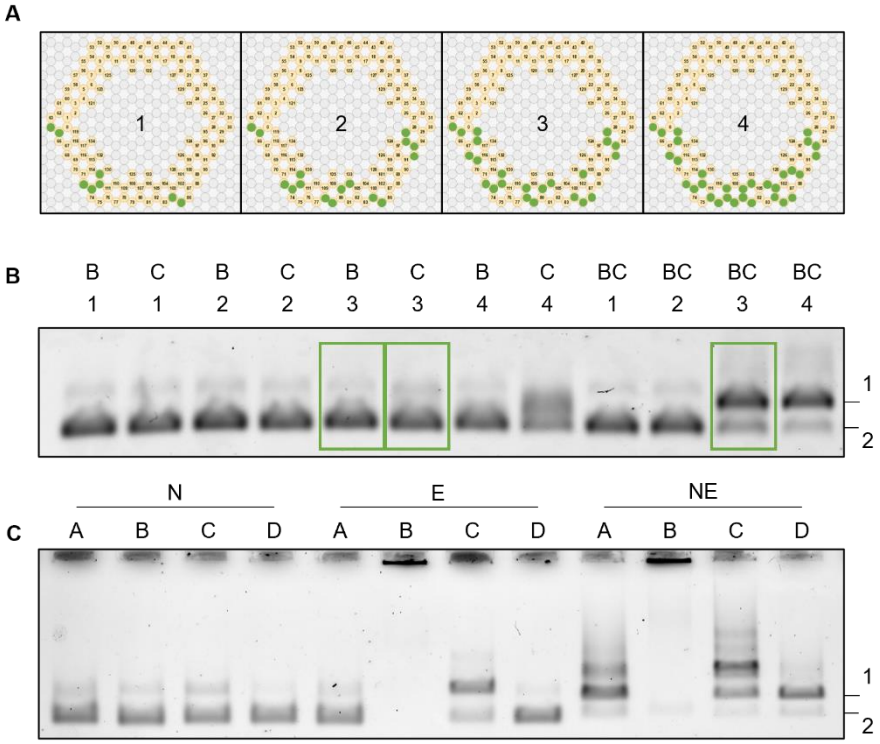

Figure 0-4: **A** Connectivity for EE interaction tested for set β. Connecting helices are depicted green, all other were passivated by six thymine overhangs. The interaction investigated was between the middle prism (B) and right prism (C) in the three prism setup. E_B half-prism contains the R_{in} staples and E_C half-prism the respective L_{ex} staples. **B** AGE of assembled E (2) with respective edge staple sets and the EE dimers. Interaction 3 (green rectangles) was chosen due to the absence of strong dimeric band (1) in the single E_C construct but with good EE interaction. **C** AGE of the adjusted NE_ANE_B interaction with adjusted L_{in} and R_{ex} staple sets while NE_BNE_C interaction was kept the same as set α. NE formation failed for B prism and shows strong multimerization in A and C.

The staple set developed for the NN and EE dimers which than was extrapolated to the B-in combination of the three prism setup (section 4.1.5 page 38 and following) was termed set α. The general design of the four base edge protrusions of the prisms A and C and respective B edge staple shortening was kept for all following design choices. The half-prism E_C was considered problematic since it formed unwanted dimers with itself (Figure 4-19 page 40). For this a completely new edge was designed similarly as before by screening different connectivity, finally resulting in a new interaction for Echo at the E_BE_C interface (Figure 0-4 A and B). As mentioned before, the edge staples were not designed in pairs left and right, therefore when L_{in} is now used instead of L_{ex} with the same staple set α the interactions were slightly different. This problem was tackled by adjusting the L_{in} staples to the used R_{ex} staples resulting in a minor increase of connectivity at the NE_ANE_B interface compared to the original set α. The interaction of for N_BN_C interface was kept the same. All together these changes were coined set β.

When using alternative connecting staple set β for the NE_ANE_B (ABβ) interface while remaining interaction BCα, no NE full prism was forming properly as monomers (Figure 0-4 C).

Next, all interactions were design from scratch. This time inspired by the work of Bayrak *et al.* the connecting helices were focusing on the vertex positions of the prism.[62] The number of connections were slightly higher than for the sets before. The staple mixes used were named set γ and tested for formation NE full prism. But again, the formation of the A and B prism was flawed (Figure 0-5).

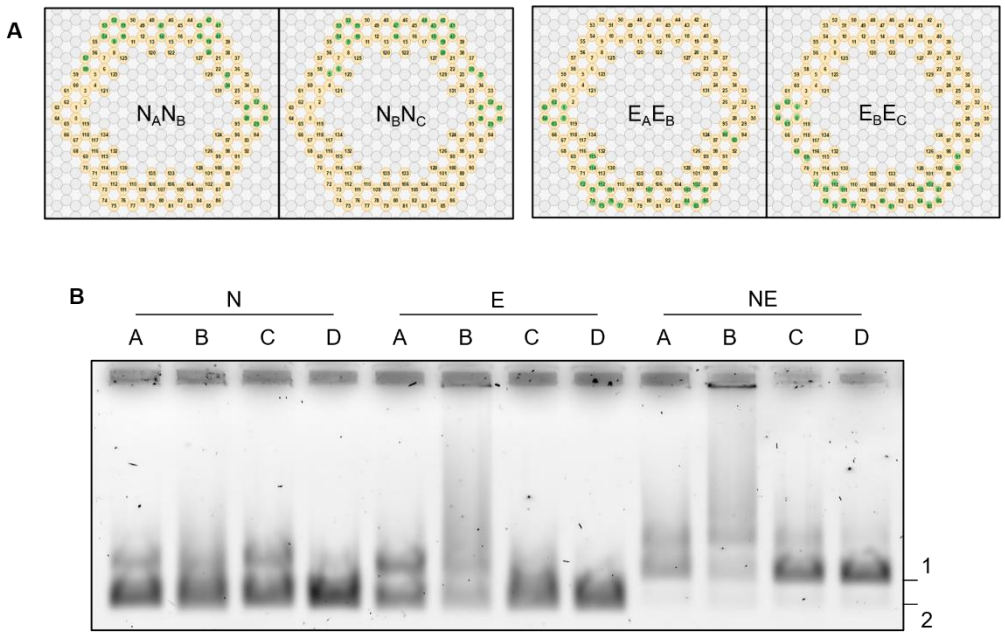

Figure 0-5: **A** Connectivity for interaction of set γ. Connecting helices are depicted in green, all other were passivated by six thymine overhangs. **B** AGE of the set γ half- and full-prisms in the three prism setup.

Some good interactions were found the combination of all three sets α-γ, however not for all prisms. Since there was no set of rules which prism would be well formed and which was not, the combination of the sets were investigated instead of further testing new arbitrary sets.

Conceptually, all interactions can be defined by the central B prism. This leaves three possible sets for the connectivity between N_A and N_B (ABα-ABγ), two for N_B and N_C (BCα and BCγ) and similarly each three sets for E_A and E_B (ABα-ABγ) and E_B and E_C (BCα-BCγ). The total number of 54 possible combinations in the B full prism were screened.

For this, all half-prisms were assembled with the respective edges and checked for half-prism formation by AGE. Only the combination of interaction ABβ and BCα in E_B led to the unsuccessful assembly and exclusion of that combination (Figure 0-6 A). Next all remaining six N_B combinations and eight E_B combinations were checked for successful formation of NE_B prisms. Due to systematic smears and dimer bands in AGE the BCγ interaction was excluded for E (Figure 0-6 B). Then the nine potential NE_A prism combinations were found to be monomeric in AGE (Figure 0-6 C), whereas only one interaction combination leads to monomeric NE_C prism, namely interaction BCα for N_C and BCβ for E_C (Figure 0-6 D). This further led to the exclusion of the other BC combinations. Finally, by investigating the negative stain TEM images of AB and BC dimers of the NE combinations some unspecific interaction can be found for the ABγ interface in two combinations (Figure 0-7). The exclusion of edge staple combinations can be followed by the color codes in Figure 0-6 and Figure 0-7 as well in overview table Table 0-52. In the end, the combination of ABα and BCα for N and ABα and BCβ for E was chosen for multimerization, since it circumvents the unwanted multimerization of prism NE_C with set α and has no drawbacks over the other five residual combinations. This combination was named B_{in+} in the main text.

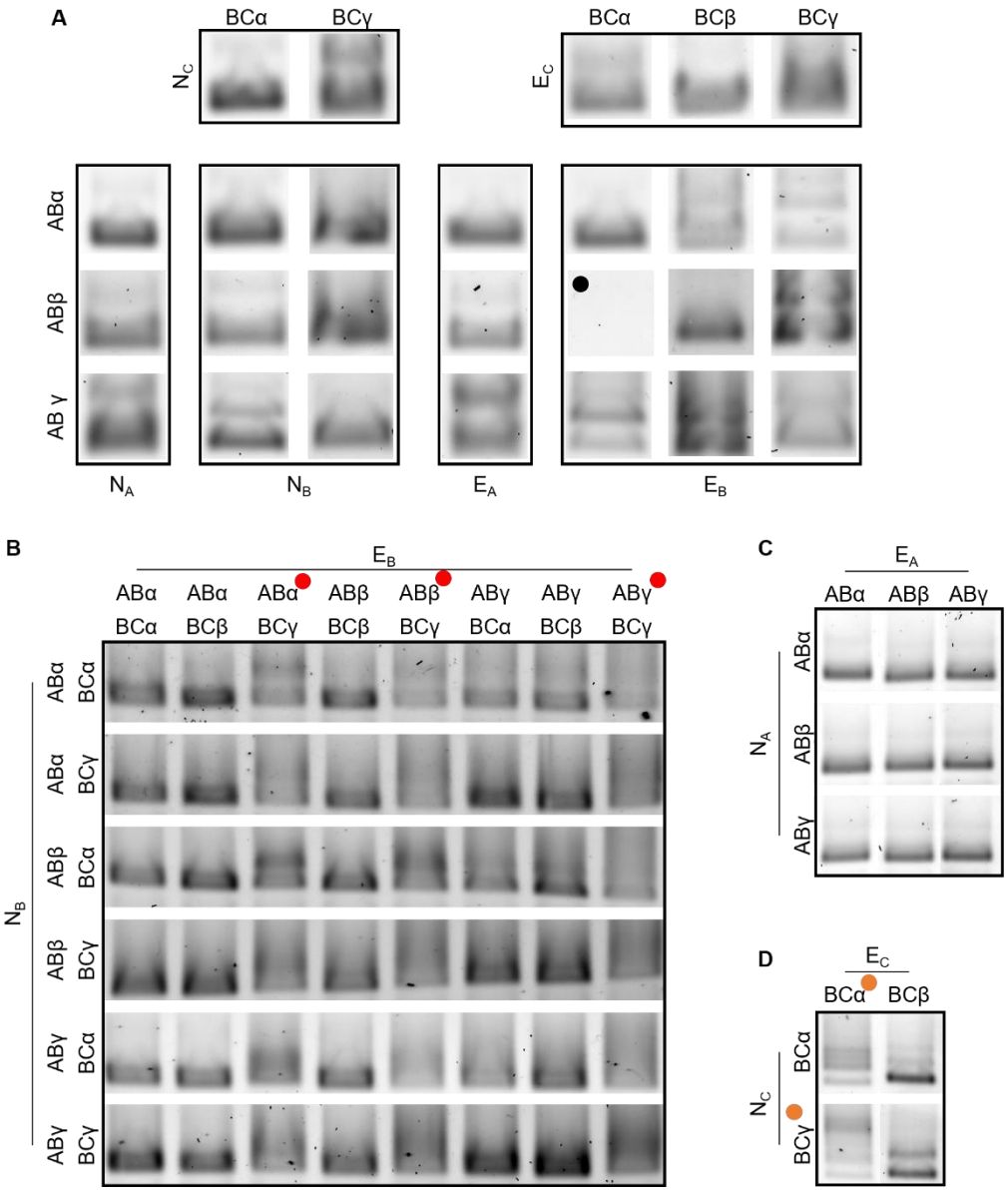

Figure 0-6: **A** AGE bands of all half-prisms possibly used with the named edge staple sets for multimerization. Only absence of bands led to exclusion, like for E_B with BCα and ABβ combination (black dot). **B** AGE bands for all NE_B constructs. Strong smearing and multimer bands were excluded, here all E BCγ interactions (red dot). **C** All residual NE A prism form well defined AGE bands. **D** Residual NE_C prism combinations were assembled, however only the combination of E BCβ and N BCα resulted in a monomer band, leading to the exclusion of the other combinations (orange dot)

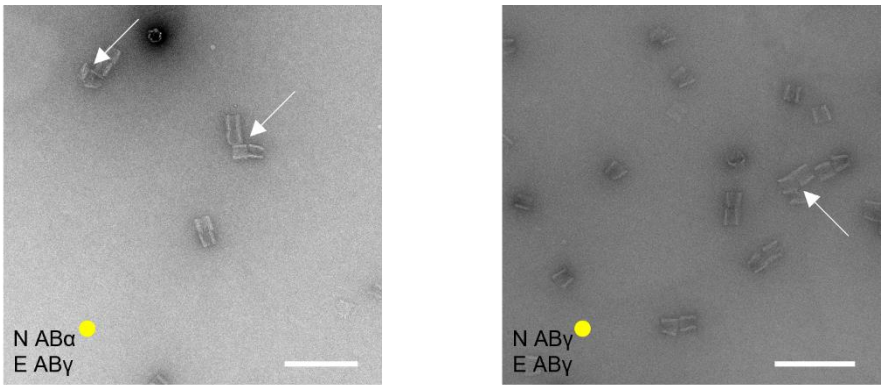

Figure 0-7: Negative stain TEM images of AB and BC combinations revealed unspecific multimerization (arrows) at the AB interaction site for two samples containing E ABγ leading to their exclusion (yellow dot).

Table 0-52: Possible interaction combinations and the exclusion inept versions thereof. Color coding similar to Figure 0-6 and Figure 0-7. Interaction used for multimerization in main text is marked in green.

N_B \ E_B	ABα BCα	ABα BCβ	ABα BCγ	ABβ BCα	ABβ BCβ	ABβ BCγ	ABγ BCα	ABγ BCβ	ABγ BCγ
ABα BCα									
ABα BCγ									
ABβ BCα									
ABβ BCγ									
ABγ BCα									
ABγ BCγ									

d. Introduction of topological markers

Figure 0-8: Cadnano design of the DNA brick based topological marker at the left edge (left), right edge (middle) and on the top of one Narcissus convex side (right). Brick staples are marked in red and blue. Other colored staples had to be adapted in either the L_{6T}, R_{6T}, core or hybr staple sets.

Both in half-prisms and full prisms the left and right side cannot be reliably distinguished in AFM and TEM analysis. Hence, topological markers became interesting for this work. Three DNA brick inspired structures were designed: a left and a right six helical bundle protruding from either the left or the right side of Narcissus and a marker laying on top near to the six-helix protrusion of Narcissus (Figure 0-8 and Figure 0-9 A) The DNA sequences were randomly generated and the staples in the origami adjusted to allow hybridization with the marker. For avoiding stacking interaction of the markers, their edges were passivated using 6T overhangs.

The combination of marker and origami was checked for both one-step and two-step assembly procedure with 200 nM marker oligonucleotides either assembled with the origami (one-step) or separately. Results for two-step and one-step assembly were very similar (not shown) and hence the one-step strategy was followed. AGE did not show a considerable shift in the band migration of the origami when topological markers were added (Figure 0-9 B). All topological markers could be described for FnS purified samples of Narcissus in negative stain TEM. Also, the left and right marker were visualized for NE in negative stain TEM and the R marker also in AFM. The position of the marker confirmed again that N was binding preferentially by its convex side to the grid (Figure 0-9 C). However, the majority of origamis found in microscope images did not contain any marker or they could not be visualized due to the resolution limit. Since a more reliable strategy was at hand by topological marking one edge of the prism with another origami, the DNA brick strategy was not further optimized.

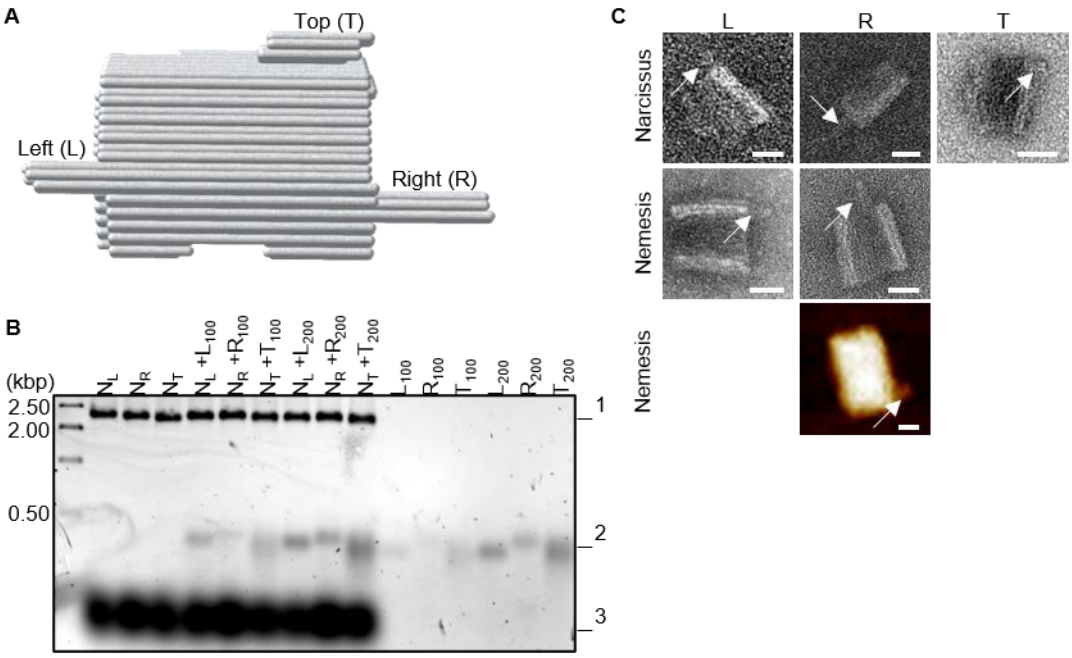

Figure 0-9: **A** Three-dimensional model of N with all three DNA brick based topological marker. **B** Assembly of N (1) with adjusted staple sets for modification for left (N_L), right (N_R) and top (N_T) marker. And co-assembly of the respective markers (L, R and T)(2), as well as their assembly without origami. Marker show lower electrophoretic mobility than staples (3). Suffixes indicate oligonucleotide concentration of the markers in nM. **C** Examples of markers found on half-prism by negative stain TEM (top row), full prisms (middle row) and in full prisms with AFM imaging (bottom) indicated by arrows. Scale bars are 20 nm.

III. Additional data for section 4.2

a. Encapsulation via natural ligand and Strep II tag

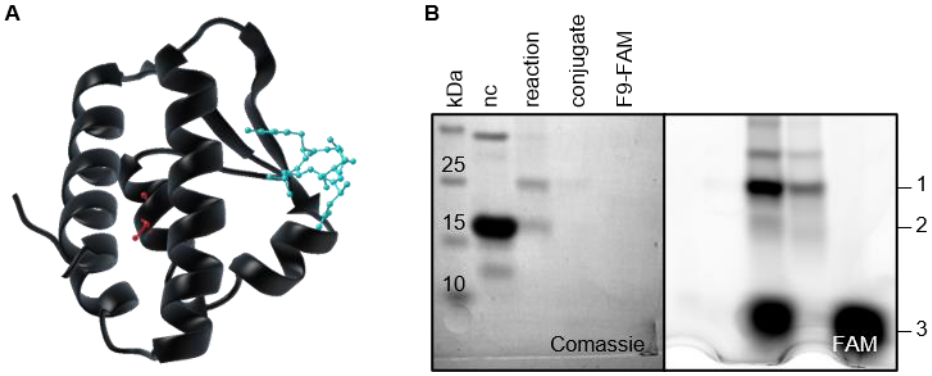

Figure 0-10: **A** Crystal structure of PUB domain (pdb 2HPL) bound to the C-terminal peptide of p97 (cyan). The domain contains only one cysteine (red) which is situated outside the peptide binding region. **B** SDS-PAGE results of the conjugation of PUB to FAM labelled F9 and the purification thereof. Conjugated bands (1) were running slower than the unconjugated PUB domain (2) or the excess oligonucleotides (3).

A variety of approaches were thinkable for encapsulation. Due to the hexameric structure of p97, every binding site and tag-molecule would hence presented six times. And, in order to force the unfoldase p97 into a defined position and orientation, only three attachment points were necessary to fix the protein to the origami. Initially a natural ligand of the p97-C-terminus, the PUB domain, was chosen for this work to avoid altering the amino acid sequence of p97 (Figure 0-10 A). The PUB domain and its conjugates with DNA oligonucleotide were produced and purified in cooperation with Mike Blüggel from the group of Prof. Dr. Peter Bayer (UDE) (see also section 3.5 p.20). The PUB domain contains one cysteine on its surface which was addressed as conjugation point with DNA. It is situated opposite to the p97 binding site (Figure **0-10** A). The amino modified oligonucleotides F9(16)-FAM and F9(16) were conjugated via sSMCC to the PUB cysteine and further purified by SEC. Successful conjugation could be confirmed by SDS PAGE (Figure 0-10 B). Concentration was estimated by single point Bradford assay.

Firstly, the interaction of conjugated PUB domain and the C-termininal peptide sequence of p97 was investigated using native PAGE (Figure 0-11 A). For this p97 was labelled via its cysteines with Alexa650-maleimide and successively purified of excess fluorophore. This fluorescent p97 was incubated with native and conjugated PUB domain. No considerable shift was found for p97, however there was colocalization of PUB-F9-FAM to the p97 band. But these bands were very smeared, hinting to a weak interaction if present at all (Figure 0-11 A, lane 4). Instead of full length p97, the FAM-labelled C-terminal peptide was used as PUB ligand and incubated with the native and conjugated PUB domain. Here, only binding was found for the native PUB domain (Figure 0-11 A, lane 5)., whereas conjugated PUB domain did not show any binding (Figure 0-11 A, lane 6).

The finding was similar for the binding to a Narcissus half-prism with one protruding arm. The origami was assembled and purified and incubated with the conjugated PUB domains. Then fluorescently labelled p97 or the FAM labelled C-terminal peptide was added to the sample. It was found that the p97 had approximately the same electrophoretic mobility in an AGE as a DNA origami making it impossible to estimate if it was bound to the half-prism in this gel (Figure 0-11 B, lanes 2, 5 and 7). Absence of FAM

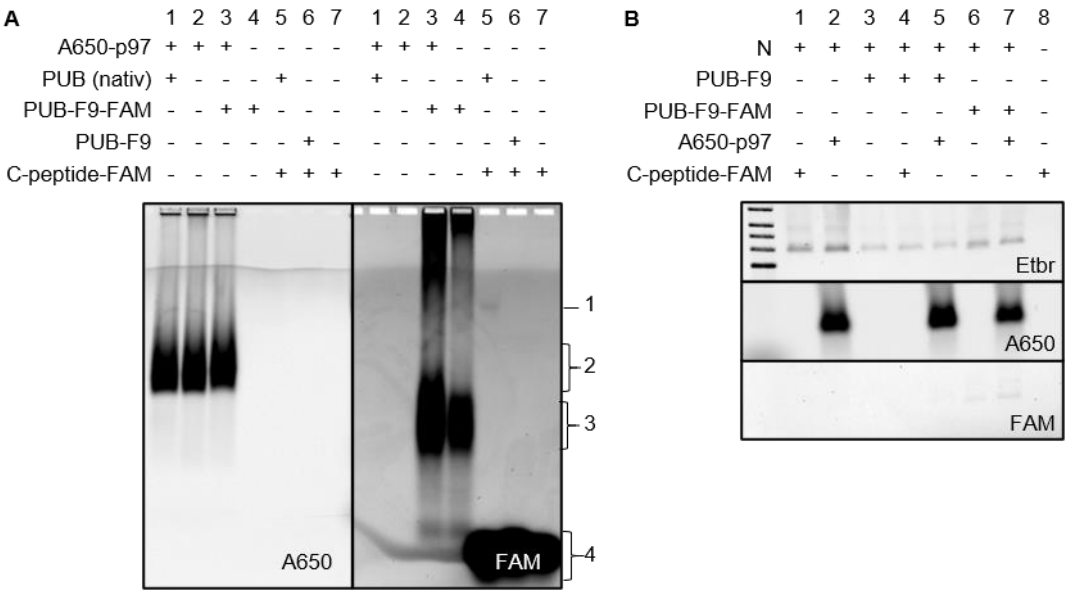

Figure 0-11: **A** Native AGE to investigate if PUB domain conjugated with F9 was binding p97. For this p97 was labelled via its cysteines with Alexa650-maleimide and successively purified from excess dye (A650-p97). Both PUB domain conjugated to F9 with and without FAM were used. Note, that native PUB seems to bind C-terminal p97 peptide labelled with FAM (C-peptide-FAM) (1), whereas PUB-F9 was not (lane 6). Concentration of p97 hexamer or the peptide was 1.4 µM, PUB concentration was 4.2 µM. Fluorescent band can be seen for p97 (2), PUB domain (3) and the peptide (4). **B** AGE of incubation of PUB domain attached to the origami with A650-p97 or the C-terminal peptide. Note that binding of the peptide (lane 4) was not found. Binding of PUB-F9-FAM to origami was however confirmed (lane 6 and 7).

fluorescence of the peptide at origami bands, indicate no strong binding interaction to the conjugated PUB domain (Figure 0-11 B, lane 4). Binding of FAM labelled conjugated PUB domain to the origami could be confirmed (Figure 0-11 B, lanes 6 and 7). It was hence assumed, that the p97 binding site of the PUB domains were distorted during the conjugation. Due to these findings, this strategy was not further investigated.

Then it was decided to use the streptavidin binding peptide (SBP) to encapsulate p97. For this a prolonged version of p97 with a SBP tag on the C-terminus was produced and purified by Johannes van den Boom in the group of Hemmo Meyer. Biotin-F9(16) binding oligonucleotides were used together with a tetrameric streptavidin as a linker between the origami and p97-SBP. p97 was co-purified with streptavidin using SEC (Figure 0-12 A). Binding of p97-SBP to streptavidin was also confirmed using native PAGE: two bands appeared for the p97 with lower mobility than the native p97 both for the purified sample as for the p97 incubated with excess streptavidin (Figure 0-12 B) without further purification. Both techniques indicate no aggregate formation of the two proteins

Binding of protein to a N half-prism containing two protrusions was confirmed only when the sample was incubated with protein on the mica (Figure 0-12 C). Also, mainly small protein spots were found on the origami which were interpreted as streptavidin. Only rarely, a protein with dimensions of p97 was found bound to an origami. When DNA origami, streptavidin and p97-SBP were incubated and then purified by FnS, only streptavidin was found bound to the half-prism (Figure 0-12 D).

Hence, this strategy was not further followed. The binding constant of SBP to streptavidin to a biotin bound DNA strand was assumed to be too low to reliably bind p97 to a DNA origami. Alternatively, biotin

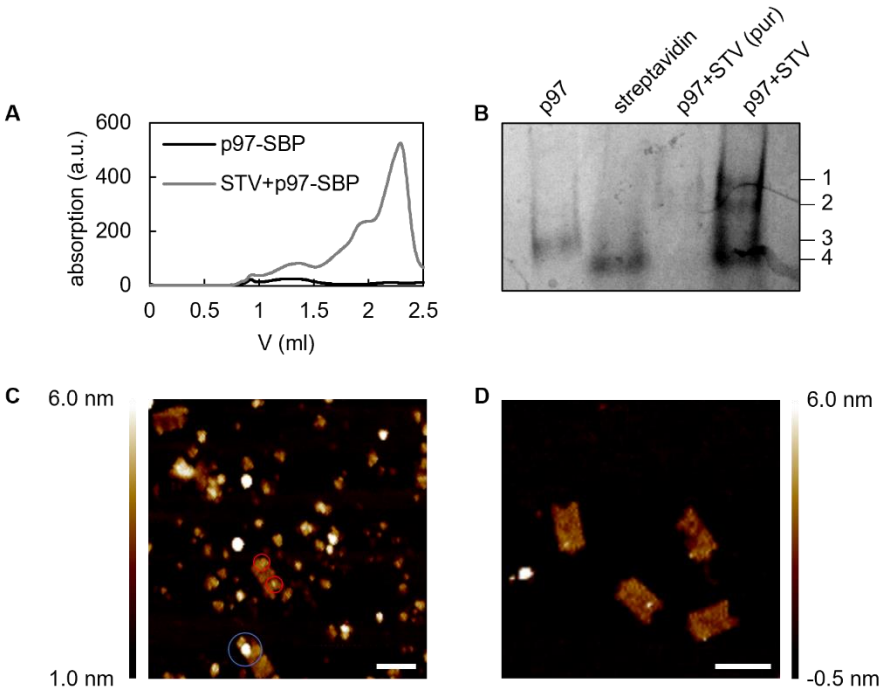

Figure 0-12: **A** SEC elution profile of only p97-SBP and the copurification with streptavidin (STV). **B** Native PAGE revealed binding that only two streptavidins were binding to p97-SBP at most (1) with one bound streptavidin (2) as additional side product. p97-SBP (3) and Streptavidin (4) were migrating faster than the hetero protein complex. **C** AFM image of N with two bt-F9 protrusions incubated with both proteins. Streptavidin binding was evident (red circles), however only rarely for p97 (blue circle). **D** When purified only binding of streptavidin was found in AFM imaging.

modified staples in vicinity might elute SBP from its binding sites.[253,301] Additionally, the binding of only one or two streptavidins to one p97 hexamer indicated that this system was not as controlled as desired.

b. AFM images of p97H encapsulation

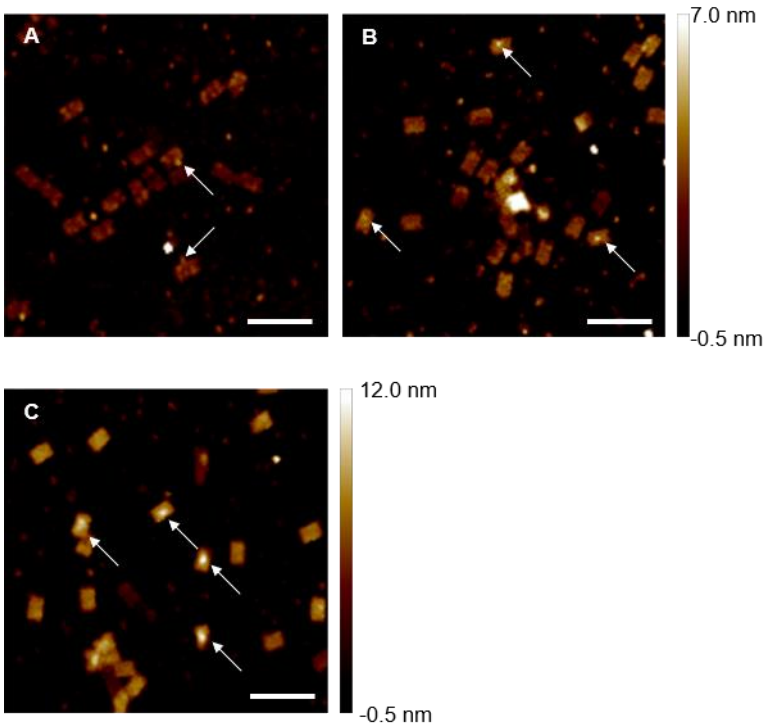

Figure 0-13: AFM images of p97H bound to DNA origamis. **A** N with one cF9 protrusion incubated with p97H. **B** E with two cF9 protrusion incubated with p97H. **C** NE with three cF9 protrusion incubated with p97H. Encapsulation events are shown with arrows. Scale bars are 200 nm.

c. PEG-block oligonucleotide data

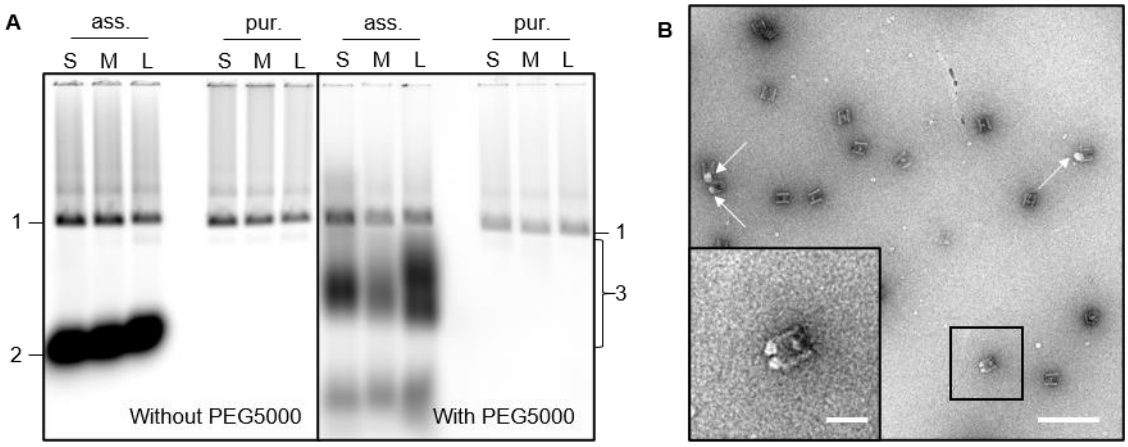

Figure 0-14: **A** AGE imaged in Cy5 channel of assembled NE(1) with Cy5 labelled blocking strands (2). Left gel for origamis assembled without PEG attachment and right gel for origamis assembled with PEG attachment. S, M and L indicate blocking oligonucleotide species. DNA orimis were purified by washing over 50 kDa MWCO filter. Electrostatic mobility of excess PEG-block strands is strongly decreased (3). Purification of PEG-block strands was still possible as seen on the right side of the right gel. **B** TEM image of NE sample with PEG-L-block in both entrances. Here, block release strand was added prior to incubation with p97H. Formation of particles found on some origami edges (arrows). Note, that the sample was also incubated with p97H. Scale bar is 200 nm. Inset shows one origami where particles were formed at two sites of an origami edge. Scale bar is 50 nm.

Some unusual behavior was found for the PEG modified block strands that could only partly be explained by the literature. During conjugation and successive purification of fluorescently labelled PEG-block strands it became evident, that PEG5000 was stabilizing the oligonucleotides in isopropanol, an effect described in literature[302,303]. The conjugates were hence purified by washing over MWCO filter rather as they could not be precipitated them. On the other hand, they were not resolving in n-butanol.

When used in DNA origami assembly PEGylated block oligonucleotides showed one or two strongly smeared bands in AGE with much higher electrophoretic mobility than the unmodified strands (Figure 0-14 A). While a slower electrophoretic mobility could be expected for a conjugate and was also found by denaturing PAGE, the strong smearing was somewhat unexpected. It indicates to some self-association, however only in absence of denaturing agents like in denaturing PAGE and presence of PEG modification. When the origamis were purified by washing over filters with 50 kDa MWCO those bands were absent. Block DNA strands were found to contain palindromic properties when analyzed by NuPack allowing self-dimerization, however unmodified strands were not showing dimerization indicating that the PEG modification might stabilize this dimerization or even multimerization at room temperature and below.

Another hint towards potential formation of PEG-DNA multimers came from negative stain TEM images of a NE prism that contain PEG-L-block strands both in the left and right PA ring and was incubated with block release strand prior to incubation with p97H. For some origamis particle formation could be found at DNA origami edges (Figure 0-14 B). This could be interpreted as released blocking strands forming particles when their concentration was high enough. This could also sterically hinder the full release of the blocking strands from all DNA origami sites, explaining the lower encapsulation yield of p97 for this kind of sample despite the addition of release strand (compare Figure 4-30 B, page 54).

d. Structural marker for p97 orientations

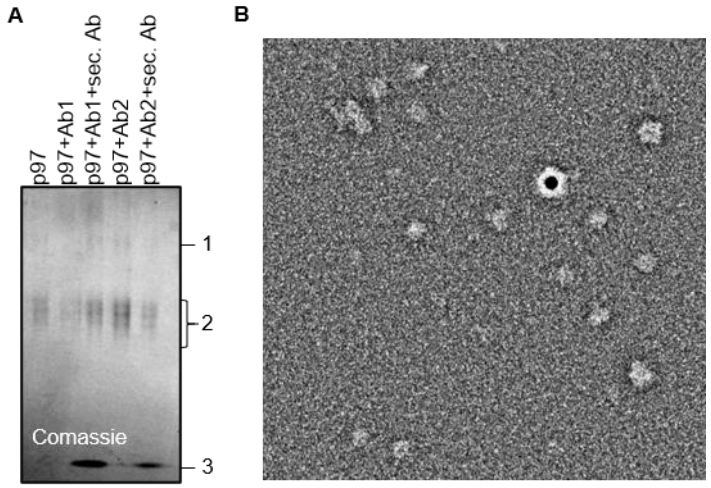

Figure 0-15: **A** Native PAGE of Halo-p97(2) does not show binding of the primary (1) or AuNP modified secondary antibody (3). **B** Negative stain TEM image (bandpass filtered) does not show localization of p97 and the AuNP. Scale bar is 50 nm.

Firstly, a Western blot inspired labelling method was envisioned[304]. Immunoglobulin G (Ab) mouse antibodies raised against the p97 segment of aa 221-310 (Ab1) was ordered. A second antibody raised against the aa 1-588 of p97 (full length, Ab2) was envisioned as control. As a secondary Ab goat IgG anti-mouse Fc conjugated to 12 nm AuNP were ordered. The AuNPs were anticipated to label the p97 N-terminus. Binding of primary and secondary Ab were checked in 4% native PAGE, however no decrease of mobility was found for the unconjugated p97H (Figure 0-15 A). AuNP labelled secondary antibodies were assumingly found in the running front while the other Ab were most likely migrating slower than p97. Binding of the AuNP to p97 was also checked in negative stain TEM. But for the very few AuNPs found on the grid no colocalization with p97 was observed (Figure 0-15 B). Due to the questionable binding between the antibody and its target in these conditions, this approach was not further followed.

As an alternative topological marker, the Ufd1-Npl4 adapter protein was envisioned. It was kindly provided by Dr. Matthias Kracht from the group of Prof. Dr. Hemmo Meyer (UDE). Ufd1-Npl4 was reported binding near to the N-terminal pore opening of p97 in the presence of ATP (Figure 0-16 A). For the resting state of p97 other modes of binding were reported for TEM investigations, however they were also associated in similar regions of p97 and hence Ufd1-Npl4 usefulness as topological marker was still anticipated.[305]

Similar as before binding of Ufd1-Npl4 was checked by native PAGE of DNA conjugated p97 with various concentration of adapter protein (Figure 0-16 B). No shift in p97 migration was found and no band was found accounting for the used adapter protein. The latter was accounted to a potential positive net charge of the complex. Binding was also investigated using negative stain TEM. But either no binding event was found, or resolution of imaging was not high enough to reliably tell if the adapter was bound. Note, that also the binding constant of this adapter might have been insufficient for labelling as p97 concentrations were in the lower nM region[306].

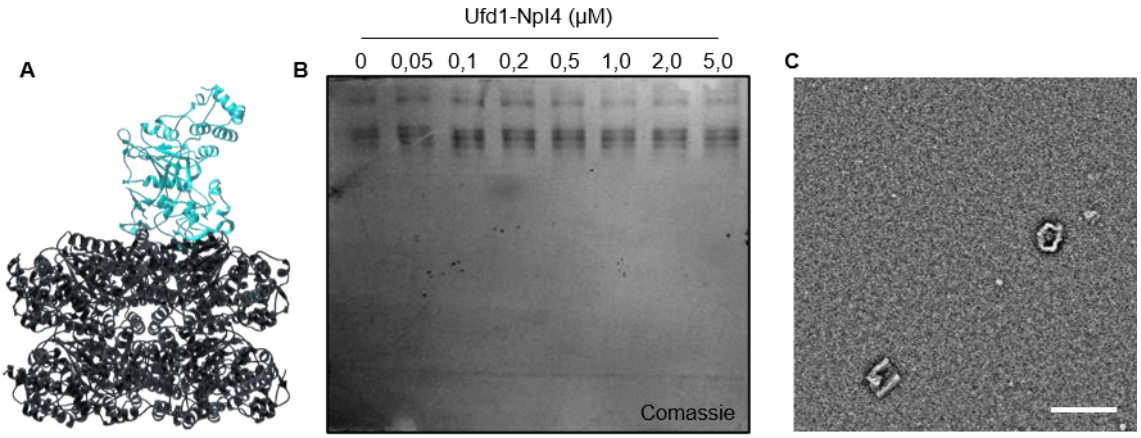

Figure 0-16: **A** Model of Udf1-Npl4 (cyan) bound to D1 ring of p97 (black) with masked N-domains (pdb: 6chs). **B** native PAGE of 50 nM conjugated p97H incubated with various concentration of Ufd1-Npl4. No shift nor band for the ligand was found. **C** Negative stain image (bandpass filtered) of purified encapsulated p97H incubated with Ufd-Npl4. Scale bar is 100 nm.

Then p37 was used as an adapter protein (Figure 0-18 A). Since it was too small to be reliably visualized in negative stain TEM a Snaptag was cloned to it which further allowed modification with AuNPs. The production and purification of p37-Snap was done by Dr. Johannes van den Boom of the group of Prof. Dr. Hemmo Meyer (UDE). Two DNA oligonucleotides were designed: one for the modification of an AuNP (Aumod) and one to be conjugated to the Snaptag (Aubind). They contained complementary 16 base pair sequences. Aumod contained a 5´ protected thiol group after a T_{10} spacer sequence used to bind to the gold nanoparticles. Aubind contained a 5´ NH_2 group that was used to conjugate a benzylguanine-NHS moiety to it (Figure 0-18 B). AuNP at 10 nm diameter were produced in the group of Prof. Dr. Sebastian Schlücker by Michael Erkelenz (UDE). Successful reaction of p37-Snap with Aubind was confirmed by SDS-PAGE (Figure 0-18 C). However, in an attempt to purify the construct by SEC the majority of protein was found eluting with the column void (Figure 0-18 C). When the purified FAM-labelled p37-Snap was incubated with purified encapsulated p97 weak colocalized bands for p37 and the origami can be found in AGE (Figure 0-18 E). AuNP seemed to quench the fluorescence of FAM as described in literature and indicating their binding.[307]

Due to the loss of sample during the purification of the conjugate, the reaction mixture was used for the imaging by negative stain TEM as follows: 15fold excess BG modified Aubind was incubated with p37-Snap overnight at 8°C. Aumod decorated AuNP were incubated with this reaction mixture on ice for 90 min. Excess of Aubind over AuNP was approx. 1,000. For purification of this excess the sample was washed over 100 kDa MWCO filter. Concentration of AuNP was measured at 400 nm. Note, that by this the number of p37 on a given AuNP was reduced avoiding potential clustering of encapsulated p97 around one AuNP. Purified encapsulated p97 were incubated for two hours on ice with the modified AuNP and then imaged by negative stain TEM. Binding was not observed. However, it became evident that statistically there should be AuNP present on or inside of NE prism which was not the case (Figure 0-18 F and Figure **0-17** A).

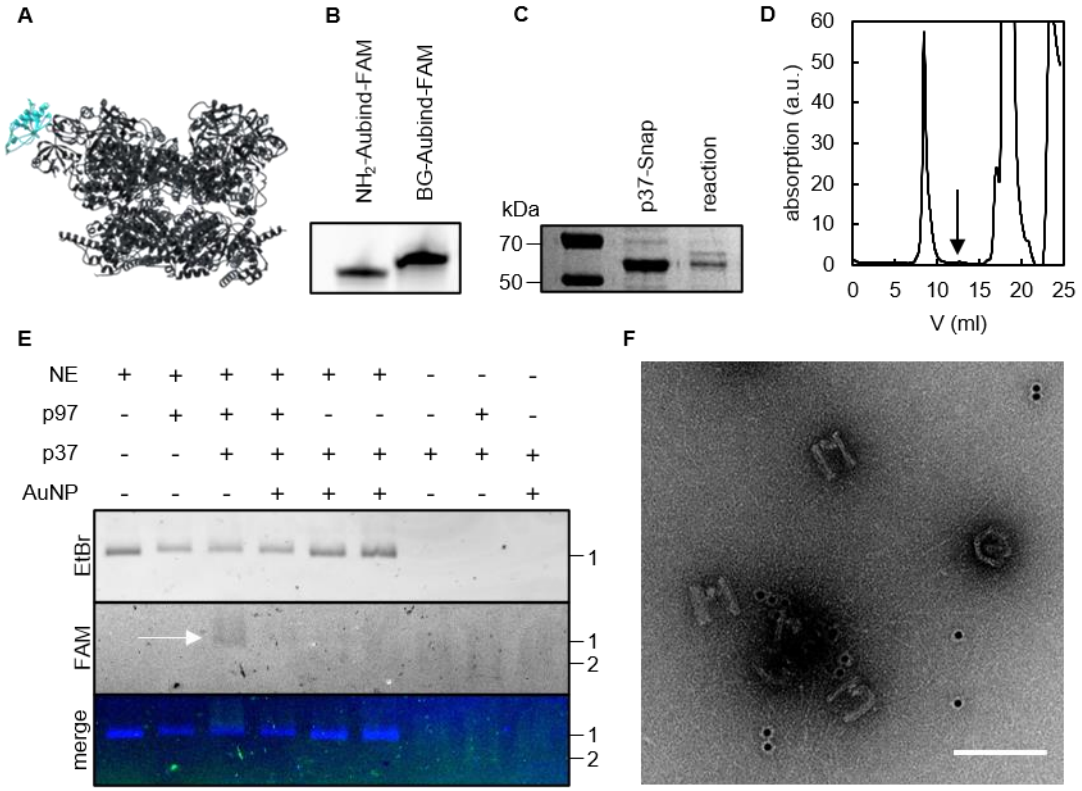

Figure 0-18: **A** Model of yeast p97 homolog Cdc48 (black) and with bound yeast p47 homolog Shp1 (cyan). Binding mode of p37 to p97 was expected to be similar. **B** Conjugation of benzylguanine moiety (Snap) to Aubind oligonucleotide. **C** SDS-PAGE confirm conjugation via Snaptag. **D** Sample purification by SEC indicate denaturation of majority of protein with only a small peak representing the native conjugate (arrow). **E** AGE NE samples (1) with Snap-p37 conjugated to FAM-oligonucleotide (2). Binding of p37-Snap labelled with FAM-Aubind to origami can be found to a small extent (arrow). FAM fluorescence was most likely suppressed by AuNP binding. **F** Negative stain TEM images of origami incubated with Aumod decorated AuNP reveal that AuNP could never be found inside DNA origami prisms. Scale bar is 100 nm.

This finding was also described in some publications and hence salt adjustments were tested[62,308,309]. For 50 mM $MgCl_2$ binding of AuNPs inside of NE prisms became evident (Figure 0-17 B). However, there was no preference of AuNP encapsulation with or without p37. Also, label efficiency with AuNP was too low for statistical analysis. One surprising finding was that p37-Snap decorated AuNP were forming clusters. These clusters seemed to be spaced evenly by some defined molecules (Figure 0-17 C and D). Due to the clusters and p37 unfolding during conjugation, the labelling technique was adjusted to circumvent usage of p37-Snap leading to the technique described in the main text (section 4.2.8 page 60). Salt adjustment in the main text for AuNP usage were based on the findings shown here.

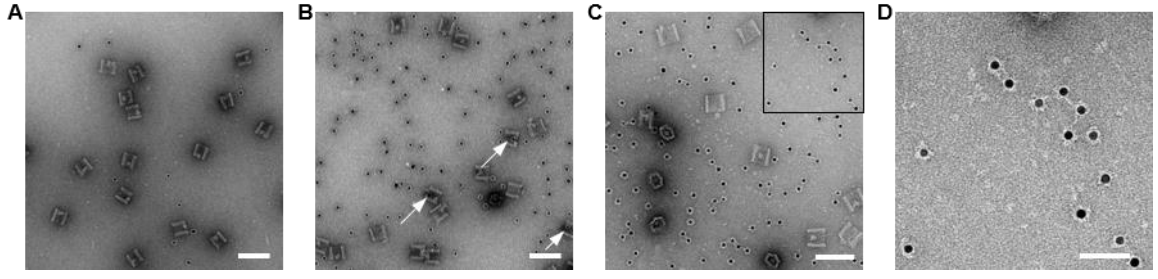

Figure 0-17: AuNP conjugated to p37 were used for all shown samples investigated. **A** Incubation overnight in p97 storage buffer with additional 500 mM NaCl. **B** Incubation in p97 storage buffer with additional 50 mM $MgCl_2$. AuNP inside origamis are indicated with arrows. **C** Exemplary negative stain TEM image of a sample and a zoom-in shown in **D**. Note the clustering of AuNPs. Scale bars for **A**-**C** are 100 nm, for **D** 50 nm.

IV. Additional data for section 4.4

a. Encapsulation of p97 via His6-tag

Site directed placement of antibodies on DNA origami surfaces was described in literature using nitriloacetic acid modified oligonucleotide.[258] Since the principle of this interaction was not limited to the His_6-tag but rather to the histidine side chain, it falls very well into the category of low regioselective non-covalent binding.

In attempt to reproduce the literature data with another protein, a modified NTA-moiety with an attached maleimide was ordered. Thiol-modified F9 oligonucleotide was deprotected and conjugated to the ligand. Only a small shift was found for ligand attachment in denaturing PAGE (Figure 0-20 A). While still suited for analytical confirmation of good conjugation yield, the technique could not be used to purifiy the conjugate. The conjugate was hence only purified from excess ligand by washing over 3 kDa MWCO filter. Conjugation could also be confirmed by MALDI (Figure 0-20 B).

The NTA ligand was used in 6p120_54cF9 together with a Alexa650 modified p97 with a C-terminal His_6-tag kindly provided by Matthias Kracht of the group of Hemmo Meyer. The origami was assembled, and the buffer exchanged to HEPESMg buffer after PEG assisted DNA origami precipitation as described in abovementioned publication. The concentration of $NiCl_2$ was 3 mM. The protein was added and incubated either for five minutes or for one hour. Surprisingly, AGE results indicate no binding of the protein (Figure **0-20** D).

When investigated by liquid AFM potential binding events could be seen, however not reliably confirmed due to the unfolding of p97 on the mica surface during imaging in this buffer (Figure 0-19). The project was put on hold due to the unforeseen weak interaction between decorated origami and protein. There were no observed adverse effects for these Ni^{2+} concentration for the origami. However, the integrity of p97 might have been disturbed by the heavy metal ions.

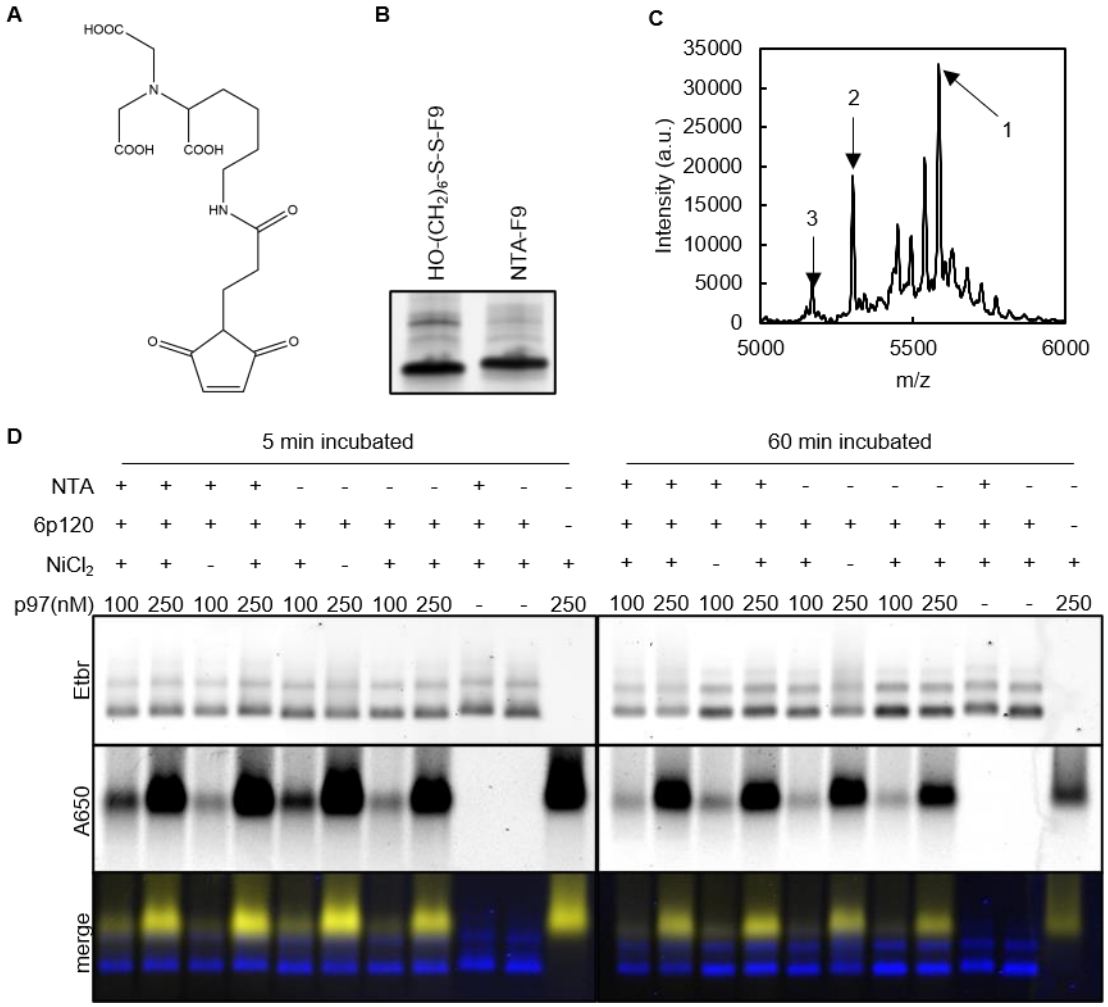

Figure 0-20: **A** NTA-maleimide structure. **B** Denaturating PAGE only shows a faint shift for the conjugate. **C** MALDI spectrum of the conjugate show masses for the conjugate at the expected 5585 Da (1), but also side products as the protected thiol modified oligonucleotides at 5303 Da (2) as well as the deprotected thiol modified one (3) at 5170 Da. **D** AGE of 6p120 with 54 protrusions decorated with NTA were incubated with p97 (C-terminal His6-tag) in HEPESMg buffer without Na_2EDTA. $NiCl_2$ was added to samples to 3 mM final concentration.

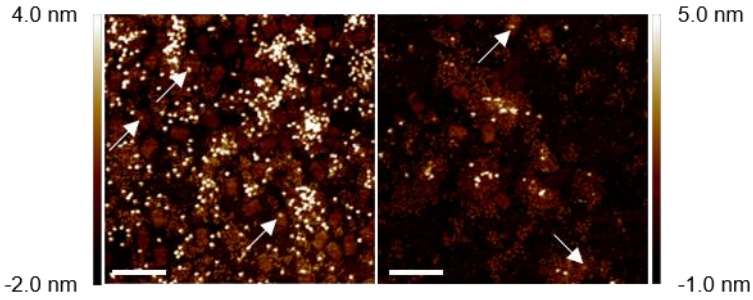

Figure 0-19: Liquid AFM images of p97 and $NiCl_2$ added to 6p120 decorated with 54 NTA-modified protrusions. Immediate imaging (left) and imaging after one hour (right) indicate p97 disassembly under these imaging conditions over time. Potential binding events indicated by arrows. Scale bars are 200 nm.

b. Other ligands for inner modification of DNA origami prisms

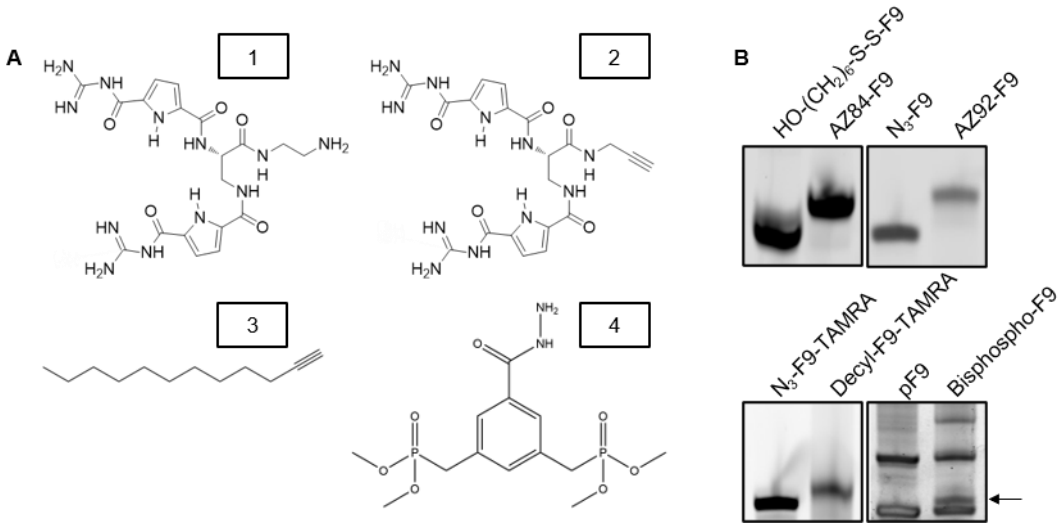

Figure 0-21: **A** Structure of four other ligands that were conjugated as potential ligands. 1 and 2 contained the same bidental GCP ligand with two possibilities of conjugation to modified oligonucleotides. 3 is dodecyne and 4 a methylester protected benzylic bisphosphonate arginine binder **B** Denaturing PAGE of the conjugates of **A** to oligonucleotides. 1 was conjugated via sSMCC to a protected thiol-modified F9. 2 and 3 were conjugate by CuAAC. 4 was conjugated by activation of the phosphate with EDC and imidazole and coupling to the hydrazide. Conjugate of 4 (arrow) was only a fraction of the total DNA amount.

To address various amino acid chains also some other moieties were conjugated to the oligonucleotides. Guanidiniocarbonyl pyrrole either modified with an amine or an alkyne were provided by Dr. Alexander Zimmermann of the former group of Prof. Carsten Schmuck (UDE). They could potentially address negatively charged amino side chains as glutamate and aspartate[310–312]. They were conjugated either via sSMCC or directly by CuAAC to respective modified F9(16). Dodecyne was clicked via CuAAC to the oligonucleotide anticipating binding aliphatic protein surface patches. Finally, a precursor of a benzylic bisphosphonate arginine binder[313] as alternative to the CLR01 tweezer was provided as a hydrazide by Phillip Rebmann by the group of Prof. Dr. Thomas Schrader (UDE). Conjugation to a 5´phosphate-F9 was carried out by phosphate activation via EDC and imidazole as prove of concept. DNA strand multimerization and low yield remained a problem (Figure 0-21).

Ligands were not further investigated due to the quantification issues mentioned in the main text.

V. List of tables

VI. List of figures

VII. List of authored and co-authored publications

Articles

Jaekel, Andreas, Pascal Lill, Stephen Whitelam, und Barbara Saccà. „Insights into the Structure and Energy of DNA Nanoassemblies". Molecules 25, Nr. 23 (Januar 2020): 5466. https://doi.org/10.3390/molecules25235466.

Jaekel, Andreas, Pierre Stegemann, und Barbara Saccà. „Manipulating Enzymes Properties with DNA Nanostructures". Molecules 24, Nr. 20 (Januar 2019): 3694. https://doi.org/10.3390/molecules24203694.

Grossi, Guido, **Andreas Jaekel**, Ebbe Sloth Andersen, und Barbara Saccà. „Enzyme-Functionalized DNA Nanostructures as Tools for Organizing and Controlling Enzymatic Reactions". MRS Bulletin 42, Nr. 12 (Dezember 2017): 920–24. https://doi.org/10.1557/mrs.2017.269.

Jaekel, Andreas, Johannes van den Boom, Hemmo Meyer, Barbara Saccà „DNA-spatial confinement improves the turnover rate of a protein segregase/unfolding machine" *in preparation*

Book chapter

Schöneweiß, Elisa-C., **Andreas Jaekel**, und Barbara Saccà. „Nanotechnology and the Unique Role of DNA". In DNA Nanotechnology for Bioanalysis, 1–26. WORLD SCIENTIFIC (EUROPE), 2017. https://doi.org/10.1142/9781786343802_0001.

Posters

Andreas Jaekel, Mike Blüggel, Matthias Kracht, Johannes van den Boom, Michelle Hechler, Peter Bayer, Hemmo Meyer and Barbara Saccà. "Rationally designed DNA-origami hosts for protein guests" on Nantec 2019 in Aalto, Finland.

Andreas Jaekel, Matthias Kracht, Johannes van den Boom, Pierre Stegemann, Michelle Hechler, Michael Ehrmann, Peter Bayer, Hemmo Meyer and Barbara Saccà. "Rationally designed DNA-origami hosts for protein guests" on 3rd CRC International Symposium 2019 in Essen, Germany

Pierre Stegemann, **Andreas Jaekel**, Andreas Sprengel, Barbara Saccá. "Understanding protein mechanisms using chemically-designed DNA cages" on Joint CRC student symposium 2018 in Billerbek, Germany

Andreas Jaekel, Michelle Hechler, Barbara Saccà. "Exploring the chemical toolbox for protein encapsulation in DNA-origami cages" on Joint CRC student symposium 2018 in Billerbek, Germany

Rosanna Matossovich, Rosa Merlo, Sonia Del Prete, Vincenzo Carginale, Clemente Capasso, Anna Valenti, **Andreas Jaekel**, Barbara Saccà, Giuliana d'Ippolito, Angelo Fontana, Maria Ciaramella, and Giuseppe Perugino, "AGTs from hot sources:from stability to applicability" on Extremophiles 2018 in Ischia, Italy

VIII. Acknowledgements

Foremost, I would like to express my gratitude to Prof. Dr. Barbara Saccà for giving me the opportunity to perform my PhD thesis under her supervision. I am thankful for her guidance through the several topics of DNA nanotechnology I was working throughout the course of the last five years as well as her inspiring mentoring spanning far beyond the scientific work.

I´d like to thank Prof. Dr. Hemmo Meyer for advising a majority of this thesis as well as evaluating it. Along this, I thank Dr. Johannes van den Boom for our smoothly running cooperation. Without his quick laboratory work and extremely sound academic input this work would have been longer in time and shorter in results.

I thank also all the former and current PhD students of the CRC1093 who synthesized chemicals or produced proteins for me during the course of this work: Dr. Elisa-Charlott Schöneweiß, Dr. Matthias Kracht, Dr. Alexander Zimmermann, Dr. Christian Heid, Pierre Stegemann, Philip Rebmann, Mike Blüggel, Michael Erkelenz thank you for allowing me to span this work across biology and chemistry alike.

Also, I´d like to express my happiness to have worked with all the members of our group and of the group of Prof. Dr. Markus Kaiser around. Dr. Wolfgang Pfeifer, Dr. Elisa-Charlott Schöneweiß, Dr. Sabrina Ninck, Dr. Florian Schulz, Dr. Steffen Köcher, Georg Homa, Svenja Heimann, Leonard Sewald, Sarah Urban, Lena Winat, Sabrina Gambietz, Pierre Stegemann, Richard Kosinski, Michael Erkelenz, Michelle Hechler, Ozan Karaman, Arne Rother, thank you for your scientific input, stories, laughs, parties and nearly every lunchtime of my last five years. I am so grateful to know you all.

Special thanks to Karoline Diesing not only for being such a great friend but also for correcting some of this work.

As a social person I was also very thankful for all the off-work distractions as new inhabitant of the Metropole Ruhr. I would like to especially thank Sarah Urban for all the evenings we spent watching bad movies or spent in Felis. Thanks to Steffen Waltenberger and André Reetz for all the game nights as well as Heinz Potztal for keeping our Männer-Vokal-Ensemble running so smoothly. I would also like to thank the A-Team, the TAMM crew, my former flatmates and my brothers putting time and energy in these long-distance friendships.

In the end, I thank my wife Katrin Haubold to bring out the better in me and having my back in good and bad times. Also, I thank my children as they were unknowingly brightening my dark hours in the last years. Thanks to my mother for her immense support throughout my whole life.

IX. Lebenslauf

Aus datenschutzrechtlichen Gründen nicht in der Onlineversion enthalten.

X. Declarations

Hiermit erkläre ich, gem. § 6 Abs. (2) g) der Promotionsordnung der Fakultät für Biologie zur Erlangung der Dr. rer. nat., dass ich das Arbeitsgebiet, dem das Thema „Rational designed DNA origami hosts for protein guests“ zuzuordnen ist, in Forschung und Lehre vertrete und den Antrag von Andreas Jaekel befürworte und die Betreuung auch im Falle eines Weggangs, wenn nicht wichtige Gründe dem entgegenstehen, weiterführen werde.

Essen, den 02.08.2021 _____

Unterschrift eines Mitglieds der Universität Duisburg-Essen

Hiermit erkläre ich, gem. § 7 Abs. (2) d) + f) der Promotionsordnung der Fakultät für Biologie zur Erlangung des Dr. rer. nat., dass ich die vorliegende Dissertation selbständig verfasst und mich keiner anderen als der angegebenen Hilfsmittel bedient, bei der Abfassung der Dissertation nur die angegeben Hilfsmittel benutzt und alle wörtlich oder inhaltlich übernommenen Stellen als solche gekennzeichnet habe.

Essen, den 02.08.2021 _____

Unterschrift des/r Doktoranden/Doktorandin

Hiermit erkläre ich, gem. § 7 Abs. (2) e) + g) der Promotionsordnung der Fakultät für Biologie zur Erlangung des Dr. rer. nat., dass ich keine anderen Promotionen bzw. Promotionsversuche in der Vergangenheit durchgeführt habe und dass diese Arbeit von keiner anderen Fakultät/Fachbereich abgelehnt worden ist.

Essen, den 02.08.2021 _____

Unterschrift des/r Doktoranden/Doktorandin